

**HYBRID MULTIDENTATE PHOSPHINE-
ALKENE LIGANDS FOR TRANSITION
METAL COORDINATION CHEMISTRY
AND CATALYSIS**

Somia Ehsan Bajwa

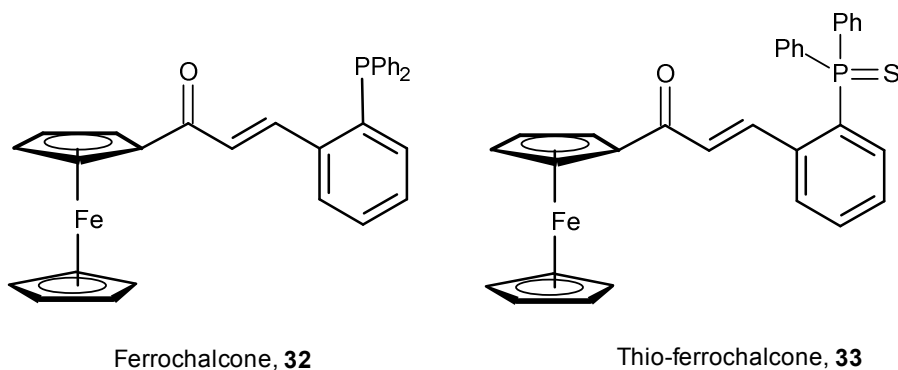
PhD

**University of York
Department of Chemistry**

March 2012

Abstract

The development of a new class of phosphine-alkene and thio-phosphine-alkene ligands based on a chalcone ferrocene framework, represents the primary focus of this study. The synthesis and characterisation of novel ligands, ferrochalcone **32** and thio-ferrochalcone **33**, are described. The related alkene-phosphine ligands, the Lei ligand **17** and novel thio-Lei ligand **46**, are further detailed.



The coordination chemistry of four ligands (**17**, **32**, **33** and **46**) with various transition metals (Pt, Pd, Cu, Rh and Au) has been investigated in a comprehensive spectroscopic study. Single crystal X-ray analysis has been conducted at suitable junctures within the project. A surprising finding was that some solution-state structures were found to be different when studied in the solid state.

The Au^I complexes-containing the ligands have been successfully used in 1,5-enyne cycloisomerisation reactions. In addition to the coordination chemistry of the novel ligand systems, some interesting findings emerged. For example, Au^I complex of Lei ligand **17** and monodbaPHOS **74** undergoes an interesting solid-state [2+2] intramolecular cycloaddition transformation, giving cycloadduct, **72** and **77**.

An interesting finding includes the presence of impurity in commercially available Pd(OAc)₂. Cyclopalladation of papaverine was carried out using pure and impure Pd(OAc)₂, which resulted in the identification of novel Pd-dimer complex, **86**. The result suggest that nitrite contaminants derive from impurities in Pd(OAc)₂, and not from the oxidation of acetonitrile mediated by metallic Pd⁰, explain the formation of Pd^{II}-nitrito cyclopalladated products. Photocrystallographic metastable linkage isomerisation and complete conversion to an oxygen-bound nitrito complex **90** was also observed.

Abstract	i
Table of Contents	ii
Acknowledgments	vi
Declaration	vii
Abbreviations	viii
Key to Thesis	x

Table of Contents

Chapter 1: Introduction	1
1.1 Phosphine as ligands	2
1.2 Alkenyl (olefin) ligands	5
1.3 Transition Metal-Alkene complexes	8
1.4 Phosphino-alkene ligands	10
1.4.1 Phosphino-alkene ligands in catalysis	12
1.5 Other metal-catalysed reaction of interest to this project	16
1.6 Ferrocene-based ligands	20
1.6.1 Pharmaceutically important ferrocene derivatives	23
1.6.2 Ferrocenyl ligands in metal catalysis	24
1.6.3 Ferrocenyl-chalcone compounds	27
1.7 Project Summary	29
Chapter 2: Synthesis of multidentate phosphino-alkene ligands	31
2.1 Design of ferrocenyl, olefin (alkene)-phosphine ligands	31
2.2 Synthesis of ligands	32
2.3 Structure of the ligands	40
2.3.1 β -[2'-(diphenylphosphino)phenyl]acrylferrocene 32	40
2.3.2 Thio-Lei ligand 46	42
2.4 Summary	43
2.5 Experimental	43

2.5.1	General Information	43
2.5.2	X-Ray Diffraction Data	50
Chapter 3:	Late transition metal complexes of alkene-phosphine and thio alkene phosphine ligands	53
3.1	Synthesis and characterization of palladium and platinum complexes with alkene phosphine ligands	54
3.1.1	Pd ^{II} complexes	54
3.1.1.1	Ferrochalcone ligand 32 complexation	54
3.1.2	Platinum metal complexes	55
3.1.2.1	Pt ^{II} complexes	55
3.1.2.1.1	Ferrochalcone ligand 32 complexation	55
3.1.2.1.2	Complexation of the Lei ligand	58
3.1.2.2	Pt ⁰ complexes	62
3.1.2.2.1	Ferrochalcone ligand 32 complexation	62
3.1.2.2.2	Complexation of the Lei ligand	66
3.2	Rhodium complexes with alkene phosphine ligands	68
3.2.1	Rh ^I complexes of the ferrochalcone 32 and Lei ligand 17	69
3.2.1.1	Ferrochalcone ligand 32 complexation	69
3.2.1.2	Complexation of the Lei ligand	73
3.3	Copper complexes with Alkene phosphine ligands	77
3.3.1	Cu ^I complexes	77
3.3.1.1	Ferrochalcone ligand 32 complexation	77
3.3.1.2	Thio-ferrochalcone ligand 33 complexation	79
3.3.1.3	Complexation of the Lei ligand	82
3.4	Experimental	87
3.4.1	General Information	87
3.4.2	X-Ray Diffraction Data	95
Chapter 4:	Gold(I) complexes of the alkene-phosphine ligands; synthesis and catalytic activity	100
4.1	Gold a-precious metal	100

4.2	Gold in chemistry	100
4.2.1	Gold(I) complexes	102
4.2.2	Gold(III) complexes	102
4.3	Cycloisomerisation	103
4.4	Results and Discussion	105
4.4.1	Catalysis	116
4.5	CV studies of Au complexes	120
4.5.1	Principle	120
4.5.2	Electrochemistry of ferrocene	121
4.5.3	Electrochemistry of ferrocalcone ligand 32	121
4.6	Experimental	124
4.6.1	General information	124
4.6.2	Catalysis	128
4.6.2.1	Without microwave	128
4.6.2.2	With microwave	129
4.6.3	X-ray Diffraction data	131
Chapter 5: Investigating nitrite impurities in “Pd(OAc) ₂ ”		133
5.1	Cyclopalladation	133
5.2	Palladium compound as catalysts	134
5.3	Palladium(II) Acetate	138
5.3.1	Preparation	139
5.4	Cyclopalladation reactions involves Pd(OAc) ₂ : a case study with Papaverine	139
5.5	Photocrystallographic study of [Pd(NO ₂)(C ^N)PPh ₃] complex; Crystallographic experiments conducted by Bath investigators)	158
5.5.1	XRD studies	158
5.5.2	Instrumentation	158
5.5.3	Photocrystallographic Experiment	158
5.5.4	Thermal Crystallographic Experiment	159
5.6	Further studies with pure and impure Pd(OAc) ₂	160
5.7	Experimental	164
5.7.1	General information	164

5.7.2	X-ray crystallography	170
5.7.2.1	X-Ray Diffraction Data for compound 90	170
5.7.2.2	Crystallographic data for compounds analysed and solved in York	173
	Chapter 6: Conclusion	177
	References for all chapters	181

Appendix 1: X-Ray crystal tables and cif files (enclosed on a CD)

Acknowledgement

First of all, I would like to thank Ian for taking me in as part of his group and for the valuable support, guidance and encouragement being given by him during my PHD. It has been a true honour to work with Ian and I could not have asked for a better supervision, as he truly is an amazing individual beyond belief.

Moreover, I also want to say my heartiest thanks to each and every person from different departments such as technical, workshop staff and administration who helped me kind heartedly whenever and where ever required. Apart from the above mentioned people, I would like to pay profound gratitude to number of individuals who helped me in keeping the things going well and on the way and making this work possible.

I would like to pay special thanks to Professor Paul Raithby (Bath) for his help on the photochemistry studies and Dr Paul (Durham) for the cyclic Voltammetric studies. Also, I would particularly like to express my great appreciation to Heather Fish, for assisting me in using the NMR instruments, and Dr Adrian Whitwood and Rob Thatcher for running and solving my crystals (X-Ray diffraction). I strongly admit that it would have been impossible to reach this day without the participation, support and encouragement of these valuable people.

This piece of writing can never be completed without mentioning the on-going valuable care and support of my labmates (past and present) during all good and bad times of my stay in York. I also want to pay thanks to all my friends whom I met in the university and who helped me sincerely to make this journey possible. A special mention goes to Tom Storr for mentoring me during my first weeks in the lab, and assisting me in every way possible.

Finally I would like to dedicate this thesis to my late mother and late sister. I would also like to pay very warm and special thanks to my Dad who stood by me at each and every step during this hard period of my life. At the end, I want to say thanks to my family especially Ayesha, Fizzan, Ruhail, Sadia, Sara and Rizwan who have always desired success and good future for me and helped me to achieve it by every mean.

Declarations

I declare that all the work presented in this thesis is my own, and that any material not my own is clearly referenced or acknowledged in the main body of the text. The work was conducted between February 2008 and May 2011.

Somia Ehsan Bajwa.

March 2012

Abbreviations

Ac	Acetyl
anal.	Analytical
Aq.	Aqueous
Ar	Aromatic group
Å	Angstroms
BINAP	2,2' – Bis(dipheylphosphino) – 1,1' - binaphthyl
Bn	Benzyl
Bu	Butyl
C(prefix)	Cyclic
Ca.	Circa
cat	Catalyst
Cp	Cyclopentadienyl
cod	1,5-Cyclooctadiene
° C	Centigrade
conc.	Concentration
conv.	Conversion
coord.	Coordinated
CDCl ₃	Deuterated chloroform
Cp	Cyclopentadienyl
CD ₂ Cl ₂	Deuterated dichloromethane
Cy	Cyclohexyl
d (NMR)	Doublet
D	Deutero
Db	Dibenzylidene acetone
DPEphos	Bis(2-diphenylphosphinophenyl)ether
DCM	Dichloromethane
DMSO	Dimethylsulfoxide
dppd	1,2- (Diphenylphosphino) benzene
dppe	1,2 – (Diphenylphosphino) ethane
dppm	Dipheylphosphinomethane
ee	Enantiomeric excess
eq.	Equivalent
ESI	Electrospray Ionisation
FAB	Fast Atom Bombardment
Fc	Ferrocene
Fesulphos	1-phosphino-2-sulfenylferrocene
g	grams
HOMO	Highest occupied molecular orbital
h	hours
HRMS	High Resolution Mass Spectrometry
HSAB	Hard-Soft-Acid-Base
HSQC	Heteronuclear Single Quantum Coherence
Hpap	papaverine
Hpbf	2-(2-pyridyl)benzo furan
Hpyi	1-(2-pyridyl)indole
Hpmi	1-(2-pyrimidyl)indole
In vacuo	Under reduced pressure
i (prefix)	Iso
IR	Infra-Red
<i>J</i>	Coupling constant

K	Kelvin
L	Ligand
LUMO	Lowest occupied molecular orbital
LIFDI	Liquid Injection Field Desorption Ionisation
LRMS	Low Resolution Mass Spectrometry
m (prefix)	Meta
m (IR)	Medium
m (NMR)	Multiplet
M	Transition Metal
Me	Methyl
mol	Mole
<i>m/z</i>	Mass to charge ratio
M.p.	Melting Point
MS	Mass Spectrometry
MeCN	Acetonitrile
n (prefix)	Normal
NHC	<i>N</i> -Heterocyclic carbene
NMR	Nuclear Magnetic Resonance
<i>o</i> (prefix)	Ortho
<i>p</i> (prefix)	Para
Ph	Phenyl
ppm	Parts per million
PCA	Photocycloaddition
PGMs	Platinum group metals
q (NMR)	Quartet
R	Organic group
rt	Room Temperature (13-25 °C)
s (IR)	Strong
s (NMR)	Singlet
S	Solvent
S-PHOS	2-Dicyclohexylphosphino-2',6'-dimethoxybiphenyl
t (NMR)	Triplet
t (prefix)	Tertiary
THF	Tetrahydrofuran
TLC	Thin Layer Chromatography (silica plates unless otherwise specified)
TMS	Trimethylsilane
uncoord.	Uncoordinated
UV	Ultraviolet
v:v	Volume ratio
w (IR)	Weak
X	Halide
XantPhos	4,5-Bis(diphenylphosphino)-9,9-dimethylxanthene
X-PHOS	2-Dicyclohexylphosphino-2',4',6'-triisopropylbiphenyl
XRD	X-ray Diffraction
Z	Aryl substituent

Key to thesis

Referencing: Each chapter is referenced individually starting at one with the references located at the end of the chapter.

Figures/Schemes: The figure numbering starts from one in each chapter and is thereafter sequential. The scheme numbering starts from one in each chapter and is thereafter sequential.

Numbering: Compounds that are referred to in the main body of text are numbered sequentially across all chapters. The main ligands described in this thesis are referred to by either abbreviated names (*e.g.* Ferrochalcone) and/or by number (**32**). Complexes are referred to by either a number and/or a formula.

Chapter 1: Introduction

A readily exploited characteristic of transition metal chemistry is its variation of oxidation states, which can be achieved with a wide variety of ligands and metal combinations. This allows the reactivity of a given transition metal complex to be tuned for use in, for example, catalytic processes or material applications. The steric and electronic factors of ligands have a profound influence upon the nature of the reactive metallic species and hence can affect the reactivity of the metal complex formed.¹ Changing the ligand can directly influence reaction efficiency and selectivity.² The use of ligands with new geometries and electronic properties may result in the catalyst possessing increased stability, selectivity and catalytic activity. Furthermore, the electronic character of the ligand can be varied over a wide range to deliver different types of catalyst for specific applications.³ Other factors which affect reactivity are the inclusion of exogenous additives, *e.g.* solvent and salts *etc.*⁴ Each component of a given catalytic system offer a means of modification and the promise of new reactivity.

The development of new carbon-carbon (C-C) and carbon-heteroatom (C-X) bond-forming reactions continues to be an essential goal in organic chemistry.⁵ Indeed, synthetic chemists are continuously looking for new methodologies for the synthesis of these compounds. The principal focus of this thesis is the design of novel ligands for potential use in homogenous catalysis.

The metals of interest in the thesis include Pd, Pt, Rh, Au and Cu, which are widely used in organic synthesis. These metals are classified as B (or soft) metals according to Pearson Hard-Soft Acid Base principle (HSAB)⁶ and therefore prefer to bind to soft bases, *e.g.* P and S; class A (hard) metals like H, Li, Na, K, Ca, Co, Fe *etc.* and prefer N and O donors.

Traditional metal-catalysed cross-coupling reactions for example, Heck,⁷ Negishi,⁸ Stille,⁹ Suzuki-Miyaura,¹⁰ and Sonogashira,¹¹ are well-established methods for the construction of C-C bonds, and widely applied in the synthesis of complex molecules. Over the last few decades considerable large research effort has been placed on the design and synthesis of highly active transition metal catalysts.¹² In obtaining the most

active catalysts, the design of ligands is of the utmost importance, as is the selected metal. Often, ligands are designed to promote the rate-limiting step, with the majority of studies focusing on the σ -donor ligands, *e.g.* phosphines and *N*-heterocyclic carbenes¹³ (NHCs).

1.1 Phosphine as ligands

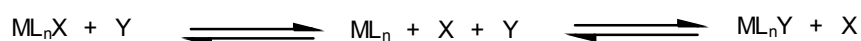
Phosphine ligands play a key role in transition metal-catalysed reactions.^{14,15} In 1857 Hofmann described the first phosphorus-metal complex, namely triethylphosphine platinum trichloride.¹⁶ Since then phosphines (PR_3) have become a traditional and versatile ligand class for transition metal-catalysed reactions, especially since the late 1960's. The ability to vary the electronic properties in a systematic fashion can significantly affect ligation properties in metal complexes. In the 1970s, Tolman quantified the dependence of the phosphine's electronic properties on R by investigating the changes in the CO stretching frequency in $[\text{Ni}(\text{CO})_3(\text{PR}_3)]$ complexes. In this study one of the CO molecules was displaced from $\text{Ni}(\text{CO})_4$ with the organophosphine of interest, allowing the resulting shift in the CO stretching frequency to be assessed by IR spectroscopy. More electron-rich R-groups increase the electron density on the phosphorus, which in turn increases the back-bonding to CO. This lengthens the C-O bond resulting in a decrease in the stretching frequency and lowering of the CO bond order.¹⁷

With advancements in computational methods and theoretical approaches alternatives have been developed to measure the electronic parameters.¹⁸ Similarly, the steric parameters of an organophosphine ligand can likewise be varied over a large range, in some cases independent of their electronic properties. Accordingly, the coordination number, geometry and electron-richness of a metal centre, the thermodynamics and the kinetics of (i) associative, and (ii) dissociative equilibria (Scheme 1) can be tailored through appropriate choice of substituents on phosphorus.

(i) Associative-A (2 steps)



(ii) Dissociative-D (2 steps)



Scheme 1: General schematic representation of ligand substitution reactions.

Tolman also quantified the steric effects of phosphines by analysing their cone angles.¹⁹ A bulkier phosphine, *e.g.* one with a larger cone angle, tends to have a greater dissociation rate than a smaller phosphine (Figure 1).

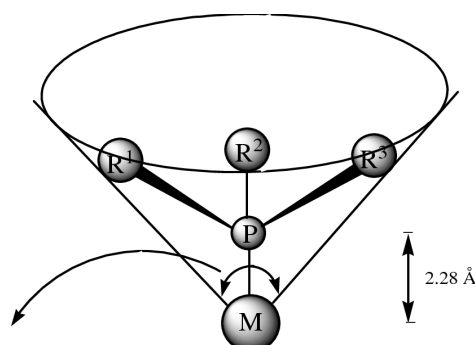


Figure 1: Steric parameters used for phosphines.

The cone angle can also dictate the geometry of the metal complex. A comparison of cone angles of common phosphine ligands in degrees is given in Table 1.

Table 1: Cone angles for some common monodentate phosphine ligands.

Phosphine ligand	Angle (°)
PH ₃	87
P(CH ₃) ₃	118
P(Ph) ₃	145
P(<i>t</i> -Bu) ₃	182
P(C ₆ F ₅) ₃	184

Phosphines are mainly regarded as σ -donors. The lone pair on phosphorus can donate electron density to a metal. Increasing the electron density on phosphorus through the use of electron-donating substituents (R) increases the strength of σ -donation. Phosphines can also act as π -acceptors, with the σ^* -orbital of the P-R bonds playing the role of the acceptor. π -Bonding arises through the donation of electron density from the metal into an empty orbital of the ligand, which exhibits phosphorus $3p$ character (Figure 2).

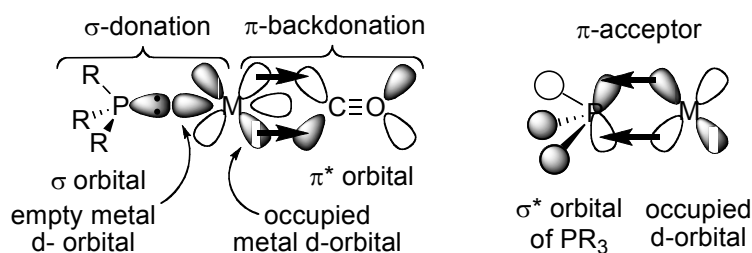


Figure 2: Phosphines are good σ -donors and π -acceptors.

Trialkylphosphines are weak π -acceptors, followed by triarylphosphines, then trialkoxyphosphites, with toxic PF_3 being similar to CO in its bonding to metals.²⁰ Common phosphine ligands used in both commercial and research laboratories range from simple alkyl and aryl phosphines, e.g. PCy_3 and PPh_3 , to more complex phosphines like those shown in Figure 3.

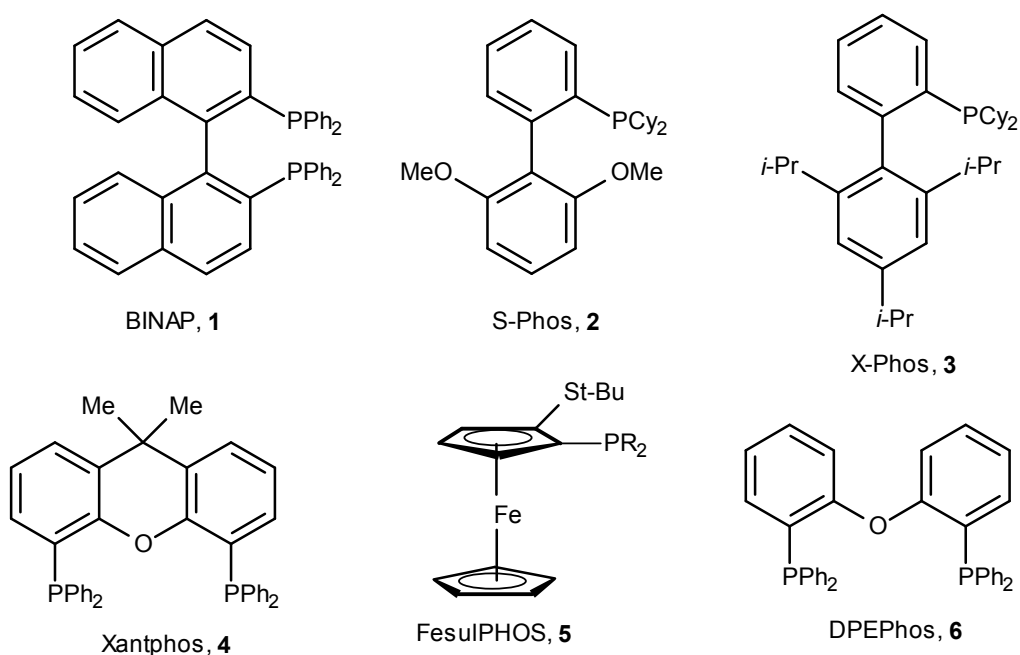
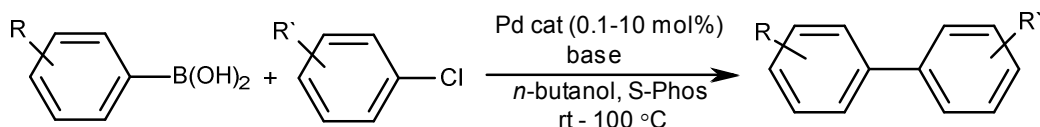


Figure 3: Commercially available phosphines.

A brief look at the history of the Buchwald-Hartwig amination highlights the evolution of the ligands used.²¹ Initially, simple phosphines such as $\text{P}(t\text{-Bu})_3$ and $\text{P}(o\text{-Tol})_3$ were employed. These were then replaced by chelating bisphosphines such as BINAP **1**, which is a well known bidentate ligand. This chiral compound is also widely used in asymmetric synthesis.

Buchwald later reported the synthesis and use of monodentate phosphines containing a biphenyl backbone. S-Phos **2** and X-Phos **3** are monodentate phosphines derived from biphenyl. They are also used in various cross-coupling reactions.^{22,23} Suzuki-Miyaura coupling reactions of aryl and heteroaryl halides with aryl-, heteroaryl-, and vinyl boronic acids proceed in very good to excellent yields using the S-Phos **2** ligand (Scheme 2).

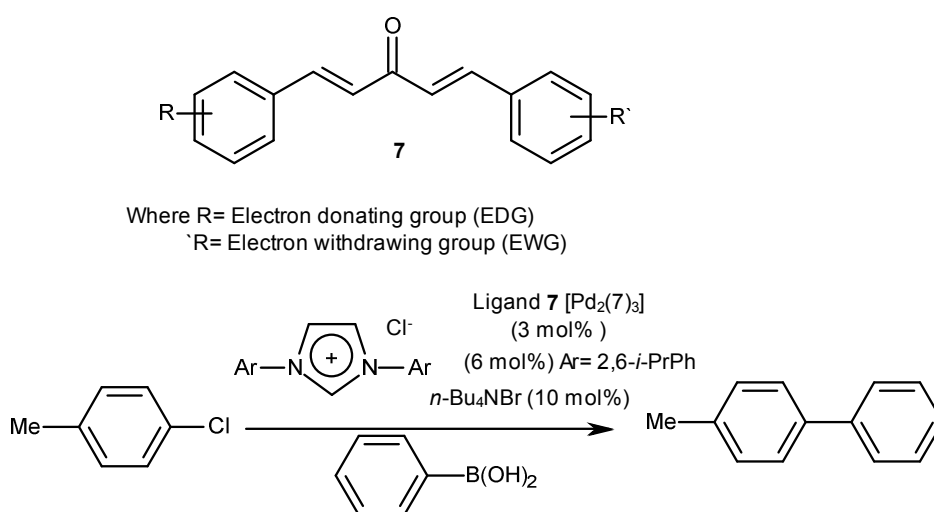


Scheme 2: General scheme for Suzuki-Miyaura coupling using S-Phos.

These ligands have also proved efficient in a number of C-C, and C-O bond forming reactions. Later work by van Leeuwen and co-workers resulted in the discovery of new bisphosphine ligands such as XantPHOS **4** and DPEPhos **6**, which also showed high activity for coupling of aryl halides with a variety of amines.²⁴

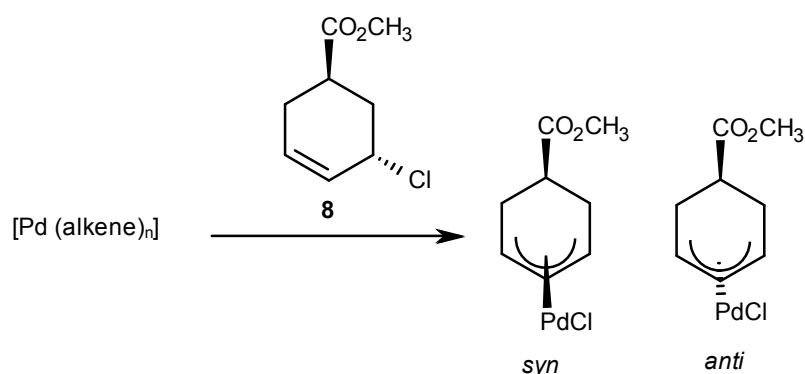
1.2 Alkenyl (olefin) ligands

The impact of alkenes as ligands in transition metal catalysis is a greatly underexploited area.²⁵ Alkenes are ubiquitous whether they are introduced in the form of substrates, in the catalyst or as an additive. There are many examples of alkenes influencing the outcome of a reaction through increased activity, stability or selectivity as depicted below in Scheme 3.²⁶



Scheme 3: General scheme for Suzuki-Miyaura cross coupling reaction.

It has been found that the electron-withdrawing substituents like NO₂ or CF₃ deactivate the Pd⁰ catalyst species, whereas strongly electron-donating substituents such as OMe increase catalytic activity over that of unsubstituted dba (dibenzylideneacetone) ligands. Independent electron-rich σ-donor ligands could increase back-bonding from the d¹⁰ palladium(0) centre to the π-acidic dba, thus strengthening this Pd⁰-alkene interaction and thereby reducing the overall concentration of the active Pd⁰L_n species. The incorporation of an electron-withdrawing substituent onto the dba ligand should further enhance this back-bonding. Conversely, the incorporation of electron-releasing substituents as part of dba ligand will destabilize back-bonding and thus increase the concentration of the active catalyst species. In C-C bond-forming cross-coupling methodology, alkene additives have been reported to increase reaction efficiency, improve selectivity and dictate new reaction mechanisms.^{27, 28} Kurosawa *et al.* reported that the stereochemical outcome of oxidative addition of Pd⁰ and Pt⁰ compounds to *trans*-5-methoxycarbonyl-2-cyclohexenylchloride **8** is altered by the presence of olefin additives (Scheme 4).

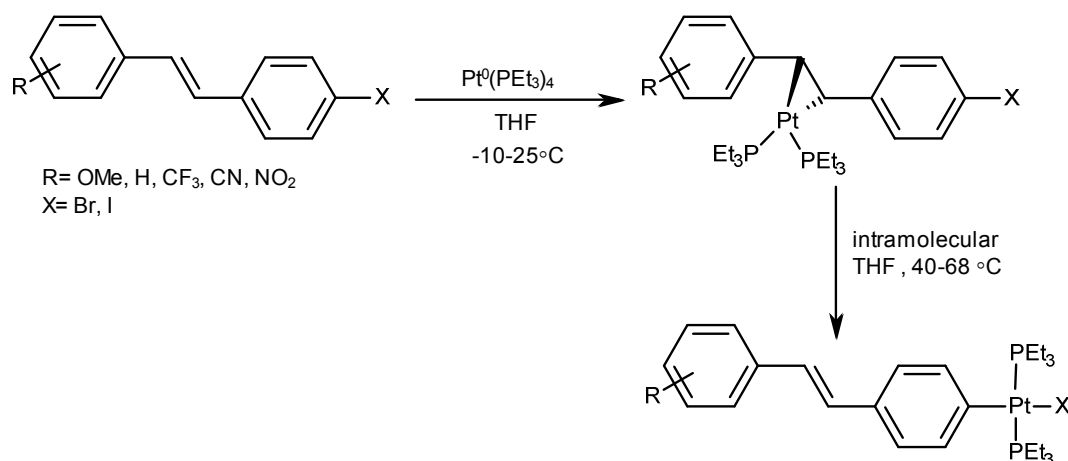


Alkene	None	45 : 55
	1,5-COD	10 : 90
		97 : 3
		97 : 3

Scheme 4: Stereoselectivity of oxidative addition of alkene metal complexes.

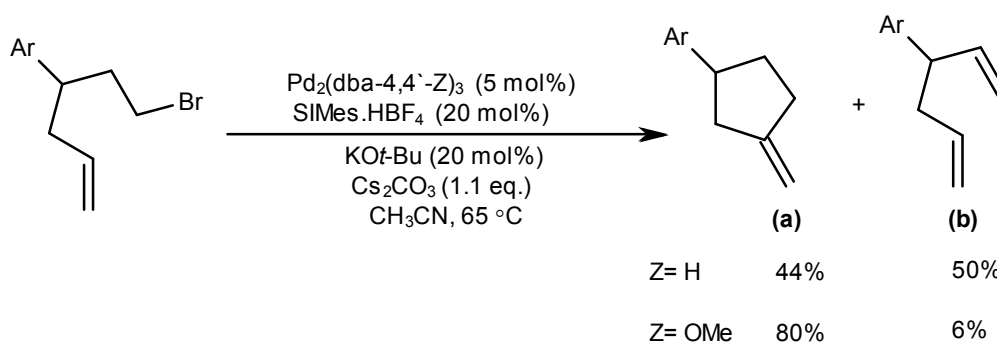
It has been observed that alkenes can be utilised in transition metal-mediated reactions in different ways. They can be part of the metal precursor source, for example, the dibenzylideneacetone (dba) in [Pd₂(dba)₃], or added as exogenous additives (*e.g.* as

shown in Scheme 4). They can be used as the “working” ligand or as an ancillary ligand, or they can form part of the substrate (*e.g.* in the Heck reaction). In a series of studies, van der Boom and co-workers showed that aryl halide substrates containing an alkene undergo η^2 -coordination to Pt^0 before oxidative addition occurs (Scheme 5).²⁹



Scheme 5: Kinetically-favoured alkene coordination, followed by oxidative addition.

Alkenes have also been used efficiently in many Pd-based catalytic studies.³⁰ It is known that electron-deficient alkenes can accelerate reductive elimination. They can also affect the product selectivity of many reactions, by interfering with carbopalladation, isomerisation and β -H elimination pathways.³¹ For example in 2007, Firmansjah and Fu reported an intramolecular Heck reaction, which showed a remarkable dba (alkene) effect.³² There are two possible products from the reaction given in Scheme 6: a) the cyclised product where intramolecular insertion of the alkene occurs before β -H elimination, and b) the diene product where β -H elimination is faster than alkene insertion (carbopalladation).



Scheme 6: Intramolecular Heck reaction displaying a remarkable dba(alkene) effect.

Using the Pd⁰ precursor [Pd₂(dba)₃] the authors obtained almost equal quantities of the cyclised and 1,5-diene products, whereas the use of [Pd₂(dba-4,4'-OMe)₃] resulted in cyclisation becoming the dominant pathway. It can be hypothesised that dba-4,4'-OMe ligand slows down β-H elimination before alkene insertion, by coordinating to the Pd^{II} oxidative addition species, thus removing the vacant site needed for β-H elimination. The dba-4,4'-OMe ligand is more electron-rich than dba-H, and so it likely interacts more strongly with Pd^{II}.

1.3 Transition Metal-Alkene Complexes

Transition metal complexes with alkenes have been known for nearly two hundred years. Zeise in 1827 for the first time prepared K[PtCl₃(C₂H₄)]·H₂O (Zeise's salt) by the dehydration of EtOH with K₂[PtCl₄].^{33,34} although its formula was not confirmed until 1861 by Griess and Martius.³⁵ Its structure was finally elucidated in the 1950's and was proven to be representative of alkene coordination to a transition metal.³⁶ Bonding of the metal centre to both carbon atoms of ethene results in an increase in the length of the C-C bond, and bending of the C-H bond, which occurs away from the metal centre. This change in geometry is described by the model of Dewar, Chatt and Duncanson who proposed synergistic alkene-metal σ-donation and complementary metal-to-alkene π-donation (Figure 4).³⁷

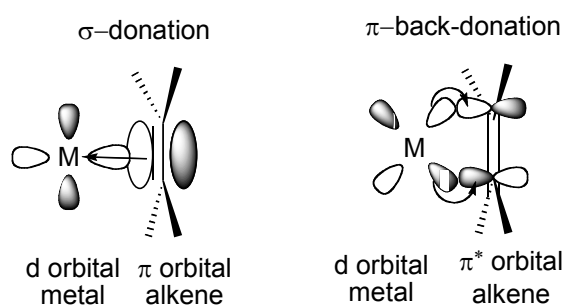


Figure 4: Frontier molecular orbitals illustrating the metal-alkene bonding interaction.

The σ-donation occurs from the highest occupied molecular orbital (HOMO) of the alkene, the C=C π-electrons, to an empty orbital on the metal centre. Concurrent π-back-donation occurs from an occupied metal d-orbital to the lowest unoccupied molecular orbital (LUMO) of the alkene, *e.g.* the vacant π*-orbital. This backbonding weakens and lengthens the C-C bond and simultaneously results in a partial rehybridization of the carbon centres. The strength of the metal-alkene bond, which in

turn relates to the length of the carbon-carbon bond, is dictated by the efficiency of π -backbonding.

A weakly π -basic metal such as Pt^{II} in Zeise's salt, provides minimal backbonding, and the resulting carbon-carbon bond length (1.375 Å) which differs relatively little from that of free ethylene (1.337 Å). This complex is representative of a simple π -complex of the alkene and metal and is typical of alkene complexes from metals in high oxidation states. Conversely coordination of an electron-deficient alkene, with a strongly π -basic metal, maximizes backbonding, in some cases leading to metallopropane type structures, with complete re-hybridisation of the carbon atoms to sp^3 (Figure 5). Most transition metal-alkene complexes lie between these two extremes.



Figure 5: Different binding modes of alkenes towards metals.

The extent to which re-hybridisation occurs, and thus the degree of back-donation can be measured by the shift in the NMR signal of the alkene carbon atoms coordinated to the metal, $\Delta\delta = (\delta_{\text{complex}} - \delta_{\text{free ligand}})$. The stronger the back-donation, the lower the frequency of the resonance of the complexed carbon atom and the greater $\Delta\delta$. One also expects a decrease in the C=C stretching frequencies in the infrared spectrum upon coordination to a late transition metal centre.^{38,39} However, compared to a carbonyl stretching bond in CO, the C=C stretching frequency is weak and overlaps with many other groups, *e.g.* organic carbonyls (amide) and aromatic groups. This makes it a less reliable indicator for the strength of back-donation.

Alkene coordination to metals has been studied extensively. In most cases alkenes are found to be more labile than the “working” ligands, *e.g.* phosphines or NHCs. The extent of lability is dependent on the strength of the metal-alkene bond (*i.e.* alkene type) and the other surrounding ligands. Electron-rich alkenes will be more labile due to decreased back-donation, which will increase reactivity. A ligand that contains both substitutionally labile and inert groups may act in a hemilabile fashion. The term “hemilabile” was first coined by Jeffrey and Rauchfuss in 1979.⁴⁰ The weakly-coordinating group can stabilise vacant sites on a transition metal centre until it is

introduced to a substrate molecule. The presence of an inert group means that the ligand remains anchored to the transition metal centre. These characteristics have meant that hemilabile ligands have found numerous applications in homogenous catalysis.⁴¹

1.4 Phosphino-alkene ligands

Bidentate ligands of the phosphino-alkenyl type have shown considerable promise, due to the combination of two beneficial types of ligand into a single framework. The phosphine component ensures strong binding to the transition metal, while the alkene provides both the opportunity to create a chiral environment in close proximity to the transition metal, as well as providing another way to vary the electronic properties of the catalyst.

The first chelating phosphino-alkene ligand (**9**) was reported by Nyholm and co-workers in 1964, followed soon after by a number of further variants (**10**, **11**, and **12**; Figure 6).⁴²

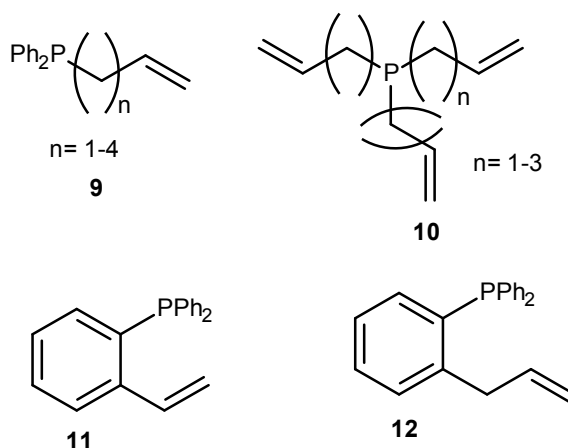


Figure 6: The 'first' phosphino-alkene ligands.

Later work by others including Grutzmacher,⁴³ Carreira,⁴⁴ Hayashi,⁴⁵ Widhalm,⁴⁶ Ellmann⁴⁷ and Lei⁴⁸ resulted in development of a new array of alkene phosphine ligands, as shown in Figure 7.

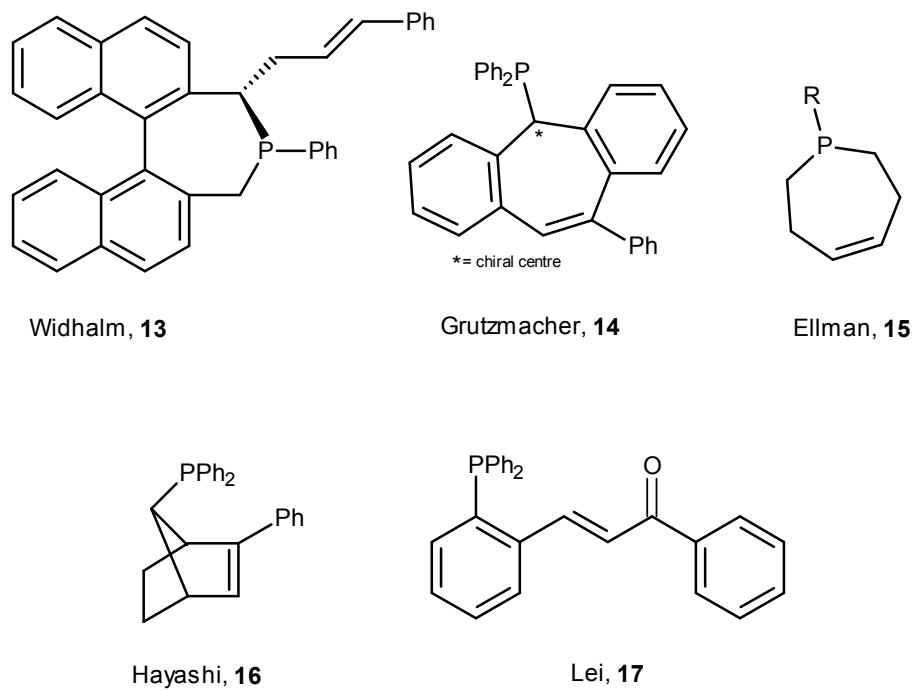
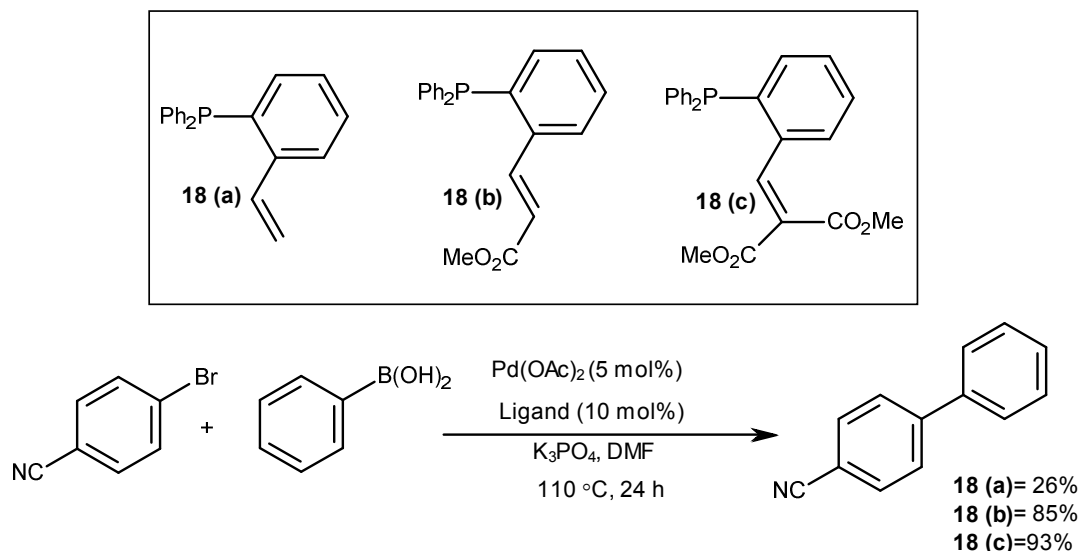


Figure 7: Second generation phosphino-alkenyl ligands.

1.4.1 Phosphino-alkene ligands in catalysis

Phosphino-alkene ligands have been utilised in a wide range of Pd, Pt, Rh, Cu and Au-catalysed reactions, as outlined below. For example, Shaw and co-workers developed a series of phosphorus-alkene bidentate ligands and used them effectively in Pd-catalysed Suzuki cross-coupling reactions (Scheme 5).⁴⁹

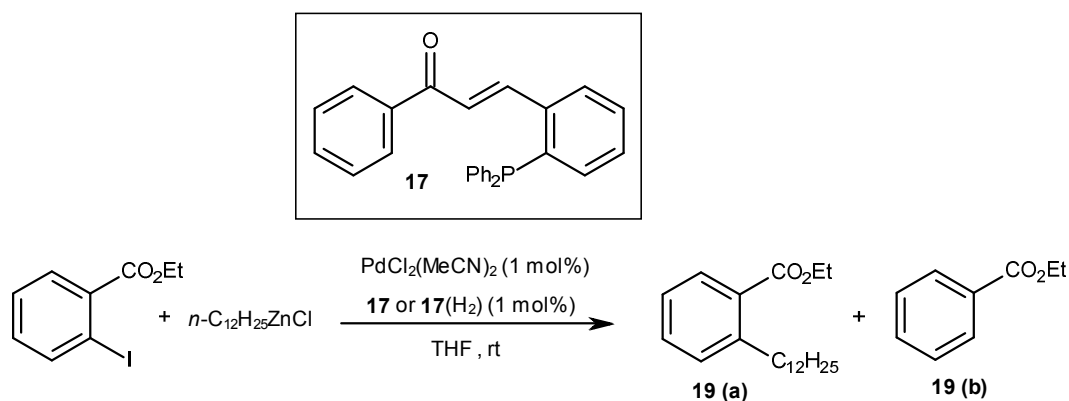


Scheme 5: A range of phosphine-alkene ligands used in the Suzuki reaction.

They found that electron-deficient and sterically hindered alkenes bring about greater yields, increasing the stability of the Pd catalyst. As complexes with only phosphine ligands catalyse cross-couplings, control reactions with the saturated ligand were carried out to see if the alkene was necessary. A saturated version of ligand **19** gave poor yields, indicating that the alkene plays a crucial role in the catalytic cycle.

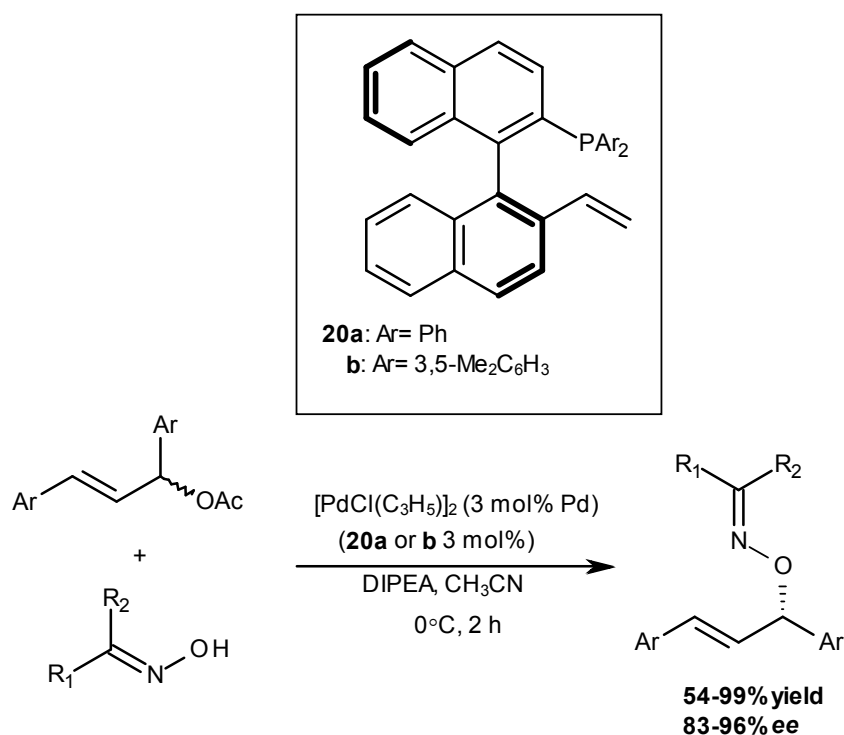
Lei and co-workers carried out a series of experiments using phosphine/electron-deficient alkene ligands and found that these ligands promoted reductive elimination. Chalcone-based phosphino-alkene ligand, **17** was used in the Negishi coupling of ethyl 2-iodobenzoate with cyclohexylzinc chloride. It is generally known that in Negishi coupling that β -H elimination competes with reductive elimination.⁵⁰ The saturated version of ligand *e.g.* **17-H₂** leads to large amounts of ethyl benzoate **19 (b)** being formed along with product **19 (a)**, whereas ligand **17** was found to be highly selective for **19 (a)**. It is assumed that the hemilabile alkene blocks the coordination sites needed for β -H elimination, reducing the electron density at Pd^{II} and hence accelerates the reductive elimination step (Scheme 6). There is also the potential for the alkene to

dissociate giving a three-coordinate Pd^{II} intermediate from which reductive elimination is facile.



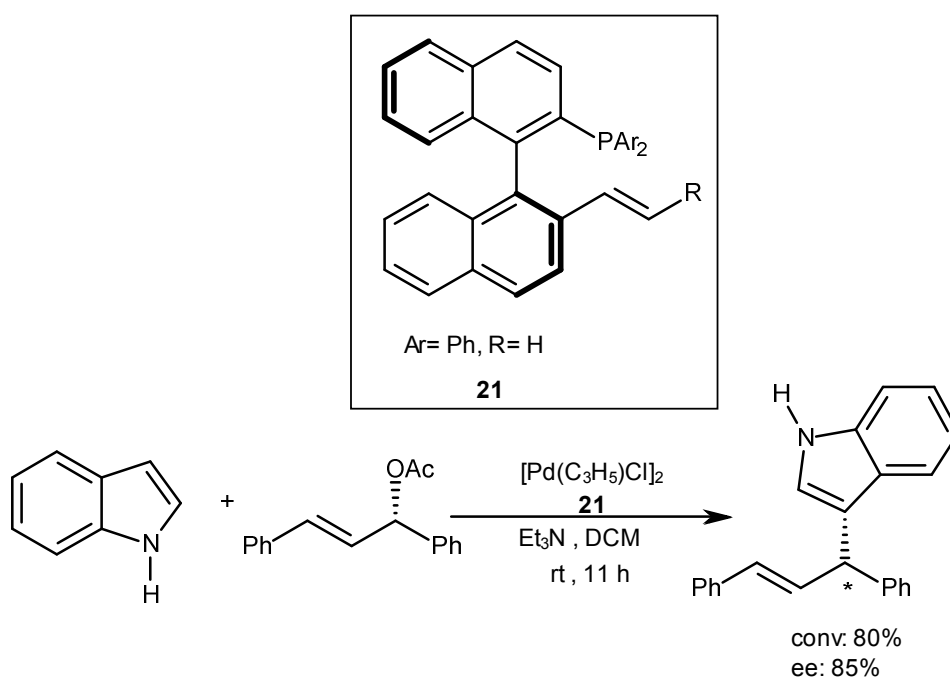
Scheme 6: Negishi cross-coupling employing a chalcone-based phosphine-alkene ligand.

Pd-catalyzed asymmetric allylic substitutions provide a practical and efficient approach to construct the C-C, C-N and C-O bonds in an enantioselective fashion. An example reaction is shown in Scheme 7, namely chiral alkene-phosphine hybrid ligands **20a** and **20b** which promote the formation of optically-active oxime ethers in high yields, with good to excellent enantioselectivities (Scheme 7).⁵¹



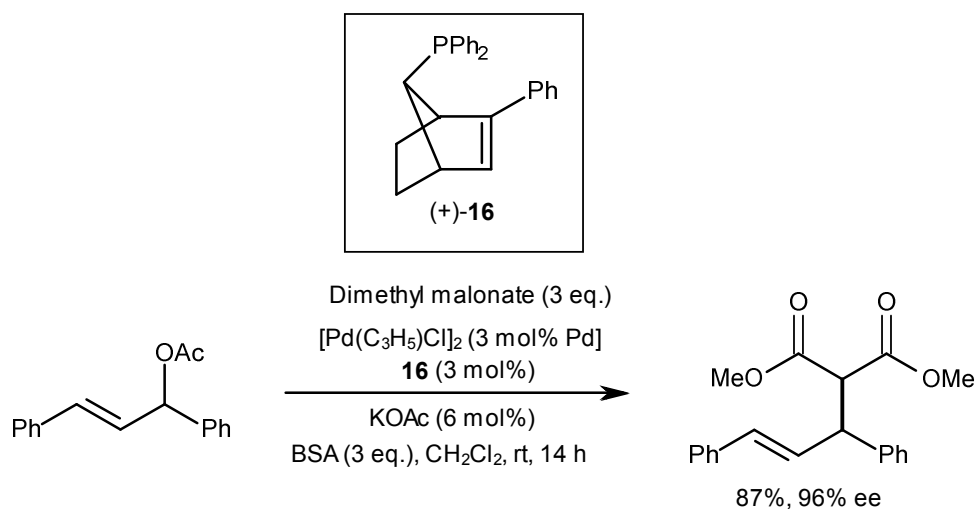
Scheme 7: Asymmetric allylic etherization of oxime using chiral ligand 20a-b.

In the same year the group of Du⁵² developed a similar version of the above ligand **21** and successfully used it in the Pd-catalyzed enantioselective allylic alkylation of indoles and pyrroles (Scheme 8).



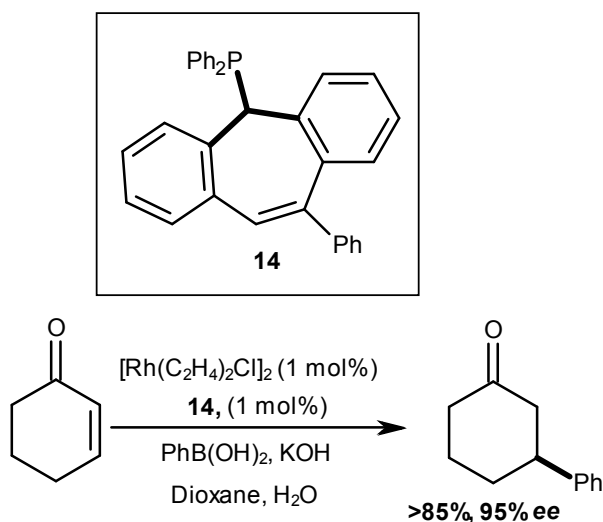
Scheme 8: Enantioselective allylic alkylation's of indoles and pyrroles employing a chiral phosphine-alkene ligand.

Hayashi and co-workers reported the use of norbornene-based phosphine-olefin ligand **16** in the Pd-catalyzed allylic alkylation of 1,3-diphenyl-2-propenyl acetate. The reaction proceeded in both high yield and enantiomeric excess (Scheme 9).⁵³



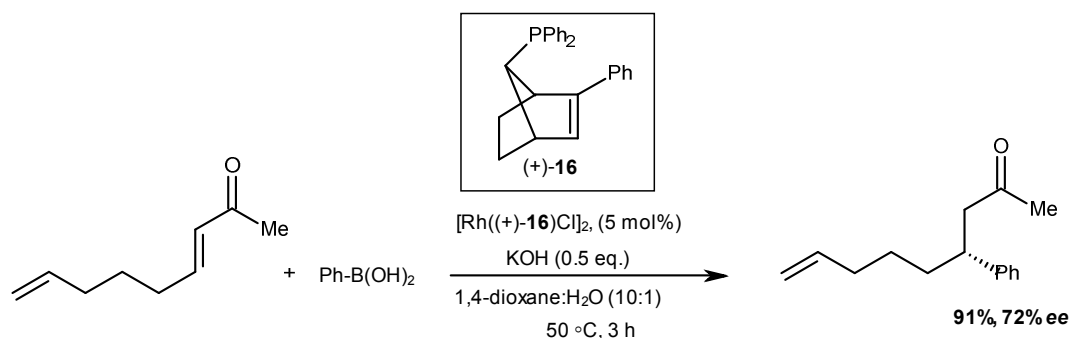
Scheme 9: Pd-catalyzed allylic alkylation using a chiral phosphine-alkene ligand.

Grutzmacher and co-workers developed a phenyl-substituted phosphino-alkene ligand based on the tropp (5-phosphanyl-5*H*-dibenzo[*a,d*]cycloheptene) framework **14**, successfully using them in the Rh-catalyzed 1,4-conjugate addition of phenylboronic acid to 2-cyclohexenone providing the product in 85% yield and 95% *ee* (Scheme 10).



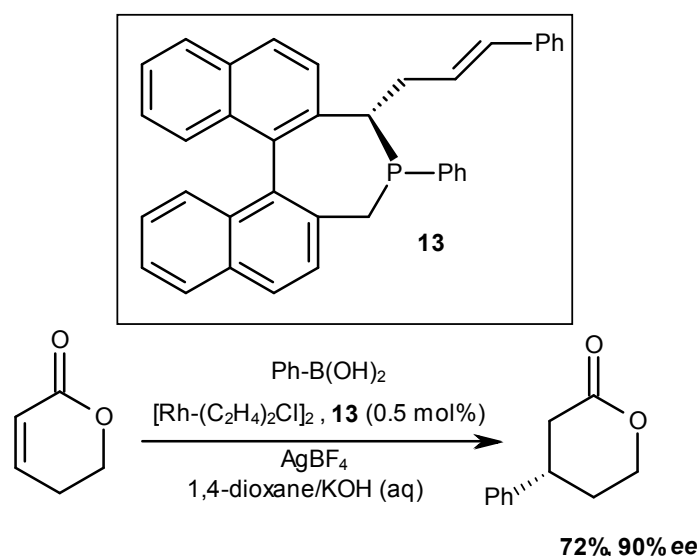
Scheme 10: Rh-catalyzed 1,4-conjugate addition using a tropp phosphine-alkene ligand.

Hayashi and co-workers successfully used a norbornene-based chiral alkene-phosphine ligand **16** in Rh-catalyzed 1,4-conjugate addition of aryl boronic acids to enones to give unsaturated ketones in high yield and enantiomeric excess (Scheme 11).



Scheme 11: Rh-catalyzed 1,4-conjugate addition of arylboronic acids to unsaturated ketones in the presence of a chiral phosphine-alkene ligand.

The work reported by Widhalm and co-workers resulted in the development of a novel phosphino-alkene ligand based on bis(naphthyl)phosphepine ring **13**. These ligands have been successfully used in the 1,4-conjugate addition of aryl boronic acids to a series of cyclic enones and enolates, resulting in the formation of products in excellent yield and enantioselectivity (Scheme 12).

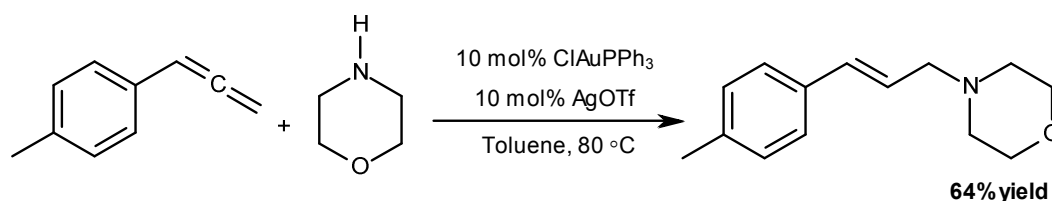


Scheme 12: Rh-catalyzed 1,4-conjugate addition of aryl boronic acids to enoates using ligand 13.

1.5 Other metal-catalysed reactions of interest to this project

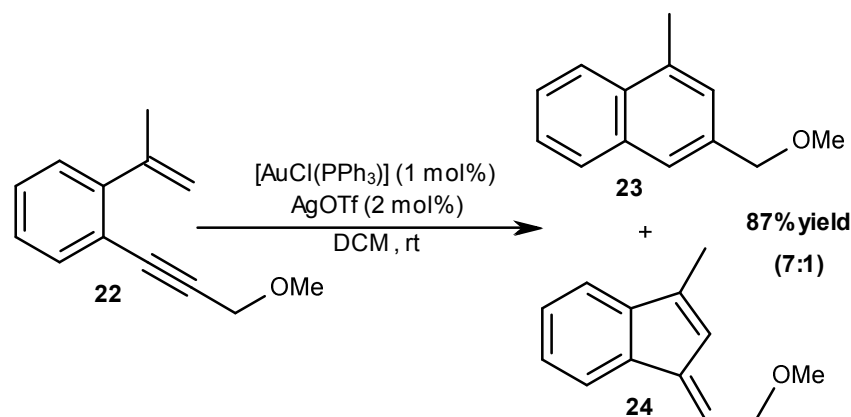
Hashmi, Toste, Echavarren, Hayashi and Haruta have fueled the advance of gold to the forefront of transition metal catalysis.⁵⁴ The use of gold(I) and gold(III) complexes as efficient homogenous catalysts in a wide-range of organic transformations has been highlighted in the last few years.⁵⁵ The popularity of these processes, which allow the formation of both C-C and C-X bonds, is largely due to the significant increase in the molecular complexity and impressive structural diversity they can obtain.⁵⁶ Phosphine-ligated gold(I) complexes are powerful C-C, C-N, and C-O bond-forming catalysts due to the ease with which they can activate unsaturated bonds, which facilitates unique rearrangements or reactions with appropriate nucleophiles.

One good example is that reported by Yamamoto and co-workers, namely gold-catalyzed intermolecular hydroamination of allenes.⁵⁷ Treatment of allenes with morpholine in the presence of a cationic gold(I) catalyst in toluene at 80 °C gave the corresponding allylic amines in good to moderate yields (Scheme 13).



Scheme 13: Gold-catalysed intermolecular hydroamination of allenes.

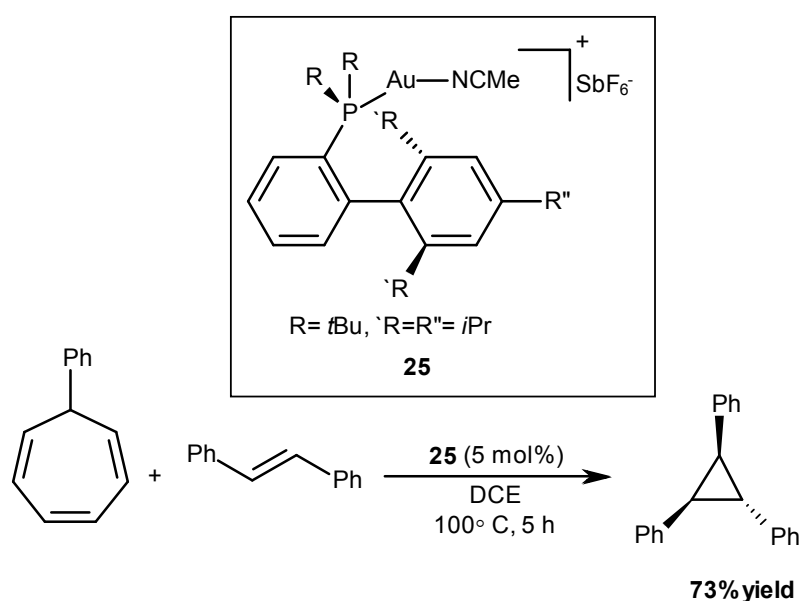
Shibata showed that a Au^I catalyst mediates the cyclisation of 1,5-enynes leading to substituted naphthalenes (Scheme 14).⁵⁸



Scheme 14: Gold-catalysed cyclisation of 1,5-enynes.

Depending on the substitution pattern of the triple bond, a 5-*exo-dig*-type cyclisation can also proceed which is competitive with the 6-*endo*-type cycloisomerisation. The benzannulation of enyne **22** gave an 87% yield of a 7:1 mixture of the naphthalene **23** and the corresponding indene **24**.

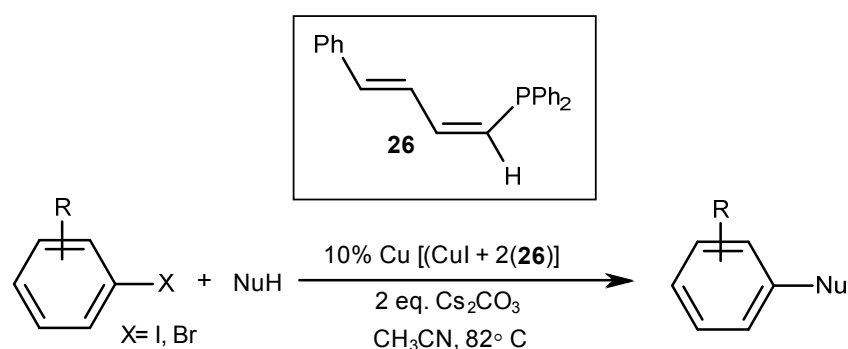
In 2011, Echavarren and co-workers carried out a series of experiments which resulted in the cyclopropanation of *trans*-stilbene with cycloheptatriene using a Au^I complex (Scheme 15).⁵⁹ Au^I-catalyzed cyclisation of 1,*n*-enynes proceeds through intermediates that can be viewed as highly distorted Au^I carbenes, which are then subsequently trapped by alkenes either intra- or intermolecularly in cyclopropanation reactions.



Scheme 15: Cyclopropanation of *trans*-stilbene with cycloheptatriene using a Au^I complex.

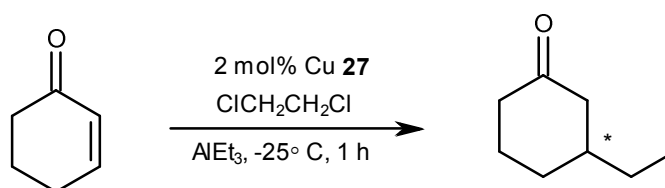
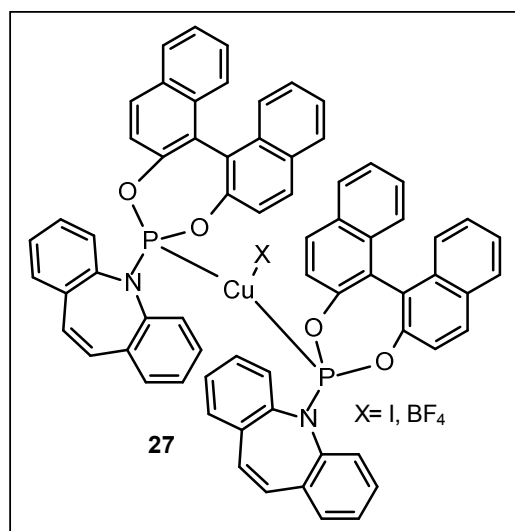
Copper has also been used in catalytic reactions as both the main metal centre (*e.g.* 1,4-conjugate addition to α,β -unsaturated carbonyl compounds,⁶⁰ *N*-arylation,⁶¹ hydroboration of styrenes⁶² and cyclopropanation reactions⁶³) and as a co-catalyst (*e.g.* direct C-H functionalisation of arenes and heteroarenes⁶⁴). A number of simple phosphino-alkenyl ligands have been coordinated to Cu^I centres and found to be effective catalysts.

In 2009, Taillefer and co-workers used 4-phenyl-1,3-butadienylphosphine as a ligand for the Ullmann-type copper-catalyzed arylations of *N*- and *O*-nucleophiles (Scheme 16).⁶⁵



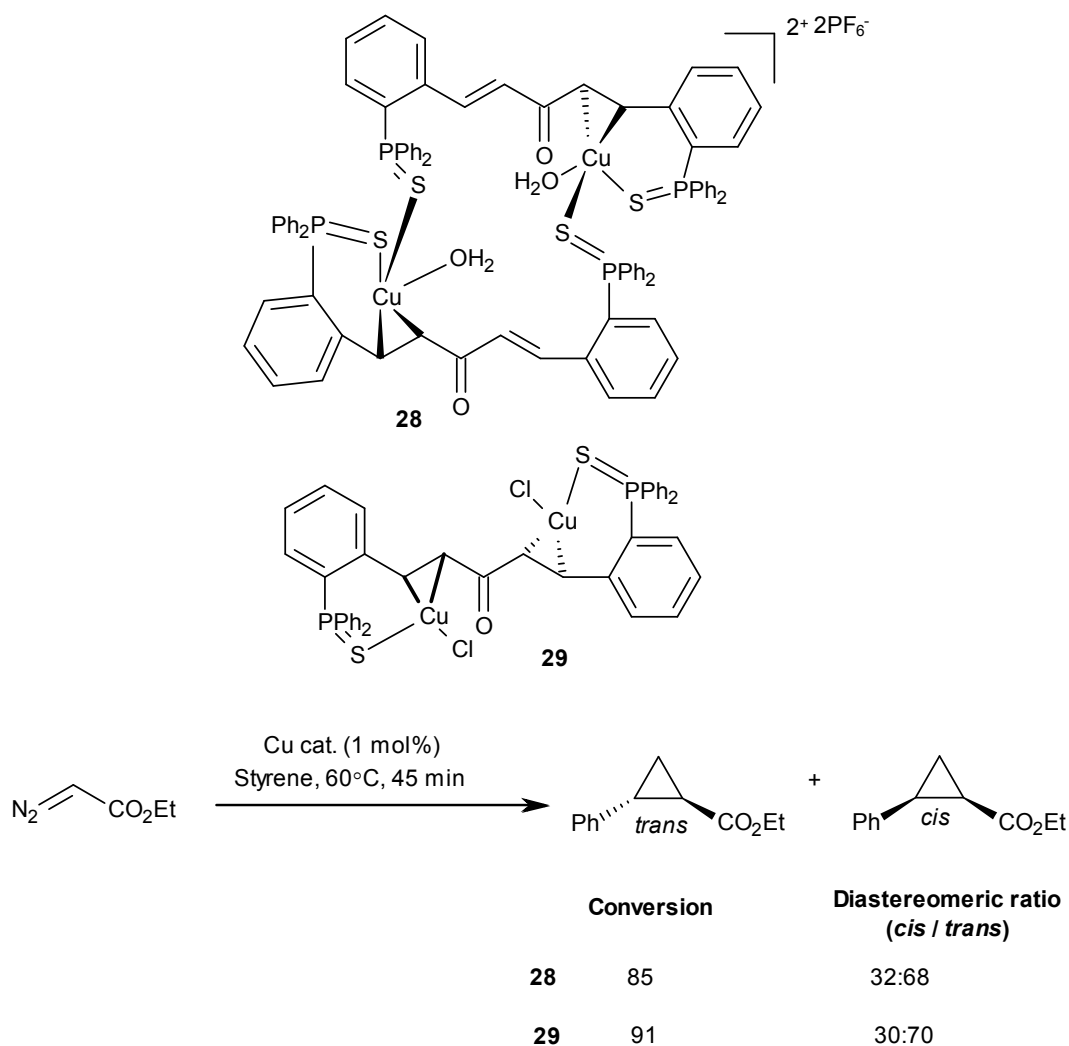
Scheme 16: Copper-catalysed arylation of N and O nucleophiles using a phosphino-alkene ligand.

Dorta and co-workers reported the use of phosphoramidate-based phosphino-alkene ligands in Cu-catalysis.⁶⁶ These complexes were evaluated in a catalytic 1,4-conjugate addition of organoaluminum reagents to conjugated enones (Scheme 17). The neutral Cu^I complexes did not catalyse the reaction; indeed, they stopped the reaction completely. However, the cationic Cu^I complexes gave excellent yields, though only with moderate enantioselectivities.



Scheme 17: Use of phosphoramidate-based phosphino-alkene ligands in Cu-catalysed conjugate addition reaction.

Very recent work by the Fairlamb group has concerned the synthesis of a multidentate conformationally-flexible ligand based on the dibenzylidene acetone core structure and its use in catalytic alkene cyclopropanation (Scheme 18).⁶⁷ It was observed that complex **28** and **29** effectively catalyses the cyclopropanation of styrene using ethyl diazoacetate at low catalyst loading.



Scheme 18: Use of dba-based phosphino-alkene ligands in Cu-catalysed cyclopropanation.

Overall, it can be seen that phosphino-alkene ligands can be used in combination with an appropriate metal to provide active catalysts for a variety of transition metal-mediated organic transformations. In a number of cases, they have been shown to be more effective than either phosphines or alkene ligands alone, and have opened-up new avenues of chemistry. Other developments not mentioned above include the use of phosphino-alkene ligands as mechanistic probes in the Pauson-Khand reaction.⁶⁸

1.6 Ferrocene-based ligands

The chemistry of ferrocene-containing compounds has received considerable attention over the years, which is associated with their utilization in organic synthesis, catalysis and material chemistry.^{69,70,71} Ferrocene-containing compounds possess properties such

as high thermal stability and reversible redox characteristics which make them quite effective for use in coordination chemistry. The functionalization of the cyclopentadienyl rings with various donor groups and subsequent ligation to metal centres are important topics of research in many fields that utilise the special properties of such species.

Ferrocene or di(η^5 -cyclopentadienyl)iron(II) was accidentally discovered by Peter L. Pauson and his graduate student Tom Kealy in 1951 when they attempted the reductive coupling of the Grignard reagent cyclopentadienyl magnesium bromide in the presence of ferric chloride.⁷² Ferrocene is an orange-coloured neutral, chemically-stable and a non-toxic molecule.⁷³ It is soluble in most of organic solvents but insoluble in water. It is stable to temperature as high as 400 °C. The structure of ferrocene **30** is depicted in Figure 8.

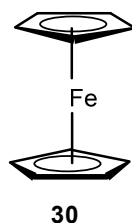


Figure 8: General structure of ferrocene.

The iron atom in ferrocene is assigned to the +2 oxidation state. Each cyclopentadienyl (Cp) ring is allocated a single negative charge, bringing the number of π -electrons on each ring to six, and thus making them aromatic. These twelve electrons (six from each ring) are then shared with the metal via covalent bonding, which, when combined with the six d-electrons on Fe^{2+} , results in a 18-electron, electronic configuration. The lack of individual bonds between the carbon atom of the Cp ring and the Fe^{2+} ion results in the Cp rings being able to freely rotate about the Cp-Fe-Cp axis. The carbon-carbon bond distances are 1.40 Å within the five membered rings, and the bond distances between the sandwiched iron and the carbons at the rings are 2.04 Å. The two cyclopentadienyl (Cp) rings of ferrocene may be orientated in two extremes of either an eclipsed (D_{5h}) or staggered (D_{5d}) conformation (Figure 9). The energy of rotation about the Fe-Cp axis is very small ($\sim 4 \text{ kJmol}^{-1}$).

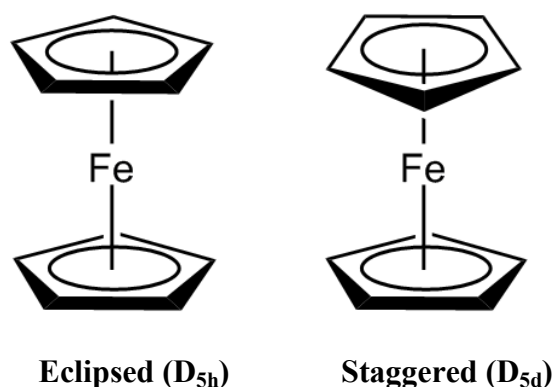


Figure 9: The different conformations of ferrocene.

Ferrocene can be easily derivatised, and functionalised and oxidised to the ferrocenium salt as depicted in Figure 10.

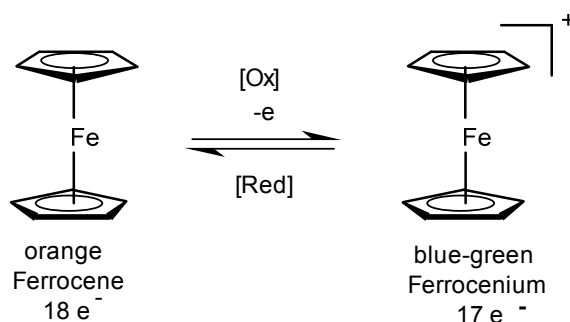


Figure 10: Oxidation of ferrocene to ferrocenium ion.

Oxidation of ferrocene gives a stable cation called a ferrocenium ion. Typical oxidising agents used are I_2 , conc. HNO_3 and silver nitrate. Ferrocenium salts are sometimes used as oxidising agents, in part because the product ferrocene is fairly inert to other compounds and readily separated from the ionic products.⁷⁴ The electrochemical property of ferrocene is based on the readiness and reversibility of the one-electron redox process. The ferrocene-ferrocenium cation system is considered as one of the most highly reversible redox systems. Ferrocenium ion is effectively used as a component in chemical sensors and as an internal standard for calibrating the redox potential in non-aqueous electrochemistry. Substituents on the cyclopentadienyl ligands alter the redox potential, for example electron-withdrawing groups such as carboxylic acid shift the potential in the anodic direction (*i.e.* they are made more positive), whereas electron-releasing groups such as a methyl group shift the potential in the cathodic direction (*i.e.* more negative). Hembre and McQueen recently reported the use of a redox-active ligand as an electron shuttle in a catalytic process.⁷⁵ Catalysts formed

from these ligands may be inactive or sluggish in one oxidation state, but active following oxidation or reduction. Alternatively, they may show selectivities for specific transformations that depend upon the oxidation state of the complex.

1.6.1 Pharmaceutically important ferrocene derivatives

Studies on bioactive organometallic compounds represent a field of research with increasing importance. In the search for novel bioorganometallic molecules exhibiting anti-cancer activity,^{76,77} ferrocene represents a promising organometallic unit. One of the examples is ferrocifen **31**, an activity-enhanced analog of the breast cancer drug tamoxifen (Figure 10).⁷⁸ The development of synthetic routes to these challenging compounds has greatly diversified the types of compounds that can be accessed.

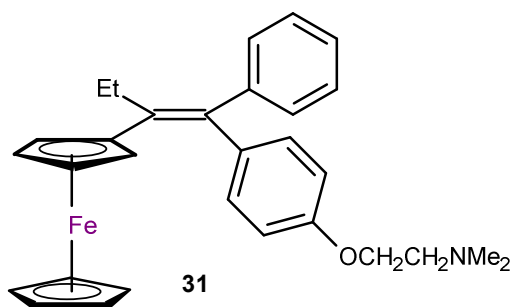


Figure 10: Ferrocifen, an analog of the breast cancer drug tamoxifen.

Many ferrocenyl compounds display interesting cytotoxic^{79,80,81} anti-tumour^{82,83} antimalarial,⁸⁴ antifungal⁸⁵ and DNA-cleavage activity.⁸⁶ Medicinal applications of ferrocene include *in vitro* (antimicrobial), *e.g.* $[\text{Mn}(\text{FcCOO})_2]$, and *in vivo* (cytotoxic), *e.g.* $[\text{Co}(\text{FcCOO})_2]$, compounds which have been used to treat several diseases.⁸⁷ Ferrocene is found to have good stability and low toxicity on biological media. Also, the lipophilicity is good for delivery. Ferrocene metabolite ferrocenium ion possesses cytotoxic activity against tumors and is easily derivatised. Given below (Figure 11), are a few well known pharmaceutically important ferrocene derivatives.

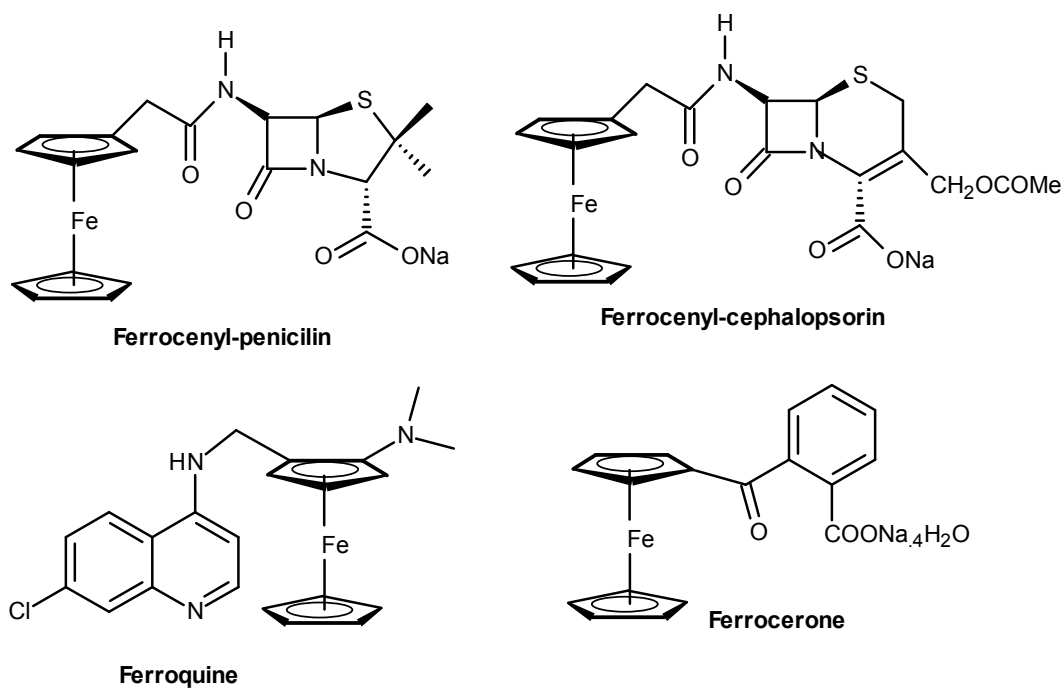


Figure 11: Pharmaceutically important ferrocene derivatives.

1.6.2 Ferrocenyl ligands in metal catalysis

In 1995, Hayashi was the first one to synthesise chiral ferrocene ligands and later on use them in asymmetric catalysis.⁸⁸ His work was followed by Kagan,⁸⁹ Richards,⁹⁰ Togni,⁹¹ Santelli,⁹² Hou,⁹³ Lemaire⁹⁴ and Guiry,⁹⁵ which resulted in the development of interesting chiral ferrocene ligands, as shown in Figure 12.

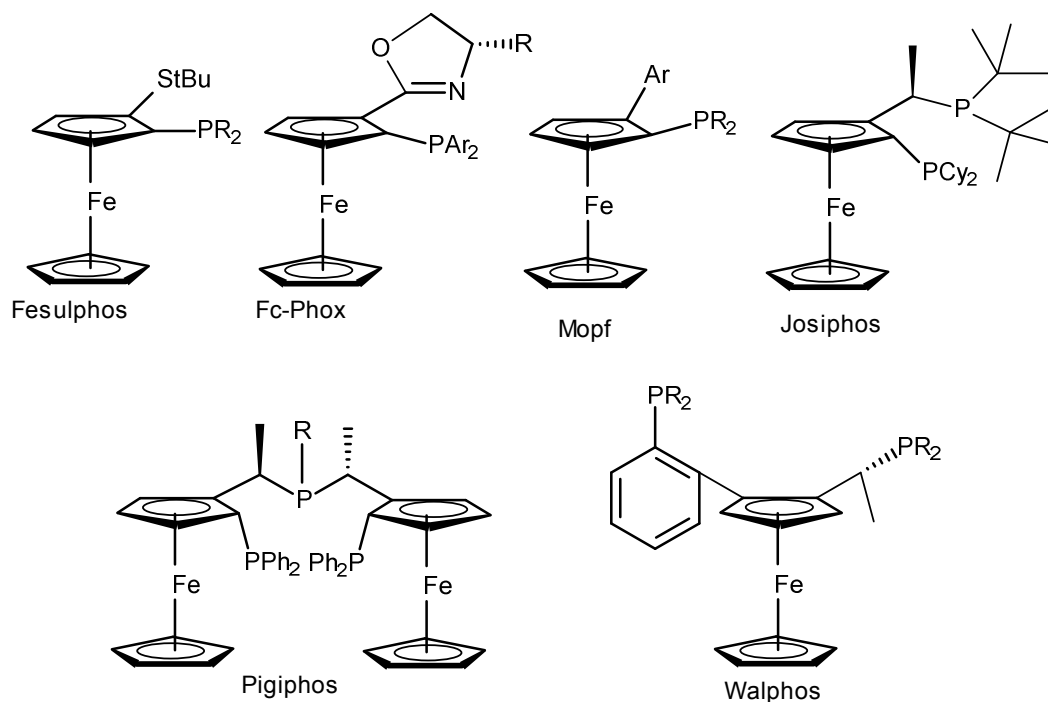
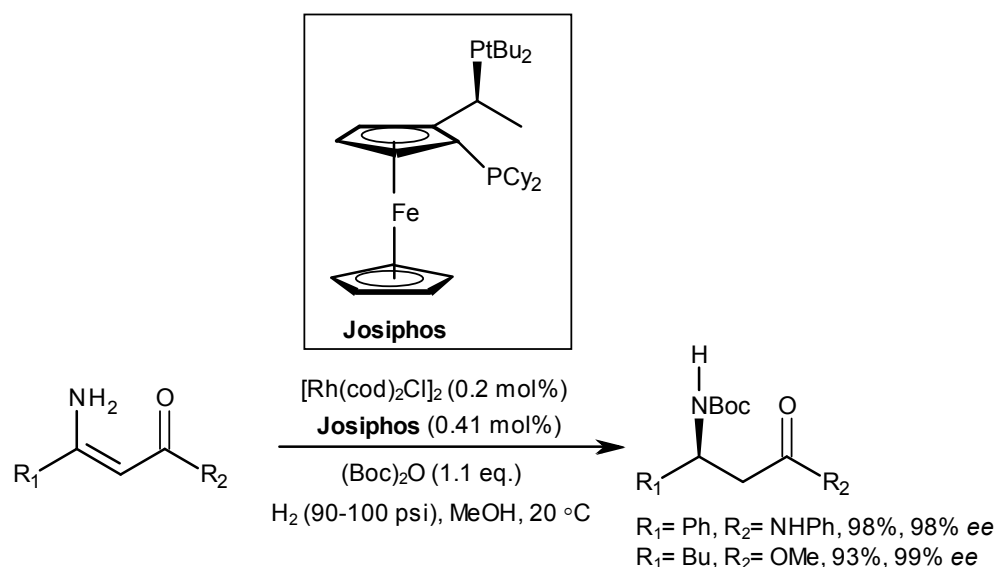


Figure 12: Examples of chiral ferrocene ligands.

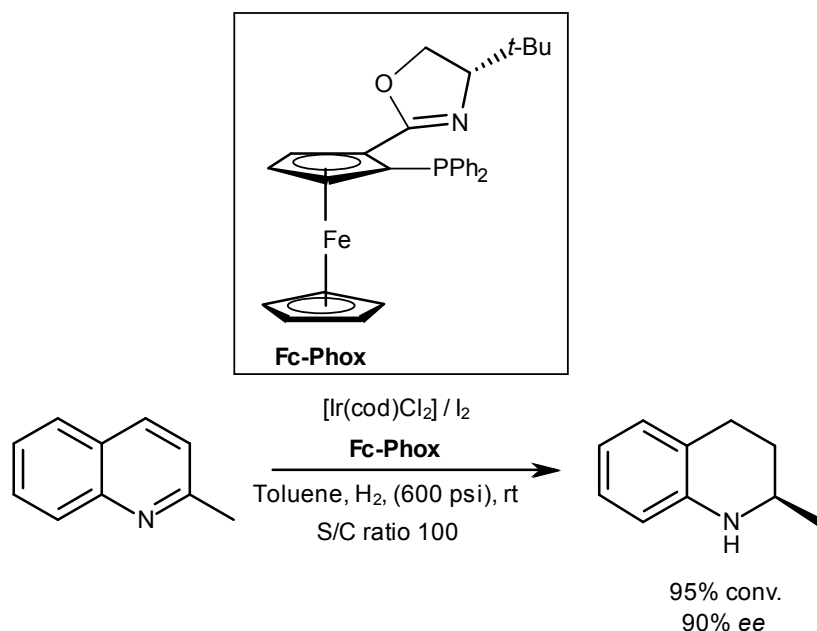
A chiral, redox-active ligand is, in theory, capable of acting as a chiral auxiliary in an organic transformation, with subsequent decomplexation of the ligand upon electrochemical oxidation, thus facilitating a complete catalytic cycle.

Ferrocenyl ligands have been successfully used in homogenous asymmetric hydrogenation of C=C and C=O bonds producing different kinds of chiral compounds on industrial scale,⁹⁶ thus showing that ligands based on the ferrocene framework can be considered as privileged structures for these types of transformations (Schemes 19 and 20).



Scheme 19: Josiphos/Rh-catalyzed asymmetric hydrogenation of unprotected enamines.

A group of researchers at Merck have effectively used Josiphos for the asymmetric hydrogenation of enamines.⁹⁷ The reaction was met with the drawback of amine-product inhibition and low-functional group compatibility, which was later improved by using Boc₂O in the presence of methanol. Under these conditions the corresponding Boc carbamates were isolated in good yields and high enantioselectivities.



Scheme 20: Fc-Phox/Ir-catalyzed asymmetric hydrogenation of 2-methylquinoline.

In another study, Zhou and co-workers showed the usefulness of Fc-Phox as a P,N ligand in the Ir-catalyzed asymmetric hydrogenation of 2-methylquinoline. It was

observed that the reaction proceeds with a slight decrease of enantioselectivity at lower catalyst loading.⁹⁸

1.6.3 Ferrocenyl-chalcone compounds

One of the most recent developments in organometallic chemistry is its interface with other sciences like biological science.⁹⁹ In many of the reported examples, a phenyl group in an organic molecule with well-known biological activities has been replaced with an organometallic moiety in order to determine whether it can be made more effective (akin to ferrocifen, **31**). In this regard, the ferrocene derivatives have featured prominently due to their excellent stability in aqueous (when substituted with appropriate water solubilising group), aerobic media, the easy accessibility of a large variety of derivatives and favourable electrochemical properties.¹⁰⁰

Chalcones are a naturally-occurring class of compounds that belong to the flavonoid family. They are aromatic ketones with two aromatic groups bridged by an enone linkage (of general structure of Ar-COCH=CH-Ar'). They have been used in a wide range of applications covering bio-materials¹⁰¹ non-linear optical¹⁰² and electroactive fluorescent materials.¹⁰³ The synthesis of chalcones is generally achieved by base-catalyzed aldol condensation.¹⁰⁴ Previous work in the Fairlamb group has shown that the hydroxy- and methoxy-chalcones display a wide range of biological properties and exert diverse pharmacological activities. Their work showed that the position of methoxy substituent on the two aromatic rings affect the anti-inflammatory action of different chalcones in relation to their ability to increase heme oxygenase-1 (HO-1) activity.¹⁰⁵

Ferrocenyl chalcones belong to the chalcone family in which one aromatic group (Ar or Ar') is substituted by the ferrocenyl group. Ferrocenyl chalcones have regularly been the subject of many interesting papers dealing with varied aspects of their chemistry¹⁰⁶ or potential uses in different fields.¹⁰⁷ Several well known examples of ferrocenyl chalcones are shown in Figure 13 overleaf.

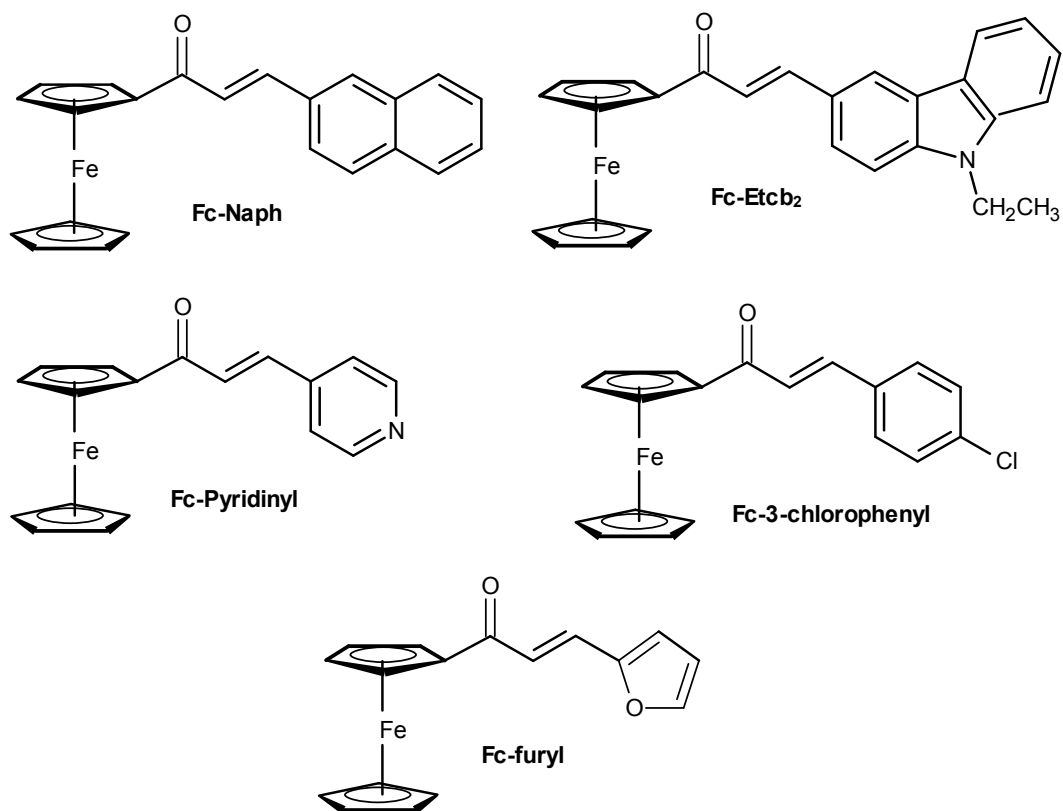


Figure 13: Selected examples of ferrocenyl chalcone compounds.

1.7 Project Summary (aims and objectives)

Chalcone-ferrocene ligands are potentially tuneable compounds.¹⁰⁸ The use of a chalcone-ferrocene ligand framework could be helpful in understanding the interaction of enone-type ligands with transition metal centres. By varying the substituents on the aryl ring connected directly to the enone π -system of the chalcone, as well as the ferrocene ring, the electronic effects could be probed.

The presence of both phosphine and alkene components enable the ligand target to possess hemilabile characteristics. The presence of a phosphine group enhances reactions such as oxidative addition. Whereas, an alkene can promote transmetallation and reductive elimination.¹⁰⁹ These chalcone-based ferrocene ligands are relatively straightforward to synthesise. The synthesis of these ligands and the assessment of the reactivity of their respective transition metal complexes will be studied in this research project.

Metal coordination behaviour of Lei ligand **17** will be further investigated (Figure 14), and compared with the chalcone-ferrocene ligands. Ligand **17** was reported during the first months in which the current project was started in York, exhibiting a similar structure as to that of ferrocene chalcone ligand class. Only a few metal complexes containing ligand **17** have been reported.¹¹⁰

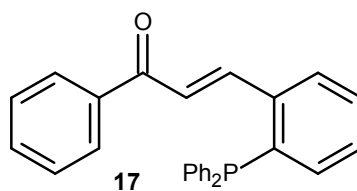
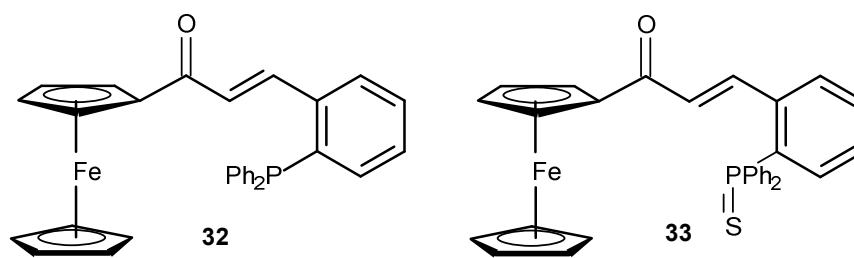


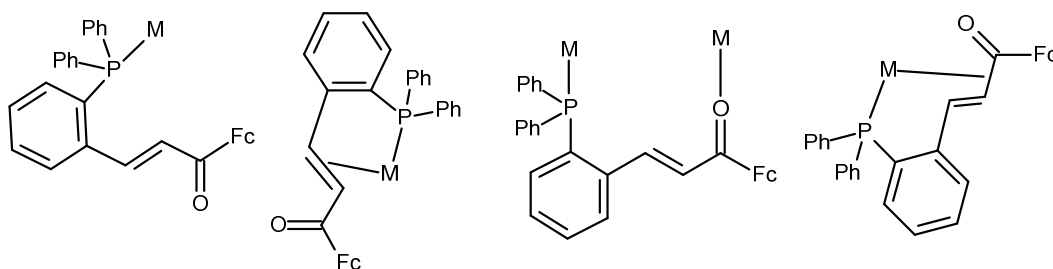
Figure 14: Structure of the Lei ligand (**17**).

Primary aims for this research project are to develop a diverse series of novel ligands based on the chalcone-ferrocene ligand framework, study their metal coordination chemistry and examine their applications in catalytic reactions. More specifically:

- To design and develop a simple methodology for the synthesis of a series of novel chalcone ferrocene ligands *e.g.* β -(2'-diphenylphosphinophenyl)-acrylferrocene **32**, and β -(2'-diphenylthiophosphinophenyl)acrylferrocene **33**.



- Study the coordination chemistry of **17**, thio-Lei, **32** and **33** with a variety of late transition metals like Pt, Pd, Rh, Au and Cu (exemplar coordination modes are shown below)



- To compare the ligating ability of the new ferrocenyl ligands with Lei's chalcone-phosphine ligand **17**.
- To explore the electrochemistry of the chalcone-ferrocene ligands and their metal complexes, with an emphasis on Au^I metal complexes.
- To use X-ray crystallography and NMR spectroscopic studies to characterise the novel alkene-phosphine and alkene thio-phosphine ligands, and their metal complexes.
- To screen novel ligands and metal complexes in benchmark catalytic reactions, in comparison with some well known catalytic systems. Cycloisomerisation chemistry will be explored using Au^I metal complexes.

Chapter 2: Synthesis of multidentate phosphino-alkene ligands

2.1 Design of ferrocenyl, olefin (alkene)-phosphine ligands

Alkene ligands can act as both σ -donors and π -acceptors.¹¹¹ A considerable amount of work has been done on the synthesis of alkene and phosphine ligands and they can be effectively used as a transition metal catalyst for a variety of organic transformations (as detailed in Chapter 1).¹¹² The aim of this chapter is to design a ligand having an alkene and phosphine moiety within the same core structure. Previous work by the Fairlamb group has been concerned with phosphine-alkenyl ligand containing a dibenzylidene acetone ligand backbone.¹¹³ Also, Professor Aiwen Lei from Wuhan university (China) designed a similar ligand having both an alkene and phosphine moiety.¹¹⁴ We have been interested in the design and development of a new class of phosphine-alkenyl ligand based on the chalcone-ferrocene backbone.¹¹⁵ Ferrocenyl chalcone belongs to a chalcone family in which one aromatic group (Ar or Ar') is substituted by an electrochemically-active ferrocenyl group.¹¹⁶ By varying the substituents on an aryl ring connected directly to an enone π -system of the chalcone, as well as the ferrocene ring, the electronic properties of the alkenes can potentially be tuned.¹¹⁷ The substituents on phosphorus could also be potentially varied and tuned, depending on the electronic and steric properties desired.¹¹⁸

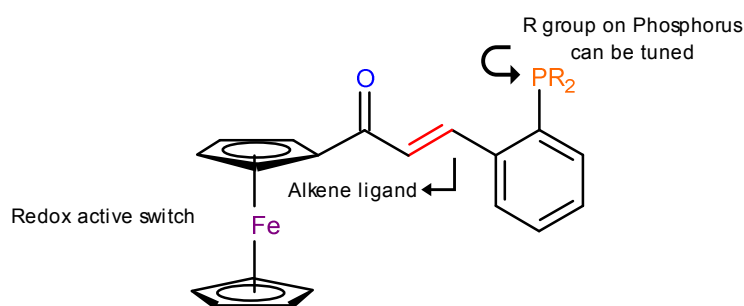


Figure 1: Design rationale for a new multidentate phosphino-alkene ligand system.

The initial target ligands for the project were **32**, and **33**, shown in Figure 2.

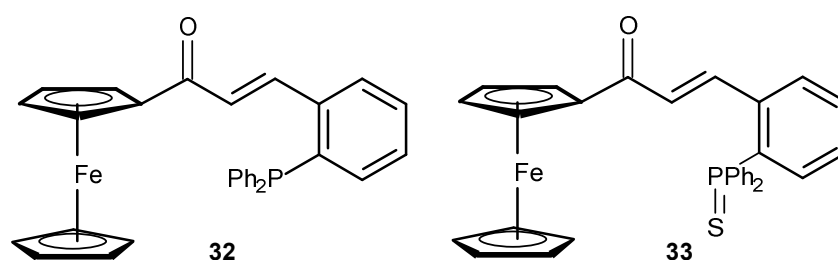
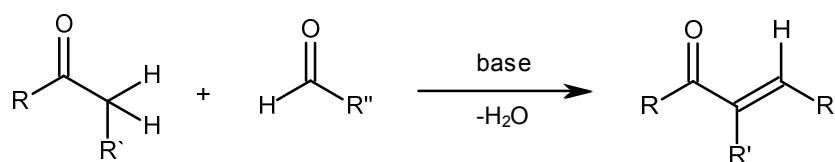


Figure 2: Initial ligand targets 32 and 33

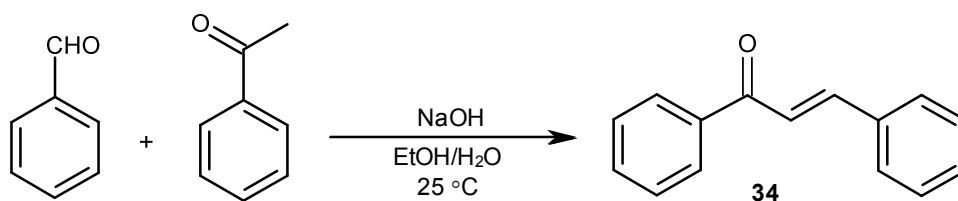
2.2 Synthesis of ligands

Chalcones are a group of naturally-occurring compounds belonging to the flavonoid family and are present in a variety of plant species such as fruits, vegetables, spices, tea, and soy based foodstuff.¹¹⁹ Chalcones, or *trans*-1,3-diaryl-2-propen-1-ones, are considered as the intermediate precursors to all flavonoid compounds. The synthesis of chalcones is generally achieved by base-catalyzed aldol condensation.¹²⁰ Different approaches were considered in this regard, such as refluxing in an organic solvent,¹²¹ the solvent-free solid-phase reaction,¹²² ultrasonication¹²³ and microwave radiation.¹²⁴ The synthesis of β -biarylacryl ferrocene is relatively straight-forward and can be accomplished by a Claisen-Schmidt condensation. The Claisen-Schmidt reaction is the aldol condensation between an aromatic aldehyde and a ketone leading to carbon-carbon bond formation, with loss of water affording a conjugated enone as the final product (Scheme 1). The Claisen-Schmidt reaction requires the use of a base as catalyst.



Scheme 1: Claisen-Schmidt condensation reaction.

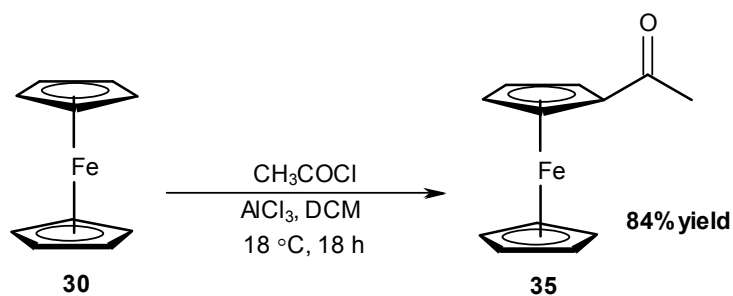
The most studied example of the Claisen-Schmidt condensation is the reaction of benzaldehyde with acetophenone to form chalcone (IUPAC naming – 1,3-diarylpropenone) **34** (Scheme 12).¹²⁵



Scheme 2: A generic synthesis of a 1,3-diarylpropenone (chalcone).

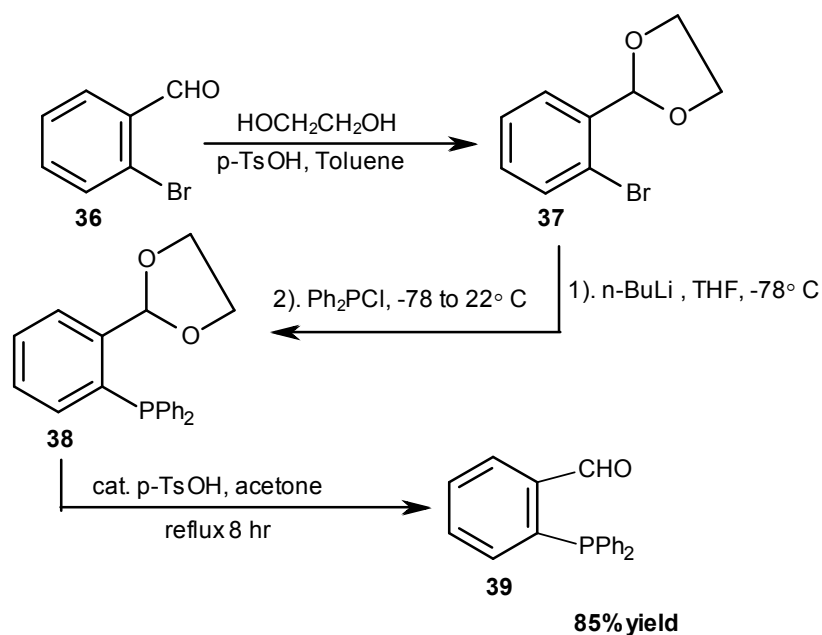
It was envisaged that the target phosphorus-containing chalcone ferrocene ligands could be accessed by base-mediated Claisen-Schmidt condensation of acetylferrocene **35** with a phosphine-substituted benzaldehyde (e.g. **39**).¹²⁶ Compounds **32** and **33** can be synthesised from commercially available acetylferrocene **35**. Also, **35** could be synthesised from ferrocene **30**, acetyl chloride and aluminium chloride in

dichloromethane. The reaction simply involves stirring at room temperature for 18 h (Scheme 13).



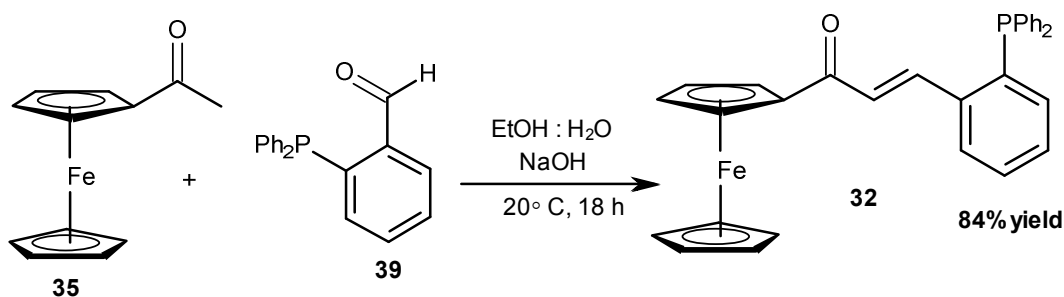
Scheme 3: Acetylation of ferrocene.

Ferrochalcone ligand **32** was obtained by reacting acetylferrocene **35** with 2-(diphenylphosphino)benzaldehyde **39**. Compound **39** could be synthesised simply from 2-bromobenzaldehyde **36** via protection of the bromoaldehyde as the acetal **37**. This was followed by halogen-lithium exchange and trapping with chlorodiphenylphosphine. Deprotection of the acetal affords aldehyde **39** as shown in Scheme 4.



Scheme 4: Synthesis of 2-(diphenylphosphino)benzaldehyde 39.

Base-catalyzed Claisen-Schmidt condensation of **39** with acetyl ferrocene **35** afforded **32** in a yield of 84% (Scheme 5).



Scheme 5: Synthesis of target ligand ferrochalcone ligand 32.

NMR and IR spectroscopy, and mass spectrometry, were used to analyse the structure of the product. The ^{31}P NMR spectrum of **32** in CDCl_3 gave a single peak at δ -13.0 confirming the formation and purity of ferrochalcone ligand **32**. The ^1H NMR spectrum showed that the α -H (alkene) appeared as a doublet ($J = 15.5$ Hz) with a chemical shift of δ 6.87, whereas the signal for β -H (alkene) appeared at *ca.* δ 8.43, spin-coupled with α -H. The signal at δ 4.06 corresponds to the five symmetrical protons of the ferrocene ring and those at δ 4.75 and δ 4.51 to the remaining four protons of the substituted ferrocene ring, with each peak corresponding to two protons. The remaining protons for the phenyl ring come in the range of *ca.* δ 6.8-7.8 as expected (Figure 3). The IR spectrum of **32** exhibited a strong band at 1653 cm^{-1} , which belongs to ν (C=O). Another strong band is observed at 1584 cm^{-1} , which is attributed to ν (C=C). The mass spectrum gave a molecular ion peak at m/z 523.3310, which corresponds to $\text{C}_{31}\text{H}_{25}\text{FePONa} [\text{MNa}]^+$ confirming the synthesis of the target ligand **32**.

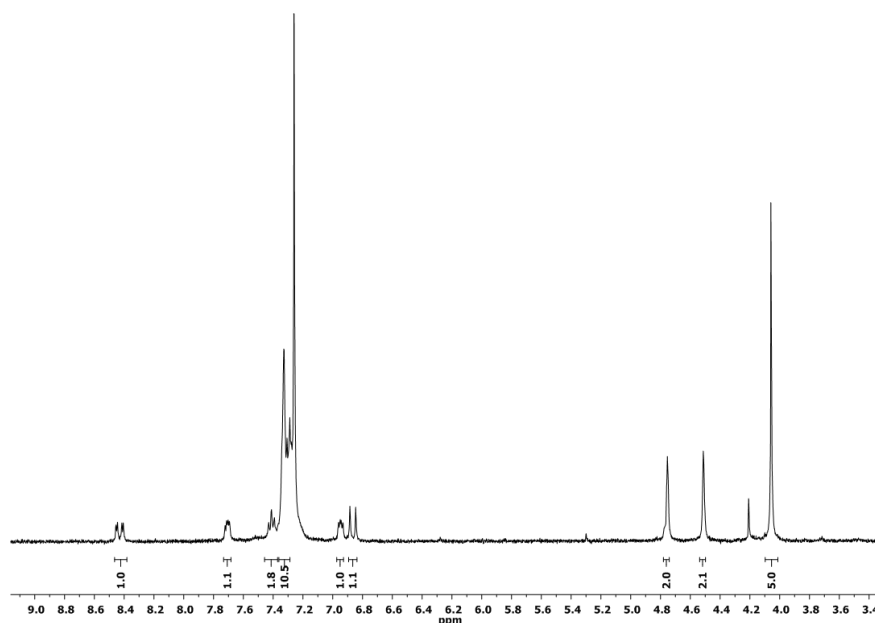
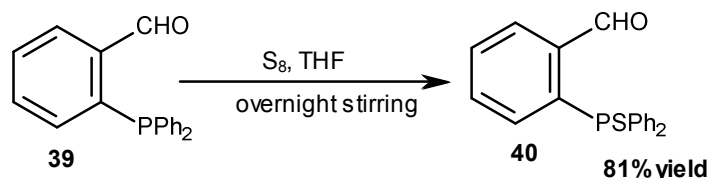


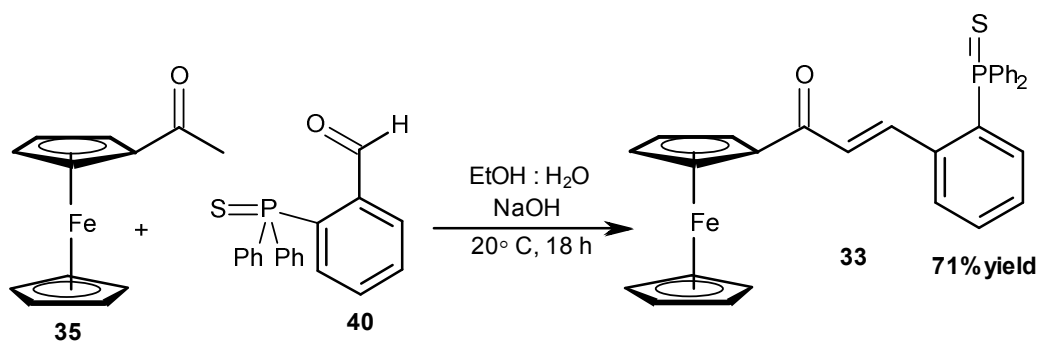
Figure 3: The ^1H NMR spectrum for ligand 32 in CDCl_3 .

Two different routes were devised for the synthesis of the “R₃P=S” compound **33**. The first route involves the synthesis of 2-(diphenylthiophosphino)benzaldehyde **40**, followed by its base-catalyzed Claisen-Schmidt condensation with acetyl ferrocene **35**. The second route involves the direct reaction of **32** with sulphur flowers (S₈) in THF. 2-(Diphenylthiophosphino)benzaldehyde **40** was synthesised by reacting **39** with excess S₈ in presence of THF to give **40** as shown in Scheme 6.



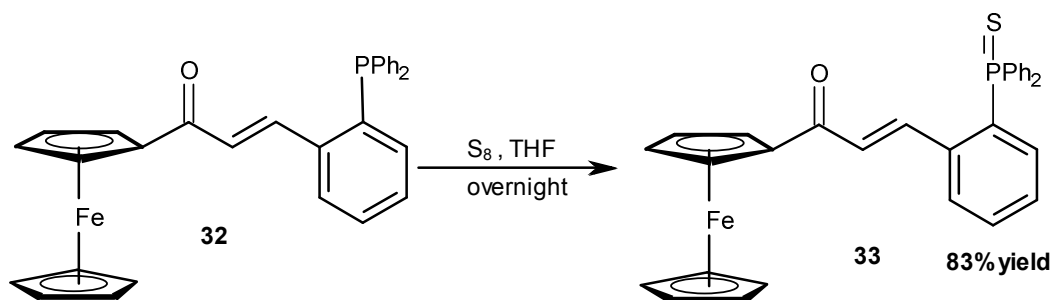
Scheme 6: Synthesis of 2-(diphenylthiophosphino)benzaldehyde 40.

Thio-ferrochalcone ligand **33** was obtained by the reaction of acetylferrocene **35** with **40** (Scheme 7).



Scheme 7: Synthesis of target ligand thio-ferrochalcone 33.

The target ligand thio-variant of ferrochalcone **33** could be synthesized by direct treatment of **32** with sulphur flowers (S₈). Overnight stirring at room temperature in THF gave the target ligand **33** in 83% yield (Scheme 8).



Scheme 8: Synthesis of target ligand thio-ferrochalcone 33.

The IR spectrum of compound **33** exhibits a band at 1643 cm^{-1} which is assigned to ν (C=O), whereas the band at 1577 cm^{-1} corresponds to ν (C=C). In the mass spectrum we observe a peak at m/z 533.4247 which corresponds to the molecular ion peak ($\text{C}_{31}\text{H}_{26}\text{FePSO} [\text{MH}]^+$) confirming the synthesis of target ligand **33**. The ^{31}P NMR spectrum of **33** in CD_2Cl_2 gave a single peak at δ 42.05 (confirming the formation and presence of single product).

The ^1H NMR spectrum of **33** in CD_2Cl_2 shows a signal at δ 8.25 which corresponds to β -H. The signal at δ 6.83 corresponds to α -H. All the proton signals in the range *ca.* δ 4-5 ppm correspond to that of ferrocene, and those between *ca.* δ 7-8 ppm represent the phenyl protons (Figure 4).

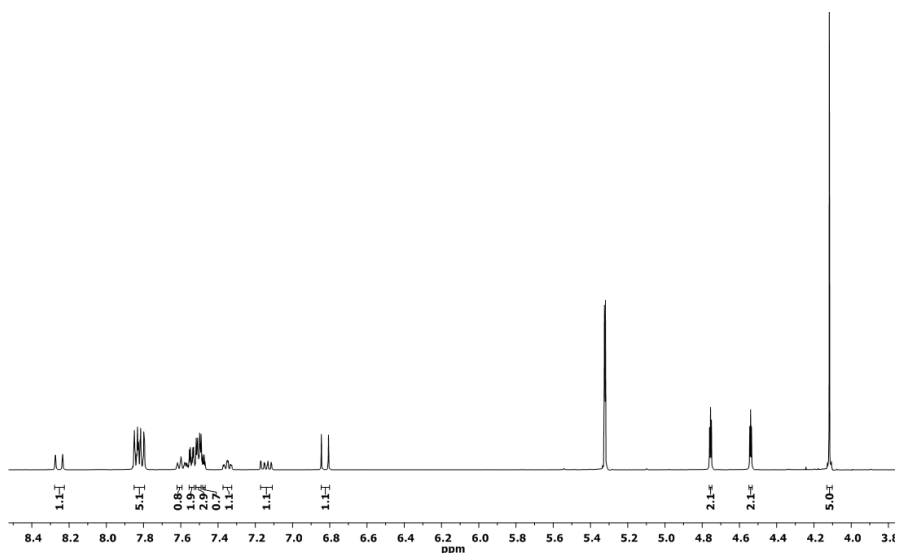


Figure 4: The ^1H NMR spectrum for ligand **33** in CD_2Cl_2 .

Alternative ferrocene chalcone derivatives **41** could be synthesised which possess different phosphorus R-groups (Figure 5). Such compounds can be effectively used as useful precursors for the synthesis of new metallocene derivatives.¹²⁷

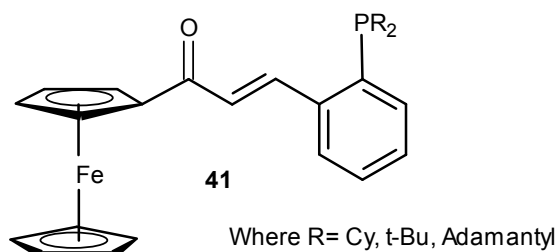


Figure 5: Representative structure for different ferrocene chalcone derivatives.

A key intermediate that could potentially be involved in the synthesis of these chalcone ferrocene derivatives is β -(2'-bromophenyl)acryl ferrocene **42** (Figure 6).

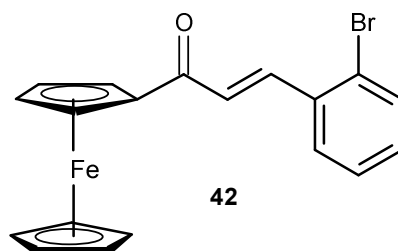
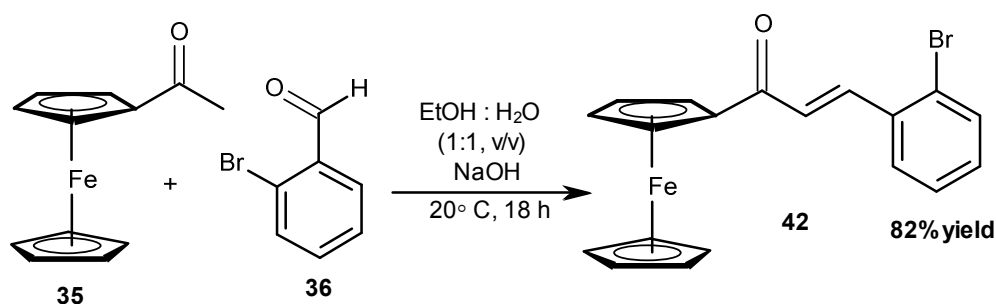


Figure 6: Structure of β -(2'-bromophenyl)aryl ferrocene **42.**

β -(2'-Bromophenyl)aryl ferrocene **42** can be prepared by a base-catalysed Claisen-Schmidt condensation reaction of acetylferrocene **35** with bromobenzaldehyde **36** at ambient temperature overnight (Scheme 9).



Scheme 9: Synthesis of β -(2'-bromophenyl)aryl ferrocene, **42.**

By the time we were working on the synthesis of these chalcone-ferrocene ligands Lei and co-workers published the synthesis of a similar ligand having a chalcone backbone with two phenyl rings as shown below **17** (as detailed in the introduction section) (Figure 7).

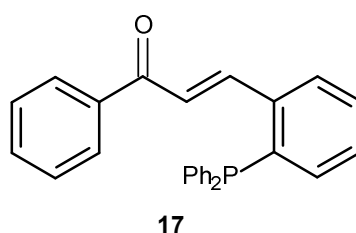
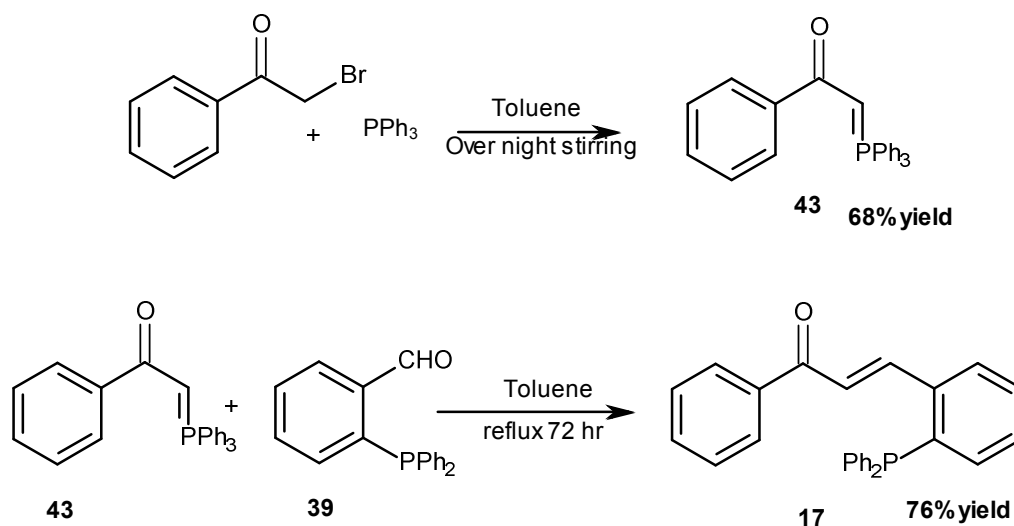


Figure 7: Structure of the Lei ligand, **17.**

The Lei ligand was synthesised by a two-step Wittig reaction. The first step involves the formation of the phosphorus ylide **43** by reaction of α -bromoacetophenone with triphenylphosphine. Whereas, in the second step the phosphorus ylide **43** reacts with **39** giving the target ligand **17**, as given in Scheme 10.



Scheme 10: Synthesis of Lei ligand, 17.

The ^{31}P NMR spectrum of **17** gave a single peak at δ -13.32 confirming the synthesis of the target ligand. MS analysis showed a molecular ion peak at $[\text{MH}]^+$ 393.1405, corresponding to $\text{C}_{27}\text{H}_{22}\text{OP}$. We struggled in the beginning to reproduce the results by Lei (usually poor yields and side products were formed). An additional product – the phosphine oxide **44**, was formed along with the target compound **17** (Figure 9). However, the reaction conditions were improved by carefully repeating the reaction under inert conditions, especially running column chromatography on silica gel under a nitrogen atmosphere. The Lei ligand was found to be air sensitive, with phosphine oxide contaminating the product in the solution-form. Another, side -product obtained was the reduced phosphine oxide-Lei ligand **45** as given in Figure 9.

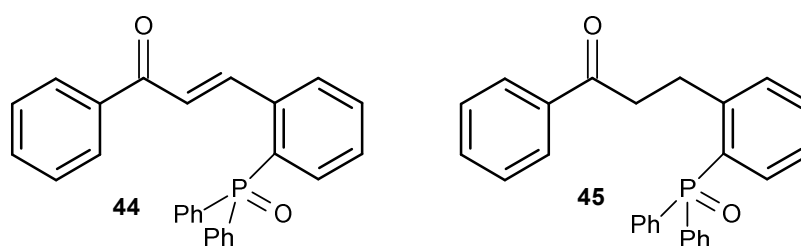
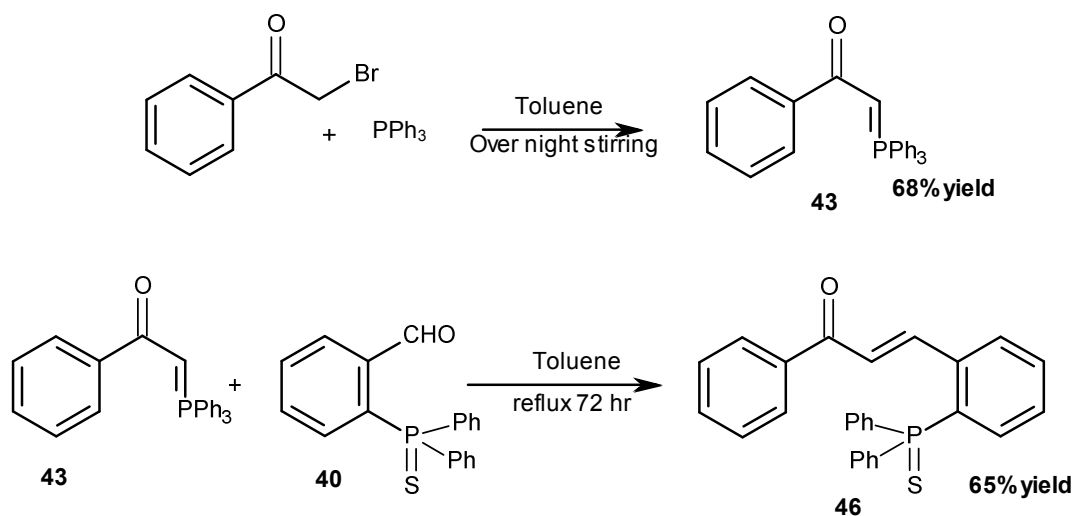


Figure 9: Side-products formed in the synthesis of the Lei ligand 17.

We also wished to prepare a novel thio-variant of the Lei ligand, **46**. A two-step reaction was used. The first step involves the formation of a phosphorus ylide obtained by reacting triphenylphosphine with α -bromoacetophenone to give **43**. A solution of α -bromoacetophenone in toluene was added dropwise to a solution of triphenylphosphine in toluene. The reaction mixture was stirred overnight at room temperature. Work-up

gave the target product **43** in 68% yield, which was used in crude form. In the final step the Wittig reaction of **40** with ylide **43** gave the product **46** in a good yield of 65%, following column chromatography on silica gel (Scheme 11).



Scheme 11: Synthesis of the thio-Lei ligand, 46.

The ^{31}P NMR spectrum for **46** in CD_2Cl_2 gave a single peak at δ 42.1 confirming the formation and purity of product. In the ^1H NMR spectrum the signal at δ 8.23 corresponds to β -H, and that at δ 7.08 corresponds to α -H. All the peaks in the range of *ca.* δ 7-8 ppm correspond to the phenyl protons.

2.3 Structure of the ligands

2.3.1 β -[2'-(diphenylphosphino)phenyl]acrylferrocene **32**.

Very fine red crystals of ferrocene ligand **32** were grown from dichloromethane and ether (2:3, v/v). The crystals were kept in solution and analysed by X-ray diffraction methods (XRD) to obtain a single crystal solid-state structure (Figure 10).

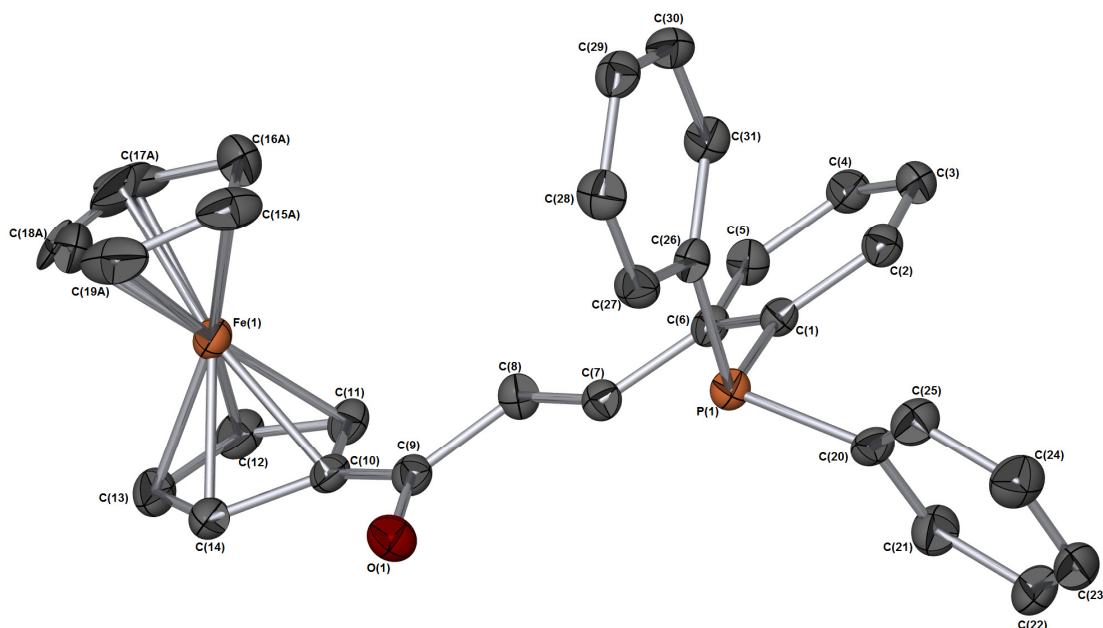


Figure 10: X-ray crystal structure of ligand 32.

Solvent and hydrogen atoms are removed for clarity. Thermal ellipsoids shown at 50%. Bond lengths (\AA): C(6)-C(7) = 1.466(3), C(7)-C(8) = 1.330(3), C(8)-C(9) = 1.487(3), C(9)-C(10) = 1.472(3), C(9)-O(1) = 1.228(3), P(1)-O(2) = 1.387(8), P(1)-C(1) = 1.832(2), P(1)-C(20) = 1.833(2), P(1)-C(26) = 1.828(2), Bond Angles ($^\circ$): C(6)-C(7)-C(8) = 126.0(2), C(7)-C(8)-C(9) = 120.2(2), C(8)-C(9)-C(10) = 117.12(19), O(1)-C(9)-C(10) = 121.3(2), O(1)-C(9)-C(8) = 121.55(19), O(2)-P(1)-C(1) = 123.1(3), O(2)-P(1)-C(20) = 109.5(3), O(2)-P(1)-C(26) = 112.5(3), C(1)-P(1)-C(20) = 102.10(9), C(26)-P(1)-C(20) = 104.93(10), C(26)-P(1)-C(1) = 102.79(10).

X-ray diffraction studies showed crystal twinning and further analysis revealed these to be a combination of both **32** and **47** (Figure 11; phosphine oxide not shown), in a ratio of *ca.* 80: 20. The unsubstituted cyclopentadienyl ring (Cp) proved to be disordered, and

was thus subsequently modelled over two positions both having equal occupancy. The disordered Cp rings were constrained as regular pentagons.

The ligand **32** was found to be sensitive to light and air in solution. The formation of the phosphine oxide of **32** was noted by ^{31}P NMR spectroscopic analysis with a resonance δ 29.74 ppm.

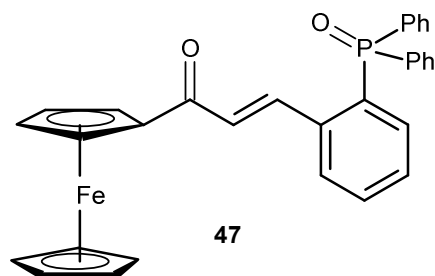


Figure 11: Structure of 47.

Various attempts to crystallise **32** without contamination by the phosphine oxide were unsuccessful. It was observed that the ligand itself is more sensitive in solution form than any metal complexes derived from it (see later). The C(7)-C(8) alkene double bond length is 1.330 Å, as expected for an alkene bond (1.334 Å for ethene).¹²⁸ However, the C-C bond length for C(6)-C(7) is 1.466 Å and C(8)-C(9) 1.487 Å higher than that for a free C=C bond, showing a single bond character for these bonds. The torsion angle for C7-C8-C9-O1 is 6.2°, exhibiting a synperiplanar conformation (*cis*-conformation) whereas the torsion angle for O1-C9-C10-C11 is -169.4°, exhibiting an antiperiplanar conformation (*trans*-conformation). The torsion angle values for O2-P1-C1-C6, O2-P1-C26-C27 and O2-P1-C20-C21 are 17.1°, 38.3° and 71.1°, showing that the first set of atoms exhibit a synperiplanar conformation, whereas the other two sets of atoms exhibit a synclinal conformation (*e.g.* gauche or skew conformation).

2.3.2 Thio-Lei ligand (C₂₇H₂₁OPS)

The thio-Lei ligand, **46** was obtained as light yellow powder, which was found to be soluble in most organic solvents, *e.g.* dichloromethane, ethyl acetate and benzene. The product was crystallised from dichloromethane. Fine yellow crystals were obtained and analysed by X-ray diffraction (Figure 12). The C=C bond length for C(8)-C(9) is 1.332 Å whereas the bond length for C(7)-C(8) is 1.488 Å, and for C(9)-C(10) 1.477 Å. This indicates a double bond order for C(8)-C(9) and a single bond order for the other two bonds. The bond length for C(8)-C(9) is similar to an alkene double bond of 1.333 Å. The bond length P(1)-S(1) is 1.956 Å. The torsion angle value for O1-C7-C6-C1 is -159.8° and for O1-C7-C8-C9 is 17.1°, showing that O1-C7-C6-C1 exhibits an antiperiplanar conformation, whereas O1-C7-C8-C9 exhibits a synperiplanar conformation. The torsion angle for S1-P1-C15-C10 is 62.66° (*e.g.* synclinal conformation), and for S1-P1-C22-C23 -125.69° (*e.g.* in an anticlinal conformation) and for S1-P1-C16-C17 is -147.85° (*e.g.* in an anticlinal conformation).

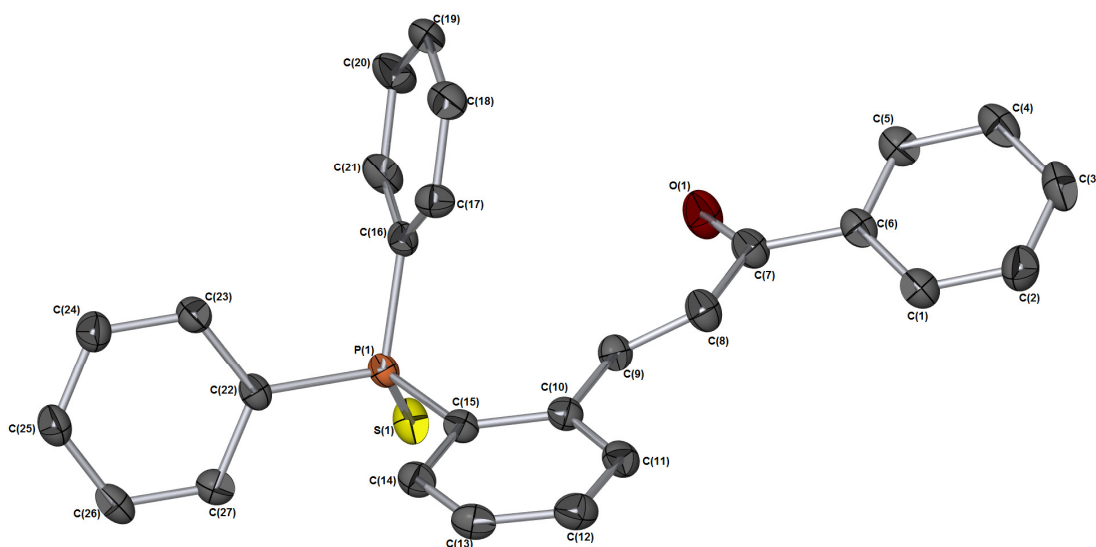


Figure 12: X-ray crystal structure of thio-Lei ligand 46.

Solvent and hydrogen atoms are removed for clarity. Thermal ellipsoids shown at 50%. Bond lengths (Å): C(6)-C(7) = 1.497(3), C(7)-C(8) = 1.488(3), C(8)-C(9) = 1.332(3), C(9)-C(10) = 1.477(3), C7-O1 = 1.222(3), P(1)-S(1) = 1.956(7), P(1)-C(15) = 1.821(2), P(1)-C(22) = 1.816(2), P(1)-C(16) = 1.811(2), Bond Angles (°): C(8)-C(7)-C(6) = 117.20(18), C(9)-C(8)-C(7) = 122.42(19), C(10)-C(9)-C(8) = 124.15(19), C(11)-C(10)-C(9) = 119.93(19), C(9)-C(10)-C(15) = 121.95(18), S(1)-P(1)-C(15) = 113.45(7), S(1)-P(1)-C(22) = 110.60(7), S(1)-P(1)-C(16) = 115.27(7), C(15)-P(1)-C(22) = 107.77(9), C(15)-P(1)-C(16) = 103.71(9), C(16)-P(1)-C(22) = 105.38(10).

A comparison of key bond lengths and torsion angles for ligands **32** and **46** are given in Table 1.

Table 1: Comparison of the bond length and torsion angle between compound 46 and 47.

Bonds	32	46
C=O	1.228(3)	1.222(3)
C=C	1.330(3)	1.332(3)
C-C	C(6)-C(7) = 1.466(3), C(9)-C(10) = 1.477(3)	C(7)-C(8) = 1.488(3), C(9)-C(10) = 1.477(3)
P=O	1.387(8)	--
P=S	--	1.956(7)
Torsion angle	(°)	(°)
C10-C9-C8-C7	-174.86	-179.2
C9-C8-C7-C6	-178.95	-163.6

2.4 Summary

The target ligands ferrochalcone **32** and thio-ferrochalcone **33** have been synthesised in good yields by a Claisen-Schmidt condensation reaction. The thio-Lei ligand **46** has also been synthesized successfully. Side-products were noted in the synthesis of Lei ligand **17**, which were not originally reported by Lei and co-workers. The XRD analysis of ferrochalcone **32** confirmed its structure, which was supported by the full spectroscopic analysis. The phosphorus ligand **32** is air sensitive and hence the structure obtained was a mixture with the corresponding phosphine oxide. With ligands (**17**, **32**, **33** and **46**) in hand, it is now possible to assess the coordination chemistry of these ligands towards a variety of metals, *e.g.* Cu, Pt, Pd, Rh, Au *etc.* (see Chapter 3).

2.5 Experimental

2.5.1 General Information

¹H-NMR spectra were obtained in the solvent indicated using a JEOL EXC400 or JEOL ECS400 spectrometer (400MHz for ¹H, 100 MHz for ¹³C and 162 MHz for ³¹P). Chemical shifts were referenced to the residual undeuterated solvent of the deuterated solvent used (CHCl₃ δ = 7.26 and 77.16 and DCM δ = 5.31 and 53.80 for ¹H and ¹³C NMR spectra, respectively). NMR spectra were processed using MestrNova software.

All ^{13}C NMR spectra were obtained with ^1H decoupling. ^{31}P NMR spectra were externally referenced to H_3PO_4 , and obtained with ^1H decoupling. For ^{13}C NMR spectra the coupling constants are quoted to ± 1 Hz. For the ^1H NMR spectra the resolution varies from ± 0.15 to ± 0.5 Hz; the coupling constants have been quoted to ± 0.5 Hz in all cases for consistency.

Melting points were recorded using a Stuart digital SMP3 machine. IR spectroscopy was undertaken using a Jasco/MIRacle FT/IR-4100typeA spectrometer with an ATR attachment on solid and liquid compounds; solution and KBr IR spectra were obtained on a Nicolet Avatar 370 FT-IR spectrometer. The relative intensities of the peaks are denoted by (s) = strong, (m) = medium and (w) = weak, whilst (br) is used to describe broad peaks. MS spectra were measured using a Bruker Daltonics micrOTOF MS, Agilent series 1200LC with electrospray ionisation (ESI and APCI) or on a Thermo LCQ using electrospray ionisation, with < 5 ppm error recorded for all HRMS samples. Mass spectral data is quoted as the m/z ratio along with the relative peak height in brackets (base peak = 100). Dry and degassed toluene, ether, DCM and hexane were obtained from a solvent system. Nitrogen gas was oxygen-free and was dried immediately prior to use by passage through a column containing sodium hydroxide pellets and silica gel. THF and benzene were dried over sodium-benzophenone ketyl and ethanol was dried and distilled from magnesium-iodine. Commercial chemicals were purchased from Sigma-Aldrich or Alfa Aesar. Elemental analysis was carried out on an Exeter Analytical CE-440 Elemental Analyser. All column chromatography was run on silica gel 60 using the solvent systems specified in the text. The fraction of petroleum ether used was that boiling at 40-60 $^\circ\text{C}$.

Dry and degassed toluene, CH_2Cl_2 and hexane were obtained from a 'Pure Solv' MD-7 solvent purification system. THF and Et_2O were either obtained from a 'Pure Solv' MD-7 solvent purification system and degassed by the freeze-pump-thaw method or purged with N_2 under sonication, or dried over sodium-benzophenone ketyl and collected by distillation. Benzene was dried over sodium-benzophenone ketyl, EtOH was dried and distilled from magnesium-iodine, and triethylamine was dried over KOH. All air sensitive procedures were carried out using Schlenk techniques.¹²⁹ Nitrogen gas was oxygen-free and was dried immediately prior to use by passage through a column containing sodium hydroxide pellets and silica. Room temperature is quoted as the

broadest range 13-25°C, but it was typically 18-20 °C. Commercial chemicals were purchased from Sigma-Aldrich and Alfa Aesar and used directly unless stated in the text. Brine refers to a saturated aqueous solution of NaCl.

β -[2'-(Diphenylphosphino)phenyl]acrylferrocene (32)

Acetyl ferrocene (0.51 g, 0.002 mol) was dissolved in ethanol (2 mL) and a solution of 2-(diphenylphosphine)benzaldehyde **39** (0.43 g, 0.002 mol) in ethanol (1 mL) was added to above mixture with stirring. After that stirring was continued for 0.5 h a solution of ethanol (2 mL), H₂O (2 mL) and NaOH (0.18 g) was added dropwise under stirring at room temperature. A red precipitate appeared after some time, which became difficult to stir. After two hours TLC analysis indicated completion of the reaction. The mixture was poured into H₂O (25 mL) and neutralized to pH=7 with 2M HCl, cooled using ice, and then filtered. The solid was washed with water (10 × 3) and dried *in vacuo*. The crude product was recrystallized from chloroform to afford the final product as a light red crystalline solid (0.94 g, 84%). Mp 147-151 °C, R_f = 0.35 (EtOAc:Pet.ether); ¹H-NMR (400 MHz, CDCl₃) δ 8.43 (dd, *J* = 15.8, 3.7 Hz, 1H), 7.85-7.60 (m, 1H), 7.40 (d, *J* = 3.8 Hz, 2H), 7.46-7.28 (m, 10H), 7.01-6.91 (m, 1H), 6.87 (d, *J* = 15.5 Hz, 1H), 4.75 (s, 2H), 4.51 (s, 2H), 4.06 (s, 5H); ¹³C-NMR (100 MHz, CDCl₃) δ 193.1, 140.5 (d, *J* = 22 Hz, 2C), 139.4 (d, *J* = 23 Hz, 2C), 138.3 (d, *J* = 11 Hz, 2C), 138.2, 136.1 (d, *J* = 10 Hz, 2C), 134.1 (d, *J* = 20 Hz, 2C), 133.8, 129.1 (d, *J* = 9 Hz, 2C), 128.7 (d, *J* = 7 Hz, 2C), 127.3 (d, *J* = 4 Hz, 2C), 126.3 (d, *J* = 4 Hz, 2C), 80.2, 72.7 (2C), 70.2 (2C), 69.9 (5C); ³¹P-NMR (162 MHz, CDCl₃) δ -13.0 (s, 1P); HRMS [MNa]⁺: 523.3310 (Calcd. for C₃₁H₂₅FePONa 523.3410); IR ν cm⁻¹ 3052 (s), 1653 (s), 1584 (s), 1457 (s), 1377 (s), 1199 (s), 1081 (s), 759 (s), 696 (s), 501 (s).

Acetylferrocene (35)

Ferrocene (0.093 g, 5 mmol) was added to a stirred suspension of acetyl chloride (0.40 g, 5.1 mmol) and aluminium chloride (0.68 g, 5.1 mmol) in dichloromethane. The resulting mixture was stirred overnight at room temperature and then washed with water (25mL). The organic layer was passed through a plug of alumina which was then washed with chloroform (3 × 10 mL) until washing become colourless. It was then finally concentrated *in vacuo* to give the crude product, which was purified by column chromatography on silica gel to give the title compound as deep red crystals (0.96 g, 84%). Mp 78-81 °C (lit. 81-86 °C)¹³⁰; ¹H-NMR (400 MHz, CDCl₃) δ 4.77 (t, *J* = 4 Hz,

2H), 4.50 (t, $J = 4$ Hz, 2H), 4.21 (s, 5H), 2.40 (s, 3H); ^{13}C -NMR (100 MHz, CDCl_3) δ 202.2, 79.2, 72.5, 69.8, 68.1, 27.3; LRMS (EI) m/z 251(M+Na, 100), 229 (50), 186 (4), 158 (2), 142 (5), 110 (3).; HRMS (ESI) m/z (MNa^+): 251.013 (Calcd. for $\text{C}_{12}\text{H}_{12}\text{FeO}$ 251); IR ν cm^{-1} 3096 (m), 1661 (s), 1653 (s), 1457 (s), 1375 (s), 1280 (s), 1103 (s), 1005 (s), 827 (s).

2-(*o*-Bromophenyl)-1,3-dioxolane (37)

2-Bromobenzaldehyde (15.0 g, 0.08 mol), ethylene glycol (6.7 mL, 0.12 mol) and *para*-toluenesulfonic acid (63 mg) were dissolved in toluene (100 ml) and refluxed, while the evolved water was collected in a Dean-Stark trap. After water was no longer evolved (*ca.* 24 h) the solution was allowed to cool to rt and washed with a saturated solution of NaHCO_3 (60 mL), followed by a saturated solution of NaCl (20 mL). The solution was dried over MgSO_4 , filtered, concentrated *in vacuo* and distilled at 100 °C, 0.5 mmHg, to give the title compound as a colourless oil (16.33 g, 89%). ^1H NMR (400 MHz, CDCl_3) δ 7.59 (ddd, $J = 15, 8, 1.5$ Hz, 1H), 7.37-7.32 (m, 1H), 7.28-7.24 (m, 1H), 7.18 (dd, $J = 7.5, 3$ Hz, 1H), 6.11 (s, 1H), 4.23-4.04 (m, 4H). ^{13}C NMR (100 MHz, CDCl_3) δ 136.7, 133.1, 130.7, 127.9, 127.5, 123.1, 102.6, 65.6. HRMS (ESI) m/z 228.9859 [MH] $^+$ (calculated for $\text{C}_9\text{H}_{10}\text{BrO}_2 = 228.99$); IR ν cm^{-1} 2955 (w, br), 2886 (m, br), 1730 (w), 1592 (w), 1571 (w), 1472 (w), 1443 (w), 1387 (m), 1270 (w), 1211 (m), 1124 (m), 1084 (s, br), 1042 (m), 1021 (m), 969 (m), 941 (m), 754 (s).

2-(*o*-Diphenylphosphinophenyl)-1,3-dioxolane (38)

A solution of 2-(*o*-bromophenyl)-1,3-dioxolane (20.95 g, 91 mmol) in dry THF (200 mL) was cooled to -78 °C and kept under an inert atmosphere of N_2 . $n\text{-BuLi}$ in hexane (40 mL, 93 mmol, 1.3 eq.) was added by syringe pump at a rate of 40 cc/h. The reaction was allowed to warm-up to 24 °C overnight, before the addition of water (240 mL). The organic phase was extracted with Et_2O (3×50 mL), dried over anhydrous Na_2SO_4 , filtered and the solvent removed *in vacuo*. The resulting oily liquid was purified by crystallisation from hot ethanol and cooled to -25 °C, to afford the title compound as a waxy white solid (21.24 g, 70%). Mp 94-95 °C; ^1H NMR (400 MHz, CDCl_3) δ 7.74-7.65 (m, 1H), 7.41-7.35 (m, 1H), 7.32 (dd, $J = 4.5, 2.0$ Hz, 6H), 7.30-7.23 (m, 5H), 6.95 (ddd, $J = 8, 4.5, 1.2$ Hz, 1H), 6.43 (d, $J = 5.0$ Hz, 1H), 4.13-4.19 (m, 4H); ^{13}C NMR (100MHz, CDCl_3) δ 142.1 (d, $J = 22$ Hz), 137.1 (d, $J = 10$ Hz), 136.1 (d,

$J = 19$ Hz), 134.2 (d, $J = 2$ Hz), 134.1, 133.8, 129.4 (d, $J = 18$ Hz), 128.7, 128.6 (d, $J = 7$ Hz), 126.6 (d, $J = 6$ Hz), 101.8, 65.5; ^{31}P NMR (162 MHz, CDCl_3) δ -15.86 (s); LRMS (ESI) m/z 291.1 [$M\text{-C}_2\text{H}_4\text{O}$] $^+$ (100), 273.1 (26), 261.1 (3), 242.1 (5), 213.0 (8).

2-(Diphenylphosphino)benzaldehyde (39)

2-(*o*-Diphenylphosphinophenyl)-1,3-dioxolane (21.24 g, 64 mmol) and *para*-toluenesulfonic acid (0.45 g) were dissolved in acetone (450 mL) and refluxed for 8 h. Whilst still warm, water (100 mL) was added and the volume reduced to ~125 mL by solvent evaporation. The resulting mixture was cooled to -25 °C overnight (freezer), and the precipitate filtered and dried *in vacuo* to afford the title compound as a bright yellow powder (15.88 g, 85%). Mp 114-117 °C; ^1H NMR (400 MHz, CDCl_3) δ 10.50 (d, $J = 5.5$ Hz, 1H), 7.97 (dd, $J = 10, 2.7$ Hz, 1H), 7.57-7.42 (m, 2H), 7.39-7.32 (m, 10H), 7.00-6.92 (m, 1H); ^{13}C NMR (100 MHz, CDCl_3) δ 191.9 (d, $J = 19$ Hz), 141.4, 136.2 (d, $J = 9$ Hz), 134.3, 134.1, 134.1, 133.8, 130.9 (d, $J = 4$ Hz), 129.3, 129.1, 128.9 (d, $J = 7$ Hz); ^{31}P NMR (162 MHz, CDCl_3) δ -11.00 (s); HRMS (ESI) m/z [$M\text{H}$] $^+$ 291.0944, (calculated for $\text{C}_{19}\text{H}_{16}\text{OP}$: 291.1016); IR ν cm^{-1} 3057 (w, br), 2851 (w), 1696 (m), 1672 (m), 1583 (w), 1432 (m), 1198 (m), 843 (m), 751 (s), 744 (s), 696 (s), 670 (s).

2-(Diphenylthiophosphino)benzaldehyde (40)

2-(Diphenylphosphino)benzaldehyde (1.48 g, 5 mmol) and S_8 (1.31 g, 5 mmol) were stirred together in THF overnight. The resulting mixture was centrifuged (3000 rpm, 3 min) to remove the solid sulfur, and the solvent removed *in vacuo*. Purification by column chromatography on silica gel eluting with petroleum ether to remove the remaining sulfur, and then diethyl ether: pentane (1:4 to 3:7), afforded the title compound as a cream powder (1.31 g, 81%). Mp 136-137 °C; ^1H NMR (400 MHz, CDCl_3) δ 10.71 (s, 1H), 8.11 (ddd, $J = 7.7, 4.0, 1.5$ Hz, 1H), 7.84-7.78 (m, 4H), 7.65-7.61 (m, 1H), 7.60-7.44 (m, 7H), 7.03 (ddd, $J = 14.6, 7.5, 1.0$ Hz, 1H); ^{13}C NMR (400 MHz, CDCl_3) δ 190.3 (d, $J = 8$ Hz), 138.0 (d, $J = 7$ Hz), 137.9 (d, $J = 79$ Hz), 132.8 (d, $J = 12$ Hz), 132.7 (d, $J = 10$ Hz), 132.5 (d, $J = 11$ Hz), 132.3 (d, $J = 3$ Hz), 132.1 (d, $J = 3$ Hz), 132.1 (d, $J = 85$ Hz), 129.9 (d, $J = 9$ Hz), 129.1 (d, $J = 13$ Hz); ^{31}P NMR (162 MHz, CDCl_3) δ 40.75 (s); HRMS (ESI) m/z [$M\text{Na}$] $^+$ 345.0478 (calculated for $\text{C}_{19}\text{H}_{15}\text{NaOPS}$: 345.0473); IR ν cm^{-1} 1685 (s), 1580 (w), 1435 (m), 1199 (m), 1099 (s), 822 (w), 749 (m), 711 (s), 691 (s), 640 (s), 633 (s), 613 (m).

β -[2'-(Diphenylthiophosphino)phenyl]acrylferrocene (33)

Acetyl ferrocene **35** (0.51 g, 0.002 mol) was dissolved in ethanol (2 mL) and a solution of 2-(diphenylthiophosphino)benzaldehyde **40** (0.43 g, 0.002 mol) in ethanol (1 mL) was added to the above mixture with stirring. After stirring for 0.5 h (until solid was dissolved) a solution of ethanol (2 mL), H₂O (2 mL) and NaOH (0.18 g) was added dropwise stirring at room temperature. A reddish precipitate appeared after some time which became difficult to stir. After two hours TLC analysis indicated the completion of the reaction. The mixture was poured into H₂O (25 mL) and neutralized to pH=7 with 2M HCl, cooled using ice, and then filtered. The solid was washed with water (3 \times 10 mL) and dried *in vacuo*. The crude product was recrystallized from chloroform to afford the final product as a light red crystalline solid (0.85g, 71%). Mp 163-165 °C; ¹H-NMR (400 MHz, CD₂Cl₂) δ 8.25 (d, *J*=15.5 Hz, 1H), 7.94-7.75 (m, 5H), 7.61 (d, *J* = 7.5 Hz, 1H), 7.54 (dd, *J*=7.0, 2.0 Hz, 2H), 7.50 (dd, *J*=7.5, 3.0 Hz, 3H), 7.48-7.47 (m, 1H), 7.35 (t, *J*=8.0 Hz, 1H), 7.14 (ddd, *J*=14.7, 7.8, 1.0 Hz, 1H), 6.83 (d, *J* = 15.5 Hz, 1H), 4.78-4.73 (m, 2H), 4.56-4.51 (m, 2H), 4.12 (m, 5H); ¹³C-NMR (100 MHz, CD₂Cl₂) δ 192.1, 139.9 (2C), 133.7 (2C), 132.9 (2C), 132.4 (2C), 132.3 (2C), 129.3 (2C), 129.2 (2C), 129.1 (2C), 126.2 (2C), 80.8, 73.2 (2C), 70.5 (2C), 70.1 (5C); ³¹P NMR (162 MHz, CD₂Cl₂) δ 42.05 (s); HRMS [*MH*]⁺: 533.4247 (Calcd. for (C₃₁H₂₆FePSO) 533.4167); IR ν cm⁻¹ 3089 (s), 1699 (s), 1643 (s), 1577 (s), 1448 (s), 1375 (s), 1244 (s), 1081 (s), 1001 (s), 976 (s), 821 (s), 743 (s).

2-Phenyl(triphenylphosphoranylidene)ethan-2-one (43)

A solution of α -bromoacetophenone (2.0 g, 1 eq., 10 mmol) in toluene (8 mL) was added dropwise to a solution of triphenylphosphine (2.63 g, 1 eq., 10 mmol) in toluene (8 mL) under a N₂ atmosphere. The mixture was stirred overnight and the resulting phosphonium salt was suspended in a mixture of water (100 mL) and methanol (100 mL). After stirring for 1 h, aqueous NaOH (1 M) was added dropwise until pH 7 was reached. The mixture was then stirred vigorously for 1 h. The white phosphorane was filtered, washed with water (15 \times 3) and dried *in vacuo*. Purification by recrystallisation from ethyl acetate afforded the title compound as an off-white solid (2.36 g, 68%). Mp 185-186 °C; ¹H NMR (400 MHz, CDCl₃) δ 7.99-7.92 (m, 2H), 7.75-7.65 (m, 6H), 7.57-7.50 (m, 3H), 7.50-7.44 (m, 6H), 7.36-7.30 (m, 3H), 4.46 (d, *J* = 24.5 Hz, 1H). ¹³C NMR (400 MHz, CDCl₃) δ 185.0 (d, *J* = 3 Hz), 141.3 (d, *J* = 15 Hz), 133.2 (d, *J* = 10

Hz), 132.1 (d, $J = 3$ Hz), 129.4, 129.0 (d, $J = 12$ Hz), 127.5, 127.2 (d, $J = 91$ Hz), 127.1, 51.1 (d, $J = 112$ Hz); ^{31}P NMR (162 MHz, CDCl_3) δ 17.80 (s). HRMS (ESI) m/z $[\text{MH}]^+$ 381.1403 (calculated for $\text{C}_{26}\text{H}_{22}\text{OP}$: 381.1403). IR ν cm^{-1} 1586 (m), 1511 (s), 1482 (m), 1435 (s), 1385 (s), 1104 (s), 871 (m), 747 (m), 707 (s), 688 (s).

Lei Ligand (17)

2-(Diphenylphosphino)benzaldehyde (0.49 g, 1 eq., 1.55 mmol) and 2-phenyl(triphenylphosphoranylidene)ethan-2-one (1.17 g, 3.1 mmol) were added to an oven-dried Schlenk flask charged with degassed toluene (10 mL) under a N_2 atmosphere. The resulting mixture was heated to reflux for 24 h. After the toluene was removed *in vacuo*, purification by column chromatography on silica gel eluting with ethyl acetate: petroleum ether (7:93) afforded the title compound as a cream solid (0.85 g, 76%). Mp 91-94 °C (no reported Mp) ^{131}I ; ^1H NMR (400 MHz, CDCl_3) δ 8.35 (dd, $J = 15.8, 4.5$ Hz, 1H), 7.75-7.71 (m, 3H), 7.55-7.51 (m, 1H), 7.42-7.25 (m, 14H), 7.18 (dd, $J = 15.8, 1.0$ Hz, 1H), 6.93 (ddd, $J = 7.7, 4.5, 1.0$ Hz, 1H). ^{13}C NMR (100 MHz, CDCl_3) δ 192.1, 143.7 (d, $J = 25$ Hz), 139.8 (d, $J = 22$ Hz), 138.5 (d, $J = 16$ Hz), 138.0, 136.0 (d, $J = 10$ Hz), 134.2 (d, $J = 20$ Hz), 133.8, 132.6, 130.1, 129.3, 129.1, 128.8, 128.7, 128.7 (d, $J = 24$ Hz), 127.1 (d, $J = 4$ Hz), 125.7 (d, $J = 4$ Hz). ^{31}P NMR (162 MHz, CDCl_3) δ -13.32 (s); HRMS (ESI) m/z $[\text{MH}]^+$ 393.1405 (calculated for $\text{C}_{27}\text{H}_{22}\text{OP}$: 393.1403); IR ν cm^{-1} 1667 (s), 1605 (s), 1432 (s), 1309 (m), 1214 (m), 1011 (m), 744 (s), 694 (s). The ^{31}P NMR peak for the (side product): δ 31.07 (s).

Thio-Lei Ligand (46)

2-(Diphenylthiophosphino)benzaldehyde (0.49 g, 1.55 mmol) and 2-phenyl(triphenylphosphoranylidene)ethan-2-one (1.17 g, 3.11 mmol) were added to an oven-dried Schlenk flask charged with degassed toluene (10 mL) under a N_2 atmosphere. The resulting mixture was heated to reflux for 24 h. After the toluene was removed *in vacuo*, purification by column chromatography on silica gel eluting with ethyl acetate: petroleum ether (7:93) afforded the title compound as a cream solid (0.85 g, 64.5%). Mp 110-113 °C (novel so no mp); ^1H NMR (400 MHz, CDCl_3) δ 8.23 (d, $J = 15.5, 1$ Hz, 1H), 7.82 (m, 1H), 7.78 (m, 2H), 7.73 (m, 2H), 7.68 (m, 2H), 7.53 (m, 1H), 7.47 (m, 3H), 7.40 (m, 6H), 7.35 (m, 1H), 7.15 (m, 1H), 7.08 (d, $J = 14.4$ Hz, 1H). ^{13}C NMR (100 MHz, CDCl_3) δ 191.9, 143.7 (d, $J = 25$ Hz), 138.9 (d, $J = 22$ Hz), 137.4 (d, $J = 16$ Hz), 134.0, 133.2 (d, $J = 10$ Hz), 132.4 (d, $J = 20$ Hz), 132.3, 132.1, 131.8, 131.7, 129.3,

128.6, 128.6, 128.4 (d, $J = 24$ Hz), 128.2 (d, $J = 4$ Hz), 126.2 (d, $J = 3$ Hz); ^{31}P NMR (162 MHz, CDCl_3) δ 42.1 (s, 1P); HRMS (ESI) m/z $[\text{MH}]^+$ 425.1134 (calculated for $\text{C}_{27}\text{H}_{22}\text{OPS}$: 425.1123); IR ν cm^{-1} 3052 (s), 2286 (s), 1664 (s), 1609 (s), 1595 (s), 1579 (s), 1558 (s), 1459 (s), 1446 (s), 1435 (s), 1332 (s), 1311 (s), 1284 (s), 1217 (s), 1178 (s), 1106 (s), 1014 (s), 997 (s), 984 (s), 734 (s), 634 (s).

β -(2-Bromophenyl)acrylferrocene (42)

Acetyl ferrocene (0.47 g, 0.002 mol) was dissolved in 95 % ethanol (1.81 mL) and a solution of *o*-bromobenzaldehyde (0.43 g, 0.002 mol) in 95% ethanol (0.5 mL) was added to the above mixture with stirring, which was continued for 0.5 h until all the solid had dissolved. A solution of ethanol (2mL), H_2O (2 mL) and NaOH (0.1 g) was added dropwise to the above mixture under stirring at room temperature. A reddish precipitate was formed, and after two hours TLC analysis indicated the completion of the reaction. The mixture was poured into water (10 mL) and neutralized to pH=7 with 2 M HCl, then cooled and filtered. The solid precipitate was washed with water (10×3) and dried *in vacuo*. The crude product was recrystallised from chloroform as dark claret red-coloured crystals (0.67 g, 82%). Mp 118-121 °C; ^1H -NMR (400 MHz, CDCl_3) δ 8.11 (d, $J = 15.7$ Hz, 1H), 7.68 (dd, $J = 24.5, 8.0$ Hz, 2H), 7.38 (t, $J = 7.5$ Hz, 1H), 7.19 (s, 1H), 7.04 (d, $J = 15.7$ Hz, 1H), 4.91 (s, 2H), 4.60 (s, 2H), 4.24 (s, 5H). ^{13}C -NMR (100 MHz, CDCl_3) δ 193.1, 139.4, 135.4, 133.6, 131.0, 127.9, 127.7, 126.2, 125.8, 80.3, 73.0 (2C), 70.2 (2C), 69.9 (5C); LRMS (EI) m/z : 394(M+H, 100), 396 (88), 392 (3), 316 (15), 315 (70), 165 (46), 121 (16), 56 (14); HRMS (ESI) m/z $[\text{MH}]^+$ 393.97 (Calcd. for $\text{C}_{19}\text{H}_{15}\text{BrFeO}$: 393.97); IR ν cm^{-1} 3096 (m), 2360 (s), 1653 (s), 1596 (s), 1454 (s), 1376 (s), 1077 (s), 1001 (s), 759 (s).

2.5.2 X-Ray Diffraction Data

Diffraction data for ferrochalcone (ijf0903) **32** was collected at 110 K on a Bruker Smart Apex diffractometer with Mo- K_α radiation ($\lambda = 0.71073$ Å) using a SMART CCD camera. Diffractometer control, data collection and initial unit cell determination was performed using "SMART". Frame integration and unit-cell refinement was carried out with "SAINT+". Absorption corrections were applied by SADABS. Structures were solved by "direct methods" using SHELXS-97 (Sheldrick, 1997)¹³² and

refined by full-matrix least squares using SHELXL-97 (Sheldrick, 1997).¹³³ All non-hydrogen atoms were refined anisotropically.

Diffraction data for thio-Lei ligand (ijf0927) **46** was collected at 120 K on an Oxford Diffraction SuperNova diffractometer with Cu-K α radiation ($\lambda = 1.5418 \text{ \AA}$) using an Enhance (Cu) X-ray source. Structures were solved by “direct methods” using SHELXS-97 (Sheldrick, 1997)¹³⁴ and refined by full-matrix least squares using SHELXL-97 (Sheldrick, 1997).¹³⁵ All non-hydrogen atoms were refined anisotropically.

Table 1: Single Crystal X-Ray details for ferrochalcone ligand (32) and Thio-Lei ligand (46).

Compound reference	ijf0903 (32)	ijf0927 (46)
Formula	C ₃₁ H ₂₅ FeO _{1.20} P	C ₂₇ H ₂₁ OPS
Formula weight	503.51	424.47
temp (K)	110(2)	120(2) K
Radiation	0.71073	1.5418
Cryst syst	Monoclinic	Monoclinic
Space group	Cc	P 2(1)/n
a(Å)	13.3506(15)	8.9290(2)
b(Å)	22.153(3)	14.3223(2)
c(Å)	10.0115(11)	17.0656(3)
α(°)	90°	90
β(°)	125.790(2)	100.6739(19)
γ(°)	90°	90
V (Å³)	2401.9(5)	2144.66(7)
Z	4	4
D_{calcd.} (Mg M⁻³)	1.384	1.315
F(000)	1046.4	888
M(mm⁻¹)	5.038	2.163
Crystal size (mm³)	0.20 x 0.17 x 0.03	0.21 x 0.21 x 0.21
θ range for data	1.84 to 28.30	4.06 to 70.90
Collection (°) Index ranges	-17 ≤ h ≤ 17, -29 ≤ k ≤ 29, -13 ≤ l ≤ 12	-10 ≤ h ≤ 10, -17 ≤ k ≤ 17, -20 ≤ l ≤ 20
No. of reflections collected	12146	19785
Refinement method	Full-matrix least-squares on F ²	Full-matrix least-squares on F ²
GOOF on F²	1.017	1.079
R1, wR2(I > 2σ(I))	0.0324, 0.0733	0.0425, 0.1186
R1, wR2(all data)	0.0389, 0.0766	0.0517, 0.1269

Further details can be found in the Appendix, including the cif files on the CD.

Chapter 3: Late transition metal complexes of alkene-phosphine and thio alkene phosphine ligands

Ferrochalcone **32** and thio-ferrochalcone **33** can be regarded as bidentate ligands. The ligand can bind through the alkene and phosphine moieties. In some cases coordination *via* the carbonyl group may also be possible. The potential coordination modes (a-d) of the ligands to metals are given in Figure 1.

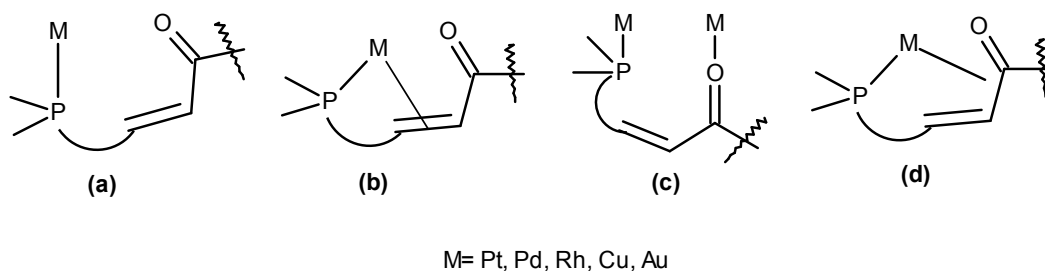


Figure 1: Potential coordination modes of phosphino-alkene ligands to metals.

In our ligands, the phosphines would be expected to be the most strongly coordinating moiety to late transition metals (a). The coordination of the alkenes (b) and/or the carbonyl (c) will depend on the oxidation state (*e.g.* Pt^0/Pd^0 are expected to be more likely to coordinate the alkene than $\text{Pt}^{\text{II}}/\text{Pd}^{\text{II}}$), the other ligands around the metal, the coordination number of the complex and the geometry of the ligand backbone as compared to the rest of the complex. In Rh complexes alkenes generally coordinate as long as there are free coordination sites. For most known copper complexes only the phosphine is bound to the Cu^{I} centre, with the alkene left non-coordinated. However, recently a few complexes did show evidence for alkene coordination in Cu^{I} complexes *e.g.* dbathiophos.¹³⁶

As shown in the introduction chapter, phosphino-alkene ligands have been utilised in Pd, Pt, Cu and Rh-catalysed reactions¹³⁷. In this chapter coordination chemistry studies involving Pd, Pt, Cu and Rh are described. These allow one to obtain a greater understanding of the ligand environment created around the metal centre.

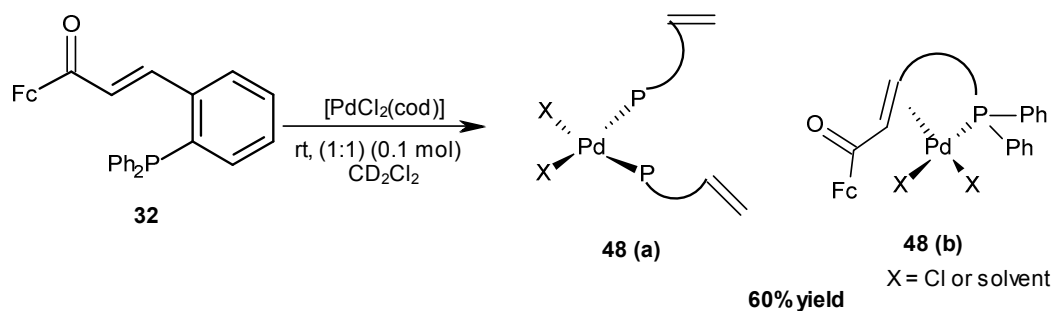
3.1 Synthesis and characterization of palladium and platinum complexes with alkene-phosphine ligands

The ferrocene ligand **32** and Lei ligand¹³⁸ **17** have three possible coordination modes.¹³⁹ In addition to the electronic nature of olefin, there are certain other factors which must be taken into account to understand the alkene-metal coordination. Several studies have examined the effect of variables such as metal oxidation state, number of d-electrons, and ligand properties on the strength of alkene binding to metal.¹⁴⁰ It was anticipated that the platinum(II) and palladium(II) complexes will exhibit a square planar geometry.¹⁴¹ In the following sub-sections are detailed the coordination of both Pd and Pt to ligands **32** and **17**.

3.1.1 Pd^{II} complexes

3.1.1.1 Ferrocene ligand (**32**) complexation

[PdCl₂(cod)] is a useful Pd^{II} precursor complex that can be used to form [PdCl₂(L)₂] complexes.¹⁴² Ferrocene ligand **32** on reaction with [PdCl₂(cod)] resulted in the displacement of the labile cod ligand to give a palladium(II) complex which could be **48a** or **48b** as a red solid. As with the free ligand the red colour is associated with the Fe^{II} centre (Scheme 1).

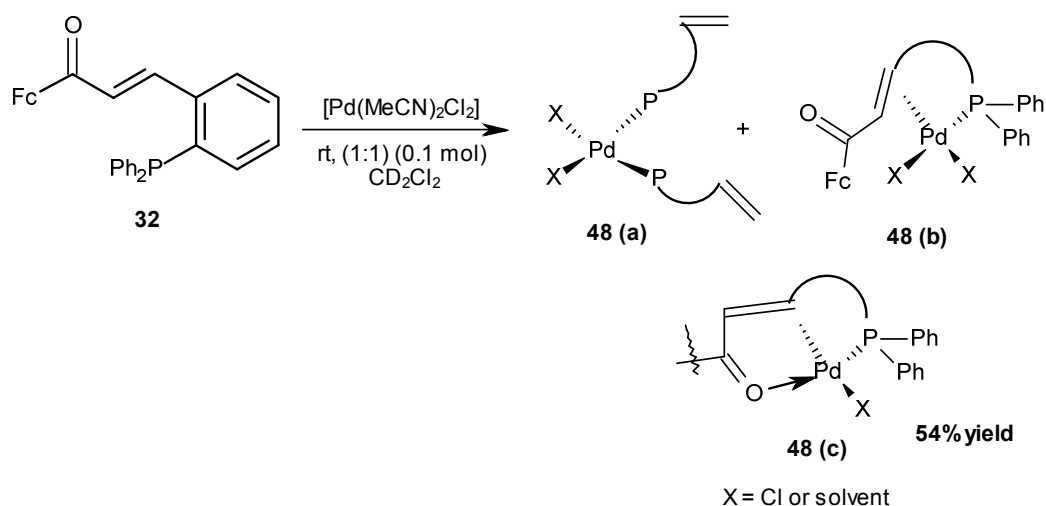


Scheme 2: Synthesis of palladium(II) complex of **32 using [Pd(cod)Cl₂].**

The Pd^{II} complex was found to be highly unstable in solution (*i.e.* it undergoes oxidation) and is also light sensitive. It was difficult to separate the cod ligand from complex **48**. Repeated attempts to crystallize the complex were unsuccessful. The ³¹P NMR showed a single peak at δ 21.4 in the complexed ligand as compared to non-coordinated ligand (δ -13.0). No evidence for alkene coordination was observed in the ¹H NMR spectrum. The ν (C=O) stretching frequency for complex **48** was almost

unchanged (1652 cm^{-1}) as compared to that of the free ligand (1653 cm^{-1}) hence it could be **48 (a)**.

Another attempt to synthesise palladium(II) complexes of ferrocene ligand **32** was carried out using an alternative precursor, namely $[\text{PdCl}_2(\text{MeCN})_2]$. Ligand **32** was reacted with $[\text{PdCl}_2(\text{MeCN})_2]$ in a ligand metal: ratio of 1:1 and 2:1 giving an insoluble reddish material **48**. The Pd^{II} complex crashed out of solution almost instantaneously (Scheme 2).



Scheme 2: Synthesis of the palladium(II) complex of 32 using $[\text{Pd}(\text{MeCN})_2\text{Cl}_2]$.

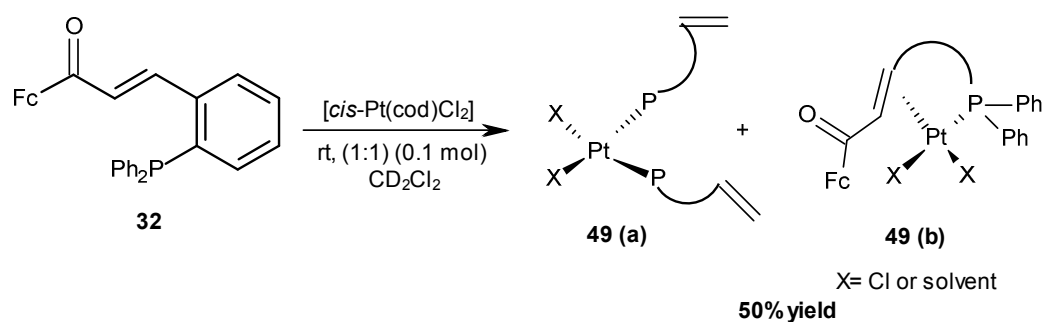
The Pd complex was insoluble in common organic solvents (slightly soluble in dichloromethane). Because of the solubility problem it was difficult to characterize the product. A weak ^{31}P NMR spectrum was obtained in both cases, in the 1:1 case a single peak at δ 21.7 was observed which has shifted from δ -13.0 in uncoordinated ligand whereas in the 2:1 complex two peaks were observed with a chemical shift value of δ 21.7 and δ 53.98 indicating two complexes in solution. A similar reaction on MonodbaPHOS conducted using $[\text{PdCl}_2(\text{MeCN})_2]$ gave a Pd complex with a structure of **48c**.¹⁴³ The ^{31}P NMR for the complex exhibited a peak at 54.0 ppm. So any of the above products could be possible. Attempts to separate the complexes by crystallisation proved unsuccessful. The material produced in this reaction is most likely polymeric.

3.1.2 Platinum metal complexes

3.1.2.1 Pt^{II} complexes

3.1.2.1.1 Ferrocene ligand (**32**) complexation

Complex **51** was prepared by reacting **32** with $[cis\text{-Pt}(\text{cod})\text{Cl}_2]$ in a ligand exchange reaction as shown in Scheme 3.



Scheme 3: Novel platinum(II) complex containing ligand 32.

Room temperature stirring of **32** with $[cis\text{-PtCl}_2(\text{cod})]$ in a metal-to-ligand ratio of 1:1 in CH_2Cl_2 resulted in a dark reddish coloured solution. Finally it was filtered to remove insoluble material. The reddish product obtained on removing the solvent *in vacuo* was characterised by different techniques. Initially the structure of the Pt complex was established by FT-IR and NMR spectroscopic analysis. The IR spectrum of **49** showed a characteristic peak at 1669 cm^{-1} for the carbonyl group as compared to that of ligand (1653 cm^{-1}). The coordination of the phosphine moiety was inferred by the significant shift of the ^{31}P signal ($\delta\ 23.3$) compared to that of the free ligand ($\delta\ -13.0$). The spin-spin coupling constant $^1J(\text{M-P})$ are a characteristic property of the metal phosphorus σ bond in phosphorus coordination compounds.¹⁴⁴ The $^1J(\text{Pt-P})$ value for the above complex was determined to be 3059 Hz, which indicates the complex is *cis*. The $^1J_{\text{PtP}}$ coupling value can be used to identify *cis* vs. *trans* coordination of the phosphines in a square planar complex. Typically, if the phosphines are *trans* a coupling constant of 1500-3000 Hz would be expected e.g. *trans*- $[\text{PtCl}_2(\text{PEt}_3)_2]$ spin-spin coupling constant is 2490, whereas the coupling constant for a *cis* complex would be higher, $>3000\text{ Hz}$ in most cases e.g. for *cis*- $[\text{PtCl}_2(\text{PPh}_3)_2]$ spin-spin coupling constant is 3673¹⁴⁵ However, no evidence for alkene coordination was observed in the ^1H NMR spectrum as two of the alkene protons have only shifted upfield to $\delta\ 8.07$ (for free ligand $\delta\ 8.43$) and $\delta\ 6.41$ (for free ligand $\delta\ 6.86$) and hence it could be concluded that the product obtained was **49a**.

On crystallisation of **49** from $\text{CH}_2\text{Cl}_2/\text{Et}_2\text{O}$ fine red crystals were formed. These crystals were then analysed by X-ray diffraction methods to obtain a solid-state structure. In this case the X-ray structure shows that the ferrocenyl phosphine ligand **32** acts as bidentate ligand

binding through both the phosphorus and the alkene moiety, giving a square planar geometry as expected for Pt^{II} complexes (Figure 2).

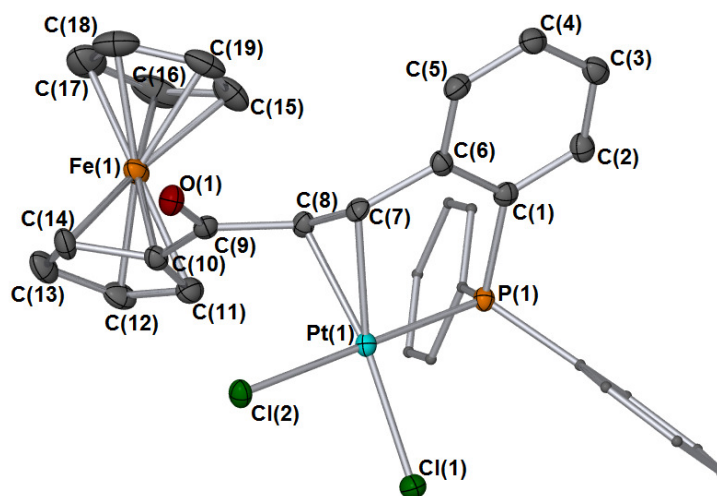


Figure 2: X-ray crystal structure of complex 49.

Hydrogen atoms removed for clarity. Thermal ellipsoids shown at 50%. Bond lengths (Å): Cl(1)-Pt(1) = 2.3072(8), Cl(2)-Pt(1) = 2.3524(7), P(1)-Pt(1) = 2.2373(8), C(8)-Pt(1) = 2.140(3), C(7)-Pt(1) = 2.174(3), C(9)-O(1) = 1.219(4), C(7)-C(8) = 1.402(4), C(6)-C(7) = 1.489(4), P(1)-C(5) = 1.797(3), P(1)-C(20) = 1.809(3), P(1)-C(26) = 1.808(3), Bond Angles(°): C(8)-Pt(1)-C(7) = 37.93(11), C(8)-Pt(1)-P(1) = 89.61(8), C(7)-Pt(1)-P(1) = 83.77(8), C(8)-Pt(1)-Cl(2) = 90.37(8), C(7)-Pt(1)-Cl(2) = 96.96(8), P(1)-Pt(1)-Cl(2) = 178.77(3), C(8)-Pt(1)-Cl(1) = 162.89(9), C(7)-Pt(1)-Cl(1) = 159.02(8), P(1)-Pt(1)-Cl(1) = 91.42(3), Cl(2)-Pt(1)-Cl(1) = 88.23(3).

The complexed alkene double bond C(7)-C(8) in [Pt(C₃₁H₂₅FePO)Cl₂] is 1.402 Å as compared to that of a non-complexed double bond in alkene (1.334 Å for ethene).¹⁴⁶ This increase in bond length indicates that there is some back-donation occurring. The Pd^{II} complex obtained on crystallization **49b** was different from the one concluded on the basis of NMR spectroscopy.

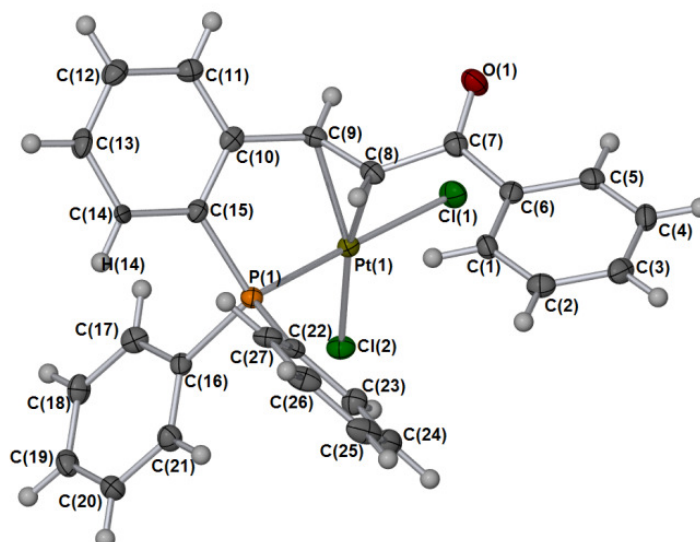


Figure 3: X-ray crystal structure of complex 50b.

Hydrogen atoms removed for clarity. Thermal ellipsoids shown at 50%. Bond lengths(Å): Cl(1)-Pt(1) = 2.3579(8), Cl(2)-Pt(1) = 2.2924(8), P(1)-Pt(1) = 2.2452(8), C(8)-Pt(1) = 2.152(3), C(9)-Pt(1) = 2.161(3), C(7)-O(1) = 1.214(4), C(8)-C(9) = 1.402(5), C(7)-C(8) = 1.402(4), C(6)-C(7) = 1.489(4), P(1)-C(5) = 1.797(3), P(1)-C(20) = 1.809(3), P(1)-C(26) = 1.808(3), Bond Angles(°): C(8)-Pt(1)-C(9) = 37.94(13), C(8)-Pt(1)-P(1) = 85.90(9), C(9)-Pt(1)-P(1) = 84.60(9), C(8)-Pt(1)-Cl(2) = 165.55(9), C(9)-Pt(1)-Cl(2) = 156.00(9), P(1)-Pt(1)-Cl(2) = 91.76(3), C(8)-Pt(1)-Cl(1) = 92.99(9), C(9)-Pt(1)-Cl(1) = 95.67(9), P(1)-Pt(1)-Cl(1) = 177.84(3), Cl(2)-Pt(1)-Cl(1) = 88.85(3).

The XRD analysis for the crystals confirmed that the Lei ligand acts as a bidentate ligand coordinating through both the phosphorus and alkene double bond. The Pt^{II} atom showed a square-planar coordination mode as expected for platinum(II) metal complexes.¹⁴⁷ On coordination there was an increase in the bond length for the alkene double bond from (1.334 Å) for the non-complexed ligand to 1.402(5) Å for the complexed ligand, providing an indication of loss of electron density on coordination to Pt^{II}.

A comparison of Pt^{II} complexes for the different ligands is given in Table 1. All of these platinum(II) metal complexes exhibit a square planar geometry.

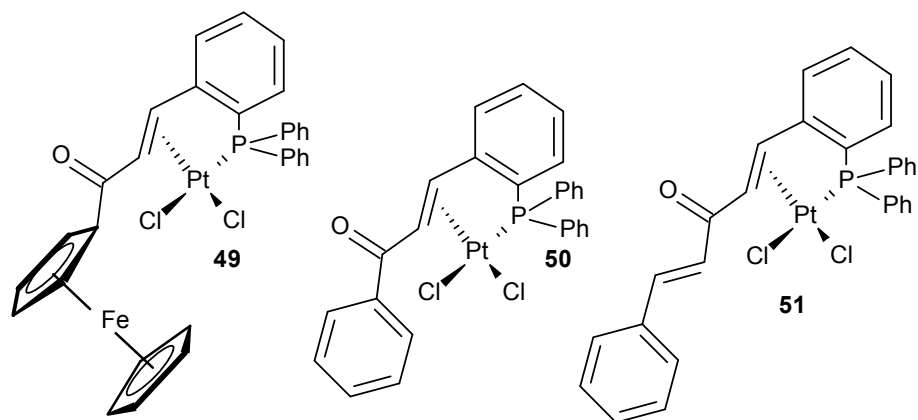
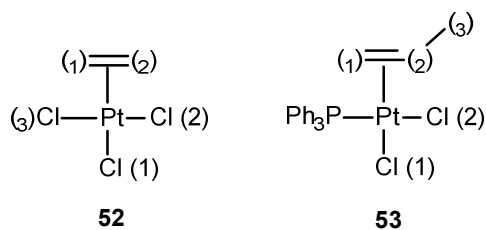


Table 1: Comparison of the bond lengths in Platinum(II) complexes of ferrochalcone, Lei ligand and MonodbaPHOS.

Bonds	PtCl ₂ (ferrochalcone) (49)	PtCl ₂ (Lei) (50)	PtCl ₂ (monodbaPHOS) ¹⁴ (51)
Pt(1)-P(1)	2.2373 (8)	2.2452 (8)	2.2363 (8)
Pt(1)-Cl cis to alkene	2.3524 (7)	2.3579 (8)	2.3429 (8)
Pt(1)-Cl trans to alkene	2.3072 (8)	2.2924 (8)	2.2995 (8)
Pt(1)-C nearest C=O	2.140 (3)	2.152 (3)	2.132 (3)
Pt(1)-C	2.174 (3)	2.161 (3)	2.175 (3)
C=C coordinated	1.402 (4)	1.402 (5)	1.399 (5)
C=C uncoordinated			1.341 (5)
C=O	1.219 (4)	1.214 (4)	1.215 (4)

In addition to this a comparison of the bond lengths between the platinum(II) complexes of ferrochalcone **32**, Lei ligand **17** and some other alkene ligands is given in Table 2.



PtCl ₂ (ferrochalcone) (49)		PtCl ₂ (Lei) (50)		Zeise's Salt (52) ¹⁴⁸		(53) ¹⁴⁹	
Bond	Length, Å	Bond	Length, Å	Bond	Length, Å	Bond	Length, Å
P(1)-Pt(1)	2.2373 (8)	P(1)-Pt(1)	2.2452 (8)	Cl(1)-Pt (<i>trans</i>)	2.340 (2)	P-Pt	2.2610 (7)
Cl(1)-Pt (1)	2.3072 (8)	Cl(1)-Pt (1)	2.3579 (8)	Cl(2)-Pt (<i>cis</i>)	2.302 (2)	Cl(1)-Pt (<i>trans</i>)	2.3195 (8)
Cl(2)-Pt (1)	2.3524 (7)	Cl(2)-Pt (1)	2.2924 (8)	Cl(3)-Pt (<i>cis</i>)	2.303 (2)	Cl(2)-Pt (<i>cis</i>)	2.3623 (8)
C(7)-Pt (1)	2.174 (3)	C(8)-Pt (1)	2.152 (3)	C(1)-Pt	2.128 (3)	C(1)-Pt	2.146 (3)
C(8)-Pt(1)	2.140 (3)	C(9)-Pt(1)	2.161 (3)	C(2)-Pt	2.135 (3)	C(2)-Pt	2.188 (3)
C(7)-C(8)	1.402(4)	C(8)-C(9)	1.402(5)	C(1)-C(2)	1.375 (4)	C(1)-C(2)	1.394 (5)
C(9)-O(1)	1.219 (4)	C(7)-O(1)	1.214 (4)			C(2)-C(3)	1.497 (6)

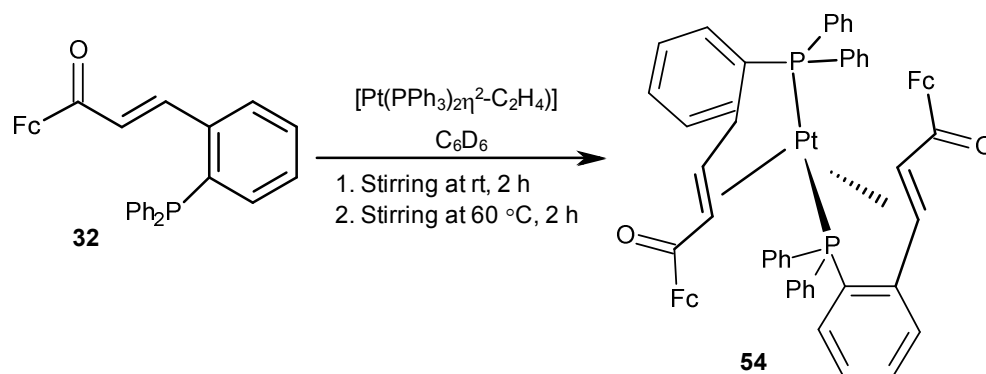
Table 2: Comparison of the bond lengths in Platinum(II) complexes of ferrochalcone, Lei ligand, Zeise's salt and compound (53).

The bond length for C=C in ethene is 1.33 Å. The non-complexed C=C bond length in all of these complexes is similar to ethene, 1.334 Å. However, the complexed C=C bond length has increased in all of these cases, indicating the increase in sp³-character on complexation. From the comparison between these complexes, it is apparent that an increase in bond length is larger in the Pt^{II} complexes for the ferrocene and Lei ligand, as compared to Zeise's salt **52** or complex **53** showing that there is more back-donation occurring. This is expected as the enone moiety is more electron-accepting than ethene.

3.1.2.2 Pt⁰ complexes

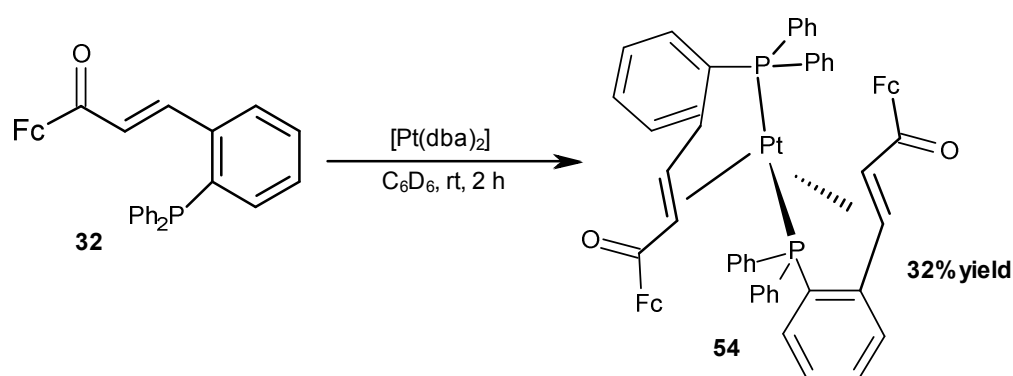
3.1.2.2.1 Ferrocene ligand (**32**) complexation

Ferrocene **32** was reacted with [Pt⁰(PPh₃)₂η²-C₂H₄]¹⁵⁰ under different reaction conditions to give the Pt⁰ complex **54**. Initially a room temperature reaction over 2 h in benzene gave a dark red solution. On removal of the solvent, a dark red solid was obtained, which was characterised. The ¹H and ³¹P NMR spectra showed the formation of a new complex along with some starting material. The reaction was repeated again by increasing the reaction time by 2 giving the same result. The reaction was again repeated by increasing the temperature to 60 °C for 2 h. On cooling the reaction mixture, filtration and solvent removal *in vacuo* which afforded a red powder. The crude material was analysed by NMR spectroscopy and found to be a mixture of starting material along a small amount of the complex. Attempts to crystallize the Pt⁰ complex from different solvents (*e.g.* chloroform, DMSO and benzene) were unsuccessful (Scheme 5).



Scheme 5: Synthesis of platinum(0) complex of **32** using [Pt⁰(PPh₃)₂η²-C₂H₄].

Another attempt at synthesising the Pt⁰ complex was made using [Pt(dba)₂], which is a common starting material for synthesizing Pt⁰ complexes.¹⁵¹ A solution of ferrochalcone **32** in benzene was added to a solution of Pt(dba)₂ in benzene in a ligand to metal ratio of 2:1 (Scheme 6). The reaction mixture was stirred at room temperature for 2 h. Finally, on removal of the solvent *in vacuo* after filtration, a red powder was obtained **54**. The crude material was analysed by ¹H and ³¹P NMR spectroscopy and was found to be a mixture of starting material **32** and the complex. The ³¹P NMR spectrum showed a shift for the phosphorus signal from δ -13.0 to δ 21.4 with platinum satellite signals (*J*_{Pt-P} = 2912 Hz). The yield of the reaction was low (32 %). Also, it was not possible to separate the Pt complex from **32**.



Scheme 6: Synthesis of platinum(0) complex of 32 using [Pt(dba)₂].

Tiny red crystals of **54** were obtained on standing a solution of the crude material in benzene for 2-3 weeks in the dark. The yield of the crystals was low and crystal picking was needed for the XRD analysis. It is not clear whether this structure is representative of the bulk material. The low quantity of the crystals prevented further characterization (by NMR, IR spectroscopy and mass spectrometry) (Figure 4).

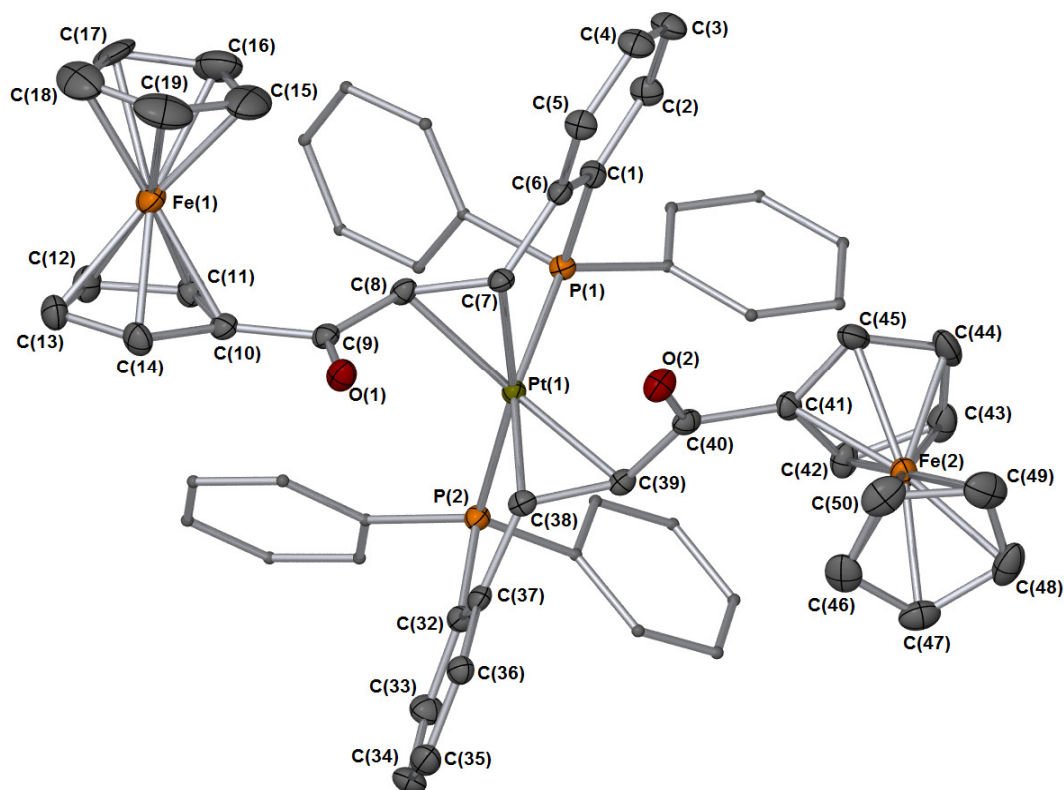


Figure 4: X-ray crystal structure of Pt⁰ metal complex of 32.

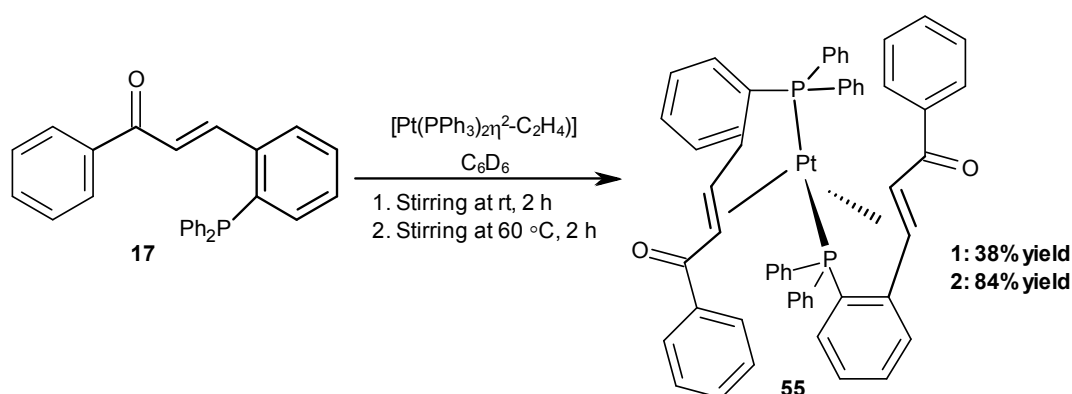
Hydrogen atoms removed for clarity. Thermal ellipsoids shown at 50%. Bond lengths(Å): C(9)-O(1) = 1.237(3), C(40)-O(2) = 1.239(3), C(8)-C(9) = 1.465(4), C(39)-C(40) = 1.467(4), C(7)-C(8) = 1.446(4), C(38)-C(39) = 1.444(4), C(8)-Pt(1) = 2.243(3), C(39)-Pt(1) = 2.206(3), C(7)-Pt(1) = 2.133(3), C(38)-Pt(1) = 2.126(3), P(1)-Pt(1) = 2.3189(7), P(2)-Pt(1) = 2.3094(7), Bond Angles (°): C(7)-C(8)-Pt(1) = 66.62(15), C(6)-C(7)-Pt(1) = 114.80(19), C(8)-C(7)-Pt(1) = 74.91(16), C(9)-C(8)-Pt(1) = 115.85(19), C(20)-P(1)-C(26) = 104.2(13), C(20)-P(1)-C(1) = 102.7(13), C(26)-P(1)-C(1) = 103.5(13), C(20)-P(1)-Pt(1) = 126.8(9), C(26)-P(1)-Pt(1) = 114.5(9), C(1)-P(1)-Pt(1) = 101.9(10).

The reaction of [Pt⁰(dba)₂] with ferrocene **32** therefore gave a novel Pt(0) complex **54**. The XRD studies showed that each of the two molecules of the ligand are both P and π -olefin bound to Pt, giving an 18 e⁻ tetrahedral complex. The chalcone ferrocene ligand is acting as a bidentate ligand coordinating through both alkene and phosphine moieties. Interestingly, the metal coordination by two P atoms and two π -olefinic bonds is intermediate between square-planar and tetrahedral, which would be expected for Pt⁰ complexes.¹⁵² The olefinic C7=C8 bond lengthens from 1.332 Å (for non-complexed

alkene) to 1.446(4) Å, whereas the bond length for olefinic bond C38=C39 lengthens to 1.444(4) Å in the metal complex.

3.1.2.2.2 Complexation of the Lei ligand

The Pt⁰ metal complex was obtained by reacting [Pt⁰(PPh₃)₂η²-C₂H₄] with two equivalents of the Lei ligand **17** in benzene. The reaction mixture was stirred for 2 h at 60 °C (Scheme 7). On cooling, the solvent was removed *in vacuo* affording a red powder.



Scheme 7: Synthesis of Pt⁰ complex of the Lei-ligand **17** using [Pt⁰(PPh₃)₂η²-C₂H₄].

The structure of the Pt⁰ complex **55** was established by NMR spectroscopy and mass spectrometry. The ³¹P NMR spectrum showed a chemical shift change from δ -13.0 to δ 21.2 with platinum satellite signals. This provides evidence of a phosphorus-platinum interaction. The ¹J(Pt-P) value for above complex was found to be 2933 Hz, which shows that the phosphorus atoms are arranged *cis*.

Similarly, the ¹H NMR spectrum of complex **55** showed a shift for both of the α- and β-protons. Interestingly, in the ¹H NMR spectrum there were platinum satellite signals confirming Pt-H interaction. A 2D Pt-H HMQC study confirmed the platinum interaction with the protons (coordinated to Pt) as shown below in Figure 5.

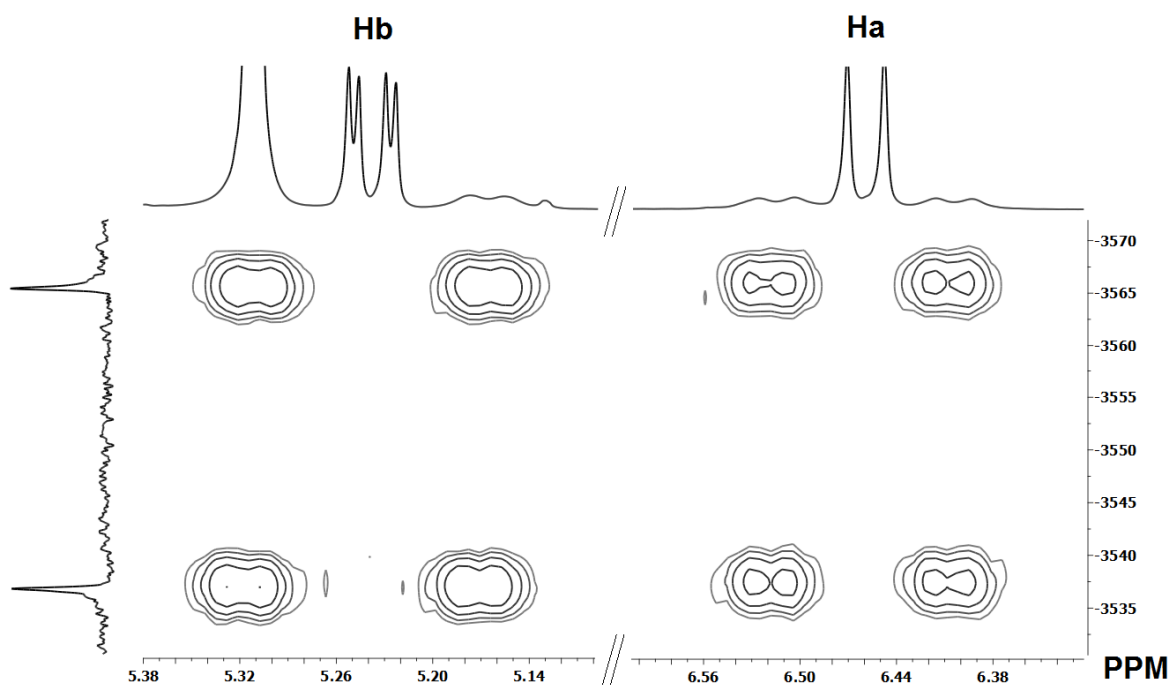


Figure 5: The ^1H - ^{135}Pt HSQC spectrum of complex **55.**

The molecular ion peak for the complex appeared at m/z 979.9470, which is $[\text{Pt}(\text{C}_{27}\text{H}_{21}\text{PO})_2]^+$. The reaction of $[\text{Pt}^0(\text{PPh}_3)_2\eta^2\text{-C}_2\text{H}_4]$ with two equivalents of Lei ligand **17** at 60 °C over 1 h gave a novel Pt^0 species. Attempts to crystallise the complex, gave light red crystals from a benzene solution. The X-ray structure for the Pt^0 complex **55** is given in Figure 6 overleaf.

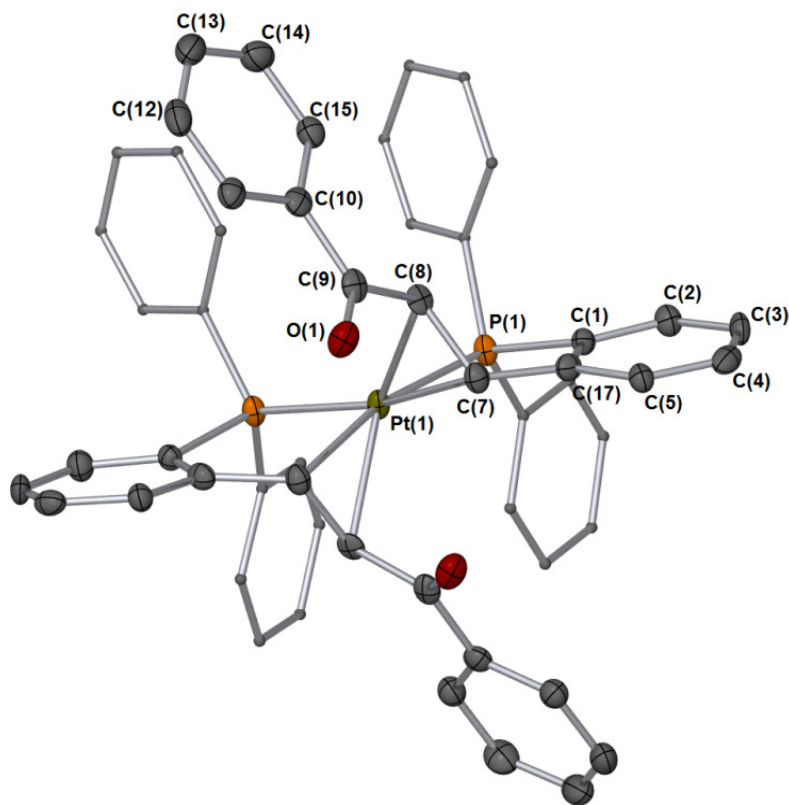


Figure 6: X-ray crystal structure of Pt⁰ metal complex of the Lei ligand 17.

Hydrogen atoms removed for clarity. Thermal ellipsoids shown at 50%. Bond lengths (Å): C(9)-O(1) = 1.238(7), C(8)-C(9) = 1.457(8), C(7)-C(8) = 1.448(8), C(8)-Pt(1) = 2.255(5), C(7)-Pt(1) = 2.125(5), P(1)-C(1) = 1.830(5), P(1)-C(22) = 1.827(6), P(1)-C(16) = 1.818(6), P(1)-Pt(1) = 2.3161(14), Bond Angles(°): C(7)-C(8)-Pt(1) = 65.9(3), C(6)-C(7)-Pt(1) = 115.4(4), C(8)-C(7)-Pt(1) = 75.6(3), C(9)-C(8)-Pt(1) = 113.0(4), C(16)-P(1)-C(22) = 106.2(3), C(16)-P(1)-C(1) = 104.1(3), C(22)-P(1)-C(1) = 106.4(3), C(16)-P(1)-Pt(1) = 121.12(19), C(22)-P(1)-Pt(1) = 114.79, C(1)-P(1)-Pt(1) = 102.79.

The XRD studies showed that the Pt metal is bonded to two of the ligands and each ligand is interacting with the metal through both alkene and phosphine moieties. The geometry obtained as a result of XRD studies gives a structure which is somewhat intermediate between square-planar and tetrahedral, as expected for Pt⁰ complexes. The olefinic C7=C8 bond lengthens from 1.332 Å (for non-complexed alkene) to the average of 1.448(8) in the metal complex due to the Pt⁰ coordination.

A comparison of the bond lengths between the Pt⁰ metal complex for the ferrochalcone **32** and Lei ligand **17** are given in Table 3.

Table 3: Comparison of the bond lengths in Pt⁰ complexes of 54 and 55.

Pt ⁰ complex (54)		Pt ⁰ complex (55)	
Bond	Length, Å	Bond	Length, Å
C(7)-C(8)	1.446(4)	C(7)-C(8)	1.448(8)
C(9)-O(1)	1.237(3)	C(9)-O(1)	1.238(7)
C(8)-Pt(1)	2.243(3)	C(8)-Pt(1)	2.255(5)
C(7)-Pt(1)	2.133(3)	C(7)-Pt(1)	2.125(5)
P(1)-C(1)	1.817(3)	P(1)-C(1)	1.830(5)
P(1)-C(20)	1.820(3)	P(1)-C(22)	1.827(6)
P(1)-C(26)	1.830(3)	P(1)-C(16)	1.818(6)
P(1)-Pt(1)	2.3189(7)	P(1)-Pt(1)	2.3161(14)

The comparison of the Pt⁰ complexes of both ferrocalcone **32** and the Lei ligand **17** showed that the ligand is acting, in both cases, as a bidentate ligand. An increase in bond length was observed on alkene metal coordination as expected. The presence of ferrocene in the ferrocenyl chalcone ligand does not alter the coordination behaviour of the ligand.

3.2 Rhodium complexes with alkene phosphine ligands

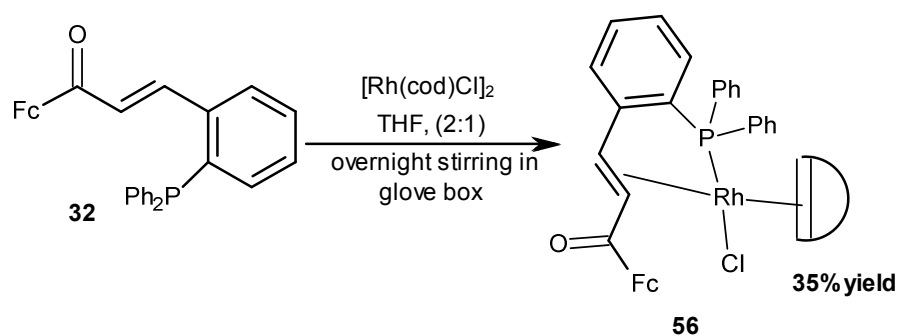
A significant part of investigations with rhodium involve the use of hemilabile ligands, mainly because the relevant complexes are of interest for their catalytic activity in several processes.¹⁵³ Rh^I complexes normally give rise to trigonal-bipyramidal complex, as well as square planar complexes.¹⁵⁴ However, in some cases, geometries closer to square-pyramidal are also observed.¹⁵⁵ Rhodium(I) complexes are industrial homogenous catalysts in number of reactions such as alkene hydroformylation, asymmetric hydrogenation and methanol carbonylation.

The metal precursor used for the synthesis of Rh metal complexes given in this study was [Rh(cod)Cl]₂. Both **32** and **17** were treated with Rh metal precursor to give the Rh^I complexes.

3.2.1 Rh^I complexes of the ferrochalcone **32** and Lei ligand **17**.

3.2.1.1 Ferrochalcone ligand (**32**) complexation

Ferrochalcone **32** was dissolved in THF and added to a solution of [Rh(cod)Cl]₂ in THF. The red suspension changed immediately to give an orange/red solution. The solution was allowed to stir overnight. The rhodium complex formed was unstable (decompose in air) and hence the reaction was conducted inside a glove box (< 0.5 ppm O₂). THF was then removed *in vacuo* and the orange/reddish residue was washed with diethyl ether, the washing was combined and concentrated *in vacuo* to give the product in a yield of 35% (Scheme 8). Precautionary measures were taken whilst analysing the Rh complex, as it was air-sensitive and decomposes in solution form (by a thermal decomposition pathway).



Scheme 8: Synthesis of Rhodium(I) complex of **32 using [Rh(cod)Cl]₂.**

The NMR sample was prepared in the glove box using a Young's tap NMR tube and data collected immediately. Initially, the product **56** was expected. However, the ³¹P NMR spectrum showed an interesting result. There was a prominent shift for the phosphorus atom in the complexed ligand. The ³¹P NMR spectrum showed two sets of doublet of doublets, along with some other ³¹P signals possibly due to cod-containing Rh^I complexes (Figure 7).

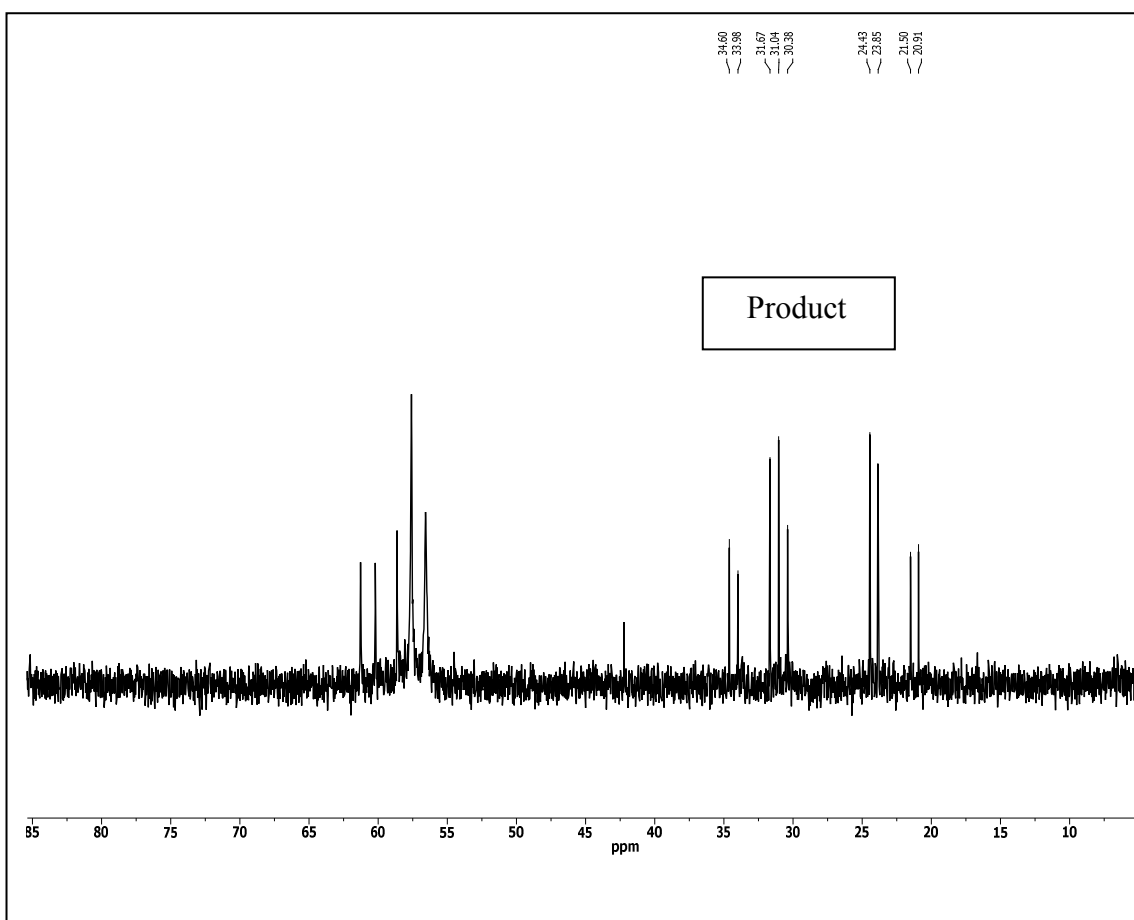


Figure 7: ^{31}P NMR spectrum for Rh^{I} complex of 32 in CD_2Cl_2 .

The chemical shift range for the first coordinated alkene phosphine ligand is δ 20.9-24.4 with spin-spin coupling constants of $J_{\text{Pa-Pb}} = 470$ Hz and $J_{\text{Rh-Pa}} = 94$ Hz. For the second ligand the chemical shift range is δ 31.0-34.6 with coupling constant value of $J_{\text{Pb-Pa}} = 470$ Hz and $J_{\text{Rh-Pb}} = 99$ Hz. The coupling constant value showed that the rhodium is bonded to two different phosphorus giving rise to an AB system- a spin-spin splitting pattern for an AB type system is given in Figure 8.

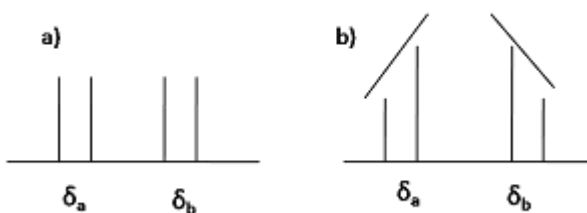
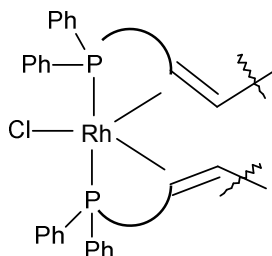


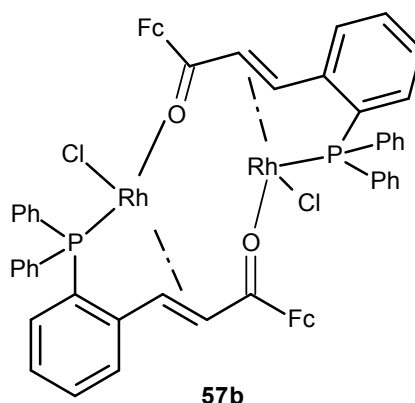
Figure 8: Spin-spin splitting pattern for an AB system, a) first-order pattern and b) second-order pattern.

The second order pattern is observed as a “roofed” pattern, e.g. the inner peaks are taller and outer peaks are shorter in case of AB system. The ^{31}P NMR spectrum suggested a Rh^{I} complex with a structure **57a**, where Rh is bonded to two ligands interacting through both alkene and phosphine **57a** (Figure 9).



57a

On standing for a long period the solution of the rhodium complex in diethyl ether led to the formation of fine orangish-red crystals. The crystals were run for the x-ray diffraction. The structure of the Rhodium(I) complex obtained on crystallization is given in Figure 10.



57b

Figure 10: Structure of Rh^{I} complex 57b.

The X-ray crystal structure for the complex is given in Figure 11.

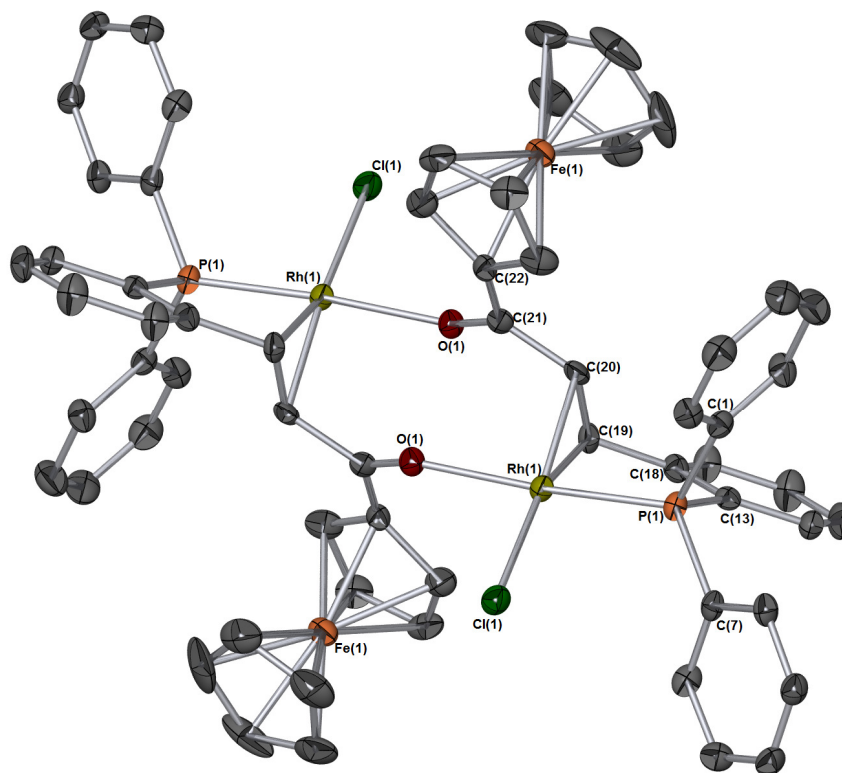


Figure 11: X-ray crystal structure of Rh^I metal complex of 57b.

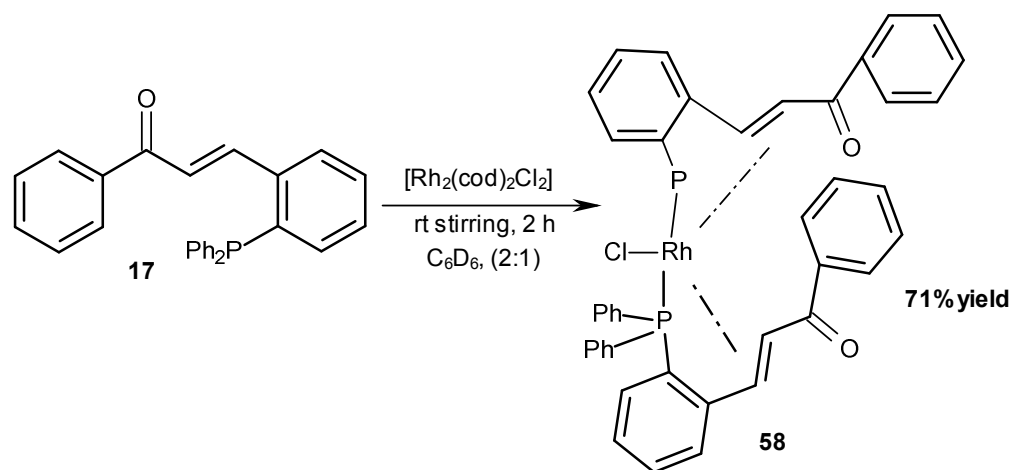
Hydrogen atoms removed for clarity. Thermal ellipsoids shown at 50%. Bond lengths(Å): C(19)-C(20) = 1.413(7), C(50)-C(51) = 1.425(7), C(21)-O(1) = 1.242(6), C(52)-O(2) = 1.240(5), C(19)-Rh(1) = 2.101(5), C(20)-Rh(1) = 2.117(4), C(50)-Rh(2) = 2.117(5), C(51)-Rh(2) = 2.103(5), Rh(1)-Cl(1) = 2.337(12), Rh(2)-Cl(2) = 2.3299(13), Rh(1)-O(1) = 2.131(3), Rh(2)-O(2) = 2.139(3), Rh(1)-P(1) = 2.1887(14), Rh(2)-P(2) = 2.1923(12), Bond Angles(°) C(19)-C(20)-Rh(1) = 71.0(3), C(50)-C(51)-Rh(2) = 70.8(3), C(18)-C(19)-Rh(1) = 113.7(3), C(49)-C(50)-Rh(2) = 115.6(3), C(19)-Rh(1)-C(20) = 39.14(18), C(51)-Rh(2)-C(50) = 39.47(18), C(19)-Rh(1)-Cl(1) = 153.08(14), C(50)-Rh(2)-Cl(2) = 161.60(3), C(20)-Rh(1)-Cl(1) = 167.79(14), C(51)-Rh(2)-Cl(2) = 158.93(14), P(1)-Rh(1)-O(1) = 175.03(10), P(2)-Rh(2)-O(2) = 177.03(9), O(1)-Rh(1)-Cl(1) = 87.35(9), O(2)-Rh(2)-Cl(2) = 86.41(9), P(1)-Rh(1)-Cl(1) = 94.27(5), P(2), Rh(2), Cl(2) = 93.70(5).

The X-ray structure of [Rh₂(ferrochalcone ligand)₂] **57b** indicated that the Rh^I is bonded to two bridging ligands. The ligand spans two Rh centres by P, alkene-coordination to one Rh and then carbonyl coordination to the other Rh atom. The X-ray structure shows that ferrochalcone **32** acts as tridentate ligand. The Rh^I complex exhibits a distorted square-planar geometry as expected for Rh^I complexes.¹⁵⁶ An increase in the bond length of the alkene bonds was expected as a result of the coordination. The alkene bond lengths for the complexed ligand are 1.413(7) Å and 1.425(7) Å, respectively which is

indicative of the carbons becoming more sp^3 -like. A comparison of the bond lengths between the two ligands around the Rh metal centre showed quite similar values.

3.2.1.2 Complexation of the Lei ligand

The Lei ligand **17** was treated with $[\text{Rh}(\text{cod})\text{Cl}]_2$ in the similar fashion to ferrochalcone **32**. Light yellow solid was obtained in a good yield of 71 % (Scheme 9).



Scheme 9: Synthesis of Rhodium(I) complex of Lei-ligand using $[\text{Rh}(\text{cod})\text{Cl}]_2$.

The IR spectrum of Rh complex **58** showed a strong absorption band at 1652 cm^{-1} corresponding to the C=O group together with the characteristic band for the C=C group (1595 cm^{-1}). ^{31}P NMR spectroscopic analysis (Figure 12) showed a similar spectrum to the Rh^{I} complex of **32** (Figure 7)

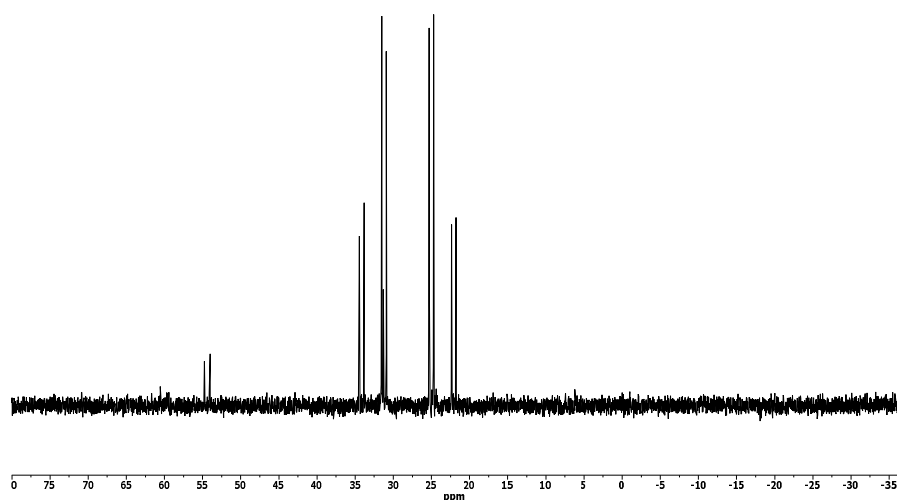


Figure 12: ^{31}P NMR spectrum for Rh^{I} complex of Lei ligand, **17.**

A pair of doublet of doublets were observed by ^{31}P NMR spectroscopic analysis for the complex (e.g. AB system). The spin-spin coupling constant values for the two doublets differ slightly indicating the difference in the environment for the two phosphorus atoms giving rise to an AB system. The chemical shift range for the first coordinated alkene phosphine ligand is δ 25.2-21.7 with a spin-spin coupling constant of $J_{\text{Pa-Pb}} = 474$ Hz and $J_{\text{Rh-Pa}} = 93$ Hz. For the second ligand the chemical shift range is δ 34.4-30.8, with coupling constant value of $J_{\text{Pb-Pa}} = 474$ Hz and $J_{\text{Rh-Pb}} = 100$ Hz.

The ^1H NMR spectrum of complex **58** is given in Figure 13.

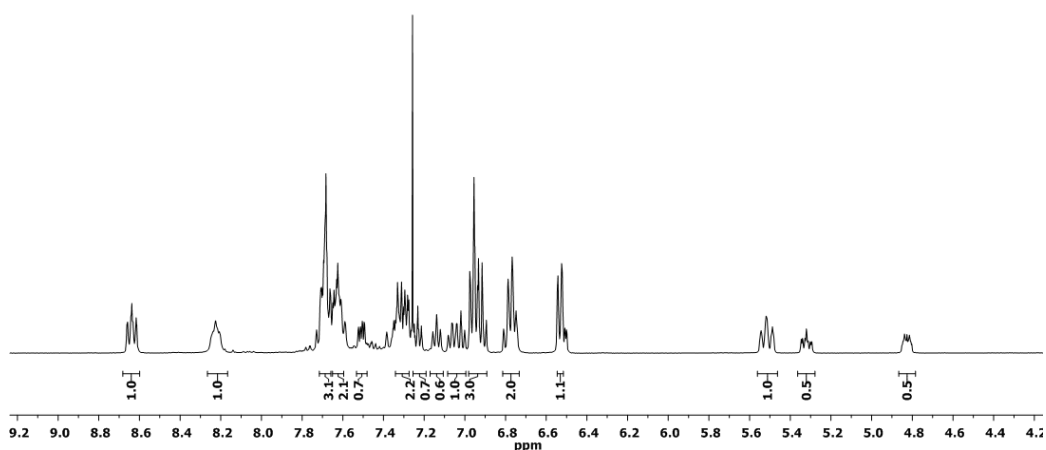


Figure 13: ^1H NMR spectrum for Rh^{I} complex of Lei ligand.

The ^1H NMR spectrum of complex **58** showed a shift for both of the α - and β -protons. The shift is more for the α -proton. The large upfield shifts from the free ligand alkene proton is evidence for the alkene binding to the rhodium centre. The phenyl proton peaks were observed between 6.5 to 8.0 ppm.

Fine yellow crystals were obtained by standing a solution of the Rh complex in benzene for a few days. The crystals were then analysed by X-ray diffraction (Figure 12).

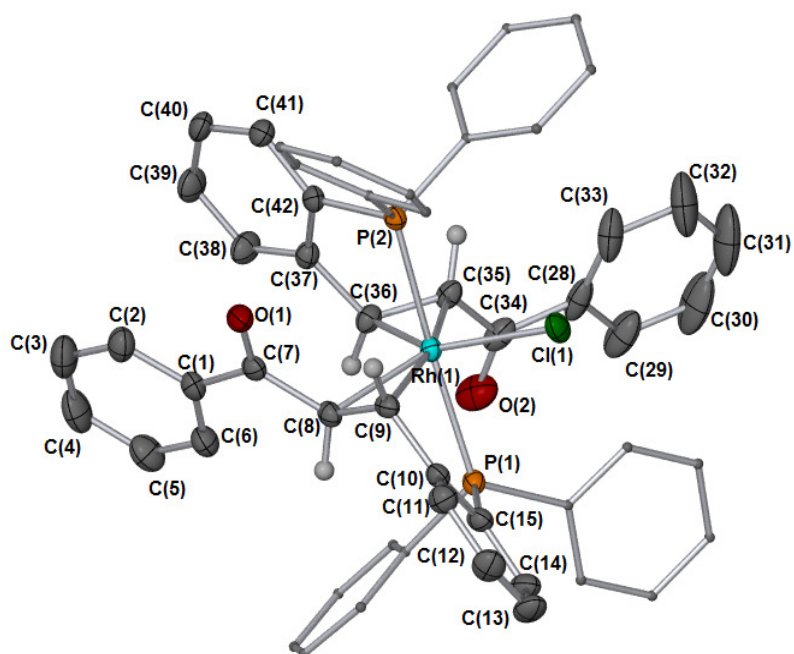


Figure 12: X-ray crystal structure of the Rh^I metal complex of Leif ligand 17.

Hydrogen atoms removed for clarity. Thermal ellipsoids shown at 50%. Bond lengths (Å): C(7)-O(1) = 1.222(2), C(34)-O(2) = 1.223(3), C(7)-C(8) = 1.489(3), C(34)-C(35) = 1.479(3), C(8)-C(9) = 1.416(3), C(35)-C(36) = 1.428(3), C(8)-Rh(1) = 2.1808(19), C(35)-Rh(1) = 2.1962(19), C(9)-Rh(1) = 2.1976(19), C(36)-Rh(1) = 2.128(2), C(15)-P(1) = 1.818(2), C(16)-P(1) = 1.830(2), C(22)-P(1) = 1.829(2), C(42)-P(2) = 1.813(2), C(43)-P(2) = 1.829(2), C(49)-P(2) = 1.842(2), Rh(1)-Cl(1) = 2.4585(6), Rh(1)-P(1) = 2.3654(6), Rh(1)-P(2) = 2.3358(6), Bond Angles(°) O(1)-C(7)-C(8) = 121.16(19), O(2)-C(34)-C(35) = 122.2(2), C(9)-C(8)-C(7) = 122.27(18), C(36)-C(35)-C(34) = 120.96(19), C(8)-Rh(1)-C(9) = 37.72(7), C(36)-Rh(1)-C(35) = 38.53(7), C(9)-C(8)-Rh(1) = 71.78(11), C(36)-C(35)-Rh(1) = 68.15(11), C(8)-C(9)-Rh(1) = 70.50(11), C(35)-C(36)-Rh(1) = 73.31(11), C(15)-P(1)-Rh(1) = 99.38(7), C(42)-P(2)-Rh(1) = 101.89(7), C(36)-Rh(1)-C(8) = 92.68(8), C(8)-Rh(1)-C(35) = 130.80(8), C(36)-Rh(1)-C(9) = 129.66(8), C(35)-Rh(1)-C(9) = 168.19(7), C(36)-Rh(1)-P(2) = 81.94(6), C(8)-Rh(1)-P(2) = 99.33(6), C(35)-Rh(1)-P(2) = 82.81(6), C(9)-Rh(1)-P(2) = 95.79(5), C(36)-Rh(1)-P(1) = 102.83(6), C(8)-Rh(1)-P(1) = 81.30(6), C(35)-Rh(1)-P(1) = 100.44(6), C(9)-Rh(1)-P(1) = 81.75(5), P(2)-Rh(1)-P(1) = 175.177(19), C(36)-Rh(1)-Cl(1) = 142.04(6), C(8)-Rh(1)-Cl(1) = 142.04(6), C(8)-Rh(1)-Cl(1) = 125.16(5), C(35)-Rh(1)-Cl(1) = 103.99(6), C(9)-Rh(1)-Cl(1) = 87.65(5), P(2)-Rh(1)-Cl(1) = 88.264(19), P(1)-Rh(1)-Cl(1) = 87.489(19).

The complex was found to exhibit an interesting geometry. The Rh^I metal is found to be coordinated to two ligands. Six and a half molecules of benzene are found in the unit cell. The metal is coordinated by two P atoms and two alkene bonds. There is a Rh(1)-Cl(1) bond, with a bond length of 2.4585(6) Å. The phosphino-alkene ligand is acting as a bidentate ligand binding through both the alkene and phosphine moiety. The bond lengths for the Rh-P bonds are similar, the Rh(1)-P(1) bond length is 2.3654(6) Å, whereas Rh(1)-P(2) bond length is 2.3358(6) Å.

The alkene bond length for the coordinated ligand C(8)-C(9) is 1.416(3) Å, which is longer than that for the non-coordinated ligand. The alkene bond length C(35)-C(36) in the other ligand is 1.428(3) Å.

A comparison of the bond lengths between the Rh^I metal complex for the ferrocyclone and Lei ligand is given in Table 4.

Table 4: Comparison of the bond lengths in Rh^I complexes 57b and 58.

Rh(I) complex (57b)		Rh(I) complex (58)	
Bond	Length, Å	Bond	Length, Å
C(19)-C(20)	1.413(7)	C(7)-C(8)	1.489(3)
C(50)-C(51)	1.425(7)	C(34)-C(35)	1.479(3)
C(21)-O(1)	1.242(6)	C(7)-O(1)	1.222(2)
C(52)-O(2)	1.240(5)	C(34)-O(2)	1.223(3)
C(19)-Rh(1)	2.101(5)	C(8)-Rh(1)	2.1808(19)
C(20)-Rh(1)	2.117(4)	C(9)-Rh(1)	2.1976(19)
C(50)-Rh(2)	2.117(5)	C(35)-Rh(1)	2.1962(19)
C(51)-Rh(2)	2.103(5)	C(36)-Rh(1)	2.128(2)
Rh(1)-Cl(1)	2.337(12)	Rh(1)-Cl(1)	2.4585(6)
Rh(2)-Cl(2)	2.3299(13)		
Rh(1)-O(1)	2.131(3)	--	--
Rh(2)-O(2)	2.139(3)		
Rh(1)-P(1)	2.1887(14)	Rh(1)-P(1)	2.3654(6)
Rh(2)-P(2)	2.1923(12)	Rh(1)-P(2)	2.3358(6)

There is an increase in the alkene bond length in both of the Rh^I complexes indicating that the alkene is interacting with the metal. Also, the Rh-P interaction was observed in both of the complexes with Rh(1)-P(1) bond lengths slightly longer than in the Lei Rh

complex, **58**. As rhodium is binding to Cl in both of the complexes, a comparison of the bond lengths of Rh(1)-Cl(1) between the two complexes showed that Rh(1)-Cl(1) bond length is higher in Lei Rh complex (**58**) as compared to ferrochalcone Rh complex (**57**).

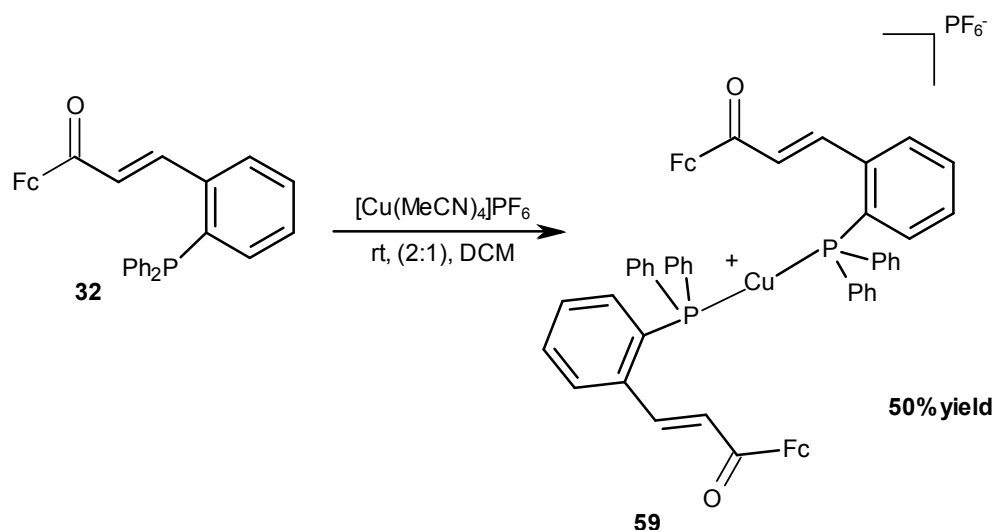
3.3 Copper complexes with Alkene phosphine ligands

Copper complexes have been of great interest to inorganic and organometallic chemists due to their varied coordination chemistry and the resulting properties. Traditionally, copper(I) is regarded as a metal ion with soft Lewis acid character,¹⁵⁷ and therefore it will form covalent bonds with soft ligands (*e.g.* with S or P as the donor atom). Copper(I) alkene complexes are known in literature, with the first reported by Brandt *et al.* The interesting feature of these copper(I) alkene complexes is that they exhibit a wide variety of coordination modes. A four coordinate copper(I) alkene complex shows a distorted tetrahedral arrangement whereas, a three coordinate copper(I) alkene complex with a bulky ligand exhibits a trigonal planar geometry. Copper(I) phosphino-alkene complexes are also known. In some cases the copper is found to be bonded to the phosphine only with no metal alkene coordination. However in a few complexes both alkene and phosphine moieties are bonded to copper. The copper metal precursors used are [Cu(MeCN)₄]PF₆ and [Cu(Cl)]. The ligands **32**, **33** and **17** were treated with the appropriate copper metal precursor under different reaction conditions to give the copper(I) metal complex, as detailed below.

3.3.1 Cu^I complexes

3.3.1.1 Ferrochalcone ligand (**32**) complexation

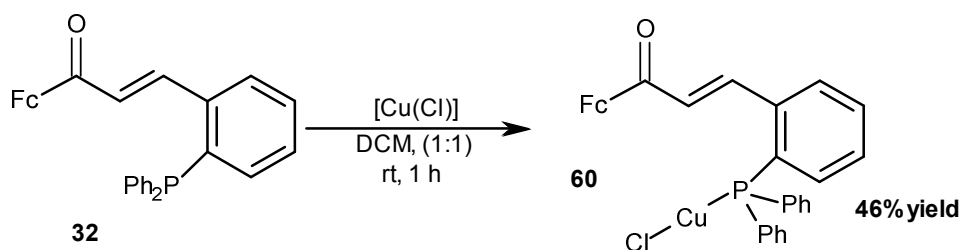
The reaction of [Cu(MeCN)₄] PF₆ with two equivalent of ferrochalcone **32** afforded the copper(I) metal complex **59** as light red powder. A solution of [Cu(MeCN)₄]PF₆ in dry degassed dichloromethane was added by cannula to ferrochalcone **32** and the resulting solution was stirred for 2 h at room temperature. Finally, the solution was filtered to give a clear solution and the solvent was removed *in vacuo* to give the solid product (Scheme 10).



Scheme 10: Synthesis of copper(I) complex of 32 using $[\text{Cu}(\text{MeCN})_4]\text{PF}_6$.

The structure of the complex **59** was analysed by NMR, IR spectroscopy and mass spectrometry. In the ^{31}P -NMR spectrum there is a shift from δ -13.0 to δ -4.80, also there is a septet at δ -143.8 corresponding to the presence of PF_6^- ion. In the ^1H -NMR spectrum there is only a slight shift for the two protons and hence no evidence of Cu-alkene coordination. The molecular ion peak in the mass spectrum appeared at m/z 563.0297 corresponding to that of $[\text{Cu}(\text{C}_{31}\text{H}_{25}\text{FePO})]^+$. Different attempts were made to crystallise the copper(I) metal complex using different solvent combinations, but couldn't succeed.

$[\text{Cu}(\text{Cl})]$ was also used as a source for the synthesis of the copper(I) complex of the chalcone ferrocene ligand. Ferrocene chalcone **32** was treated with $[\text{Cu}(\text{Cl})]$ in a ligand to metal ratio of 1:1, at a room temperature reaction for 1 h giving dull red powder **60** (Scheme 11).



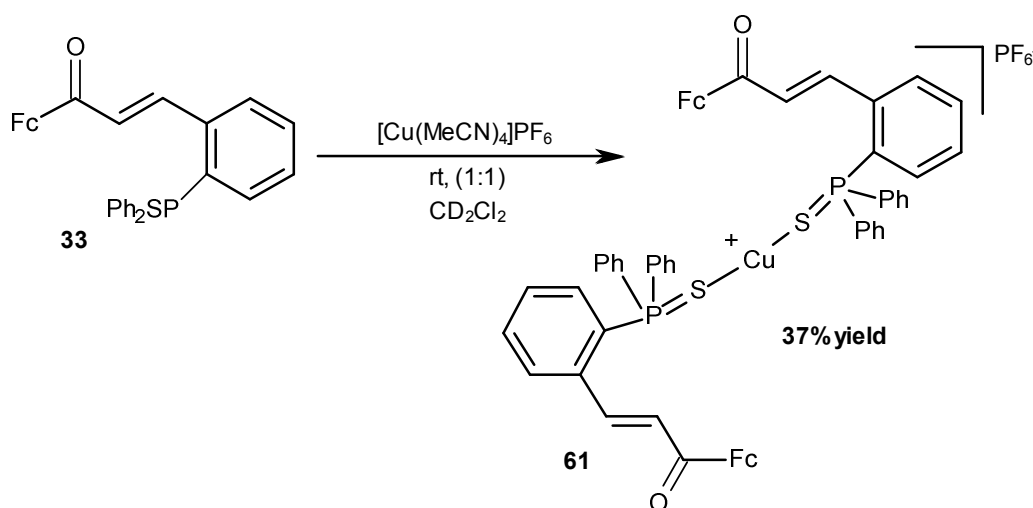
Scheme 11: Synthesis of Copper(I) complex of 32 using $[\text{Cu}(\text{Cl})]$.

The structure of the complex was established by FT-IR and NMR spectroscopy. The IR spectrum of the complex **60** showed a characteristic peak at 1652 cm^{-1} for the carbonyl group. The ^{31}P -NMR spectrum showed a singlet at δ -4.38, which is, compared to the

ligand δ -13.0 shifted more downfield. This provides evidence of some sort of phosphorus-metal interactions. The $^1\text{H-NMR}$ spectrum showed no evidence of Cu-alkene interaction. Fine crystals were obtained by layering ether over a CH_2Cl_2 solution of copper complex but they were too small to be analysed by XRD.

3.3.1.2 Thio-ferrochalcone ligand (33) complexation

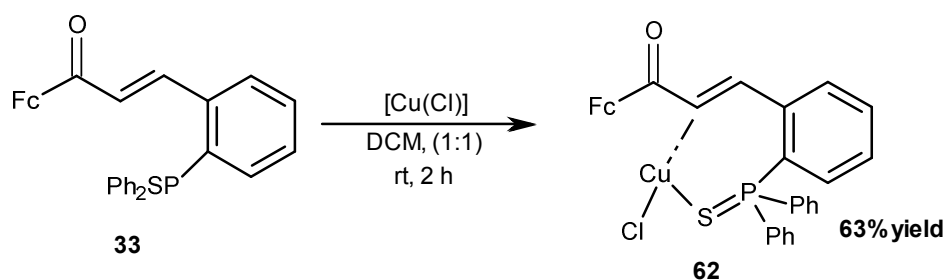
Cu^{I} being regarded as a metal ion with soft Lewis acid character shows good reactivities towards soft ligands like S or P by forming covalent bond and hence metal coordination behaviour of thio-ferrochalcone was explored. Alkene thio-phosphine Cu^{I} metal complex **61** was prepared by reaction of thio-ferrochalcone **33** with $[\text{Cu}(\text{MeCN})_4]\text{PF}_6$ (Scheme 12).



Scheme 12: Synthesis of copper(I) complex of 33 using $[\text{Cu}(\text{MeCN})_4.\text{PF}_6]$.

There is only very slight shift in the ^{31}P NMR spectrum showing that the metal is not coordinating to phosphorus in fact it's the sulfur forming a bridge with the Cu metal. A molecular ion was seen in the mass spectrum at m/z 1127.07 corresponding to $[\text{Cu}(\text{C}_{31}\text{H}_{25}\text{FePSO})_2]^+$. Fine crystals were grown from dichloromethane but were too small for XRD analysis.

Thio-ferrochalcone **33** was also treated with $[\text{CuCl}]$ in dichloromethane to obtain the copper(I) complex. Reaction over a 2 h at room temperature, with ligand metal ratio of 1:1, afforded a giving light red solid product, believed to be **62** (Scheme 13).



Scheme 13: Synthesis of copper(I) complex of 33 using [CuCl].

The structure of the complex was established by FT-IR and NMR spectroscopy. The ^{31}P -NMR spectrum showed a chemical shift change from δ 42.05 to δ 41.2. The shift is not very prominent indicating that phosphorus is not directly coordinating to metal and perhaps its sulfur forming the bond with metal. Similarly, a slight shift in the ^1H -NMR spectrum was observed.

In order to gain further information about the coordination mode involved, attempts were made to crystallize the complex. Fine red crystals were grown from a dichloromethane solution of the complex after *ca.* 1 week. The determined X-ray structure obtained is shown in Figure 13.

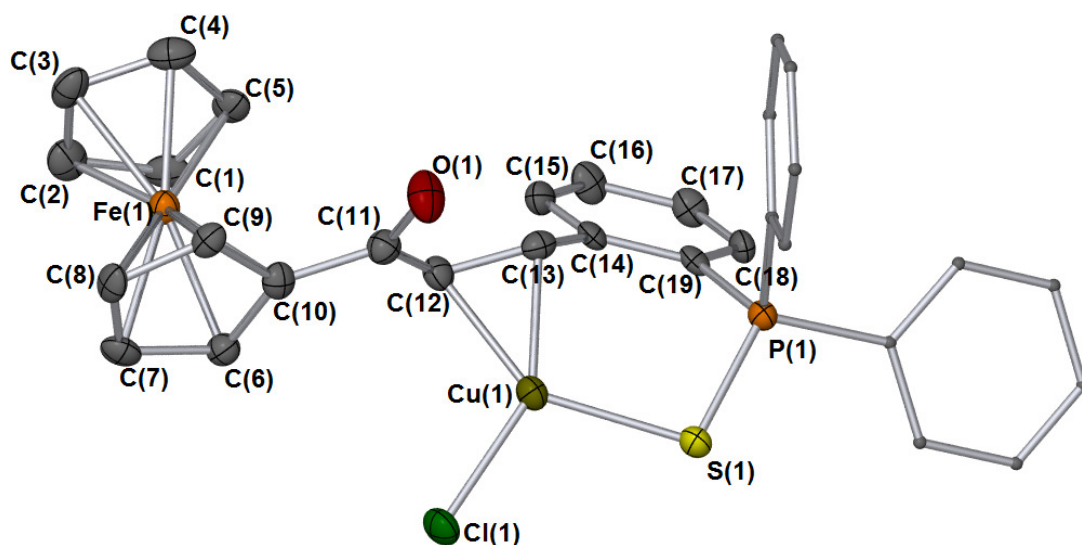


Figure 13: X-ray crystal structure of the Cu^I metal complex containing ligand 33.

Hydrogen atoms removed for clarity. Thermal ellipsoids shown at 50%. Bond lengths (Å): C(10)-C(11) = 1.467(5), C(11)-C(12) = 1.499(5), C(12)-C(13) = 1.384(5), C(13)-C(14) = 1.496(5), C(11)-O(1) = 1.229(4), P(1)-C(19) = 1.807(4), P(1)-C(20) = 1.802(4), P(1)-C(26) = 1.807(4), P(1)-S(1) = 1.9991(13), S(1)-Cu(1) = 2.2526(11), Cu(1)-Cl(1) = 2.1892(10), C(12)-Cu(1) = 2.056(4), C(13)-Cu(1) = 2.039(4), Bond Angles (°) : C(12)-Cu(1)-C(13) = 39.49(14), C(12)-Cu(1)-S(1) = 142.69(11), C(13)-Cu(1)-S(1) = 103.32(11), C(12)-Cu(1)-Cl(1) = 109.88, C(13)-Cu(1)-Cl(1) = 149.34(11), S(1)-Cu(1)-Cl(1) = 107.14(4), P(1)-S(1)-Cu(1) = 100.86(5), C(19)-P(1)-S(1) = 111.48(12), C(26)-P(1)-S(1) = 113.30(13), C(20)-P(1)-S(1) = 110.28(13).

The structure of the Cu^I complex exhibits a trigonal geometry. The X-ray structure showed that the crystal contained a molecule of dichloromethane (solvent) in the unit cell. The thio-ferrochalcone acts as a bidentate ligand, binding through both the sulphur and the alkene moiety. The C=C bond distance of the alkene double bond is 1.384 Å, which is slightly longer than that for non-complexed alkene double bond (1.334 Å), confirming a weak alkene-metal interaction.

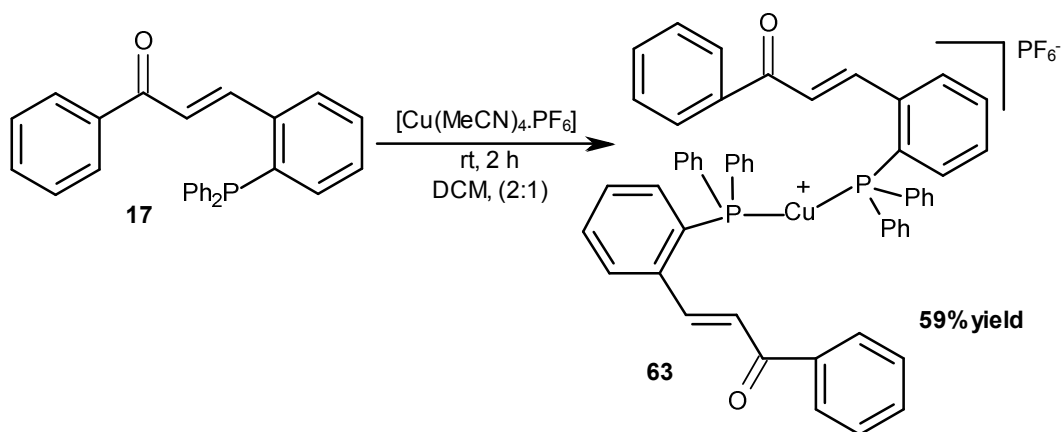
An comparison of the torsion angle for some important atom combinations is given in Table 5.

Table 5: Torsion angle for the copper(I) complex of 33.

Bonds	Torsion angle (°)	Conformation
C(11)-C(12)-C(13)-C(14)	-159.3(4)	antiperiplanar(trans)
Cl(1)-Cu(1)-S(1)-P(1)	174.9(5)	antiperiplanar(trans)
C(12)-Cu(1)-S(1)-P(1)	2.4(2)	synperiplanar(cis)
C(13)-Cu(1)-S(1)-P(1)	-1.46(3)	synperiplanar(cis)
O(1)-C(11)-C(12)-Cu(1)	78.9(4)	synclinal(gauche/skew)
C(19)-P(1)-S(1)-Cu(1)	-44.37(14)	synclinal(gauche/skew)
C(26)-P(1)-S(1)-Cu(1)	75.95(14)	synclinal(gauche/skew)
C(20)-P(1)-S(1)-Cu(1)	-164.39(13)	antiperiplanar(trans)

3.3.1.3 Complexation of the Lei ligand

Both the chalcone ferrocene ligand **32** and the Lei ligand **17** exhibit a similar structure, having the common chalcone backbone. The major difference is the presence of ferrocene instead of a phenyl ring. A reaction of the Lei ligand **17** was conducted with $[\text{Cu}(\text{MeCN})_4]\text{PF}_6$ in a ligand to metal ratio of 2:1 (Scheme 14), conducted which afforded a light yellow product believed to be **63**.

**Scheme 14: Synthesis of copper(I) complex of the Lei ligand 17.**

The ^{31}P -NMR spectrum of **63** showed a singlet at δ -4.51, also there is a septet at -143.8 corresponding to the presence of the PF_6^- anion. The molecular ion peak in the mass spectrum appeared at m/z 849.2133 corresponding to that of $[\text{Cu}(\text{C}_{27}\text{H}_{21}\text{PO})_2]^+$.

In order to ascertain the geometry of the copper metal complex **63** crystals were grown from dichloromethane XRD analysis confirmed the structure of the copper metal complex **63** (Figure 14).

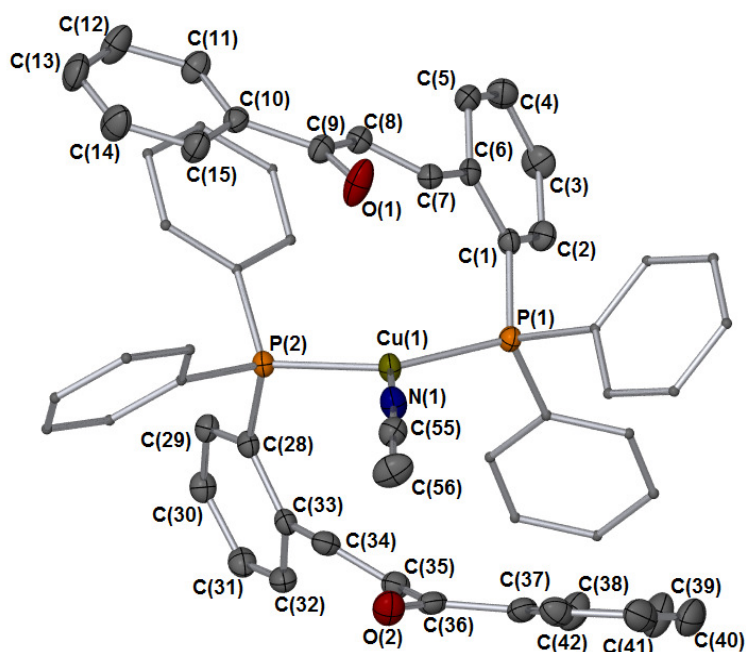


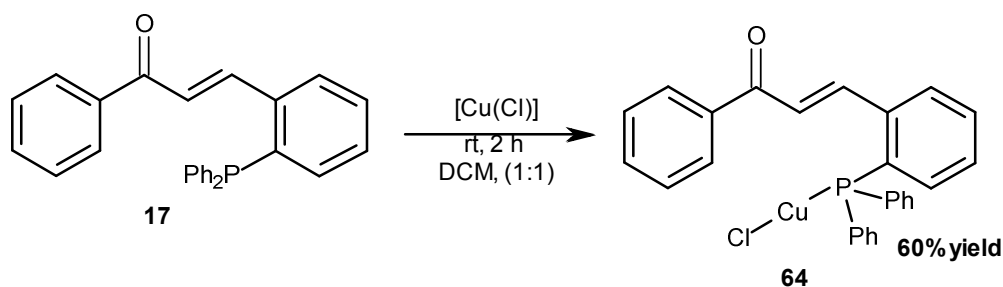
Figure 14: X-ray crystal structure of Cu (I) metal complex 63.

Hydrogen atoms removed for clarity. Thermal ellipsoids shown at 50%. Bond lengths (Å): C(9)-O(1) = 1.217(2), C(8)-C(7) = 1.337(2), P(1)-C(1) = 1.8232(17), P(1)-C(16) = 1.8255(17), P(1)-C(22) = 1.8233(17), P(1)-Cu(1) = 2.2421(5), C(36)-O(2) = 1.225(2), C(34)-C(35) = 1.335(2), P(2)-C(28) = 1.8314(17), P(2)-C(43) = 1.8234(17), P(2)-C(49) = 1.8237(16), P(2)-Cu(1) = 2.2451(5), Cu(1)-N(1) = 1.9593(15), N(1)-C(55) = 1.138(2), Bond Angles(°) C(1)-P(1)-C(16) = 104.47(8), C(1)-P(1)-C(22) = 104.66(8), C(22)-P(1)-C(16) = 103.40(8), C(1)-P(1)-Cu(1) = 112.59(5), C(16)-P(1)-Cu(1) = 115.14(6), C(22)-P(1)-Cu(1) = 115.34(6), C(43)-P(2)-C(49) = 104.91(8), C(43)-P(2)-C(28) = 103.14(7), C(49)-P(2)-C(28) = 104.65(7), C(43)-P(2)-Cu(1) = 115.39(5), C(49)-P(2)-Cu(1) = 115.92(5), C(28)-P(2)-Cu(1) = 111.51(5), P(1)-Cu(1)-P(2) = 131.018(18), N(1)-Cu(1)-P(1) = 115.78(5), N(1)-Cu(1)-P(2) = 113.20(5), C(55)-N(1)-Cu(1) = 172.55(16).

One of the dichloromethane of crystallisation was disordered and modelled over two sites with a refined relative occupancy of 4:1. The two ligands were bounded to Cu metal centre through phosphorus only and there is no alkene metal coordination. The

C=C bond length for C(7)-C(8) is 1.337 Å, whereas for C(34)-C(35) it is 1.335 Å in the complexed ligand. If we do a comparison of the alkene bond length in the complexed ligand with the non-complexed ligand (1.33 Å), they are almost identical confirming that the alkene is not interacting with the metal. Another, interesting comparison of the bond lengths is between Cu(1)-P(1) (2.2421 Å) and Cu(1)-P(2) (2.2451 Å) which is also quite similar. The bond length for P(1)-C(1) (1.8232 Å) is similar to that of P(2)-C(43) (1.8234 Å) showing that both ligands are attached symmetrically to the metal centre. Also there was a copper metal coordination with a molecule of acetonitrile. The torsion angle for C(43)-P(2)-Cu(1)-P(1) is $-49.26(7)^\circ$ which is similar to that of C(1)-P(1)-Cu(1)-P(2) $47.39(6)^\circ$, with the only difference noted in the direction of rotation. Hence, both of torsions exhibit a synclinal conformation. Similarly, C(43)-P(2)-Cu(1)-N(1) and C(1)-P(1)-Cu(1)-N(1) give $131.08(8)^\circ$ and $-132.96(8)^\circ$ exhibit an anticlinal conformation.

Reaction of the Lei ligand **17** with [CuCl] in a ligand metal ratio of 1:1, for 2 h in dichloromethane afforded a copper(I) complex which is believed to be **64** in 60% yield as given in Scheme 15.



Scheme 15: Synthesis of copper(I) complex of Lei ligand using [CuCl].

The ^{31}P -NMR spectrum of **63** showed a chemical shift change from $\delta -13.0$ to $\delta -3.47$ confirming a phosphorus-metal interaction. The shift in the ^1H -NMR spectrum is very negligible, highlighting little if any alkene-Cu interaction. The mass spectrum gives a molecular ion peak at m/z 455.1 corresponding to $[\text{Cu}(\text{C}_{27}\text{H}_{21}\text{PO})]^+$.

The Lei copper(I) complex **64** was crystallized from a dichloromethane solution layered with pentane, which afforded slight yellow crystals suitable for XRD analysis. The X-ray structure of the copper(I) complex is given in Figure 15, which exists as a dimer in the solid-state.

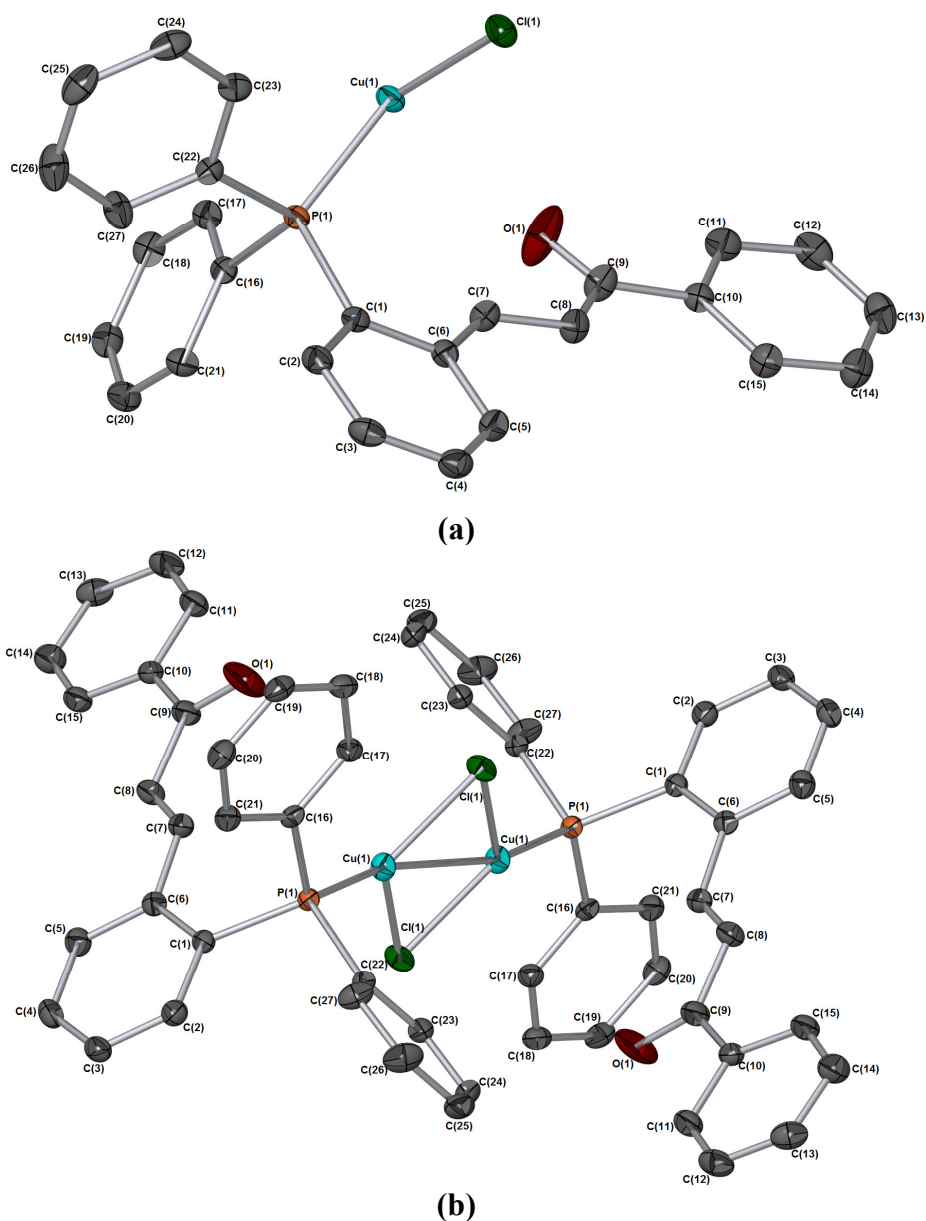


Figure 15: X-ray crystal structure of Cu^I metal complex 64, (a) asymmetric unit (b) molecular structure

Hydrogen atoms removed for clarity. Thermal ellipsoids shown at 50%. Bond lengths (Å): C(6)-C(7) = 1.468(2), C(7)-C(8) = 1.334(2), C(8)-C(9) = 1.483(2), C(9)-O(1) = 1.2193(19), P(1)-Cu(1) = 2.1765(4), Cu(1)-Cl(1) = 2.2635(4), Cu(1)-Cu(1¹) = 2.8915(3), Cu(1)-Cl(1¹) = 2.2635(4), P(1)-C(1) = 1.8338(14), P(1)-C(16) = 1.8182(14), P(1)-C(22) = 1.8192(14), Bond Angles(°) C(7)-C(8)-C(9) = 119.41(14), C(8)-C(9)-O(1) = 120.13(15), C(10)-C(9)-O(1) = 119.52(14), C(1)-P(1)-Cu(1) = 115.80(4), C(16)-P(1)-Cu(1) = 116.55(5), C(22)-P(1)-Cu(1) = 107.80(4), P(1)-Cu(1)-Cl(1) = 122.133(15), P(1)-C(1)-C(6) = 119.36(10), P(1)-Cu(1)-Cu(1¹) = 167.505(15), P(1)-Cu(1)-Cl(1¹) = 134.555(16).

The Lei ligand acts as monodentate ligand binding through the phosphorus only and there is no alkene metal interaction. The C(7)-C(8) distance of the alkene double bond is 1.334(2) Å which is similar to that for an alkene in a non-coordinated metal complex. A comparison of the torsion angle between the different atoms is given in Table 6.

Table 6: Torsion angle for the copper(I) complex of Lei ligands(64).

Bonds	Torsion angle (°)
Cu(1 ¹)-Cl(1)-Cu(1)-Cl(1 ¹)	0.0
C(1)-P(1)Cu(1)-Cl(1)	-48.87(5)
C(1)-P(1)-Cu(1)-Cu(1 ¹)	-96.56(8)
P(1)-Cu(1)-Cl(1)-Cu(1 ¹)	-167.94(18)
P(1)-C(1)-C(2)-C(3)	-174.04(11)
P(1)-C(1)-C(6)-C(5)	173.62(10)

A comparison of the bond lengths between Cu complex **63** and **64** is given in Table 7.

Table 7: Comparison of the bond lengths in copper(I) complexes of Lei ligand.

Cu(I) complex (63)		Cu(I) complex (64)	
Bond	Length, Å	Bond	Length, Å
C(7)-C(8)	1.337(2)	C(7)-C(8)	1.334(2)
C(9)-O(1)	1.217(2)	C(9)-O(1)	1.2193(19)
P(1)-Cu(1)	2.2421(5)	P(1)-Cu(1)	2.1765(4)
Cu(1)-N(1)	1.9593(15)	Cu(1)-Cl(1)	2.2635(4)
P(1)-C(1)	1.8232(17)	P(1)-C(1)	1.8338(14)
P(1)-C(16)	1.8255(17)	P(1)-C(16)	1.8182(14)
P(1)-C(22)	1.8233(17)	P(1)-C(22)	1.8192(14)

The bond length for C=C bond in both of these copper complexes is similar to the bond length of a non-complexed alkene (1.33 Å), which showed that both of these alkene bonds were not involved in any kind of interaction with the metal.

3.4 Experimental

3.4.1 General Information

NMR spectra were obtained in the solvent indicated, using a JEOL ECX400 or JEOL ECS400 spectrometer (400 MHz for ^1H , 100 MHz for ^{13}C and 162 MHz for ^{31}P). Chemical shifts were referenced to the residual undeuterated solvent of the deuterated solvent used (CHCl_3 $\delta = 7.26$ and 77.16 , CDHCl_2 $\delta = 5.31$ and 53.80 and $\text{C}_6\text{D}_5\text{H}$ $\delta = 7.16$ and 128.0 for ^1H and ^{13}C NMR spectra, respectively). All ^{13}C NMR spectra were obtained with ^1H decoupling. ^{31}P NMR spectra were externally referenced to H_3PO_4 , and obtained with ^1H decoupling. For ^{13}C NMR spectra the coupling constants are quoted to ± 1 Hz. For the ^1H NMR spectra the resolution varies from ± 0.15 to ± 0.5 Hz; the coupling constants have been quoted to ± 0.5 Hz in all cases for consistency. For ^{31}P NMR spectra the coupling constants have been quoted to either ± 0.5 or ± 1 Hz. NMR spectra were processed using MestrNova software.

Melting points were recorded using a Stuart digital SMP3 machine. IR spectroscopy was undertaken using a Jasco/MIRacle FT/IR-4100typeA spectrometer with an ATR attachment on solid and liquid compounds; KBr and solution IR spectra were obtained on a Nicolet Avatar 370 FT-IR spectrometer as stated. MS spectra were measured using a Bruker Daltonics micrOTOF machine with electrospray ionisation (ESI) or on a Thermo LCQ using electrospray ionisation, with <5 ppm error recorded for all HRMS samples. LIFDI mass spectrometry was carried out using a Waters GCT Premier MS Agilent 7890A GC, with <15 ppm error recorded for all HRMS. Mass spectral data is quoted as the m/z ratio along with the relative peak height in brackets (base peak = 100). TLC analysis was carried out on Merck TLC aluminium sheets (silica gel 60 F254) and visualised with UV light (254 nm) and iodine vapour. All column chromatography was run on silica gel 60 using the solvent systems specified in the text. The fraction of petroleum ether used was $40\text{-}60$ °C.

Dry and degassed toluene, CH_2Cl_2 and hexane were obtained from a Pure-Solv MD-7 solvent purification system. THF and Et_2O were either obtained from a Pure-Solv MD-7 solvent purification system and degassed by the freeze-pump-thaw method or purged with N_2 under sonication; or dried over sodium-benzophenone ketyl and collected by distillation. Benzene was dried over sodium-benzophenone ketyl, and ethanol was dried and distilled from magnesium-iodine. All air-sensitive reactions were carried out using

Schlenk techniques or in a MBraun MG-20-G with TP170b glove-box with an N₂ atmosphere. Nitrogen gas was oxygen-free and was dried immediately prior to use by passage through a column containing sodium hydroxide pellets and silica. Room temperature was typically between 13-25 °C. Commercial chemicals were purchased from Sigma-Aldrich or Alfa Aesar.

Pd^{II} complex (48 b): Synthesis using PdCl₂(cod)

A solution of PdCl₂(cod) (0.020 g, 0.1 mmol) and ferrochalcone **32** (0.050 g, 0.1 mmol) in CH₂Cl₂ (5 mL) was stirred at room temperature for 1 h. Addition of hexane and concentration in vacuo to two-thirds the volume afforded a dark red-coloured precipitate, which was filtered and dried *in vacuo* (0.041 g, 60%). Mp 192-194 °C; ¹H-NMR (400 MHz, CDCl₃) δ 8.41 (d, *J* = 15.7, 1H), 7.93 (s, 3H, Ph), 7.80 (m, 1H), 7.43-7.51(m, 10H), 6.83 (d, *J* = 15.7, 1H), 4.70-4.83 (m, 2H), 4.54-4.51 (m, 2H), 4.10-4.23 (m, 5H); ¹³C-NMR (100 MHz, CDCl₃) δ 192.1, 133.8, 133.6, 129.0, 128.8, 128.7, 128.6, 116.8, 74.5, 71.1, 70.5, 70.2, 69.9, 69.8, 69.7; ³¹P-NMR (162 MHz, CDCl₃) δ 21.4 (s, 1P); HRMS (LIFDI) [M]⁺ *m/z* 639.9518 (Calcd. for [Pd(C₃₁H₂₄FePO)Cl] 639.9637); IR ν cm⁻¹ 3438 (s), 2924 (s), 1652 (s), 1554 (s), 1456 (s), 1377 (s), 1099 (s), 996 (s), 693 (s).

Pd^{II} complex (48 a): Synthesis using PdCl₂(MeCN)₂

To a solution of ferrochalcone **32** (0.050 g, 0.1 mmol) in CH₂Cl₂ (2.5 mL) was added a solution of [Pd(MeCN)₂Cl₂] (0.025 g, 0.1 mmol) in CH₂Cl₂ (5 mL). The product immediately crystallizes out after stirring for 1 h. The product was filtered and dried *in vacuo* (0.037 g, 54 %). Mp 193-195 °C; ¹H-NMR (400 MHz, CDCl₃) δ 9.00 (d, *J* = 16 Hz, 1H), 8.27 (m, 3H), 7.44 (m, 1H), 7.20 (m, 3H), 6.99 (m, 3H), 6.94 (m, 3H), 6.91 (m, 1H), 6.80 (d, *J* = 16 Hz, 1H), 4.68 (s, 2H), 4.09 (m, 2H), 3.81 (s, 5H); ³¹P-NMR (162 MHz, C₆D₆) δ (ppm): 21.7 (s, 1P); IR (KBr, ν cm⁻¹): 3444 (bs), 2917 (s), 2349 (s), 2324 (s), 1653 (s), 1553 (s), 1456 (s), 1436 (s), 1383 (s), 1262(s), 1233 (s), 1099 (s), 1017 (s), 825 (s), 763 (s), 686 (s), 653 (s); HRMS (LIFDI) [M-Cl]⁺ *m/z* 607.01 (Calcd. for [Pd(C₃₁H₂₆FePO)] 607.01).

Pt^{II} complex (49)

A solution of [*cis*-PtCl₂(cod)] (0.046 g, 0.1 mmol) and ferrochalcone **32** (0.048 g, 0.012 mmol) in CH₂Cl₂ (5 mL) was stirred for 30 mins. Addition of hexane and concentration

to two-thirds the volume to afford a red solid, which was filtered and dried *in vacuo* (0.037 g, 50%). Mp 278-285 °C; ¹H-NMR (400 MHz, CDCl₃) δ 8.05-8.10 (m, 2H), 7.78-7.85 (m, 4H), 7.50-7.58 (m, 2H), 7.38-7.43 (ddt, *J* = 7.1, 5.1, 3 Hz, 5H), 7.20-7.23 (m, 1H), 6.41 (d, *J* = 11.8 Hz, 1H), 5.17 (dd, *J* = 11.7, 3.3 Hz, 1H), 4.63 (dd, *J* = 2.5, 1.3 Hz, 1H), 4.46 (q, *J* = 2.5 Hz, 1H), 4.39-4.40 (m, 2H), 3.88 (s, 5H); ¹³C-NMR (100 MHz, CDCl₃) δ 193.2, 133.8, 134.1, 134.2, 136.1 (d, *J* = 10 Hz), 138.2 (d, *J* = 16 Hz), 139.4 (d, *J* = 23 Hz), 140.3 (d, *J* = 22 Hz), 129.5, 129.1, 129.0, 128.7 (d, *J* = 7 Hz), 127.2 (d, *J* = 4 Hz), 126.3 (d, *J* = 4 Hz), 80.1, 72.7, 70.2, 69.9; ³¹P-NMR (162 MHz, CDCl₃) δ 23.3 (s, ¹*J*_{PtP} = 3059 Hz); HRMS (ESI) [*M-Cl*]⁺ *m/z* 731.0325 (Calcd. for [Pt(C₃₁H₂₆FePO)Cl] 731.0342); IR ν cm⁻¹ 2922 (s), 1739 (s), 1695 (s), 1669 (s), 1652 (s), 1558 (s), 1583 (s), 1533 (s), 1464 (s), 1436 (s), 1419 (s), 1105 (s), 728 (s).

Pt^{II} complex (50 b)

A solution of [*cis*-PtCl₂(cod)] (0.017 g, 0.06 mmol) and Lei ligand **17** (0.023 g, 0.06 mmol) in CH₂Cl₂ (4 mL) was stirred for 1 h at room temperature. The solvent was removed *in vacuo* giving light yellowish powder (0.020 g, 52%). Mp 211-213 °C; ¹H-NMR (400 MHz, CDCl₃) δ 8.02 (ddd, *J* = 12.5, 8.0, 1.5 Hz, 3H), 7.79 (dd, *J* = 8.0, 3.0 Hz, 2H), 7.75 (dd, *J* = 4.0, 2.5 Hz, 2H), 7.73 (d, *J* = 2.5 Hz, 1H), 7.69-7.72 (m, 2H), 7.51-7.56 (m, 3H), 7.46 (s, 1H), 7.42 (d, *J* = 4.3 Hz, 2H), 7.39 (d, *J* = 2.5 Hz, 2H), 7.37 (s, 1H), 7.27 (d, *J* = 1.5 Hz, 1H), 6.54 (d, *J* = 11.5 Hz, 1H); ¹³C-NMR (100 MHz, CDCl₃) δ 188.1, 150.1 (d, *J* = 17.5 Hz), 137.6, 136.6, 134.4 (d, *J* = 2.5 Hz), 133.8 (d, *J* = 11.0 Hz), 133.4, 133.2, 133.1 (d, *J* = 10.5 Hz), 132.6 (d, *J* = 5.0 Hz), 131.6, 130.8, 130.2, 130.1 (d, *J* = 11.6 Hz), 129.2, 128.9, 128.8, 128.8, 128.7, 128.6, 128.4, 128.2, 127.5, 126.9, 125.6, 125.3, 124.9, 124.7; ³¹P-NMR (162 MHz, CDCl₃) δ 24.8 (s, 1P, ¹*J*_{Pt-P} = 3038 Hz); HRMS (ESI) [*MH*]⁺ *m/z* 623.0662 (Calcd. for [Pt(C₂₇H₂₂PO)Cl] 623.0665); IR ν cm⁻¹ 3056 (s), 2918 (s), 1682 (s), 1641 (s), 1595 (s), 1481 (s), 1447 (s), 1435 (s), 1307 (s), 1320 (s), 1240 (s), 1103 (s), 998 (s), 988 (s), 769 (s), 692 (s).

Pt⁰ complex (54)

A solution of [Pt(dba)₂] (0.07 g, 0.095 mmol) and ferrocene **32** (0.05 g, 0.095 mmol) in benzene (1 mL) was stirred for 2 h at room temperature. The solvent was removed *in vacuo*, giving a red powder (0.037 g, 32%). ³¹P-NMR (162 MHz, CDCl₃) δ 21.3 (s, 1P, *J*_{Pt-P} = 2912 Hz).

Pt⁰ complex (55) containing ligand 17

a. Room temperature stirring

A solution of [Pt⁰(PPh₃)₂η²-C₂H₄] (0.04 g, 0.057 mmol) and Lei ligand (0.02 g, 0.057 mmol) in benzene (5 mL) was stirred for 2 h at room temperature. The mixture was filtered and the solvent was removed *in vacuo* giving a red powder (0.021 g, 38%).

b. On heating at 60 °C

A solution of [Pt⁰(PPh₃)₂η²-C₂H₄] (0.04 g, 0.057 mmol) and Lei ligand (0.02 g, 0.057 mmol) in benzene (5 mL) was stirred for 2 h at 60 °C. The mixture was filtered and the solvent was removed *in vacuo* giving a red powder (0.047 g, 84 %).

Mp 263-265 °C (decomp.); ¹H-NMR (400 MHz, C₆D₆) δ 7.73-7.79 (m, 1H), 7.62 (d, *J* = 7.7 Hz, 1H), 7.44 (s, 1H), 7.34-7.44 (m, 10H), 7.03-7.05 (m, 9H), 6.91-6.96 (m, 4H), 6.76-6.80 (m, 3H), 6.66-6.73 (m, 6H), 5.43 (dd, *J* = 9.3, 6.6 Hz, 1H), 5.04 (m, 1H); ¹³C-NMR (100 MHz, C₆D₆) δ 189.2, 141.2, 134.1, 132.4, 130.6 (d, *J* = 30.7 Hz), 129.7 (d, *J* = 3.4 Hz), 129.5, 129.0, 128.9, 128.8, 128.7, 128.6, 128.5, 128.4, 128.3, 128.2, 126.7, 126.6, 73.4 (d, *J* = 53.8 Hz), 65.7 (d, *J* = 2.1 Hz); ³¹P-NMR (162 MHz, C₆D₆) δ 21.2 (s, 1P, ¹*J*_{Pt-P} = 2933 Hz); HRMS (ESI) [M]⁺ *m/z* 979.9470 (Calcd. for [Pt(C₂₇H₂₁PO)₂]⁺ 979.9472); IR ν cm⁻¹ 3052 (s), 2920 (s), 1652 (s), 1622 (s), 1570 (s), 1558 (s), 1464 (s), 1456 (s), 1436 (s), 1411 (s), 1297 (s), 1213 (s), 1196 (s), 1118 (s), 1095 (s), 1069 (s), 1018 (s), 998 (s), 745 (s), 693 (s).

Rh^I complex (57)

A Schlenk tube was charged with a suspension of [RhCl(cod)]₂ (0.037 g, 0.11 mmol) in THF (10 mL) was added ferrochalcone **32** (0.110 g, 0.22 mmol) in THF (5 mL). The dark reddish suspension changed immediately to a dull red solution. The solution was left to stir overnight at room temperature under a N₂ atmosphere. After this time, the THF was removed *in vacuo*. The red residue was washed with diethyl ether (3 × 15 mL) and the organic washings were collected and filtered, combined and concentrated *in vacuo* to *ca.* 5 mL. After 24 h a red microcrystalline solid formed, which was separated by filtration and the filtrate was left for crystallization giving the title complex (0.088 g, 35%). Mp 236-238 °C (decomp.); ¹H-NMR (400 MHz, CDCl₃) δ 8.20 (d, *J* = 15.7 Hz, 1H), 7.79 (dd, *J* = 8.0, 4.0 Hz, 1H), 7.71 (m, 4H), 7.61 (m, 2H), 7.53 (m, 2H), 7.49 (dd, *J* = 7.5, 2.5 Hz, 3H), 7.39 (m, 2H), 6.86 (d, *J* = 15.7 Hz, 1H), 4.83 (t, *J* = 4.0 Hz, 2H),

4.52 (t, $J = 4.0$ Hz, 2H), 4.10 (s, 5H); ^{13}C -NMR (100 MHz, CDCl_3) δ 167.8, 133.8, 133.6, 132.8, 132.7, 132.5, 132.2, 132.1, 131.1, 130.8, 130.7, 130.6, 129.2, 128.9 (d, $J = 5.5$ Hz), 128.7, 127.1, 78.8 (d, $J = 14.0$ Hz), 72.8, 70.2, 70.1, 69.8, 69.7, 68.3; ^{31}P -NMR (162 MHz, CDCl_3) δ 34.6-31.0 (dd, 1P, $J_{\text{Rh-Pb}} = 99.2$ Hz, $J_{\text{Pb-Pa}} = 468.8$ Hz), 24.4-20.9 (dd, 1P, $J_{\text{Rh-Pa}} = 94.4$ Hz, $J_{\text{Pa-Pb}} = 470.4$ Hz), 56.55 (s), 57.59 (s), 58.62 (s), 60.74 (d, $J_{\text{Rh-P}} = 172.80$ Hz, 1P); HRMS LIFDI $[M]^+$ m/z 637.99 (Calcd. for $[\text{Rh}(\text{C}_{31}\text{H}_{25}\text{FePO})_2\text{Cl}]$ 637.97); IR ν cm^{-1} 3044 (s), 2821 (s), 1627 (s), 1553 (s), 1473 (s), 1456 (s), 1325 (s), 1225 (s), 1189 (s), 1044 (s), 759 (s), 696 (s).

Rh^I complex (58)

A solution of $[\text{RhCl}(\text{cod})]_2$ (0.037 g, 0.11 mmol) and Lei ligand (0.086 g, 0.22 mmol) in benzene (10 mL) was stirred for 2h at room temperature. Finally, solvent was removed and concentrated to *ca.* 5 mL giving light yellow crystalline solid (0.145 g, 71%). Mp 221-223 °C; ^1H -NMR (400 MHz, CDCl_3); 8.64 (m, 1H), 8.22 (m, 1H), 7.69 (m, 3H), 7.63 (td, $J = 7.0, 6.0, 2.7$ Hz, 2H), 7.51 (dd, $J = 7.3, 4.0$ Hz, 1H), 7.30 (m, 2H), 7.23 (m, 1H), 7.14 (t, $J = 7.5$ Hz, 1H), 7.04 (m, 1H), 6.95 (m, 3H), 6.78 (q, $J = 8.0, 7.5$ Hz, 2H), 6.53 (m, 1H), 5.52 (m, 1H), 5.32 (ddd, $J = 10.5, 7.5, 2.5$ Hz, 0.5H), 4.82 (ddd, $J = 7.5, 4.0, 1.7$ Hz, 0.5 H); ^{13}C -NMR (100 MHz, CDCl_3) δ 197.3, 192.5, 138.7, 137.5, 135.4 (d, $J = 7.3$ Hz), 134.8 (d, $J = 8.5$ Hz), 134.1, 133.8 (d, $J = 6.8$ Hz), 132.6 (d, $J = 7.0$ Hz), 131.9, 131.5, 130.4, 130.1, 129.9, 129.8, 129.5, 129.4, 129.2 (d, $J = 8.7$ Hz), 128.9, 128.8, 128.7, 128.5, 128.1, 127.9, 127.9 (d, $J = 7.5$ Hz), 127.7, 127.7, 127.3, 127.1, 127.1, 126.9, 126.1 (d, $J = 6.0$ Hz), 125.5 (d, $J = 5.3$ Hz), 125.1, 124.5; ^{31}P -NMR (162 MHz, CDCl_3) δ 34.4-30.8 (dd, 1P, $J_{\text{Pb-Pa}} = 474$ Hz, $J_{\text{Rh-Pb}} = 100$ Hz), 25.2-21.7 (dd, 1P, $J_{\text{Pa-Pb}} = 474$ Hz, $J_{\text{Rh-Pa}} = 93$ Hz); HRMS LIFDI $[M]^+$ m/z 887.16 (Calcd. for $[\text{Rh}(\text{C}_{27}\text{H}_{21}\text{PO})_2]$ 887.17); IR ν cm^{-1} 3054 (s), 2923 (s), 1695 (s), 1652 (s), 1635 (s), 1595 (s), 1482 (s), 1456 (s), 1433 (s), 1384 (s), 1325 (s), 1225 (s), 1189 (s), 1092 (s), 1044 (s), 1022 (s), 791 (s), 751 (s), 697 (s).

Cu^I complex (59)

$[\text{Cu}(\text{MeCN})_4]\text{PF}_6$ (0.028 g, 0.075 mmol) was dissolved in CH_2Cl_2 (2.5 mL) and transferred by cannula to a solution of ferrocalcone **32** (0.075 g, 0.15 mmol) in CH_2Cl_2 (2.5 mL) and stirred for 2 h at room temperature. The solvent was removed *in vacuo* and the crude product redissolved in minimum amount of CH_2Cl_2 . Toluene was added and the mixture stirred for 1 h to give dark reddish precipitate, which was then filtered and washed with toluene and a small amount of ether to afford title compound (0.081 g, 50

%). Mp 214-219 °C; ¹H-NMR (400 MHz, CD₂Cl₂) δ 8.12 (d, *J* = 16.5 Hz, 1H), 7.73 (s, 1H), 7.51 (m, 2H), 7.40 (m, 10H), 7.30 (s, 1H), 6.85-6.90 (m, 1H), 4.71 (m, 2H), 4.67 (m, 2H), 4.14 (m, 5H); ¹³C-NMR (100 MHz, CD₂Cl₂) ; 190.5, 137.8 (d, *J* = 8.3 Hz), 134.4 (d, *J* = 13 Hz), 134.1 (d, *J* = 7.0 Hz), 133.5 (d, *J* = 12 Hz), 132.9 (d, *J* = 11.5 Hz), 132.0, 131.2, 130.7 (d, *J* = 19 Hz), 129.7 (d, *J* = 12 Hz), 129.5 (d, *J* = 12.6 Hz), 126.4, 125.5, 117.3, 101.6 (d, *J* = 9 Hz), 95.7, 74.5, 70.6, 70.1; ³¹P-NMR (162 MHz, CD₂Cl₂) δ -4.80 (s, 1P), -143.8 (septet, ¹*J*_{P-F} = 719.5 Hz); HRMS (ESI) [*M*]⁺ *m/z* 563.0297 (Calcd. For [Cu(C₃₁H₂₅FePO)] 563.0283); IR ν cm⁻¹ 3092 (bs), 2891 (s), 2223 (s), 1671 (s), 1643 (s), 1561 (s), 1428 (s), 1389 (s), 1182 (s), 1092 (s), 997 (s), 831 (s), 776 (s), 692 (s).

Cu^I complex (60)

To a stirred solution of ferrochalcone (0.028 g, 0.057 mmol) in CH₂Cl₂ (2.5 mL) was added a solution of [CuCl] (0.056 g, 0.057 mmol) in CH₂Cl₂ (2.5 mL) and reaction mixture was stirred for 1 h at room temperature. Finally it was filtered, and the filtrate was concentrated giving light reddish powder (0.016 g, 46 %). Mp 197-199 °C (decomp); ¹H-NMR (400 MHz, CD₂Cl₂) δ 8.28 (d, *J* = 13.7 Hz, 1H), 7.69 (m, 1H), 7.53 (m, 6H), 7.39 (dt, *J* = 13.0, 6.5 Hz, 5H), 7.32 (d, *J* = 7.6 Hz, 1H), 6.99 (t, *J* = 8.8 Hz, 1H), 6.78 (d, *J* = 15.0 Hz, 1H), 4.68 (bs, 2H), 4.49 (bs, 2H), 4.04 (s, 5H); ¹³C-NMR (100 MHz, CD₂Cl₂) δ 145.1, 140.6 (d, *J* = 13.5 Hz), 134.9 (d, *J* = 15.5 Hz), 134.3 (d, *J* = 5.8 Hz), 132.3, 131.3, 131.2, 131.1, 130.1, 129.8 (d, *J* = 6.5 Hz), 129.5 (d, *J* = 10.7 Hz), 129.1, 128.7 (d, *J* = 6.0 Hz), 80.8, 73.4, 72.8, 70.6, 70.6, 70.4, 70.3 (d, *J* = 5.0 Hz), 70.1; ³¹P-NMR (162 MHz, CD₂Cl₂) δ -4.38 (s, 1P); HRMS (ESI) [*M*]⁺ *m/z* 563.0284 (Calcd. For [Cu(C₃₁H₂₅FePO)] 563.0277); IR ν cm⁻¹ 2921 (bs), 2850 (s), 2359 (s), 1700 (s), 1652 (s), 1575 (s), 1506 (s), 1465 (s), 1436 (s), 1398 (s), 1314 (s), 1277 (s), 1168 (bs), 1070 (s), 998 (s), 824 (s), 751 (s), 694 (s).

Cu^I complex (61)

[Cu(MeCN)₄]PF₆ (0.028 g, 0.075 mmol) was dissolved in CH₂Cl₂ (2.5 mL) and transferred by cannula to a solution of thio-ferrochalcone (0.079 g, 0.15 mmol) in CH₂Cl₂ (2.5 mL) and stirred for 2 h at room temperature. The solvent was removed in *vacuo* and the crude product redissolved in minimum amount of dichloromethane. Toluene was added and the mixture stirred for 1 h to give red precipitate, which was then filtered and washed with toluene and a small amount of ether to afford title compound as a red solid (0.063 g, 37 %). Mp 231-233 °C (decomp.); ¹H-NMR (400

MHz, C₆D₆) δ 7.78-7.73 (m, 2H), 7.72 (s, 1H), 7.70-7.66 (m, 4H), 7.64 (dd, *J* = 7.5, 3.7 Hz, 4H), 7.60 (m, 1H), 7.46 (tdd, *J* = 7.5, 2.8, 1.0 Hz, 1H), 7.10-6.99 (m, 1H), 6.84 (d, *J* = 14.0 Hz, 1H), 6.38 (d, *J* = 14.0 Hz, 1H), 4.92 (app.t, *J* = 4.0 Hz, 2H), 4.72 (app.t, *J* = 4.0 Hz, 2H), 4.23 (s, 5H); ¹³C-NMR (100 MHz, C₆D₆) ; 189.5, 137.1 (d, *J*=9), 134.3 (d, *J*=13), 133.4 (d, *J*=12), 133.1 (d, *J*=7.0), 132.8 (d, *J*=12), 132.0, 131.2, 130.6 (d, *J*=9), 129.7 (d, *J*=19), 129.5 (d, *J*=13), 126.4, 125.4, 116.3, 99.6 (d, *J*=9), 96.7, 74.5, 70.6, 70.1; ³¹P-NMR (162 MHz, C₆D₆) δ 44.5 (s, 1P), -142.06 (septet, ¹*J*_{P-F} = 713 Hz); HRMS (ESI) [*M*]⁺ *m/z* 1127.0701 (Calcd. For [Cu(C₃₁H₂₅FePSO)₂] 1127.0701); IR (KBr, ν cm⁻¹): 3438 (bs), 2922 (s), 2359 (s), 2340 (bs), 1652 (s), 1635 (s), 1599 (s), 1437 (s), 1377 (s), 1307 (s), 1104 (s), 1083 (s), 841 (s), 752 (s), 692 (s), 604 (s).

Cu^I complex (62)

To a stirred solution of thio-ferrochalcone ligand **33** (0.030 g, 0.057 mmol) in CH₂Cl₂ (2.5 mL) was added a solution of [CuCl] (0.056 g, 0.057 mmol) in CH₂Cl₂ (2.5 mL) and reaction mixture was stirred for 2 h at room temperature. Finally the reaction mixture was filtered, and the filtrate concentrated *in vacuo* affording a light red powder (0.023 g, 63%). Mp 203-205 °C (decomp.); ¹H-NMR (400 MHz, CD₂Cl₂) δ 7.82 (ddt, *J* = 13.5, 7.0, 1.3 Hz, 6H), 7.56-7.59 (m, 3H), 7.51-7.54 (m, 3H), 7.49-7.50 (m, 1H), 7.37 (tdd, *J* = 7.5, 2.3, 1.2 Hz, 1H), 7.10 (dd, *J* = 7.8, 1.1 Hz, 1H), 6.70 (d, *J* = 14.5 Hz, 1H), 4.78 (app.t, *J* = 4.0 Hz, 2H), 4.55 (app.t, *J* = 4.0 Hz, 2H), 4.14 (s, 5H); ¹³C-NMR (100 MHz, CD₂Cl₂) δ 192.1, 139.9 (d, *J* = 8 Hz), 134.1, 133.6 (d, *J* = 11 Hz), 133.3, 132.9 (d, *J* = 11 Hz), 132.7, 132.6, 129.5, 129.3 (d, *J* = 13 Hz), 80.7, 73.3, 70.5, 70.2; ³¹P-NMR (162 MHz, CD₂Cl₂) δ 41.2 (s, 1P); HRMS (ESI) [*M*]⁺ *m/z* 595.0 (Calcd. for [Cu(C₃₁H₂₅FePSO)] 595.00); IR ν cm⁻¹ 2919 (s), 2849 (s), 2361 (s), 1700 (s), 1684 (s), 1645 (s), 1558 (s), 1520 (s), 1457 (s), 1437 (s), 1374 (s), 1304 (s), 1255 (s), 1104 (s), 1074 (s), 998 (s), 755 (s), 691 (s), 609 (s).

Cu^I complex (63)

[Cu(MeCN)₄]PF₆ (0.022 g, 0.060 mmol) was dissolved in CH₂Cl₂ (2.5 mL) and transferred by cannula to a solution of Lei ligand (0.047 g, 0.12 mmol) in CH₂Cl₂ (2.5 mL) and the reaction mixture was stirred for 2 h at room temperature. The solvent was removed *in vacuo* and the crude product redissolved in a minimum amount of CH₂Cl₂. Toluene was added and the mixture stirred for 1 h to give a light yellowish precipitate, which was then filtered and washed with toluene and a small amount of ether to give the product (0.061 g, 59%). Mp 171-173 °C (decomp.); ¹H-NMR (400 MHz, CD₂Cl₂) δ

8.09 (d, $J = 15.0$ Hz, 1H), 7.73 (d, $J = 7.7$ Hz, 2H), 7.64 (t, $J = 7.5$ Hz, 1H), 7.59 (s, 1H), 7.47 (q, $J = 8.0$ Hz, 5H), 7.39 (s, 3H), 7.24 (t, $J = 7.7$ Hz, 3H), 7.05 (d, $J = 6.5$ Hz, 4H), 7.01-6.90 (m, 1H); ^{13}C -NMR (100 MHz, CD_2Cl_2) δ 141.5 (d, $J = 9.0$ Hz), 137.7, 135.1, 134.3 (d, $J = 11.3$ Hz), 134.1 (d, $J = 12.0$ Hz), 131.6, 130.7, 129.8, 129.4, 128.8, 118.1; ^{31}P -NMR (162 MHz, CD_2Cl_2) δ -4.51 (s, 1P), -143.8 (septet $^1J_{\text{P-F}} = 712.8$ Hz); HRMS (ESI) $[\text{M}+\text{H}]^+$ m/z 849.2133 (Calcd. for $[\text{Cu}(\text{C}_{27}\text{H}_2\text{PO})_2]$ 849.2132); IR ν cm^{-1} 3446 (s), 3056 (s), 2956 (s), 2924 (s), 2853 (s), 2359 (s), 1652 (s), 1600 (s), 1480 (s), 1436 (s), 1332 (s), 1261 (s), 1215 (s), 1096 (s), 1016 (s), 839 (s), 748 (s), 693 (s).

Cu^{I} complex (64)

To a stirred solution of Lei ligand (0.022 g, 0.057 mmol) in CH_2Cl_2 (2.5 mL) was added a solution of $[\text{CuCl}]$ (0.005 g, 0.057 mmol) in CH_2Cl_2 (2.5 mL) and reaction mixture was stirred for 2 h at room temperature. Finally the reaction mixture was filtered, and the filtrate concentrated *in vacuo* to give light yellow powder (0.017 g, 60%). Mp 197-199 °C (decomp.); ^1H -NMR (400 MHz, CD_2Cl_2) δ 8.03 (d, $J = 15.5$ Hz, 1H), 7.69 (dd, $J = 7.7, 4.0$ Hz, 1H), 7.63 (dd, $J = 8.3, 1.2$ Hz, 2H), 7.53 (m, 1H), 7.51 (dd, $J = 3.0, 1.3$ Hz, 2H), 7.48 (d, $J = 1.5$, 1H), 7.44 (m, 3H), 7.39 (m, 4H), 7.35 (s, 1H), 7.32 (m, 3H), 7.05 (d, $J = 15.5$ Hz, 1H), 6.99 (ddd, $J = 9.5, 7.8, 1.0$ Hz, 1H); ^{13}C -NMR (100 MHz, CD_2Cl_2) δ 190.5, 140.4, 138.2, 134.8 (d, $J = 16$ Hz), 134.3 (d, $J = 6.5$ Hz), 132.9, 132.6, 132.2, 131.2, 131.1 (d, $J = 8.0$ Hz), 130.8, 130.1 (d, $J = 7.0$ Hz), 129.5 (d, $J = 10$ Hz), 129.1 (d, $J = 15.5$ Hz), 128.8 (d, $J = 6.3$ Hz); ^{31}P -NMR (162 MHz, CD_2Cl_2) δ -3.47 (s, 1P); HRMS (ESI) $[\text{M}]^+$ m/z 455.0621 (Calcd. for $[\text{Cu}(\text{C}_{27}\text{H}_{21}\text{PO})]$ 455.0623); IR ν cm^{-1} 2922 (s), 1739 (s), 1695 (s), 1669 (s), 1652 (s), 1558 (s), 1583 (s), 1558 (s), 1533 (s), 1464 (s), 1436 (s), 1419 (s), 1105 (s), 728 (s).

3.4.2 X-Ray Diffraction Data

Diffraction data for complex **49**, **50**, **54**, **55**, **57**, **58**, **62** and **63** was collected at 110 K on a Bruker Smart Apex diffractometer with Mo- K_{α} radiation ($\lambda = 0.71073 \text{ \AA}$) using a SMART CCD camera. Diffractometer control, data collection and initial unit cell determination was performed using “SMART”. Frame integration and unit-cell refinement was carried out with “SAINT+”. Absorption corrections were applied by SADABS. Structures were solved by “direct methods” using SHELXS-97 (Sheldrick, 1997)¹⁵⁸ and refined by full-matrix least squares using SHELXL-97 (Sheldrick, 1997).¹⁵⁹ All non-hydrogen atoms were refined anisotropically.

Diffraction data for complex **64** was collected on a SuperNova diffractometer with Mo- K_{α} radiation ($\lambda = 0.7107 \text{ \AA}$) using an Enhance (Mo) X-ray source. OLEX2¹⁶⁰ was used for overall structure solution, refinement and preparation of computer graphics and publication data. Within OLEX2, the algorithms used for structure solution were “direct methods”, using the “A short history of SHELX (Sheldrick, 2007)/Bruker”. Refinement by full-matrix least-squares used the SHELXL-97¹⁶¹ algorithm within OLEX2.¹⁶² All non-hydrogen atoms were refined anisotropically. Hydrogen atoms were placed using a “riding model” and included in the refinement at calculated positions.

Table 14: Single Crystal X-Ray details for Pt^{II} complex of ferrochalcone ligand (32) and Lei ligand (17).

Compound reference	ijf0845	ijf1009
Formula	C ₃₁ H ₂₅ FePOCl ₂ Pt	C ₂₇ H ₂₁ POCl ₂ Pt
Formula weight	1005.06	658.40
temp (K)	110(2)	110(2) K
Radiation	0.71073	0.71073
Cryst syst	Triclinic	Monoclinic
Space group	P-1	P 2(1)/n
a(Å)	11.8386(5)	9.1527(13)
b(Å)	12.7592(5)	14.931(2)
c(Å)	13.7222(6)	16.591(2)
α(°)	107.9840(10)	90
β(°)	110.4270(10)	96.855(3)
γ(°)	98.6050(10)	90
V (Å³)	1768.81(13)	2251.2(5)
Z	2	4
D_{calcd.} (Mg M⁻³)	1.887	1.943
F(000)	976	1272
M(mm⁻¹)	5.038	2.163
Crystal size (mm³)	0.27 x 0.05 x 0.03	0.20 x 0.05 x 0.04
θ range for data	2.56 to 28.27	1.84 to 28.31
Collection (°)	-15 ≤ h ≤ 15,	-12 ≤ h ≤ 12,
Index ranges	-16 ≤ k ≤ 17, -18 ≤ l ≤ 18	-19 ≤ k ≤ 19, -22 ≤ l ≤ 21
No. of rflns collected	18390	22990
Refinement method	Full-matrix least-squares on F ²	Full-matrix least-squares on F ²
GOOF on F²	1.038	1.038
R1, wR2(I>2σ(I))	0.0264, 0.0572	0.0242, 0.0536
R1, wR2(all data)	0.0325, 0.0597	0.0308, 0.0562

Further details can be found in the Appendix, including the cif files on the CD.

Table 15: Single Crystal X-Ray details for Pt⁰ complex of ferrochalcone ligand (32) and Lei ligand (17).

Compound reference	ijf0924	ijf0908
Formula	C ₇₄ H ₆₂ Fe ₂ P ₂ O ₂	C ₅₄ H ₄₂ P ₂ O ₂

	Pt	Pt
Formula weight	1351.97	979.91
temp (K)	110(2)	110(2)
Radiation	0.71073	0.71073
Cryst syst	Monoclinic	Monoclinic
Space group	P2(1)/c	C2/c
a(Å)	18.7251(11)	10.6144(14)
b(Å)	18.9632(11)	19.110(3)
c(Å)	17.6708(10)	20.148(3)
α(°)	90	90
β(°)	110.0790(10)	92.197(2)
γ(°)	90	90
V (Å³)	5893.3(6)	4083.8(10)
Z	4	4
D_{calcd.} (Mg M⁻³)	1.524	1.594
F(000)	2728	1960
M(mm⁻¹)	2.956	3.559
Crystal size (mm³)	0.11 x 0.08 x 0.02	0.16 x 0.14 x 0.06
θ range for data	1.58 to 30.01	2.02 to 25.10
Collection (°)	-26 ≤ h ≤ 26,	-12 ≤ h ≤ 12,
Index ranges	-26 ≤ k ≤ 25,	-22 ≤ k ≤ 22,
	-24 ≤ l ≤ 24	-23 ≤ l ≤ 23
No. of rflns collected	66489	15767
Refinement method	Full-matrix least-squares on F ²	Full-matrix least-squares on F ²
GOOF on F²	1.017	1.072
R1, wR2(I>2σ(I))	0.0336, 0.0640	0.0376, 0.0882
R1, wR2(all data)	0.0552, 0.0707	0.0484, 0.0930

Further details can be found in the Appendix, including the cif files on the CD.

Table 16: Single Crystal X-Ray details for Rh^I complex of ferrochalcone ligand (32) and Lei ligand (17).

Compound reference	ijf0932	ijf0923
Formula	C _{64.5} H ₅₅ Cl ₇ Fe ₂ O ₂ P ₂ Rh ₂	C ₅₄ H ₄₂ P ₂ O ₂ . Cl Rh
Formula weight	1489.69	1274.66
temp (K)	110.0	110(2)
Cryst syst	Triclinic	Triclinic

Space group	P-1	P-1
a(Å)	12.8584(11)	12.6642(19)
b(Å)	13.2521(12)	14.165(2)
c(Å)	20.6616(18)	19.638(3)
α(°)	82.442(2)	109.472(3)
β(°)	74.112(2)	103.210(3)
γ(°)	62.002(2)	93.300(3)
V (Å³)	2989.9(5)	3199.0(8)
Z	2	2
D_{calcd.} (Mg M⁻³)	1.655	1.323
F(000)	1498	1326
M(mm⁻¹)	1.429	0.408
Crystal size (mm³)	0.16×0.06×0.03	0.23 x 0.22 x 0.12
θ range for data	3.7 to 56.66	1.56 to 28.33
Collection (°)	-17 ≤h≤17,	-16 ≤h≤16,
Index ranges	-17≤k≤17, -27≤l≤27	-18≤k≤18, -26≤l≤26
No. of rflns collected	23986	33292
Refinement method	Full-matrix least-squares on F ²	Full-matrix least-squares on F ²
GOOF on F²	0.687	1.031
R1, wR2(I>2σ(I))	0.0490, 0.0829	0.0398, 0.0931
R1, wR2(all data)	0.1038, 0.0959	0.0490, 0.0997

Further details can be found in the Appendix, including the cif files on the CD.

Table 17: Single Crystal X-Ray details for Cu^I complex of ferrochalcone ligand (32) and Lei ligand (17).

Compound reference	ijf0933	ijf0919	ijfsf1105
Formula	C ₃₁ H ₂₅ FePSOCl Cu	C ₅₆ H ₄₅ P ₂ O ₂ · PF ₆ Cu	C ₅₄ H ₄₂ Cl ₂ O ₂ P ₂ Cu ₂
Formula weight	716.31	1204.23	982.80
temp (K)	110(2)	110(2)	110.0
Cryst syst	Triclinic	Triclinic	Monoclinic
Space group	P-1	P-1	P2 ₁ /c
a(Å)	10.9354(12)	13.2476(11)	9.30005(17)
b(Å)	11.7472(13)	14.7778(12)	18.4790(3)
c(Å)	12.8931(14)	15.8400(13)	13.1567(3)

$\alpha(^{\circ})$	67.871(2)	80.960(2)	90.00
$\beta(^{\circ})$	73.376(3)	71.685(2)	97.4728(18)
$\gamma(^{\circ})$	84.793(3)	67.983(2)	90.00
$V(\text{\AA}^3)$	1469.9(3)	2726.5(4)	2241.84(7)
Z	2	2	2
$D_{\text{calcd.}}(\text{Mg M}^{-3})$	1.618	1.467	1.456
$F(000)$	728	1232	1008
$M(\text{mm}^{-1})$	1.641	0.749	1.182
Crystal size (mm³)	0.08 x 0.06 x 0.05	0.42 x 0.22 x 0.05	0.2107 x 0.1733 x 0.1132
θ range for data	1.77 to 25.04	1.36 to 28.30	6.14 to 64.18
Collection ($^{\circ}$)	-12 $\leq h \leq$ 13,	-17 $\leq h \leq$ 17,	-13 $\leq h \leq$ 13,
Index ranges	-13 $\leq k \leq$ 13, -15 $\leq l \leq$ 15	-19 $\leq k \leq$ 19, -21 $\leq l \leq$ 21	-26 $\leq k \leq$ 27, -18 $\leq l \leq$ 19
No. of rflns collected	11967	28307	21151
Refinement method	Full-matrix least- squares on F^2	Full-matrix least- squares on F^2	Full-matrix least- squares on F^2
GOOF on F^2	1.004	1.026	1.032
R1, $wR2(I > 2\sigma(I))$	0.0416, 0.0854	0.0355, 0.0877	0.0312, 0.0705
R1, $wR2(\text{all data})$	0.0622, 0.0950	0.0462, 0.0938	0.0397, 0.0746

Further details can be found in the Appendix, including the cif files on the CD.

Chapter 4: Gold(I) complexes of the alkene-phosphine ligands; synthesis and catalytic activity

“All that glitters may not be gold, but at least it contains free electrons”

(John Desmond Bernal, Irish Physicist)

4.1 Gold – a precious metal

Gold has been present in the collective conscience of mankind since the beginning of known history.¹⁶³ Alchemy, whose main goal was to produce gold starting from other metals, is considered nowadays as the precursor of modern chemistry.¹⁶⁴ The main use of gold was and still is in jewellery and decorative arts. Being unaffected by air,

moisture and most corrosive reagents, gold is well-suited either as a base metal for various objects, or as a protective-coating on other more reactive materials. Being the most malleable and ductile of all metals it can be easily shaped into different things. However, because of its softness in its pure-state, it is often mixed with other metals (such as silver, copper, nickel, palladium *etc.*) in order to modify its physical properties. It equally and effectively possesses numerous industrial applications and used as a protective-coating against radiation in the aeronautical and spatial industry, as a heat shield in various high tech industries (including in Formula 1 cars) and as reflective layer on some optical devices, and as colouring agent in special types of glass, or as a toner in photography.

The most important industrial applications are found in electronics due to its excellent conductivity and its good general chemical resistance. Gold is also used in medicine. Radioactive gold isotopes are utilized in diagnosis, while several gold complexes proved to be active against cancer¹⁶⁵ or arthritis.¹⁶⁶ In dentistry, gold alloys are often employed for fillings, crowns, bridges and orthodontic appliances. High quality pure metallic gold is non-toxic and non-irritating and can be used in food, having the E175 label.¹⁶⁷ However, it is tasteless and it does not have any nutritional effect, leaving the body unaltered.

4.2 Gold in chemistry

The chemistry of gold has lived in the shadow of other metals for a long time until recently chemists have focused their work in this golden direction. Recently, synthetic chemists have started paying great interest to the catalytic properties of the gold complexes,¹⁶⁸ with gold emerging as one of the most discussed topic with in the catalysis community.¹⁶⁹ The research group of Hashmi, Toste, Bond, Haruta, Hutchings, Ito and Hayashi has initiated key contributions towards gold reactivity and opened new perspectives for the chemical community.¹⁷⁰

For economical reasons, the catalytical transformations involving gold are of course much more interesting than the stoichiometrical ones. Examples of catalysis by gold have been known since the beginning of the last century,¹⁷¹ but, despite the evidence, chemists continued to consider gold as “catalytically dead” because of its stability in

elementary state. However, the recent work on the high catalytic activity of gold compounds in catalysis proved the opposite.¹⁷²

Gold-catalyzed reactions fall into two major categories, heterogeneous catalysis and homogenous catalysis. Au-complexes catalyze the transformation of C=C and C≡C bonds¹⁷³ into a diverse array of reactions including: nucleophilic substitution,¹⁷⁴ hydration,¹⁷⁵ cycloaddition,¹⁷⁶ rearrangement,¹⁷⁷ hydrosilylation,¹⁷⁸ oxidation,¹⁷⁹ carbene transfer (C-H functionalisation),¹⁸⁰ epoxidation,¹⁸¹ hydroamination¹⁸² and cycloisomerisation.¹⁸³

Heterogeneous catalysis can involve gold nanoparticles and thiol-monolayer gold surfaces. Solid gold catalysts can be recycled, and when prepared in the form of smaller clusters (particle size of *ca.* 5 nm) are highly active and selective for reactions such as CO oxidation in the presence of H₂,¹⁸⁴ water-gas shift,¹⁸⁵ alcohol oxidation,¹⁸⁶ and some C-C forming reactions.¹⁸⁷

Homogenous catalysis involves gold(I) and gold(III) metal complexes and is widely used in organic synthesis.¹⁸⁸ Since 2000, homogenous gold catalysis of organic reactions has experienced exponential growth and now chemists working in homogenous catalysis routinely consider gold complexes in their investigation. The use of gold(I) and gold(III) complexes as efficient homogenous catalysts in a wide variety of organic transformations has been highlighted in the last years.¹⁸⁹ The popularity of these processes, which allow the formation of both C-C and C-X bonds, is largely due to the significant increase in molecular complexity and the impressive structural diversity that they can provide.¹⁹⁰

4.2.1 Gold(I) complexes

Gold(I) complexes are d^{10} and exhibit either LAuX or L₂Au⁺ composition. They all show a linear, bicoordinated geometry. They usually require a strong σ -donor ligand in order to stabilize the metal centre. The most common ligands include phosphines, phosphites, N-heterocyclic carbenes or alkenes. The X ligand is generally weakly coordinating, which can be easily displaced by the substrate during the catalysis reaction. LAuX complexes can be either covalent (X= Cl or Br) or cationic (X= BF₄, PF₆, TfO *etc.*) Some of the most common gold(I) complexes are given below in Figure 1.

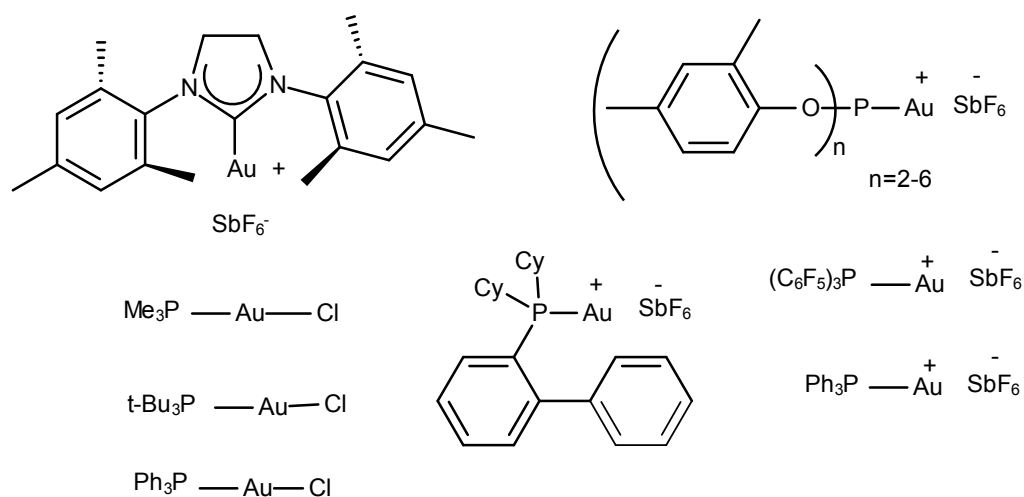


Figure 1: Some of the most common Au^I complexes with LAuX composition.

4.2.2 Gold(III) complexes

Gold(III) catalysts are d^8 complexes with AuX_3 , AuX_4^- anion or sometimes $LAuX_3$ composition. Most of these complexes show a square planar geometry. They exhibit reduced specificity and are less active as compared to the gold(I) catalyst. Below are given some of the important examples of gold(III) catalyst (Figure 2).

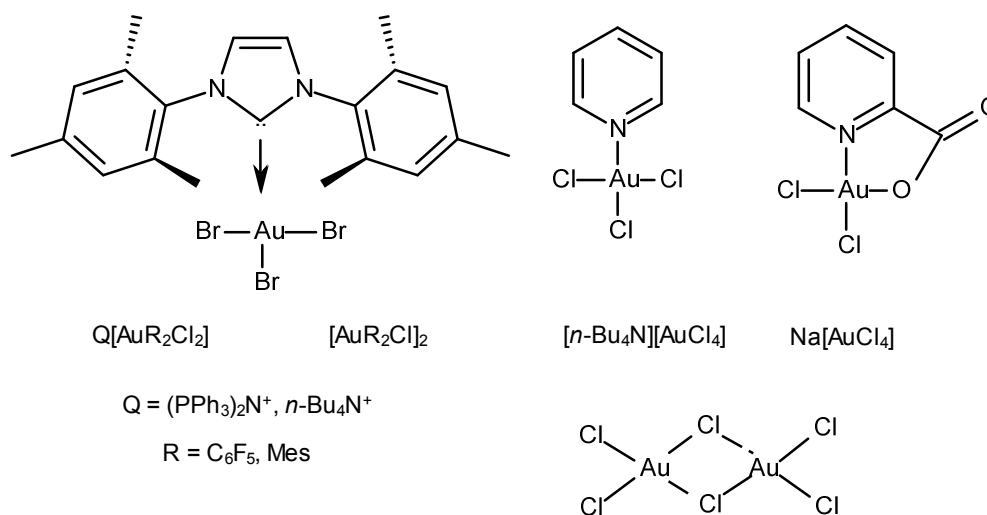


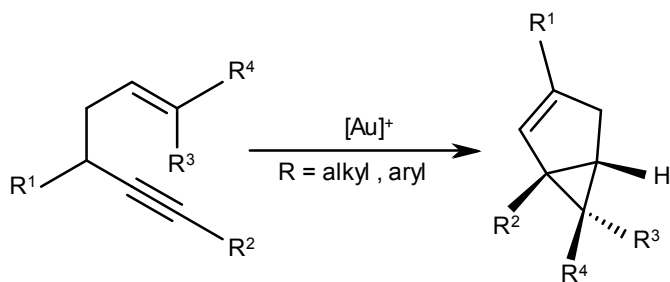
Figure 2: Some common examples of Au^{III} complexes.

Au(I) and Au(III) complexes display markedly different behaviour in similar reactions depending on the reaction pathway, leading to different products and substitution pattern.¹⁹¹ It is observed that Au(I) could be the active species where a soft π -acid is required (such as in cycloisomerisation), whereas Au(III) may be the active species where lewis acidity is required (in neutral or cationic form).¹⁹²

It has been found recently that transition metal-catalysed cycloisomerisation reactions of enyne systems have been a subject of intense research affording a range of structurally diverse products,¹⁹³ by appropriate choice of the catalyst and substrates.¹⁹⁴ The selective synthesis of different cyclic products from the same starting materials by subtle modifications to the catalytic conditions is an interesting but often troublesome topic for chemists.¹⁹⁵ However, the gold catalyst has widened its application in this regard by its versatile catalytic activities.¹⁹⁶

4.3 Cycloisomerisation

The cycloisomerisation of 1,n-enynes ($n=5-8$), mediated by Au^{I} and Au^{III} complexes has received considerable attention, particularly 1,5- and 1,6-, although 1,7- and 1,8-enynes have also been investigated. Enyne cycloisomerisation can be catalysed by Ru,¹⁹⁷ Pd,¹⁹⁸ Pt,¹⁹⁹ Ir,²⁰⁰ Rh²⁰¹ and Cu²⁰² however Au^{I} is usually more active and displays very high selectivity.²⁰³ We have concentrated on the cycloisomerisation of 1,5-enynes resulting in the synthesis of bicyclo[3.1.0]hexanes, which is particularly facile.²⁰⁴ The group of Toste has shown that a range of alkyl and aryl substituted 1,5-enynes undergo $\text{Au}(\text{I})$ -catalysed cycloisomerisation to afford bicyclo[3.1.0]hexyl ring systems (Scheme 1).²⁰⁵



Scheme 1: Au^{I} -catalyzed cycloisomerisation of 1,5-enynes.

There are a number of natural products containing the bicyclo[3.1.0]hexane core, for example prostaglandin EI analogues such as **65** (Figure 3).²⁰⁶

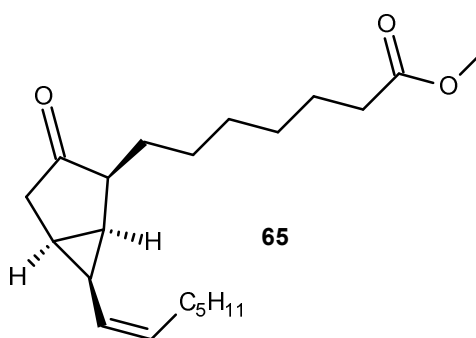


Figure 3: The structure of the prostaglandin EI analogue (65**).**

Another well known example is of α -cubebene **66** (a tricyclic sesquiterpene), which contain a tricyclo[4.4.0.0]decane core synthesized by Fürstner using a 1,5-enyne cycloisomerisation reaction (Figure 4).²⁰⁷

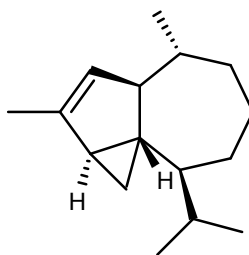
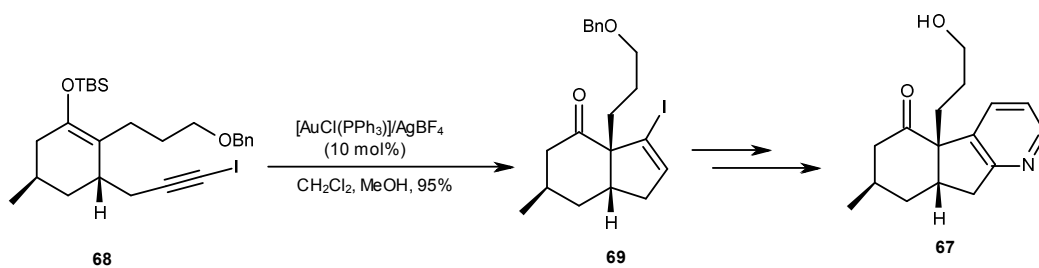


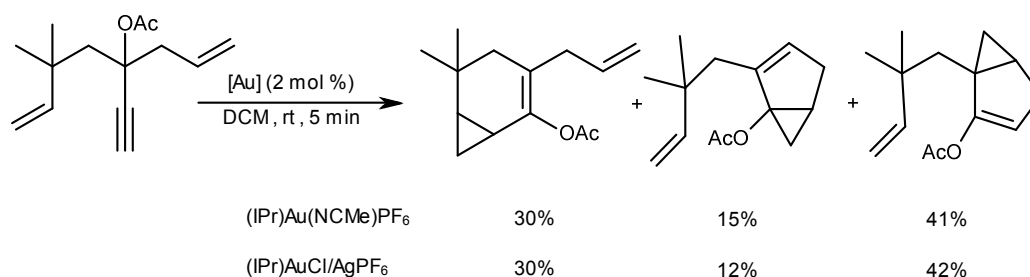
Figure 4: The structure of α -cubebene (66).

Another example from the group of Toste is that of (+)-lycopoladine A (**67**),²⁰⁸ a natural product from the club moss *Lycopodium complanatum*.²⁰⁹ An Au-catalysed cycloisomerisation of 1,5-enyne **68** affords the bicyclo[4.3.0]nonane core.



Scheme 2: Key Au-catalysed transformation in the total synthesis of (+)-lycpladine A.

Nolan *et al* also reported the synthesis of an unexpected bicyclo[3.1.0]hexene as a product in a Au(I)-catalysed cycloisomerisation of 1,5-enyne (Scheme 3).²¹⁰

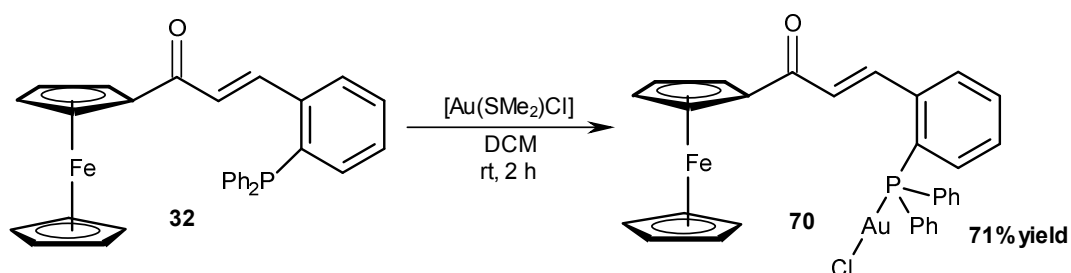


Scheme 3: Au^I catalyzed cycloisomerisation of 1,5-enynes bearing a propargylic acetate.

The aim of this part of project was to prepare Au^I complexes containing the chalcone- based alkene-phosphine and alkene-thio phosphine ligands. Previously considerable work has been done on both alkene- and phosphine-based ligands, however the chemistry of Au complexes involving hybrid alkene-phosphine ligands has not been fully explored in benchmark catalytic reactions, which is thus addressed in this chapter.

4.4 Results and Discussion

Ferrochalcone gold(I) chloride complex **70** was formed by the reaction of ferrochalcone **32** with dimethylsulfide gold(I) chloride in presence of dry CH₂Cl₂. Room temperature stirring for 2 h, followed by filtration gave clear solution resulting from the formation of Au^I complex (Scheme 4).



Scheme 4: Synthesis of Au^I complex of **32 using [Au(SMe₂)Cl].**

The product was analysed by NMR spectroscopy and mass spectrometry. The ³¹P NMR spectrum of **70** showed a shift from δ -13.0 (free ligand) to δ 28.3 in the complexed ligand. The ¹H NMR spectrum showed a very negligible shift for the α -H ($\Delta\delta = \delta_{\text{free}} - \delta_{\text{coordinated}}$ (0.03 ppm)) as compared to the shift for the β -H (0.33 ppm). Elemental analysis of the product obtained was low in carbon and hydrogen showing the presence of an impurity in the complex. However, mass spectrometry (LIFDI) confirmed the formation of [Au(C₃₁H₂₅FePO)Cl]⁺ complex with m/z of 732.0269.

The reaction was performed in the dark, as the complex is light sensitive. Different solvents were used to crystallize the complex, and small red crystals were formed in CD₂Cl₂ solution, which were then analysed by XRD to obtain a solid-state single crystal structure.

The X-ray structure shows that ferrochalcone **32** acts as a monodentate ligand binding through the phosphorus moiety only and there is no alkene interaction at all as given in (Figure 5).

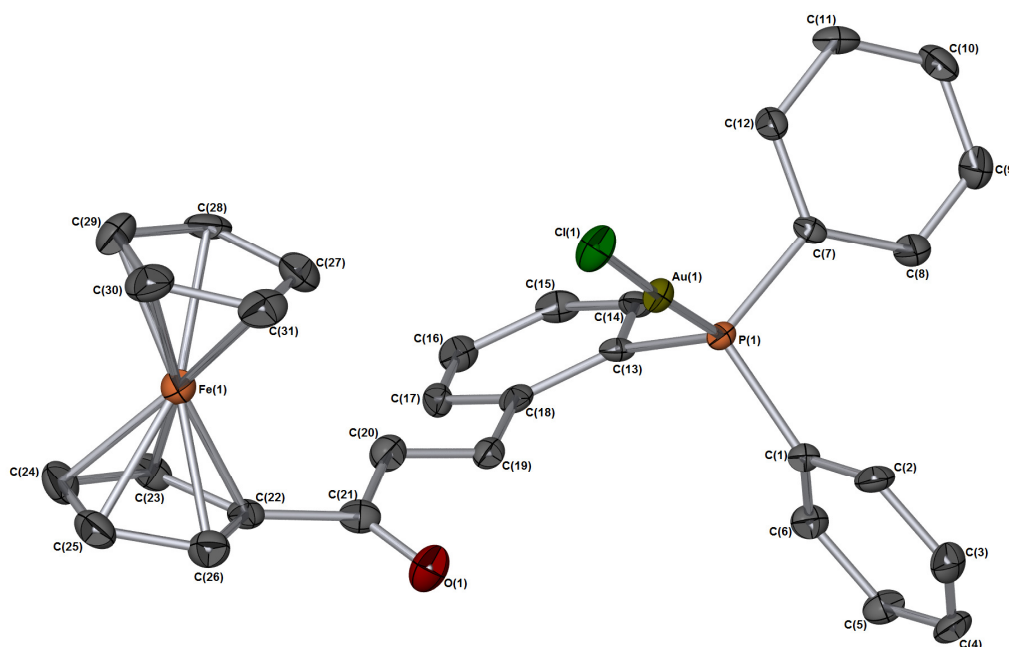


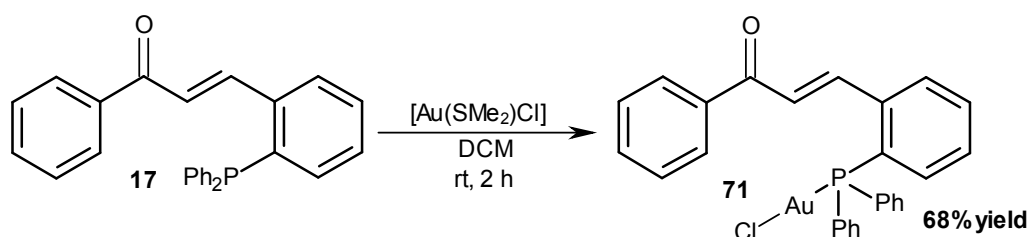
Figure 5: X-ray crystal structure of Au^I complex of **32.**

Hydrogen atoms removed for clarity. Thermal ellipsoids shown at 50%. Bond lengths (Å):
C(19)-C(20) = 1.340(8), C(20)-C(21) = 1.490(7), C(21)-O(1) = 1.224(7), Au(1)-Cl(1) =

2.2878(13), Au(1)-P(1) = 2.2350(13), C(1)-P(1) = 1.807(6), C(7)-P(1) = 1.819(5), C(13)-P(1) = 1.829(5), Bond Angles (°) : P(1)-Au(1)-Cl(1) = 178.05(5), C(13)-C(18)-C(19) = 123.1(5), C(20)-C(19)-C(18) = 122.9(5), C(19)-C(20)-C(21) = 121.9(6), C(22)-C(21)-C(20) = 117.2(5), C(1)-P(1)-C(7) = 104.2(3), C(1)-P(1)-C(13) = 107.2(2), C(7)-P(1)-Au(1) = 111.33(17), C(7)-P(1)-C(13) = 104.2(2), C(13)-P(1)-Au(1) = 114.96(18).

The Au^I complex **70** showed a linear geometry with a P-Au-Cl bond angle of 178.05(5) as expected for most of the Au^I complexes. The alkene bond length for C19-C20 (1.340 Å) is similar to that for the ethene C=C bond (1.333 Å) showing that the alkene is not involved in bonding with the metal.

As for ligand **32**, Lei ligand **17** was also treated with dimethylsulfide gold(I) chloride to obtain the Au complex (Scheme 5).



Scheme 5: Synthesis of Au^I complex of 17 using [Au(SMe₂)Cl].

The product obtained was then analysed by both ¹H and ³¹P NMR spectroscopy along with mass spectrometry. A shift in the position of α-H from δ 6.93 to δ 6.97 and for β-proton from δ 8.35 to δ 8.12 was observed. A shift by ³¹P NMR from δ -13.0 to δ 28.7 (Δδ=δ_{free}-δ_{coordinated} (41.65 ppm)) which confirmed an interaction between metal and the ligand. The LIFDI mass spectrum showed a ion at *m/z* 624.05 corresponding for [Au(C₂₇H₂₁PO)Cl]⁺. The yellow complex **71** is soluble in most solvents. Yellow needles were grown from a CD₂Cl₂ solution of Lei (Au) complex. The crystals were analysed by XRD analysis. Surprisingly a [2+2] cycloaddition product was found to have formed (Figure 6). As the [2+2] cycloaddition product was formed through photochemical reaction, hence it's not possible to characterise the product.

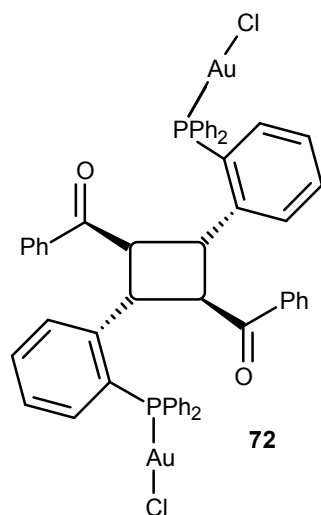


Figure 6: [2+2] cycloaddition product of complex 71.

These crystals from the same batch were further analysed by Professor Paul Raithby at the University of Bath. The structure obtained is shown in Figure 7.

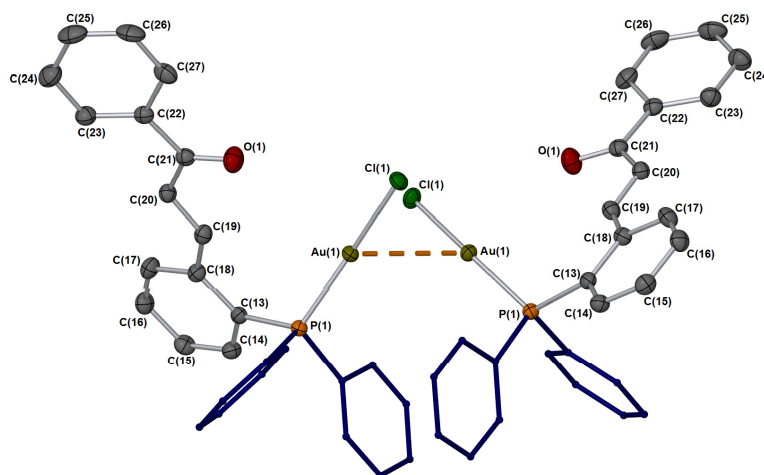


Figure 7: X-ray crystal structure of Lei-(Au) complex 71 (determined in Bath).

Hydrogen atoms removed for clarity. Thermal ellipsoids shown at 50%. Bond lengths(Å):
 C(19)-C(20) = 1.333(6), C(20)-C(21) = 1.485(6), C(21)-O(1) = 1.217(5), Au(1)-Cl(1) =
 2.2870(11), Au(1)-P(1) = 2.2356(11), C(13)-P(1) = 1.824(4), C(7)-P(1) = 1.816(4), C(1)-P(1) =
 1.816(4), Bond Angles(°) : P(1)-Au(1)-Cl(1) = 176.90(4), C(22)-C(21)-O(1) = 120.1(4), C(20)-
 C(21)-O(1) = 121.9(4), C(18)-C(19)-C(20) = 126.5(4), C(13)-C(18)-C(19) = 121.6(4), P(1)-
 C(13)-C(18) = 120.2(3).

The crystal-packing for the above structure is given in Figure 8.

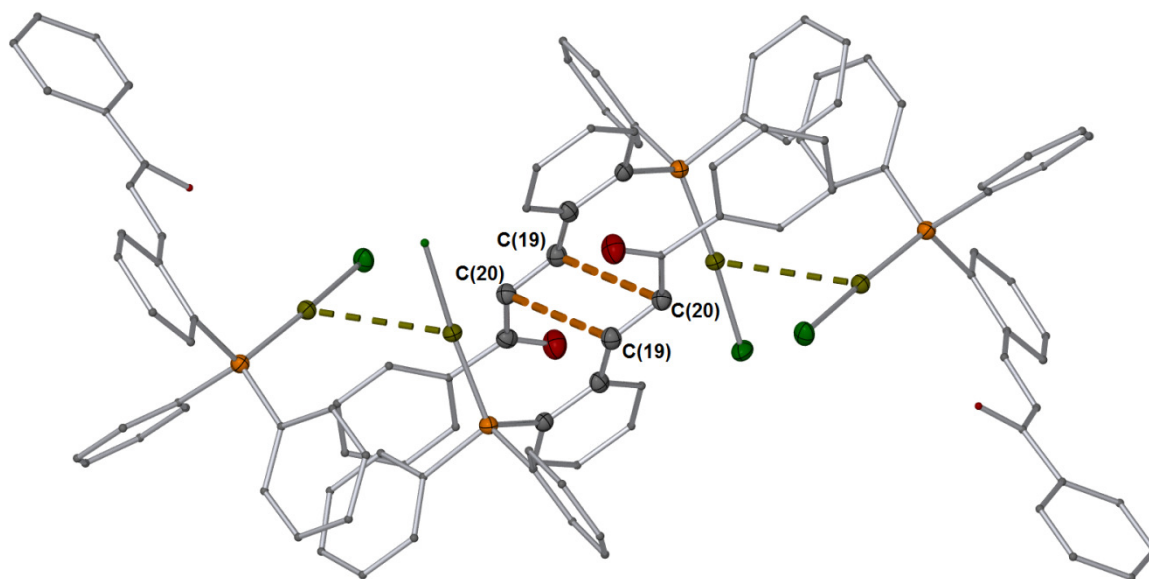


Figure 8: Crystal packing of Lei-(Au) complex 71 (determined in Bath).

The packing distance between C=C bonds was found to be 4.38 Å, which is outside Schmidt's idealized distance for facile [2+2] cycloaddition (*ca.* 4 Å). The important bond length to be considered is C(19)-C(20) alkene double bond which is 1.333(6) Å showing no involvement in either alkene metal bonding nor any type of cycloaddition reaction as previously observed. Whereas, the bond angle for P-Au-Cl is 176.90°. The two alkene bonds are placed quite far apart to be involved in any kind of interaction with Au^I.

The X-ray analysis for the crystal analysed in York showed that the structure was subjected to disorder arising from the presence of the 2+2 cycloaddition dimer. The occupancies of the disordered residue were refined to a 70:30 ratio of the dimer:monomer respectively.

Cinnamoyl derivatives (chalcones) are prone to photoinduced [2 π +2 π] photocycloaddition (PCA). Two types of cycloaddition are possible: “head-to-head” or “head-to-tail”.²¹¹ It is the *E*-isomer that is usually involved in the PCA reaction. Also, it is found that the conformational transitions of chalcones can affect, to a considerable extent, the reactivity of the CH=CH bonds and the stereoisomerism of the PCA products.²¹²

The single crystal X-ray structure shows that gold is bonded to the Lei ligand through phosphorus only and no alkene involvement is observed. The alkene moiety of the ligand undergoes a PCA reaction in the solid-state to give a cyclobutane ring as shown below in Figure 9.

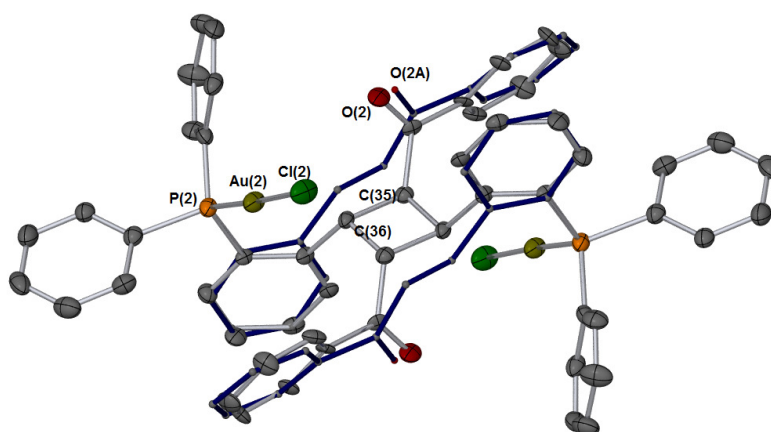


Figure 9: X-ray crystal structure of Lei-(Au) complex (72), [2+2] cycloaddition product of complex 71.

Selected bonds/angles for the [2+2] cycloaddition product. Hydrogen atoms removed for clarity.

Thermal ellipsoids shown at 50%. Bond lengths (Å): C(35)-C(36) = 1.547(8), C(34)-C(35) = 1.517(10), C(34)-O(2) = 1.211(18), Au(2)-Cl(2) = 2.2877(10), Au(2)-P(2) = 2.2336(11), C(42)-P(2) = 1.818(10), C(43)-P(2) = 1.813(4), C(49)-P(2) = 1.817(4), C(36)-C(35#) = 1.594(8), C(36#)-C(35) = 1.594(8), Bond Angles(°) : P(2)-Au(2)-Cl(2) = 176.70(4), C(41)-C(42)-P(2) = 116.9(7), C(37)-C(42)-P(2) = 122.8(7), C(35)-C(36)-C(37) = 118.8(5), C(34)-C(35)-C(36) = 115.5(5), C(33)-C(34)-C(35) = 116.2(7), C(35)-C(34)-O(2) = 122.1(10), C(33)-C(34)-O(2) = 121.6(9), C(37)-C(36)-C(35#) = 117.5(5), C(36)-C(35)-C(36#) = 90.7(4).

The bond length for C=C bond was 1.547(8) Å showing a shift from a C=C double bond character to single bond, as a result in the formation of a cyclobutane ring. The PCA of alkenes (chalcones) can proceed by two paths, through either the singlet state or triplet state (due to intersystem crossing). In the former case, the concerted PCA reaction occurs, which is allowed by orbital symmetry (through the formation of an excimer). In the second case, the PCA reaction proceeds according to the radical mechanism to form

an intermediate 1,4-biradical. The crystal structure obtained for the Lei (Au) complex confirmed the formation of a cyclobutane ring as a result of photocycloaddition in the alkene moiety of the Lei (Au) complex **71**.

We then further explored the Au metal coordination chemistry with phosphine variants of dba (dibenzylidene acetone). Dba is one of the most widely used ligand in our research group. DbaPHOS **73** and monodbaPHOS **74** are the two ligands used for the Au metal coordination studies, and the reason why they were selected is that both of these ligands contain an alkene and phosphine moiety similar to that of chalcone alkene-phosphine ligands (Figure 10).

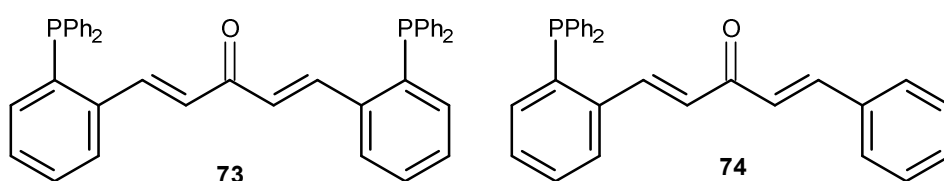
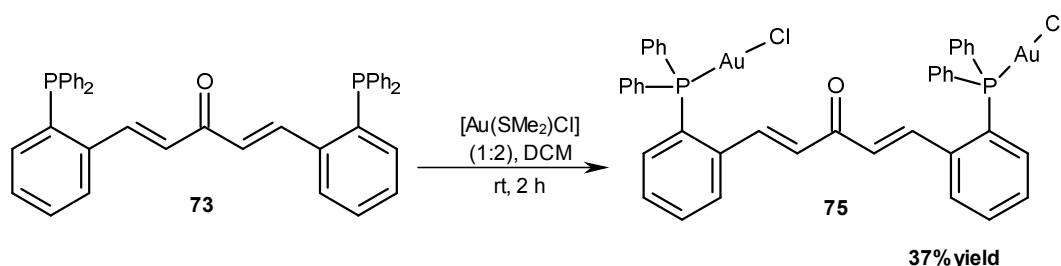


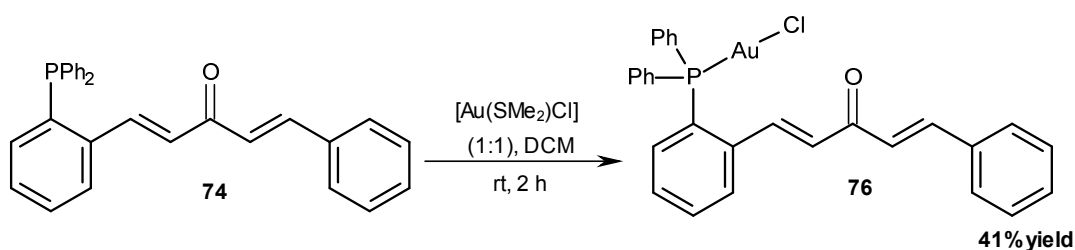
Figure 10: The structure of dbaPHOS (73**) and monodbaPHOS (**74**).**

The plan was to conduct a small scale study (by NMR) on the synthesis of Au complexes with dbaPHOS and monodbaPHOS.²¹³ The reaction of dbaPHOS **73** with [Au(SMe₂)Cl] was conducted in CH₂Cl₂ in a ligand metal ratio of (1:2) (Scheme 6). The product obtained was analysed by different analytical techniques. There is a shift in the ³¹P NMR spectrum from δ- 14.09 to δ 33.64 showing a phosphorus Au interaction; also there is a signal at δ 31.17. Similarly, a small shift in the position of both α-H and β-H was observed.



Scheme 6: Synthesis of Au-complex of dbaPHOS using [Au(SMe₂)Cl].

Monodba-PHOS was reacted in the same way with [Au(SMe₂)Cl] in CD₂Cl₂ (Scheme 7).



Scheme 7: Synthesis of Au-complex of monodbaPHOS using $[\text{Au}(\text{SMe}_2)\text{Cl}]$.

A shift in the ^{31}P NMR spectrum from $\delta -13.75$ (free ligand) to $\delta 28.02$ with a shift of 38.76 ppm ($\Delta\delta = \delta_{\text{free}} - \delta_{\text{coordinated}}$) was observed in the ^{31}P NMR spectrum. A slight shift for the two protons was also observed in the ^1H NMR spectrum. The LIFDI mass spectrum gives a mass ion at m/z 650.0698 corresponding to $[\text{C}_{29}\text{H}_{23}\text{POAuCl}]^+$, confirming the formation of Au^{I} complex for the MonodbaPHOS. It was observed that the monodbaPHOS Au complex crystallizes out as yellow needles from the NMR sample after a few days. XRD analysis confirmed **77** as the structure (Figure 11).

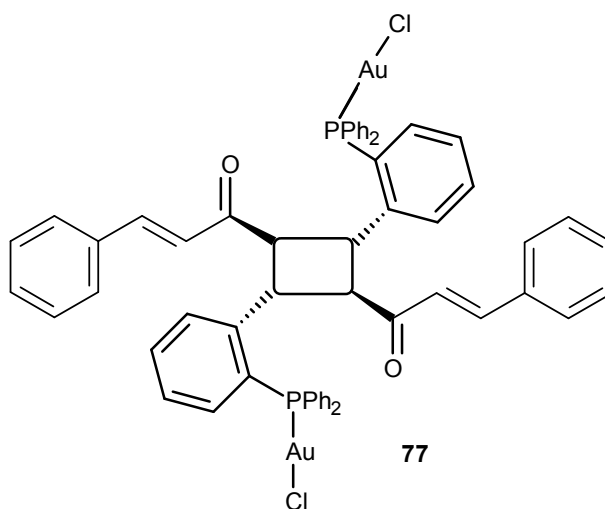


Figure 11: [2+2] cycloaddition product of complex 76.

The X-ray crystal structure for the monodba-PHOS (Au) complex is given in Figure 12.

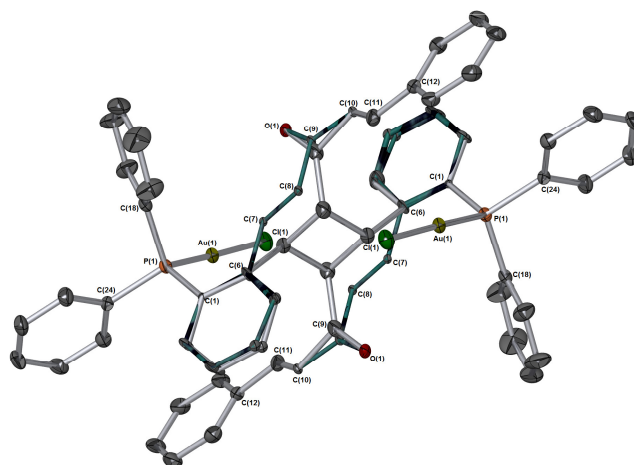


Figure 12: X-ray crystal structure of monodbaPHOS-(Au) complex.

Selected bonds/angles for the [2+2] cycloaddition product **77**. Hydrogen atoms removed for clarity. Thermal ellipsoids shown at 50%. Bond lengths (Å): C(6A)-C(7A) = 1.57(4), C(7A)-C(8A) = 1.551(14), C(8A)-C(9A) = 1.53(3), C(9A)-C(10) = 1.56(5), C(9A)-O(1) = 1.29(4), C(7A)-C(8A¹) = 1.596(16), C(8A)-C(7A¹) = 1.596(16), Au(1)-Cl(1) = 2.2880(8), Au(1)-P(1) = 2.2305(8), Bond Angles(°) : C(6A)-C(7A)-C(8A) = 113.9(14), C(7A)-C(8A)-C(9A) = 115(2), C(6A)-C(7A)-C(8A¹) = 127(2), C(7A)-C(8A)-C(7A¹) = 89.1(8), C(8A)-C(7A)-C(8A¹) = 90.9(8), C(9)-O(1)-C(9A) = 14(2), O(1)-C(9A)-C(8A) = 129(3), O(1)-C(9A)-C(10) = 109(2), P(1)-Au(1)-Cl(1) = 175.12(3).

The presence of the dimerised cycloaddition product is not unprecedented for dba. Dba has been shown to undergo intermolecular [$\pi 2s + \pi 2s$] cycloaddition in the solution state.²¹⁴ In isolation dba does not undergo photochemical [$\pi 2s + \pi 2s$] cycloaddition in the solid-state as the structure does not meet the required criteria. According to Schmidt's topochemical principles dba cannot undergo cycloaddition in the solid-state as the C=C double bonds in adjacent molecules are more than 4 Å apart. Dba has been shown to undergo photochemical cycloadditions when co-crystallised with additives such as UO₂Cl₂ and SnCl₄.²¹⁵ These additives change the crystal packing of the dba molecules, therefore aligning the alkene bonds in an orientation that allows them to react. It is worthy of note that the [2+2] cycloaddition reaction has occurred on the most hindered alkene. The presence of the mixture of compounds in the crystal suggested that a photochemical [$\pi 2s + \pi 2s$] reaction could be occurring in the solid-state.

A comparison of Au^I complexes for ligand **(32)**, **(17)** and **(74)** is given in Table 1. All of these Au^I metal complexes exhibit a linear geometry.

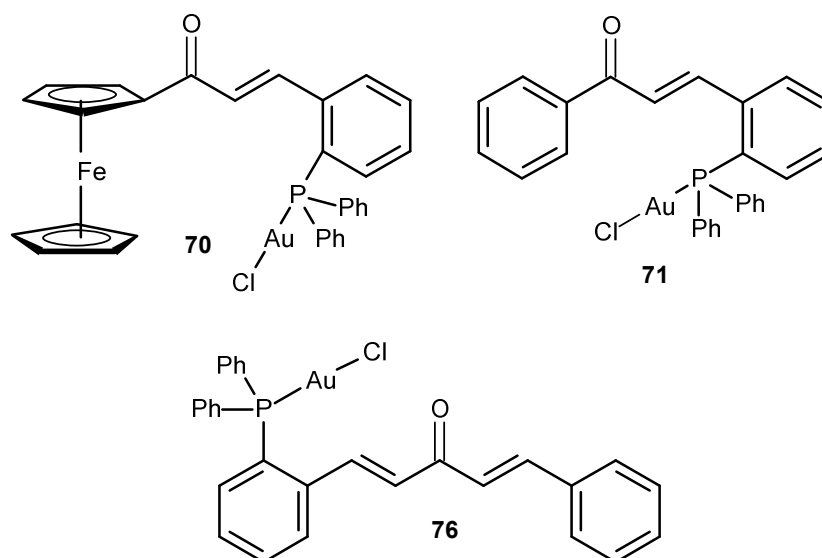


Table 1 : Comparison of the bond lengths in Au(I) complexes of ferrocchalcone (70), Lei ligand (71).

Au(I) complex (70)		Au(I) complex (71)	
Bond	Length, Å	Bond	Length, Å
C(19)-(20)	1.340(8)	C(19)-C(20)	1.333(6)
C(20)-(21)	1.490(7)	C(20)-C(21)	1.485(6)
C(21)-O(1)	1.224(7)	C(21)-O(1)	1.217(5)
C(1)-P(1)	1.807(6)	C(1)-P(1)	1.816(4)
C(7)-P(1)	1.819(5)	C(7)-P(1)	1.816(4)
C(13)-P(1)	1.829(5)	C(13)-P(1)	1.824(4)
Au(1)-P(1)	2.2350(13)	Au(1)-P(1)	2.2356(11)
Au(1)-Cl(1)	2.2878(13)	Au(1)-Cl(1)	2.2870(11)

The bond length for the C=C double bond in ethane is 1.33 Å.²¹⁶ The bond length for the non-complexed and complexed ligand is similar to ethene, 1.334 Å indicating that alkene is not involved in any interaction with the metal. The ligand is coordinated to

metal through phosphorus giving a linear geometry. A comparison between other important bonds showed very similar values.

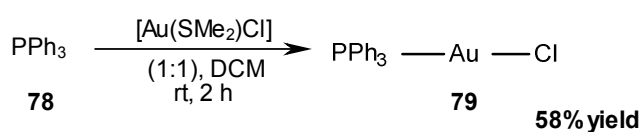
In addition to this a comparison of the bond lengths between gold(I) complexes of Lei ligand ([2+2] cycloaddition product) **72** and monodbaPHOS ligand ([2+2] cycloaddition product) **77** was done as given in Table 2.

Table 2: Comparison of the bond lengths in gold(I) complexes of Lei ligand (72) and monodbaPHOS ligand (77).

Au(I) complex (72) (2+2) cycloaddition product of 71		Au(I) complex (77) (2+2) cycloaddition product of 76	
Bond	Length, Å	Bond	Length, Å
C(35)-C(36)	1.547(8)	C(7A)-C(8A)	1.551(14)
C(34)-C(35)	1.517(10)	C(8A)-C(9A)	1.53(3)
C(34)-O(2)	1.211(18)	C(9A)-O(1)	1.29(4)
C(36)-C(35#)	1.594(8)	C(7A)-C(8A ¹)	1.596(16)
C(36#)-C(35)	1.594(8)	C(8A)-C(7A ¹)	1.596(16)
Au(2)-P(2)	2.2336(11)	Au(1)-P(1)	2.2305(8)
Au(2)-Cl(2)	2.2877(10)	Au(1)-Cl(1)	2.2880(8)

The C=C bond length in the cyclobutane of the Lei-Au(I) complex **72** is 1.547(8) Å which is quite higher than the bond length for C=C double bond in ethane 1.33 Å and is similar to that of a single bond. The same phenomena were observed for the monodbaPHOS-Au^I complex **77**.

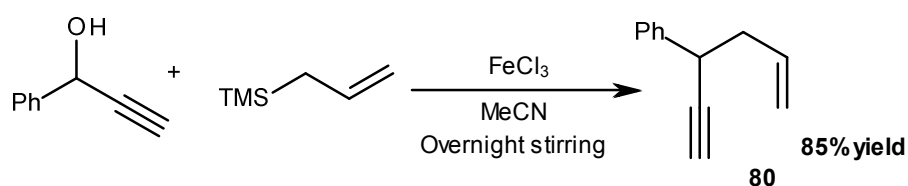
A small scale reaction (by NMR) was conducted for the synthesis of Au complex for the triphenylphosphine ligand. To a CD₂Cl₂ solution of [Au(SMe₂)Cl] was added PPh₃ and the reaction mixture was stirred for 2 h. The solution was filtered to get a clear solution, reduced in *vacuo* and analysed by NMR spectroscopy (Scheme 8). The ³¹P NMR spectrum showed a shift in the position of phosphorus peak from δ -4.57 (ligand) to δ 34.1. The synthesis of complex was further confirmed by mass spectrometric analysis.



Scheme 8: Synthesis of Au-complex of PPh₃ using [Au(SMe₂)Cl].

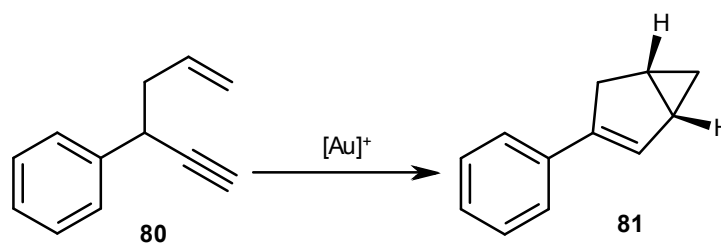
4.4.1 Catalysis

As we have successfully managed to synthesise Au complexes for different alkene phosphine ligands including the chalcone ferrocene ligand, the Lei ligand and the dba ligand, the plan was to use them in homogenous catalysis. The reactivity of these complexes as catalysts for the cycloisomerisation of 4-phenyl-1-hexen-5-yne was thus assessed. The substrate, 4-phenyl-1-hexen-5-yne **80** was synthesised by reacting 1-phenyl-prop-2-yn-1-ol with allyltrimethylsilane in acetonitrile. Dropwise addition of solution of anhydrous FeCl₃ in acetonitrile was necessary, which resulted in the synthesis of the target 1,5-enyne **80** (Scheme 9).



Scheme 9: Synthesis of 4-phenyl-1-hexen-5-yne (80**).**

4-phenyl-1-hexen-5-yne **80** has been shown to undergo Au^I catalysed cycloisomerisation to afford a bicyclo[3.1.0]hexyl ring system **81** (Scheme 10).

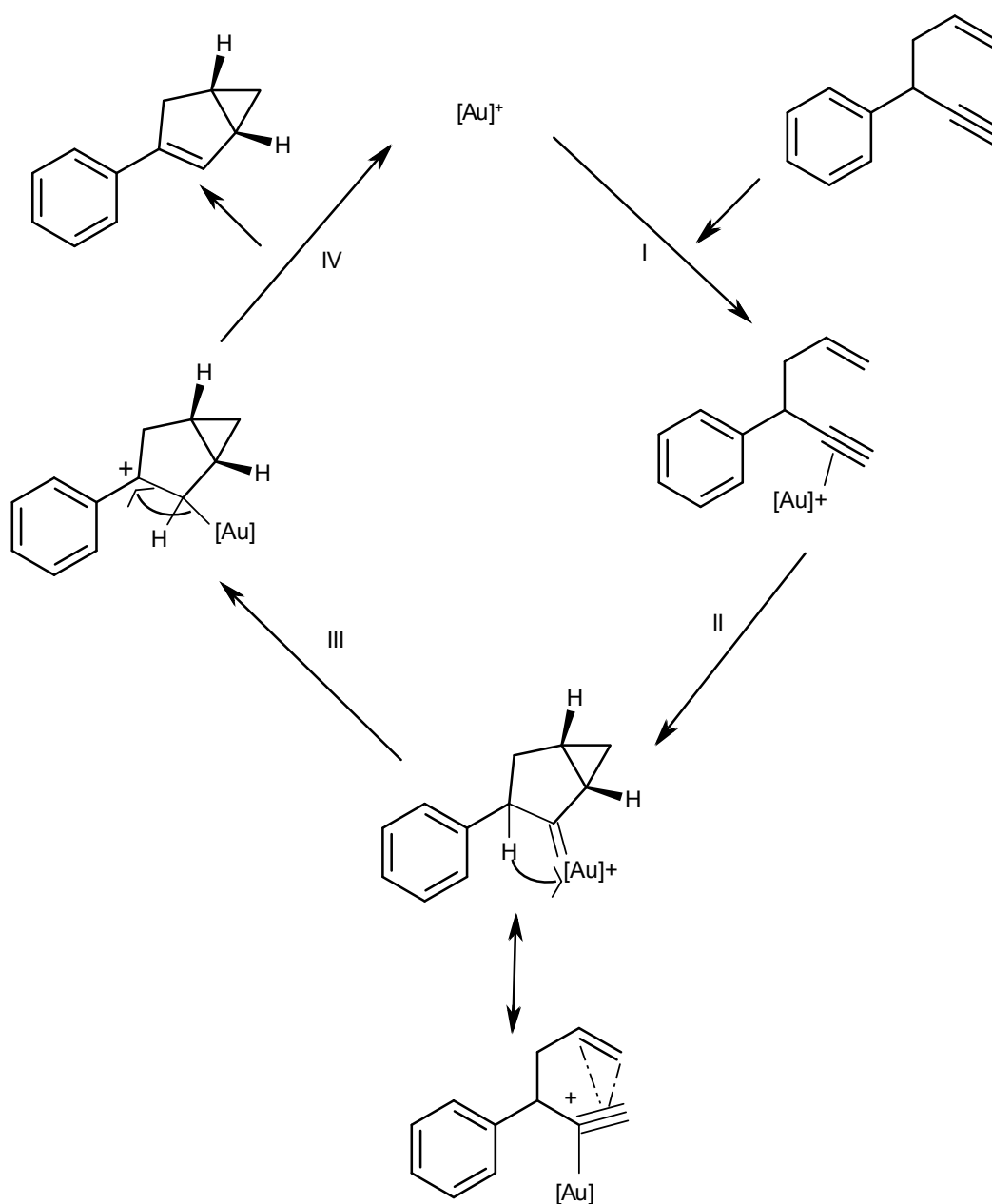


Scheme 10: The Au-catalysed cycloisomerisation of 4-phenyl-1-hexen-5-yne (80**) to produce 3-phenylbicyclo[3.1.0]hex-2-ene (**81**).**

The group of Toste²¹⁷ has shown that the simple Pd or Pt complexes PdCl₂(MeCN)₂ and PtCl₂ achieve less than 5% conversion. However, when Au^{III} complex was used 50 % conversion after 3 hours was observed (without added salts), and quantitative conversion when 3 equivalents of AgBF₄ (relative to substrate) was added at 5 mol% Au loading.

The first step of the reaction involves the binding of a gold cation (typically formed by halide abstraction from a gold complex by a silver salt) to the alkyne (Scheme 11, step

I). This withdraws electron density from the bond, due to a lack of backbonding from gold to the alkyne antibonding orbitals, making it susceptible to nucleophilic attack. The alkene acts as a nucleophile and attacks the alkyne in the Markovnikov position to form the bicyclo[3.1.0]hexane structure via a 5-*endo*-dig cyclisation (Step II). The Au complex is thought to help stabilise the carbocation by a π -backbonding to give the Au-carbon bond carbene character (the lower energy of the empty carbocation p orbital allows backbonding c.f. gold alkyne bonding). A hydride then migrates to form a carbocation at the adjacent position (step III) which is quenched by elimination of Au to give the bicyclohexene (Step IV). From this mechanism it would be logical to assume that a more electropositive Au cation would bind and activate the alkyne more strongly.



Scheme 11: The mechanism of gold-catalysed 5-endo-dig cycloisomerisation of 4-phenyl-1-hexen-5-yne (80) to produce 3-phenylbicyclo[3.1.0]hex-2-ene (81).

The cycloisomerisation of 4-phenyl-1-hexen-5-yne using gold complexes (**70**, **71**, **75**, **76** and **79**) was carried out using two different experimental conditions, with microwave and without microwave.

In the absence of microwave irradiation 1 equiv. of 4-phenyl-1-hexen-5-yne was reacted with 0.01 equiv. of Au catalyst at 25 °C for 3 mins using AgSbF₆ as an additive. The reaction proceeded with good conversions in almost all cases except for the dbaPHOS. No reaction was observed when the cycloisomerisation was carried out using gold complex of dbaPHOS.

A brief summary of the cycloisomerisation of 4-phenyl-1-hexen-5-yne without microwave irradiation is given in Table 3.

Table 3: Cycloisomerisation of 4-phenyl-1-hexen-5-yne without microwave.

	Au catalyst	Amount (mol %)	Ag additive	Amount (mol %)	Temp (°C)	Time (hours)	Conv. (%)
1	71	1	AgSbF ₆	1	25	3	>98
2	70	1	AgSbF ₆	1	25	3	>98
3	79	1	AgSbF ₆	1	25	3	>98
4	75	1	AgSbF ₆	1	25	3	No rex
5	76	1	AgSbF ₆	1	25	3	70

The cycloisomerisation was also carried out using microwave irradiation. 4-phenyl-1-hexen-5-yne was treated with Au catalysts at 50 °C for 5 mins. The best result was obtained using Lei(Au) catalyst **71** giving a conversion of >99%. However, for the ferrocene(Au) catalyst **70** a conversion of 39% was observed. It was found that reaction did not go to completion even after increasing the reaction time perhaps due to the decomposition of ferrocene complex under microwave conditions. The Ph₃P(Au) catalyst gave an intermediate yield of 45%. No reaction was observed for dbaPHOS whereas a poor conversion was obtained using MonodbaPHOS. An interesting result was that no reaction was observed in the absence of a Au complex confirming that the reaction is not catalysed independently by either Au catalyst or AgSbF₆. This is consistent with previous work and suggests that a cationic Au centre is required for effective catalytic cycloisomerisation.

A brief summary of the cycloisomerisation of 4-phenyl-1-hexen-5-yne with microwave is given in Table 4.

Table 4: Cycloisomerisation of 4-phenyl-1-hexen-5-yne with microwave.

	Au catalyst	Amount (mol %)	Ag additive	Amount (mol %)	Temp (°C)	Time (mins)	Conv. (%)
1	71	1	AgSbF ₆	1	50	5	>99
2	70	1	AgSbF ₆	1	50	5	39
3	--	1	AgSbF ₆	1	50	5	No rex

4	79	1	AgSbF ₆	1	50	5	45
5	76	1	AgSbF ₆	1	50	5	8
6	75	1	AgSbF ₆	1	50	5	No rex

4.5 CV studies of Au complexes

Cyclic voltammetry is a versatile electrochemical technique for the characterization of electroactive species. This method provides valuable information regarding the stability of the oxidation states and the rate of electron transfer between the electrode and the analyte. Applications of the cyclic voltammetry have been extended to almost every aspect of chemistry; for example, the investigation of biosynthetic reaction pathways and the examination of the ligand effect on the metal complex potential as well as enzymatic catalysis.²¹⁸

4.5.1 Principle

Cyclic voltammetry is a method in which information about the analyte is obtained from the measurement of the Faradic current as a function of the applied potential. The current response over a range of potentials is measured, starting at an initial value and varying the potential in a linear manner up to a limiting value. At this limiting potential the direction of the potential scan is reversed and the same potential range is scanned in the opposite direction (hence the term “cyclic”). Consequently, the species formed by oxidation on the forward scan can be reduced on the reverse scan. This technique is accomplished with a three-electrode arrangement: the potential is applied to the working electrode with respect to a reference electrode while an auxiliary (or counter) electrode is used to complete the electrical circuit. A typical cyclic voltammogram is shown in Figure 13.

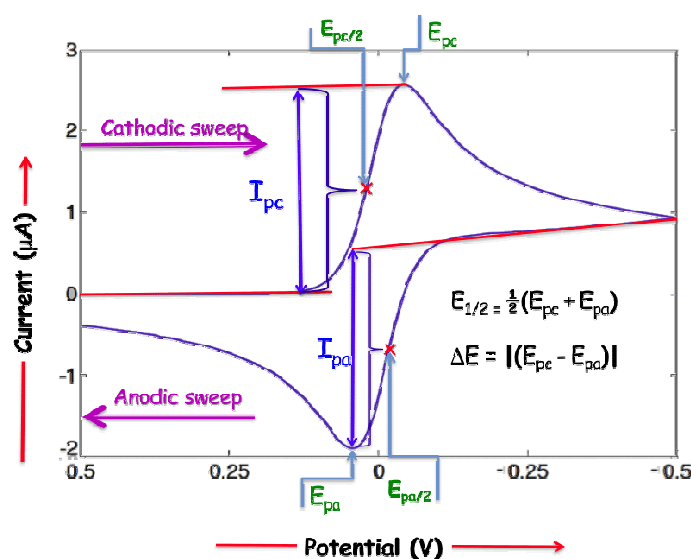


Figure 13: Diagrammatic representation of a typical cyclic voltammogram.

The scan starts at a slightly negative potential, E_i up to some positive switching value, E_{switch} at which scan is reversed back to the starting potential. The current is first observed to peak at E_{pa} (with value i_{pa}) indicating that an oxidation is taking place and then drops due to depletion of the reducing species from the diffusion layer. During the return scan the processes are reversed (reduction is now occurring) and a peak current is observed at E_{pc} (corresponding value, i_{pc}).

4.5.2 Electrochemistry of ferrocene

The oxidation of ferrocene $[\text{Fe}(\text{C}_5\text{H}_5)_2]$ to the ferrocenium cation $[\text{Fe}(\text{C}_5\text{H}_5)_2]^+$ is a standard one-electron transfer reversible process because the rate of electron transfer is incredibly fast.²¹⁹ Consequently, the redox system $[\text{Fe}(\text{C}_5\text{H}_5)_2]^+/\text{Fe}(\text{C}_5\text{H}_5)_2$ has received considerable attention in electrochemistry because it can be used for instrumental and reference potential calibrations in organic media.²²⁰ Oxidation of ferrocene can be done by different oxidants such as silver nitrate or conc. H_2SO_4 .

4.5.3 Electrochemistry of ferrochalcone ligand **32**

We were interested in tuning the electronic properties of these chalcone ferrocene ligands by converting them to ferrocenium ion. The electrochemical behaviour of chalcone ferrocene based phosphine-alkene ligands is of interest due to the *ideal* reversible redox behaviour of ferrocene, for which the $[\text{Fe}(\text{C}_5\text{H}_5)_2]^+ / [\text{Fe}(\text{C}_5\text{H}_5)_2]$ couple has received notable attention in the electrochemistry field. Thus, a system containing ferrocene along with another transition metal (*e.g.* Pt, Pd) can behave as a electroactive species, that could help in tuning the metal complex (and alkene).

The cyclic voltammetric experiments were conducted using 0.1 M TBAPF₆ in CH_2Cl_2 . A Glassy carbon working electrode was used with a decamethylferrocene internal reference. $\text{FcH}^*/[\text{FcH}^*]^+ = -0.48$ V (which places ferrocene at 0.0 V). $E_{1/2}$ value displayed for ferrochalcone ligand **32** was performed at *ca.* -40 °C, whereas for the metal complex it was performed at room temperature. The CV results obtained for ligand **32** and Au^I complex **70** are summarised in Table 5.

Table 5: Cyclic Voltammetric results for ferrochalcone ligand (32) and complex (70).

Complex	Oxidation, $E_{1/2}$ / V	Reduction, E_{pa} / V
B-Ligand	0.35	-1.20
B-Au Complex	0.32	-1.12

An FcH* internal standard near -0.5 volts was observed which is not the part of the sample and is likely to be an impurity. The cyclic voltammogram (Figure 14) displayed a ferrocene-based oxidation, more or less reversible, between $0.30 - 0.40$ V (i.e. harder to oxidise than ferrocene itself, likely a consequence of the vinyl ketone, for ferrochalcone **32**). There is also irreversible vinyl-ketone most likely based reduction. The second irreversible oxidation is harder to ascribe with confidence as it could easily be a decomposition product formed from the first irreversible reduction.

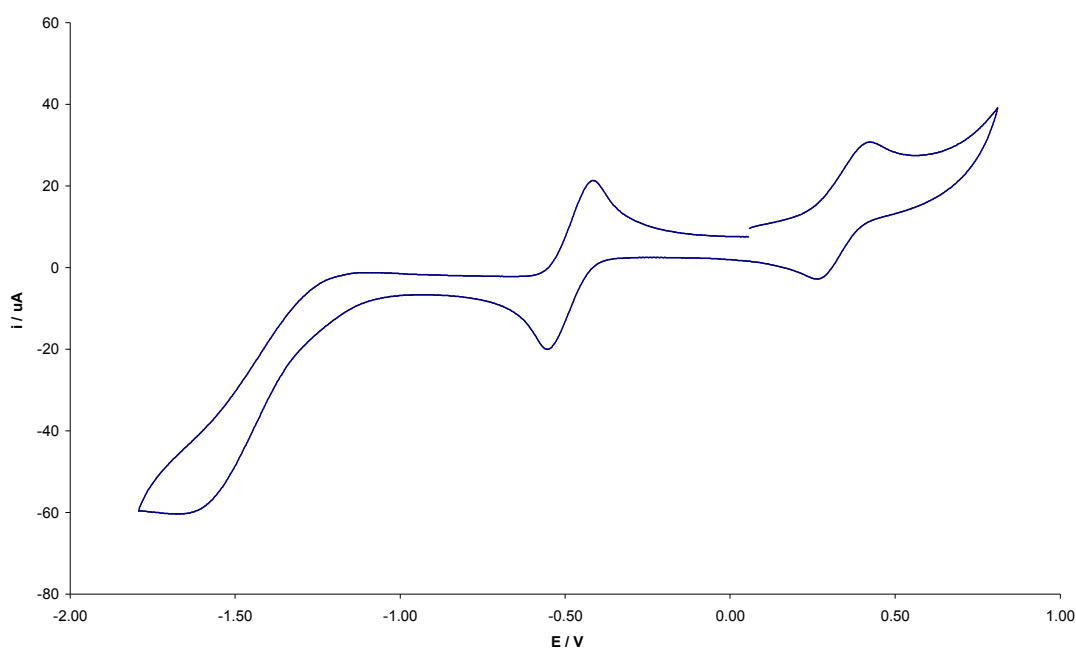


Figure 14: The cyclic voltammogram for ferrochalcone 32.

The CV of the Au^I metal complex for ferrochalcone **32** showed a reversible cycle at $E_{1/2} = 0.32$ V, corresponding to the redox process of the ferrocenyl unit and an anodic peak (E_{pa}) value of -1.12 V.

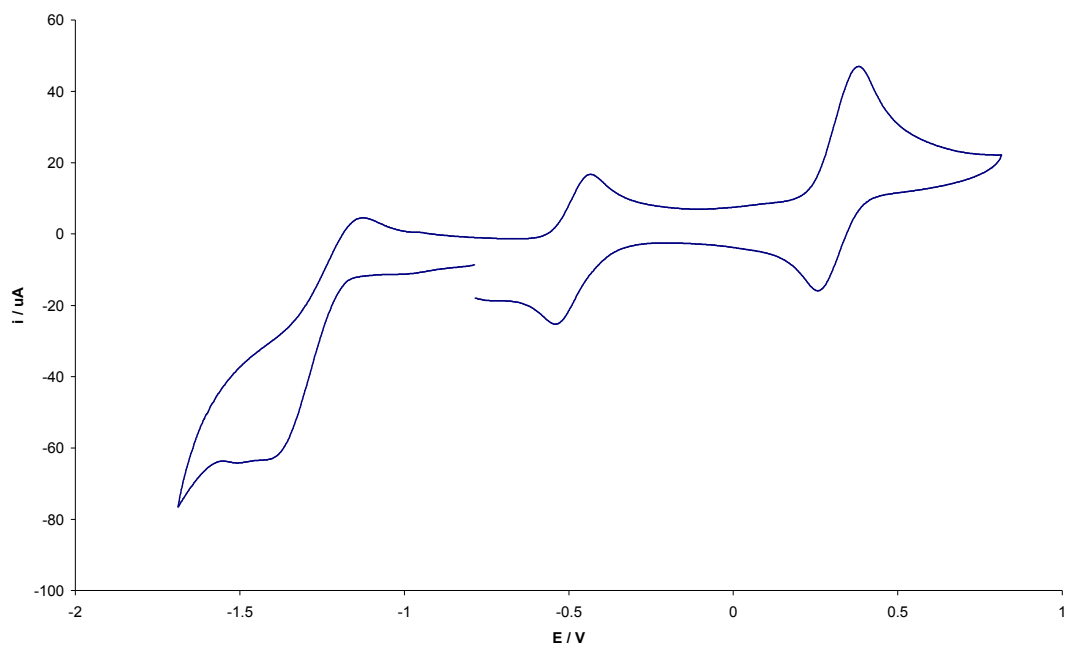


Figure 15: The cyclic voltammogram for Au^I complex of ligand 32.

4.6 Experimental

4.6.1 General Information

¹H-NMR spectra were obtained in the solvent indicated using a JEOL EXC400 or JEOL ECS400 spectrometer (400MHz for ¹H, 100 MHz for ¹³C and 162 MHz for ³¹P). Chemical shifts were referenced to the residual undeuterated solvent of the deuterated solvent used (CHCl₃ δ = 7.26 and 77.16 and DCM δ = 5.31 and 53.80 for ¹H and ¹³C NMR spectra respectively). NMR spectra were processed using MestrNova software. All ¹³C NMR spectra were obtained with ¹H decoupling. ³¹P NMR were externally referenced to H₃PO₄, and obtained with ¹H decoupling. For ¹³C NMR spectra the coupling constants are quoted to ±1 Hz. For the ¹H NMR spectra the resolution varies from ±0.15 to ±0.5 Hz; the coupling constants have been quoted to ±0.5 Hz in all cases for consistency.

Melting points were recorded using a Stuart digital SMP3 machine. IR spectroscopy was undertaken using a Jasco/MIRacle FT/IR-4100typeA spectrometer with an ATR attachment on solid and liquid compounds; solution and KBr IR spectra were obtained on a Nicolet Avatar 370 FT-IR spectrometer. The relative intensities of the peaks are denoted by (s) = strong, (m) = medium and (w) = weak, whilst (br) is used to describe broad peaks. MS spectra were measured using a Bruker Daltronics micrOTOF MS, Agilent series 1200LC with electrospray ionisation (ESI and APCI) or on a Thermo LCQ using electrospray ionisation, with <5 ppm error recorded for all HRMS samples. Mass spectral data is quoted as the *m/z* ratio along with the relative peak height in brackets (base peak = 100). Dry and degassed toluene, ether, DCM and hexane were obtained from a solvent system. Nitrogen gas was oxygen-free and was dried immediately prior to use by passage through a column containing sodium hydroxide pellets and silica gel. THF and benzene were dried over sodium-benzophenone ketyl and ethanol was dried and distilled from magnesium-iodide. Commercial chemicals were purchased from Sigma-Aldrich or Alfa Aesar. Elemental analysis was carried out on an Exeter Analytical CE-440 Elemental Analyser. All column chromatography was run on silica gel 60 using the solvent systems specified in the text. The fraction of petroleum ether used was that boiling at 40-60 °C.

Dry and degassed toluene, CH₂Cl₂, MeCN and hexane were obtained from a 'Pure Solv' MD-7 solvent purification system. THF and Et₂O were either obtained from a 'Pure

Solv' MD-7 solvent purification system and degassed by the freeze-pump-thaw method or purged with N₂ under sonication, or dried over sodium-benzophenone ketyl and collected by distillation. All air sensitive procedures were carried out using Schlenk techniques.²²¹ Nitrogen gas was oxygen-free and was dried immediately prior to use by passage through a column containing sodium hydroxide pellets and silica. Room temperature is quoted as the broadest range 13-25°C, but it was typically 18-20 °C. Commercial chemicals were purchased from Sigma-Aldrich and Alfa Aesar and used directly unless stated in the text. Brine refers to a saturated aqueous solution of NaCl.

Ferrochalcone gold(I) chloride complex (70)

A solution of [Au(SMe₂)Cl] (0.087 g, 0.297 mmol) in dry CH₂Cl₂ (5 ml) and β-[2'-(diphenylphosphino)phenyl]acryl ferrocene (0.148 g, 0.297 mmol) in dry CH₂Cl₂ (10 ml) was mixed together and stirred for 2 h at room temperature. The reaction mixture was then filtered and the solvent was removed under *vacuo* giving light reddish solid (0.155 g, 71%). Mp 210-211°C; ¹H-NMR (400 MHz, CDCl₃) δ 8.10 (d, *J* =14.8 Hz, 1H), 7.75 (s, 2H), 7.63 (dd, *J* =13.4, 7.1 Hz, 4H), 7.50-7.55 (m, 7H), 7.39 (m, 1H), 7.01-7.06 (m, 1H), 6.84 (d, *J* =15.2 Hz, 1H), 4.77-4.79 (m, 2H), 4.51-4.55 (s, 2H), 4.21 (s, 1H), 4.16 (s, 4H); ¹³C-NMR (100 MHz, CDCl₃) δ 191.5, 140.1 (d, *J* =10 Hz), 137.6 (d, *J* =12 Hz), 134.6 (d, *J* =14 Hz), 134.1 (d, *J* =9 Hz), 132.4 (d, *J* =2 Hz), 132.3 (d, *J* =2 Hz), 129.6, 129.5, 129.5, 128.9, 128.8 (d, *J* =4 Hz), 128.1, 127.7, 127.4, 79.9, 73.1, 70.2, 69.9; ³¹P-NMR (162 MHz, CDCl₃) δ 28.31 (s, 1P); HRMS (LIFDI) [M]⁺: 732.0269 (Calcd. for [Au(C₃₁H₂₅FePO)Cl] 732.0347); IR ν cm⁻¹ 2920 (s), 2359 (s), 1653 (s), 1601 (s), 1559 (s), 1456 (s), 1436 (s), 1377 (s), 1314 (s), 1277 (s), 1101 (s), 1078 (s), 1027 (s), 998 (s), 824 (s), 693 (s), 543 (s), 504 (s). ; Anal. Calcd for [Au(C₃₁H₂₅FePO)Cl]: C, 39.84; H, 2.90; N, 0. Found: C, 50.81; H, 3.44; N, 0.

Lei gold(I) chloride complex (71)

A solution of [Au(SMe₂)Cl] (0.087 g, 0.297 mmol) in dry CH₂Cl₂ (5 ml) and Lei ligand (0.116 g, 0.297 mmol) in dry CH₂Cl₂ (10 ml) was mixed together and stirred for 2 h at room temperature. The reaction mixture was then filtered and the solvent was removed under *vacuo* giving light reddish solid (0.127 g, 68%). Mp 172-174 °C; ¹H-NMR (400 MHz, CD₂Cl₂) δ 8.12 (d, , *J* =15.5 Hz, 1H), 7.83 (dd, *J* =7.7, 4.7 Hz, 1H), 7.76 (d, *J* =1.1 Hz, 1H), 7.74 (d, *J* =1.5 Hz, 1H), 7.63-7.55 (m, 8H), 7.52-7.46 (m, 6H), 7.43-7.38 (m, 1H), 7.17 (d, *J* =15.4 Hz, 1H), 6.97 (ddd, *J* =13.0, 7.8, 1.1 Hz, 1H); ¹³C-NMR (100

MHz, CD₂Cl₂) δ 191.1, 142.1 (d, *J* = 13 Hz), 139.8 (d, *J* = 10 Hz), 135.1 (d, *J* = 14 Hz), 134.3 (d, *J* = 8 Hz), 133.1, 132.8 (d, *J* = 2.5 Hz), 132.7 (d, *J* = 2 Hz), 130.4 (d, *J* = 10 Hz), 130.1, 129.9, 129.2, 129.1, 129.1, 128.9, 128.8, 128.4, 127.8, 127.7; ³¹P-NMR (162 MHz, CD₂Cl₂) δ 28.33 (s, 1P); HRMS (LIFDI) [M]⁺: 624.0586 (Calcd. for [Au(C₂₇H₂₁PO)Cl] 624.0684); IR ν cm⁻¹ 3054 (s), 2359 (s), 1663 (s), 1642 (s), 1604 (s), 1577 (s), 1480 (s), 1460 (s), 1436 (s), 1319 (s), 1268 (s), 1219 (s), 1181 (s), 1101 (s), 1014 (s), 997 (s), 963 (s), 754 (s), 712 (s), 693 (s), 658 (s), 586 (s), 504 (s); Anal. Calcd for [Au(C₂₇H₂₁PO)Cl]: C, 51.90; H, 3.39; N, 0. Found: C, 48.16; H, 3.30; N, 0

Dbu PHOS gold(I) chloride complex (75)

A solution of [Au(SMe₂)Cl] (73 mg, 0.25 mmol) in dry, degassed CH₂Cl₂ (5 mL) was added by cannula to a solution of dbaPHOS, (150 mg, 0.25 mmol) in dry degassed CH₂Cl₂ (10 mL) in a metal ligand ratio of (2:1). The resulting solution was stirred for 2 h at room temperature. CH₂Cl₂ was removed *in vacuo* to give a yellowish powder. (79 mg, 37%). Mp 176-179°C (dec.); ¹H-NMR (400 MHz, CDCl₃) δ 8.00 (d, *J* = 16 Hz, 2H), 7.68 (d, *J* = 6.8 Hz, 10H), 7.51 (t, *J* = 7.5 Hz, 2H), 7.45 (t, *J* = 7.5 Hz, 4H), 7.36 (t, *J* = 7.8 Hz, 10H), 6.95 (m, 2H), 6.42 (d, *J* = 16 Hz, 2H); ¹³C-NMR (100 MHz, CDCl₃) δ 140.9 (t, *J* = 8.1 Hz), 137.8 (t, *J* = 5.7 Hz), 134.9 (t, *J* = 8.1 Hz), 133.4 (t, *J* = 3.0 Hz), 131.4, 130.9, 130.1 (t, *J* = 3.7 Hz), 129.3 (t, *J* = 5.5 Hz), 128.2, 127.5 (t, *J* = 3.2 Hz); ³¹P-NMR (162 MHz, CDCl₃) δ 33.64 (bs, 1P), 31.17 (s, 1P); HRMS (LIFDI) [M]⁺: 799.1320 (Calcd. for [Au(C₄₁H₃₂P₂O)] 799.1594); IR ν cm⁻¹ 3051 (s), 2953 (s), 1651 (s), 1605 (s), 1581 (s), 1428 (s), 1410 (s), 1289 (s), 1212 (s), 1174 (s), 1042 (s), 1014 (s), 954 (s), 787 (s), 732 (s), 644 (s); Anal. Calcd for [Au(C₄₁H₃₂P₂O)Cl]: C, 58.97; H, 3.86; N, 0. Found: C, 55.75; H, 3.72; N, 0

Mono dba PHOS gold(I) chloride complex (76)

A solution of [Au(SMe₂)Cl] (73 mg, 0.25 mmol) in dry, degassed CH₂Cl₂ (5 mL) was added by cannula to a solution of Mono dbaPHOS, (104 mg, 0.25 mmol) in dry, degassed CH₂Cl₂ (10 mL) in a metal ligand ratio of (1:1). The resulting solution was stirred for 2 h at room temperature. CH₂Cl₂ was removed *in vacuo* to give a yellowish powder. (68 mg, 41%) 197-198°C (dec.); ¹H-NMR (400 MHz, CDCl₃) δ 8.28 (d, *J* = 15.8 Hz, 1H), 7.72 (dd, *J* = 7.6, 4.7 Hz, 1H), 7.66 (d, *J* = 2.2 Hz, 1H), 7.64 (d, *J* = 1.6 Hz, 1H), 7.63 (d, *J* = 1.2 Hz, 1H), 7.61 (t, *J* = 1.5 Hz, 1H), 7.59 (s, 1H), 7.58-7.57 (m, 2H), 7.54 (d, *J* = 2.2 Hz, 1H), 7.52 (dd, *J* = 3.3, 1.5 Hz, 1H), 7.48 (d, *J* = 2.6 Hz, 2H),

7.47-7.45 (m, 2H), 7.45-7.44 (m, 1H), 7.43 (s, 1H), 7.42-7.40 (m, 2H), 7.39 (s, 1H), 7.05 (d, $J=15.8$ Hz, 1H), 6.95 (ddd, $J=12.9, 7.8, 1.0$ Hz, 1H), 6.65 (d, $J=15.9$ Hz, 1H); ^{13}C -NMR (100 MHz, CDCl_3) δ 188.9, 144.1, 139.7 (d, $J=13.5$ Hz), 139.4 (d, $J=10$ Hz), 134.8, 134.71, 134.6, 133.7 (d, $J=8.5$ Hz), 132.6 (d, $J=2.5$ Hz), 132.4 (d, $J=2.0$ Hz), 131.3, 130.7, 129.9, 129.8, 129.6 (d, $J=12.0$ Hz), 129.1, 128.8, 128.7 (d, $J=3.5$ Hz), 128.1, 127.8, 127.2, 122.5; ^{31}P -NMR (162 MHz, CDCl_3) δ 27.49 (s, 1P); HRMS (LIFDI) $[\text{M}]^+$: 650.0698 (Calcd. for $[\text{Au}(\text{C}_{29}\text{H}_{23}\text{OP})\text{Cl}]$ 650.0841); IR ν cm^{-1} 3023 (w), 2928 (w), 1629 (s), 1610 (s), 1573 (s), 1567 (m), 1431 (w), 1414 (w), 1419 (m), 1335 (m), 1167 (s), 1079 (s); Anal. Calcd for $[\text{Au}(\text{C}_{29}\text{H}_{24}\text{OP})\text{Cl}]$: C, 53.43; H, 3.71; N, 0. Found: C, 51.21; H, 3.44; N, 0.

Triphenylphosphine gold(I) chloride complex (79)²²²

A solution of $[\text{Au}(\text{SMe}_2)\text{Cl}]$ (88 mg, 0.3 mmol) in dry, degassed CH_2Cl_2 (5 mL) was added to a solution of Ph_3P (78 mg, 0.3 mmol) in dry, degassed CH_2Cl_2 (5 mL). The resulting solution was stirred for 2 h at room temperature. The reaction solution was filtered to get a clear solution. CH_2Cl_2 was removed under vacuum giving a concentrated solution (4 mL), which was then layered with ether (5 mL) to afford off-white precipitates (87 mg, 58%) separated by filtration. Mp 235-237 °C; ^1H -NMR (400 MHz, CDCl_3) δ 7.55 (t, , $J=1.3$ Hz, 1H), 7.53 (d, $J=1.6$ Hz, 2H), 7.52-7.50 (m, 3H), 7.49 (d, $J=2.6$ Hz, 3H), 7.46 (d, $J=2.6$ Hz, 2H), 7.44 (d, $J=1.4$ Hz, 3H), 7.43-7.41 (m, 1H); ^{13}C -NMR (100 MHz, CDCl_3) δ 134.2 (d, $J=13$ Hz), 132.1 (d, $J=3$ Hz), 129.3 (d, $J=12$ Hz), 128.6; ^{31}P -NMR (162 MHz, CDCl_3) δ 34.14 (s, 1P); HRMS (LIFDI) $[\text{M}]^+$: 494.7042 (Calcd. for $[\text{Au}(\text{C}_{18}\text{H}_{15}\text{P})\text{Cl}]$ 494.7068); IR ν cm^{-1} 3057 (s), 1898 (s), 1816 (s), 1683 (s), 1585 (s), 1479 (s), 1433 (s), 1312 (s), 1179 (s), 1109 (s), 1026 (s), 998 (s); Anal. Calcd for $[\text{Au}(\text{C}_{18}\text{H}_{15}\text{P})\text{Cl}]$: C, 43.98; H, 3.09; N, 0. Found: C, 43.70; H, 3.06; N, 0

4-Phenyl-1-hexen-5-yne (80)

1-Phenyl-2-propyn-1-ol (2.53 ml, 20.4 mmol, 1 equiv.) and allyltrimethylsilane (9.78 ml, 61.4 mmol, 3 equiv.) were mixed in 40 ml of dry acetonitrile. FeCl_3 (anhydrous, 166 mg, 1.02 mmol, 0.05 equiv.) in 5 ml dry acetonitrile was added dropwise. The reaction was stirred for 2 hours at room temperature. Again, FeCl_3 (anhydrous, 166 mg, 1.02 mmol, 0.05 equiv.) in 5 ml dry acetonitrile was added dropwise and the reaction was stirred for further 1 hour at room temperature. The solution was reduced in *vacuo* and the product was purified by column chromatography, eluting with 100 % petroleum

ether (40-60) to give the title compound as colourless oil (2.70 g, 17.3 mmol, 85%). ¹H-NMR (400 MHz, CDCl₃) δ 7.41-7.32 (m, 4H), 7.29-7.24 (m, 1H), 5.87 (ddtd, *J* = 17.1, 10.2, 7.0 and 1.3 Hz, 1H), 5.13-5.06 (m, 2H), 3.72 (td, *J* = 7.2 and 2.4 Hz, 1 H), 2.54 (t, *J* = 7.2 Hz, 2H), 2.32 (app.d, *J* = 2.4 Hz, 1H); ¹³C-NMR (100 MHz, CDCl₃) δ 140.7, 135.1, 128.5, 127.4, 126.9, 117.1, 85.3, 71.4, 42.4, 37.6; HRMS (EI) [M]⁺: 156.0943 (Calcd. for [C₁₂H₁₂] 156.0939). Data in accordance with the literature.²²³

4.6.2 Catalysis; Synthesis of 3-Phenylbicyclo[3.1.0]hex-2-ene (81)

4.6.2.1 With out Microwave

1. Using Lei-(Au)Cl complex

To a solution of 4-phenyl-1-hexen-5-yne (50.0 mg, 321 μmol, 1 equiv.) in dichloromethane (0.64 mL, 0.50 M), AgSbF₆ (0.8 mg, 3.1 μmol, 0.01 equiv.) and gold complex (3.2 μmol, 0.01 equiv.) were added. The solution was stirred at 25 °C for 3 hours and filtered through a plug of silica gel which was washed with dichloromethane (2 ml). The solution was reduced in *vacuo* and conversion was determined by ¹H NMR spectroscopy and is found to be > 98 %.

2. Using Ferrochalcone-(Au)Cl complex

To a solution of 4-phenyl-1-hexen-5-yne (50.0 mg, 321 μmol, 1 equiv.) in dichloromethane (0.64 mL, 0.50 M), AgSbF₆ (0.8 mg, 3.1 μmol, 0.01 equiv.) and gold complex (3.2 μmol, 0.01 equiv.) were added. The solution was stirred at 25 °C or 3 hours and filtered through a plug of silica gel which was washed with dichloromethane (2 ml). The solution was reduced in *vacuo* and conversion was determined by ¹H NMR spectroscopy and is found to be > 98 %.

3. Using PPh₃-(Au)Cl complex

To a solution of 4-phenyl-1-hexen-5-yne (50.0 mg, 321 μmol, 1 equiv.) in dichloromethane (0.64 mL, 0.50 M), AgSbF₆ (0.8 mg, 3.1 μmol, 0.01 equiv.) and gold complex (3.2 μmol, 0.01 equiv.) were added. The solution was stirred at 25 °C or 3 hours and filtered through a plug of silica gel which was washed with dichloromethane (2 ml). The solution was reduced in *vacuo* and conversion was determined by ¹H NMR spectroscopy and is found to be > 98 %.

4. Using dba-PHOS (Au) complex

To a solution of 4-phenyl-1-hexen-5-yne (50.0 mg, 321 μmol , 1 equiv.) in dichloromethane (0.64 mL, 0.50 M), AgSbF_6 (0.8 mg, 3.1 μmol , 0.01 equiv.) and gold complex (3.2 μmol , 0.01 equiv.) were added. The solution was stirred at 25 $^\circ\text{C}$ for 3 hours and filtered through a plug of silica gel which was washed with dichloromethane (2 ml). The solution was reduced in *vacuo* and analysed by ^1H NMR spectroscopy confirming the presence of starting material only and hence no reaction has occurred.

5. Using mono dba-PHOS

To a solution of 4-phenyl-1-hexen-5-yne (50.0 mg, 321 μmol , 1 equiv.) in dichloromethane (0.64 mL, 0.50 M), AgSbF_6 (0.8 mg, 3.1 μmol , 0.01 equiv.) and gold complex (3.2 μmol , 0.01 equiv.) were added. The solution was stirred at 25 $^\circ\text{C}$ for 3 hours and filtered through a plug of silica gel which was washed with dichloromethane (2 ml). The solution was reduced in *vacuo* and analysed by ^1H NMR spectroscopy confirming 70 % conversion by NMR.

4.6.2.2 With Microwave

1. Using Lei-(Au)Cl complex

To a solution of 4-phenyl-1-hexen-5-yne (50.0 mg, 321 μmol , 1 equiv.) in dichloromethane (0.64 mL, 0.50 M) in microwave reaction tube was added AgSbF_6 (0.8 mg, 3.1 μmol , 0.01 equiv.) and gold complex (3.2 μmol , 0.01 equiv.). The solution was stirred at 50 $^\circ\text{C}$ for 5 mins and filtered through a plug of silica gel which was washed with dichloromethane (2 ml). The solution was reduced in *vacuo* and conversion was determined by ^1H NMR spectroscopy and is found to be > 99 %.

2. Using B-(Au)Cl complex

To a solution of 4-phenyl-1-hexen-5-yne (50.0 mg, 321 μmol , 1 equiv.) in dichloromethane (0.64 mL, 0.50 M) in microwave reaction tube was added AgSbF_6 (0.8 mg, 3.1 μmol , 0.01 equiv.) and gold complex (3.2 μmol , 0.01 equiv.). The solution was stirred at 50 $^\circ\text{C}$ for 5 mins and filtered through a plug of silica gel which was washed with dichloromethane (2 ml). The solution was reduced in *vacuo* and conversion was determined by ^1H NMR spectroscopy and is found to be 39 %. The reaction was repeated on same scale by increasing the reaction time to 15 mins instead of 5 mins giving the product in 26 % yield.

3. Without using Au complex, only in the presence of AgSbF₆

To a solution of 4-phenyl-1-hexen-5-yne (50.0 mg, 321 μmol , 1 equiv.) in dichloromethane (0.64 mL, 0.50 M) in microwave reaction tube was added AgSbF₆ (0.8 mg, 3.1 μmol , 0.01 equiv.). The solution was stirred at 50 °C for 5 mins and filtered through a plug of silica gel which was washed with dichloromethane (2 ml). The solution was reduced in *vacuo*. The ¹H NMR showed the starting material only hence reaction did not occur at all.

4. Using PPh₃-(Au)Cl complex

To a solution of 4-phenyl-1-hexen-5-yne (50.0 mg, 321 μmol , 1 equiv.) in dichloromethane (0.64 mL, 0.50 M) in microwave reaction tube was added AgSbF₆ (0.8 mg, 3.1 μmol , 0.01 equiv.) and gold complex (3.2 μmol , 0.01 equiv.). The solution was stirred at 50 °C for 5 mins and filtered through a plug of silica gel which was washed with dichloromethane (2 ml). The solution was reduced in *vacuo* and conversion was determined by ¹H NMR spectroscopy and is found to be 45 %.

5. Using mono dba-PHOS-(Au)Cl complex

To a solution of 4-phenyl-1-hexen-5-yne (50.0 mg, 321 μmol , 1 equiv.) in dichloromethane (0.64 mL, 0.50 M) in microwave reaction tube was added AgSbF₆ (0.8 mg, 3.1 μmol , 0.01 equiv.) and gold complex (3.2 μmol , 0.01 equiv.). The solution was stirred at 50 °C for 5 mins and filtered through a plug of silica gel which was washed with dichloromethane (2 ml). The solution was reduced in *vacuo* and conversion was determined by ¹H NMR spectroscopy and is found to be 8 %.

6. Using dba-PHOS-(Au)Cl complex

To a solution of 4-phenyl-1-hexen-5-yne (50.0 mg, 321 μmol , 1 equiv.) in dichloromethane (0.64 mL, 0.50 M) in microwave reaction tube was added AgSbF₆ (0.8 mg, 3.1 μmol , 0.01 equiv.) and gold complex (3.2 μmol , 0.01 equiv.). The solution was stirred at 50 °C for 15 mins and filtered through a plug of silica gel which was washed with dichloromethane (2 ml). The solution was reduced in *vacuo*. The ¹H NMR showed the starting material only hence reaction did not occur at all.

^1H NMR (400 MHz, CDCl_3) δ 7.45-7.42 (m, 2H), 7.38-7.33 (m, 2H), 7.26 (m, 1H), 6.48 (q, $J=2$ Hz, 1H), 3.08 (ddd, $J=17, 7.5, 2$, 1H), 2.80 (app. D, $J=17$ Hz, 1H), 2.01 (m, 1H), 1.79 (m, 1H), 1.00 (td, $J=7.5, 4$ Hz, 1H), 0.17 (dd, $J=7.0, 4.0$ Hz, 1H); ^{13}C NMR (100 MHz, CDCl_3) δ 139.7, 136.6, 129.6, 128.2, 126.7, 125.1, 36.3, 23.8, 17.6, 15.4; HRMS (EI) $[\text{M}]^+$: 156.0943 (Calcd. for $[\text{C}_{12}\text{H}_{12}]$ 156.0939). Data in accordance with the literature.²²⁴

4.6.3 X-Ray Diffraction Data

Diffraction data for Lei Au^I complex ijf1018 **71** was collected at 110 K on a Bruker Smart Apex diffractometer with Mo- K_α radiation ($\lambda = 0.71073$ Å) using a SMART CCD camera. Diffractometer control, data collection and initial unit cell determination was performed using “SMART”.²²⁵ Frame integration and unit-cell refinement was carried out with “SAINT+”.²²⁶ Absorption corrections were applied by SADABS.²²⁷ Structures were solved by “direct methods” using SHELXS-97 (Sheldrick, 1997)²²⁸ and refined by full-matrix least squares using SHELXL-97 (Sheldrick, 1997).²²⁹ All non-hydrogen atoms were refined anisotropically.

Diffraction data for ferrochalcone Au^I complex (ijf1116) **70**, monodbaPHOS Au^I complex ijf1117 **76** were collected at 110 K on an Oxford Diffraction SuperNova diffractometer with Mo- K_α radiation ($\lambda = 0.71073$ Å) using a EOS CCD camera. The crystal was cooled with an Oxford Instruments Cryojet. Diffractometer control, data collection, initial unit cell determination, frame integration and unit-cell refinement was carried out with “Crysalis”.²³⁰ Face-indexed absorption corrections were applied using spherical harmonics, implemented in SCALE3 ABSPACK scaling algorithm.²³¹ OLEX2²³² was used for overall structure solution, refinement and preparation of computer graphics and publication data.

Table 6: Single Crystal X-Ray details for Au^I complex of ferrochalcone (32), Lei ligand (17) and monodba-PHOS (76).

Compound reference	ijf1116	ijf1018	ijf1117
Formula	C ₃₁ H ₂₅ AuClFePO	C ₁₀₈ H ₈₄ Au ₄ Cl ₄ P ₄ O ₄	C ₂₉ H ₂₃ AuClPO
Formula weight	732.75	2499.31	650.86
temp (K)	110(10)	110(2)	110(10)
Cryst syst	Monoclinic	Monoclinic	Monoclinic
Space group	C2/c	P 2(1)/c	C2/c
a(Å)	30.0863(15)	9.1617(5)	27.4947(4)
b(Å)	8.8904(6)	18.2335(9)	9.21591(14)
c(Å)	19.2451(10)	28.1227(14)	18.9937(3)
α(°)	90.00	90	90
β(°)	93.235(4)	97.0600(10)	90.4571(14)
γ(°)	90.00	90	90
V (Å³)	5139.5(5)	4662.3(4)	4812.64(12)
Z	8	2	8
D_{calcd.} (Mg M⁻³)	1.894	1.780	1.797
F(000)	2848	2416	2528
M(mm⁻¹)	6.457	6.511	6.311
Crystal size (mm³)	0.2026 x 0.1082 x 0.0524	0.21 x 0.20 x 0.14	0.1984 x 0.1517 x 0.0566
θ range for data	6.12 to 58	1.46 to 28.32	5.92 to 64.34
Collection (°)	-39 ≤ h ≤ 37,	-12 ≤ h ≤ 12,	-24 ≤ h ≤ 41,
Index ranges	-12 ≤ k ≤ 6, -24 ≤ l ≤ 23	-24 ≤ k ≤ 24, -37 ≤ l ≤ 37	-12 ≤ k ≤ 12, -24 ≤ l ≤ 27
No. of rflns collected	11219	47922	12407
Refinement method	Full-matrix least-squares on F ²	Full-matrix least-squares on F ²	Full-matrix least-squares on F ²
GOOF on F²	1.149	1.050	1.101
R1, wR2(I>2σ(I))	0.0411, 0.0807	0.0343, 0.0647	0.0305, 0.0566
R1, wR2(all data)	0.0512, 0.0861	0.0473, 0.0684	0.0385, 0.0595

Further details can be found in the Appendix, including the cif files on the CD.

Chapter 5: Investigating nitrite impurities in “Pd(OAc)₂”

The work detailed in this chapter resulted in the following publication: On the appearance of nitrite anion in [PdX(OAc)L₂] and [Pd(X)(C[^]N)PPh₃]syntheses (X = OAc or NO₂): photocrystallographic identification of metastable Pd(η¹-ONO)(C[^]N)PPh₃: S. E. Bajwa, T. E. Storr, L. E. Hatcher, T. J. Williams, C. G. Baumann, A. C. Whitwood, D. R. Allan, S. J. Teat, R. R. Raithby* and I. J. S. Fairlamb* Chemical Science DOI:10.1039/c2sc01050j

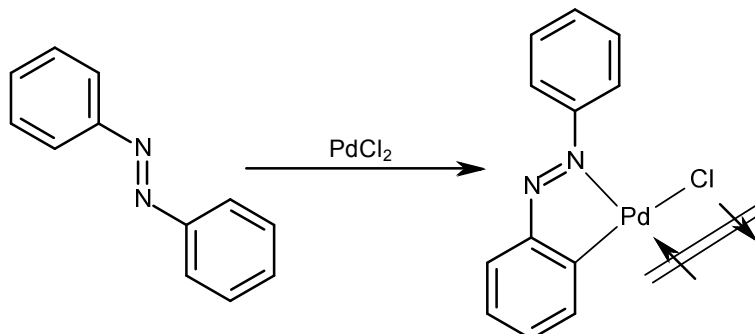
Palladium chemistry has rapidly become an indispensable tool for synthetic organic chemists. Palladium is a chemical element with the chemical symbol Pd and an atomic number of 46. It is a rare and lustrous silvery-white metal discovered in 1803 by William Hyde Wollaston.²³³ It basically belongs to a group of elements called the platinum group metals (PGMs).²³⁴ They all have very similar chemical properties but pall

adium has the lowest melting point and is least dense. The common oxidation states of palladium are 0, +1, +2 and +4. Palladium is a versatile metal for homogenous catalysis and is effectively used in combination with a broad variety of ligands for highly selective chemical transformations.²³⁵ Palladium catalysis has gained widespread use in industrial and academic synthetic chemistry laboratories as a powerful methodology for the formation of C-C and C-heteroatom bonds.²³⁶ Palladium is also used in electronics, dentistry, medicine, hydrogen purification, chemical applications and groundwater treatment. Palladium catalysts are effectively used in the field of organic and organometallic chemistry. When it is finely divided, such as palladium on carbon, palladium forms a versatile catalyst and speeds up hydrogenation and dehydrogenation reactions as well as in the petroleum cracking. A large number of carbon-carbon bond forming reactions in organic chemistry are facilitated by catalysis with palladium compounds.

5.1 Cyclopalladation

Cyclopalladation involves the formation of a chelated metallocycle from the reaction of a suitable C-H substrate containing a donor group e.g. nitrogen or sulphur. The C-H bond *ortho*- to the reacting centre is activated by the metal, leading to the formation of a

metal carbon-bond. This reaction was first discovered by Arthur C. Cope and co-workers, who found that azoerenes²³⁷ and benzylamines react with Pd^{II} to give a cyclopalladated product.²³⁸ The cyclopalladation of azobenzene was one of the first examples, reported in 1965 (Scheme 1).



Scheme 1: The cyclopalladation of azobenzene.

Cyclopalladation represents one of the most powerful methods for the activation of Csp²-H bonds and *ortho*-functionalization of aromatic compounds. The application of cyclopalladated compounds, especially those bearing nitrogen-chelating atom have been widely used in organic synthesis, e.g. in the Heck reaction,²³⁹ and Suzuki coupling reaction,²⁴⁰ as palladacyclic precatalyst. A leading example is Hermann's commercially available [Pd(OAc)C[^]N]₂ complex.

5.2 Palladium compound as catalysts

Palladium compounds are effectively used as catalyst in various types of reactions. Well known palladium catalyst precursors include, allylpalladiumchloride dimer, *bis*(acetonitrile)palladium(II) chloride, *bis*(benzonitrile)palladium(II) chloride, *bis*(dibenzylideneacetone)palladium, palladium(II) acetate, palladium(II) chloride, *tetrakis*(acetonitrile)palladium(II) tetrafluoroborate. Whereas following palladium compounds are efficiently used as catalysts in various types of reactions, [1,2-*bis*(diphenylphosphino)ethane]dichloropalladium(II), *bis*(triphenylphosphino)palladium(II) acetate, *bis*[tri(*o*-tolyl)phosphine]palladium(II) chloride, dichloro*bis*(tricyclohexylphosphine)palladium(II), *tetrakis*(triphenylphosphine)palladium (0). A few selected but representative examples are given in Figure 1.

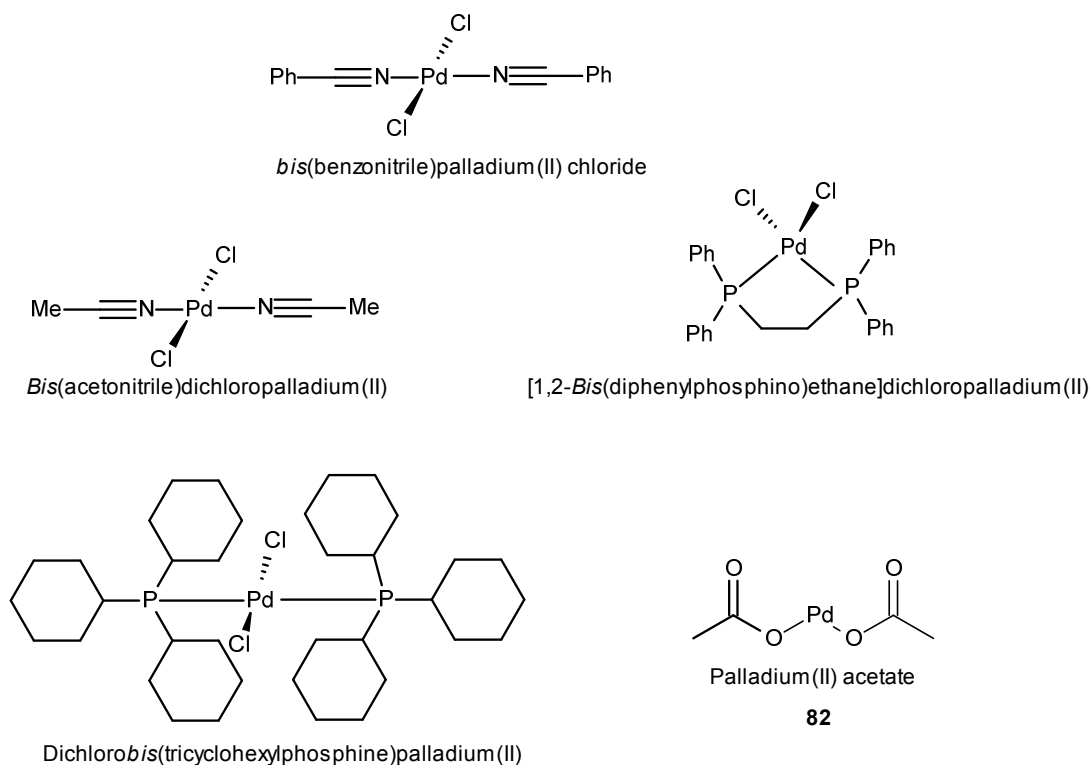


Figure 1: Some commonly used Palladium catalysts.

The aim of this part of the project was to investigate the purity of palladium(II) acetate and its employment in cyclopalladation reactions. Its origin is in the work reported by Nonoyama on the cyclopalladation of papaverine using $\text{Pd}(\text{OAc})_2$ where they observed a nitro-palladated product on reacting papaverine with $\text{Pd}(\text{OAc})_2$ in presence of acetonitrile.²⁴¹ The formation of nitro-derived palladated product was unexpected and hence a detailed study involving the cyclopalladation of papaverine was conducted to address this issue.

Papaverine **83**, 1-[(3,4-dimethoxyphenyl)methyl]-6,7-dimethoxyisoquinoline (abbreviated as Hpap) (Figure 2), is found in the opium plant is an alkaloid with medicinal properties. For example it exhibits smooth muscle relaxation and is a vasodilator (cerebral). The structure of Hpap made this alkaloid suitable for doing cyclopalladation studies using $\text{Pd}(\text{OAc})_2$.

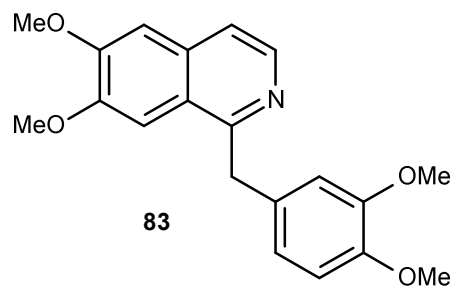
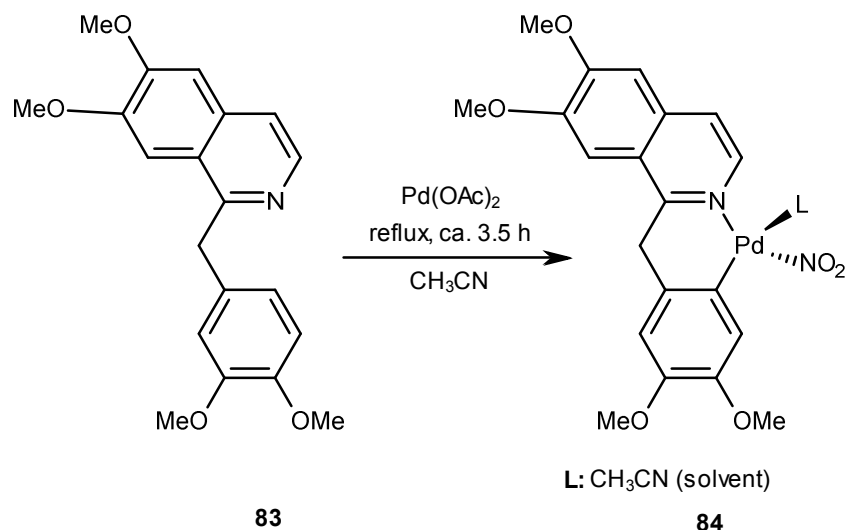


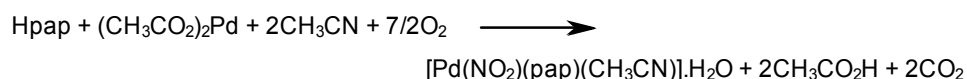
Figure 2: Structure of papaverine (abbreviated as Hpap)

The reaction of Hpap with Pd(OAc)₂ in refluxing acetonitrile resulted in the formation of a complex with the unexpected composition [Pd(NO₂)(pap)(CH₃CN)].H₂O, **84** (Scheme 2).²⁴¹



Scheme 2: Reaction of Hpap with Pd(OAc)₂ as reported by Nonoyama.

It was reported that decomposition of CH₃CN and the formation of NO₂⁻ was catalysed by metallic Pd (the dark colour of the reaction mixture suggested formation of colloidal Pd) during the reaction. The following stoichiometry was suggested without supporting evidence, as given in Scheme 3.



Scheme 3: Stoichiometric equation explaining the formation of the nitrite Pd adduct reported by Nonoyama.

The result reported was supported mostly on the basis of IR. Two characteristic strong bands at 1379 and 1336 cm^{-1} were associated with a nitrite group. A band at 314 cm^{-1} was assigned to ν (Pd-N). No band assignable to an acetate group was present.

In the same year Nonoyama conducted further cyclopalladation reactions of 2-(2-pyridyl)benzo[b]furan (Hpbf), (**85**) and 1-(2-pyridyl and 2-pyrimidyl)indole (Hpyi & Hpmi) (**86 & 87**) using Palladium(II) acetate (Figure 3).²⁴² On refluxing the Hpyi and Hpmi ligands with $\text{Pd}(\text{OAc})_2$ in the presence of acetonitrile, the solution darkens and the formation of metallic palladium was noted.

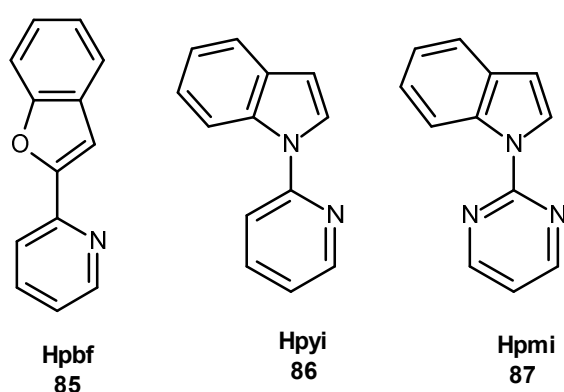


Figure 3: Structure of furan (Hpbf) and indole derived (Hpyi & Hpmi) ligands.

The product obtained was formulated on the basis of the analytical results, as $[\text{Pd}(\text{NO}_2)(\text{L})(\text{CH}_3\text{CN})]$ (Figure 4).

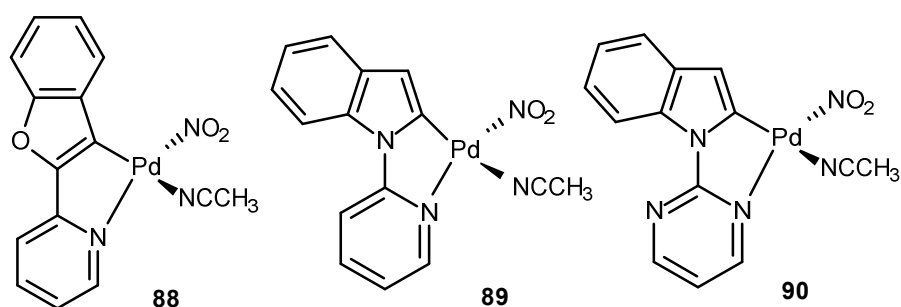


Figure 4: Palladium complexes containing nitrite ligands.

Again, the formation of palladium-derived “ NO_2 ” complexes was unexpected and was supposed to result from the oxidation of CH_3CN catalyzed by metallic palladium as given in Scheme 3 earlier.

Some reactions of CH_3CN are known but there seems to be no precedent for its oxidation reaction to form NO_2^- . It seemed unlikely to us that nitrite was being formed by oxidation of acetonitrile. Therefore we set about assessing this reaction in further detail.

5.3 Palladium(II) Acetate

Palladium(II) acetate **82** is a chemical compound of formula $\text{Pd}(\text{O}_2\text{CCH}_3)_2$ or $\text{Pd}(\text{OAc})_2$. When warmed with alcohols or on prolonged boiling with other solvents, $\text{Pd}(\text{OAc})_2$ decomposes to give Pd^0 .²⁴³ It catalyses many organic reactions, is easily reduced by light or heat to form thin films of Pd and can produce colloids and nanowires.²⁴⁴ The primary use of Palladium(II) acetate is as a starting material for the syntheses of other Pd(II) compounds as well as for the preparation of palladium catalysts and their precursors.

Palladium(II) acetate is trimeric, consisting of an equilateral triangle of Pd atoms each pair of which is bridged with two acetate groups in a butterfly conformation.²⁴⁵ Each metal atom achieves approximate square planar co-ordination. In the solid state, the structure is generally trinuclear with nearly idealized D_{3h} symmetry in which each of the three palladium atoms is in square planar environment and there are six bridging acetate groups.

In solution, the structure of palladium acetate has remained somewhat controversial. Claims have been made supporting the persistence of the trinuclear molecules in solution, while other evidence is said to support the formation of various aggregates of $[\text{Pd}(\text{OAc})_2]_n$ ($n=1, 2, 3$ etc.) (Figure 5).²⁴⁶ The ^1H NMR spectrum of palladium acetate in methanol has been reported to show a large number of signals in the range where single acetate signal would be expected for the symmetrical triangular structure. This was said to be indicative of a variety of aggregated and possibly even the occurrence of ionic species.²⁴⁷

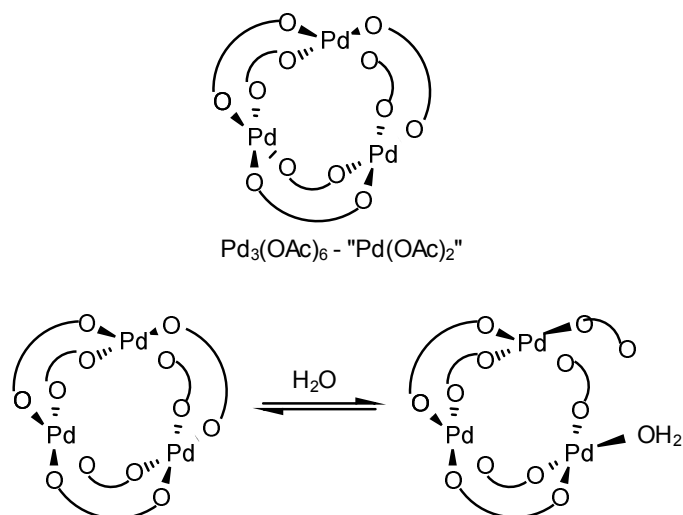


Figure 5: Structure of palladium acetate in solution, $\text{Pd}_3(\text{OAc})_6\text{OH}_2$.

5.3.1 Preparation of $\text{Pd}(\text{OAc})_2$

Palladium(II) acetate is commercially available and there are several routes describing its preparation. One of the most successful and commonly used synthetic routes was reported by Zhang and co-workers.²⁴⁸ The method is summarized by the following pair of reactions, (Scheme 4).



Scheme 4: Route used for the synthesis of $\text{Pd}(\text{OAc})_2$.

The first reaction occurs as reported with rapid formation of finely divided palladium metal. The freshly formed powder is subsequently oxidized by a mixture of HNO_3 and acetic acid, and the product is extracted into a 1:2 mixture of CH_2Cl_2 :hexane. Crystals are obtained by evaporation under a stream of N_2 . This last step is very important as it allows the nitrous gases to be removed, *vide infra*.

5.4 Cyclopalladation reactions involves $\text{Pd}(\text{OAc})_2$: a case study with papaverine

The plan was to do cyclopalladation reaction of papaverine using $\text{Pd}(\text{OAc})_2$. Before carrying on the reaction the purity of different substrates involved was checked.

Papaverine is commercially available from Sigma Aldrich and was >99 % pure, as confirmed by ^1H NMR spectroscopic analysis. The acetonitrile used in the reaction was dried and purified by triply-distillation over anhydrous AlCl_3 , Li_2CO_3 and lastly CaH , according to a procedure reported by Walter and Ramaley (*method A*).²⁴⁹ Finally the purity of $\text{Pd}(\text{OAc})_2$ was confirmed by running a ^1H NMR spectrum of commercial samples (Figure 6).

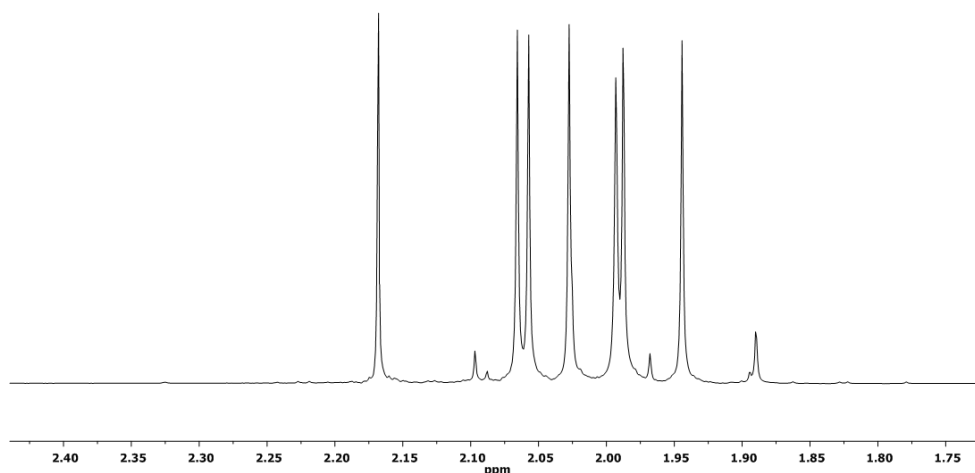


Figure 6: ^1H NMR spectrum of commercially available $\text{Pd}(\text{OAc})_2$.

The commercially available sample of $\text{Pd}(\text{OAc})_2$, was a mixture of Pd compounds as confirmed by ^1H NMR spectrum and hence a detailed study over the synthesis and purity of $\text{Pd}(\text{OAc})_2$ was carried out.

In an important study Cotton and Murillo highlighted the non-trivial behaviour of $\text{Pd}(\text{OAc})_2$.²⁵⁰ $\text{Pd}_3(\text{OAc})_6$ is prepared by oxidation of metallic Pd (derived from PdCl_2) with $\text{HNO}_3 / \text{AcOH}$,²⁵¹ as shown above and as a consequence of poor N_2 flow, nitrogen oxides bring about the formation of the purple complex, $\text{Pd}_3(\text{OAc})_5\text{NO}_2$.²⁵² A ^1H NMR spectroscopic comparison of the two different products obtained during synthesis of $\text{Pd}(\text{OAc})_2$ is shown in Figure 7.

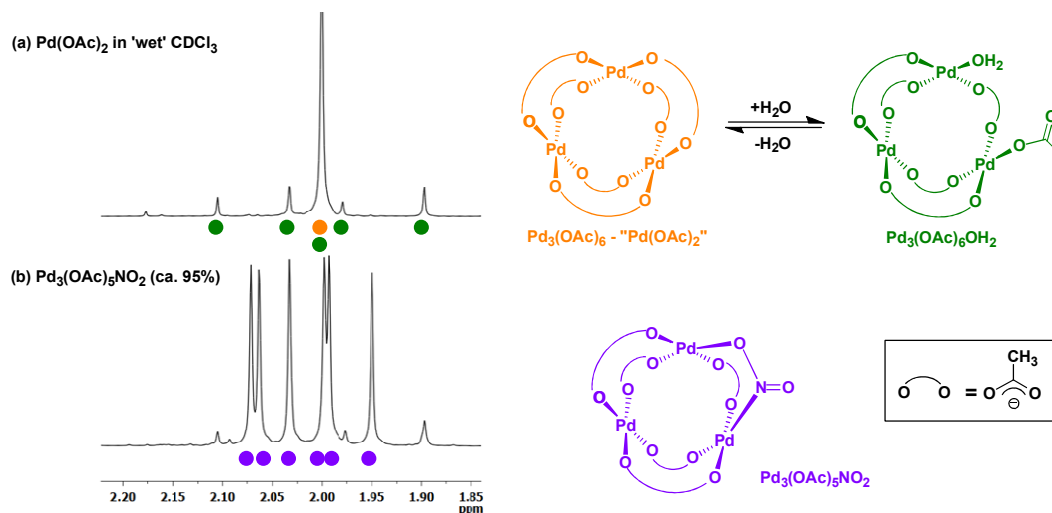


Figure 7: A comparison of the two different products obtained during synthesis of Pd(OAc)₂ by ¹H NMR spectroscopic analysis.

The ¹H NMR spectroscopic analysis of commercially available Pd(OAc)₂ in CDCl₃ showed the presence of Pd₃(OAc)₅NO₂. In order to check the ratio of the impurity, the Pd complex was subjected to elemental analysis. A comparison of elemental analysis of impure Pd(OAc)₂ with pure Pd(OAc)₂ is given below in Table 1.

Table 1: The comparison of E.A of Impure Pd(OAc)₂ with pure Pd(OAc)₂.

		% C	% H	% N
Observed	Impure material Pd material	18.47	2.24	1.72
Calculated	Pd ₃ (OAc) ₅ NO ₂	18.18	2.29	2.12
Calculated	Pd ₃ (OAc) ₆	21.40	2.69	-

The percentage ratio of Pd₃(OAc)₅NO₂ (based on nitrogen content) in the commercially available sample of Pd(OAc)₂ is $(1.72/2.12) \times 100 = \underline{81.1\%}$

Ratio of NO₂:OAc in 81% Pd₃(OAc)₅NO₂

Ratio of Pd₃(OAc)₅NO₂:Pd₃(OAc)₆ = 81.1:18.9 = 4.3:1

Total (relative) OAc content =

4.3x5 OAc {from $\text{Pd}_3(\text{OAc})_5\text{NO}_2$ }

6 OAc {from $\text{Pd}_3(\text{OAc})_6$ }

Total= 27.5 OAc

Total (relative) NO_2 content = 4.3 NO_2 {from $\text{Pd}_3(\text{OAc})_5\text{NO}_2$ }

Ratio of OAc: NO_2 = 27.5:4.3 = 6.4:1

Different samples of $\text{Pd}(\text{OAc})_2$ (a variety of commercial suppliers) from the Department of chemistry (University of York) were collected and analysed by ^1H NMR spectroscopy. Surprisingly, almost all of them showed the presence of nitrite impurities, with the exception of a samples (>99%) $\text{Pd}_3(\text{OAc})_6$ (Figure 8).

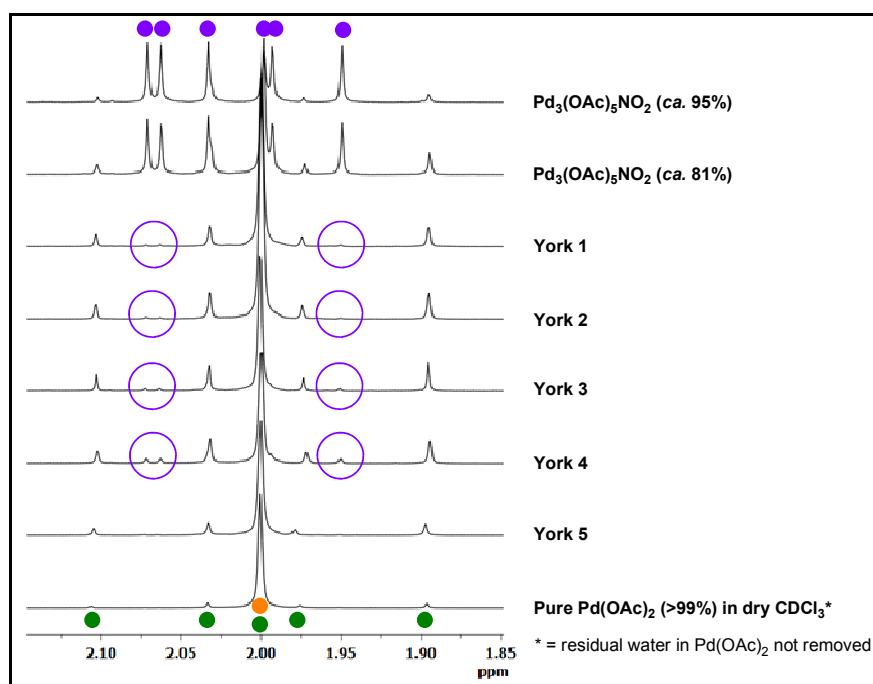


Figure 8: The ^1H NMR comparison of different samples of $\text{Pd}(\text{OAc})_2$ from University of York. (using reagent grade ‘wet’ CDCl_3 unless otherwise specified) (400 MHz). The purple circles highlight trace $\text{Pd}_3(\text{OAc})_5\text{NO}_2$. For reference purposes, ^1H NMR spectra of $\text{Pd}_3(\text{OAc})_5\text{NO}_2$ (ca. 95% and 81% purity materials) and pure $\text{Pd}(\text{OAc})_2$ in dry CDCl_3 are included.

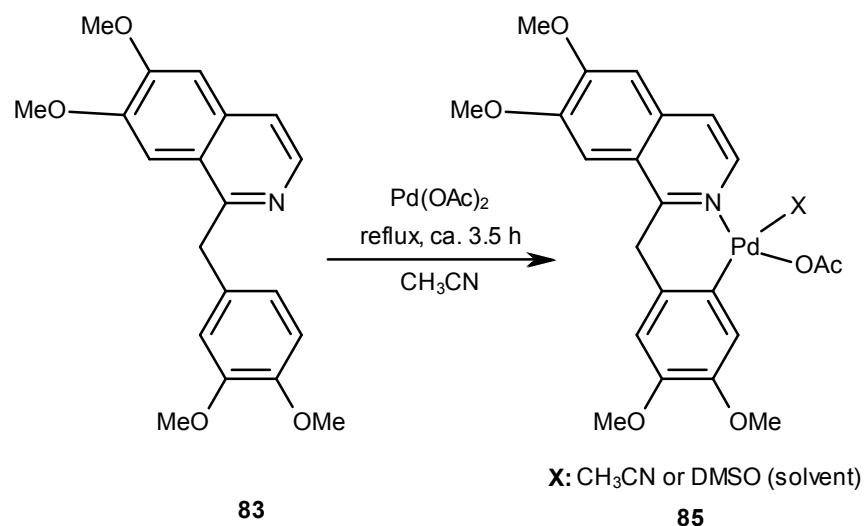
Also, it was observed that this trinuclear ‘triangle’ complex, formally $\text{Pd}_3(\text{OAc})_6$, has a nearly idealized D_{3h} symmetry in the solid-state. In the presence of trace H_2O in CDCl_3

(e.g. laboratory grade CDCl_3), $\text{Pd}_3(\text{OAc})_6$ readily gives $\text{Pd}_3(\text{OAc})_6(\text{OH}_2)$ (OAc displacement by H_2O results in desymmetrization) as reported by Cotton and co workers.

The presence of nitrite impurity in $\text{Pd}(\text{OAc})_2$ could explain the result reported by Nonoyama on the cyclopalladation of papaverine as shown in Scheme 13. It was found that the reaction of $\text{Pd}(\text{OAc})_2$ with papaverine **83** in CH_3CN at reflux in air for 3.5 h (filtered whilst hot to remove metallic Pd^0 residues) gave a filtrate containing **84**· CH_3CN , which precipitates out of solution (overnight) as reported by Nonoyama. Recrystallization of this precipitate from warm DMSO afforded **84**·DMSO.

The reaction of papaverine **83** was repeated with pure (>99%) $\text{Pd}_3(\text{OAc})_6$ under air using reagent grade CH_3CN . The reaction mixture was heated at reflux for 3.5 h. Finally it was filtered while hot to remove metallic Pd^0 residues and left for precipitation. The precipitates was slow to appear (ca. 3-14 days at 5 °C),²⁵³ although **83** had been fully consumed (as shown by ^1H NMR spectroscopy). Finally, a yellow semi-crystalline material appeared, which was filtered and analysed. Elemental analysis and LIFDI mass spectrometric analysis showed this material to have the composition of $[\text{Pd}(\text{OAc})(\text{C}^{\wedge}\text{N})]$ and not $[\text{Pd}(\text{NO}_2)(\text{C}^{\wedge}\text{N})]$. ^1H NMR spectroscopy (in d_6 -DMSO) revealed that cyclopalladation had occurred, and whilst being similar to the data for **84**·DMSO, some differences were apparent. The reaction was repeated several times and in all cases the same result was observed.

A series of control reactions with triply-distilled CH_3CN (from AlCl_3 , Li_2CO_3 and CaH)²⁵⁴, in both the presence and absence of air, gave the same product as detailed above. In the absence of DMSO the product formed was suspected to be $[\text{Pd}(\text{OAc})(\text{C}^{\wedge}\text{N})]$ · CH_3CN **85** as given in Scheme 5.



Scheme 5: Cyclopalladation of Hpap with Pd(OAc)₂.

Yellowish-coloured crystals grew from CH₃CN solution after a week, which were analysed by XRD analysis. The X-ray studies gave a novel dimeric Pd(II) acetate bridged complex **86** (representative of the bulk material) with the following structure (Figure 9), and the X-ray structure is given in Figure 10.

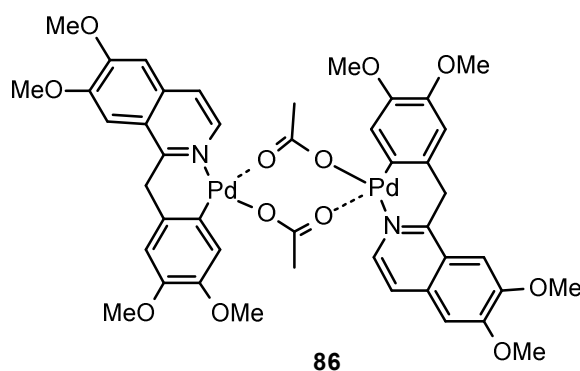


Figure 9: The structure of novel dimeric Pd(II) acetate bridged complex, 86.

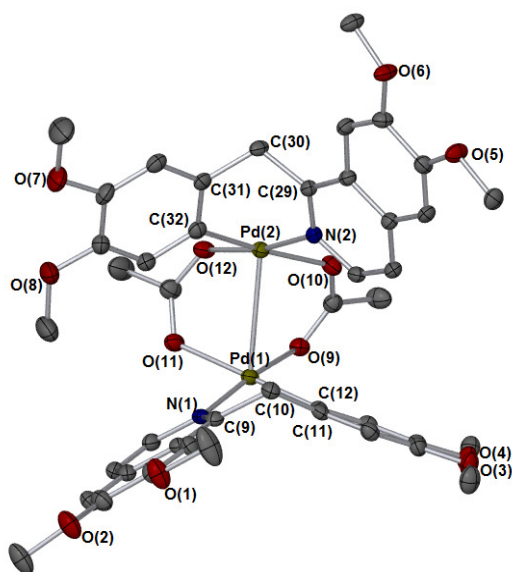


Figure 10: X-ray structure of 86 with 3 CH₃CN molecules and H-atoms omitted for clarity; selected atoms labelled.

Solvent and hydrogen atoms are removed for clarity. Thermal ellipsoids shown at 50%. Bond lengths (Å): Pd(1)-Pd(2) = 3.0258(4), Pd(1)-N(1) = 2.033(2), Pd(2)-N(2) = 2.032(2), Pd(1)-C(12) = 1.980(3), Pd(2)-C(32) = 1.959(3), Pd(1)-O(9) = 2.0523(19), Pd(1)-O(11) = 2.166(2), Pd(2)-O(10) = 2.135(2), Pd(2)-O(12) = 2.0571(19), Bond Angles(°) O(10)-Pd(2)-O(12) = 92.36(8), O(9)-Pd(1)-O(11) = 90.70(8), O(9)-Pd(1)-Pd(2) = 79.30(6), O(10)-Pd(2)-Pd(1) = 75.71(5), N(1)-Pd(1)-O(11) = 90.27(8), C(12)-Pd(1)-O(9) = 89.63(10), C(32)-Pd(2)-N(2) = 87.44(10), C(32)-Pd(2)-O(12) = 89.13(10), N(2)-Pd(2)-O(10) = 90.48(9).

The complex crystallises in the triclinic space group *P*-1, with one dimeric complex and three CH₃CN molecules in the asymmetric unit. *N*-coordination (from the papaverine ligand) to Pd^{II} leads to a pseudo-*anti* relationship of the two palladated ligands. The palladacyclic moiety 1 {containing Pd(1)} is found in a true boat conformation whereas the palladacyclic moiety 2 {containing Pd(2)} is slightly twisted as a result of modest π - π stacking interactions between neighbouring quinolinyl groups (*ca.* 4.1 Å between both aromatic ring systems). The Pd(1)-Pd(2) bond distance is 3.0258(4)Å. Thus in the solid-state and in the presence of CH₃CN, **85**·CH₃CN is not observed, and only binuclear Pd complex **86**·CH₃CN is obtained. Moreover, there was no sign of nitrite anion.

The complex also crystallized from DMSO giving yellow crystals, which were analysed

by XRD. The X-ray analysis confirmed the formation of a novel dimeric Pd(II) acetate bridged complex as above. However, an interesting observation was that the CH₂ bridged carbons has been oxidised, giving following structure (Figure 11).

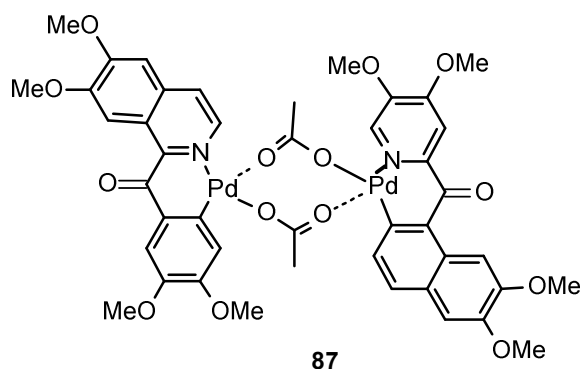


Figure 11: The structure of novel dimeric Pd(II) acetate bridged complex, 87.

DMSO has been previously reported to be involved in oxidation of cyclometallated product. Oxidation of Pt(II) by coordinated DMSO was established in 1968 upon treatment of *cis*-[PtCl₂(DMSO)₂] with concentrated aqueous HCl to give *trans*-[PtCl₄(SMe₂)₂]²⁵⁵ and is more widely recognised reaction now.²⁵⁶ A similar type of oxidation was also observed by Bruce and co-workers in their work on liquid crystalline organoplatinum(II) complexes.²⁵⁷

The X-ray crystal structure of the Pd-dimer complex **87** is given in Figure 12.

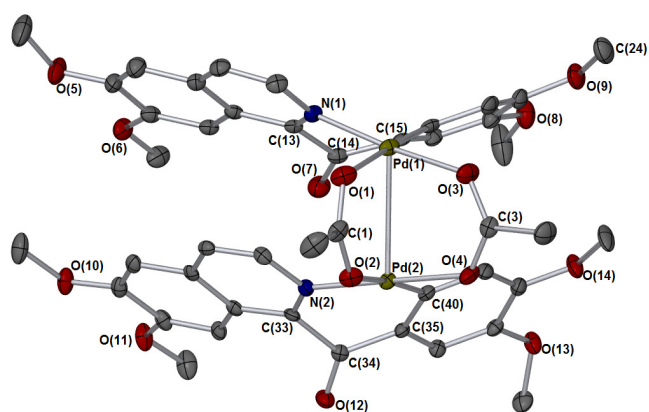


Figure 12: X-ray structure of **87 with 2 (CH₃)₂SO molecules and H-atoms omitted for clarity; selected atoms labelled.**

Solvent and hydrogen atoms are removed for clarity. Thermal ellipsoids shown at 50%. Bond lengths(Å): Pd(1)-Pd(2) = 2.9539(3), Pd(1)-N(1) = 2.0092(19), Pd(2)-N(2) = 2.0310(19), Pd(1)-C(20) = 1.953(3), Pd(2)-C(40) = 1.961(2), Pd(1)-O(1) = 2.1548(18), Pd(1)-O(3) = 2.0462(17), Pd(2)-O(2) = 2.1307(17), Pd(2)-O(4) = 2.0687(16), C(14)-O(7) = 1.217(3), C(34)-O(12) = 1.224(3), Bond Angles(°) O(1)-Pd(1)-O(3) = 87.43(7), O(2)-Pd(2)-O(4) = 84.49(7), O(1)-C(1)-O(2) = 125.2(2), O(3)-C(3)-O(4) = 115.0(2), Pd(1)-N(1)-C(13) = 124.25(16), Pd(2)-N(2)-C(33) = 128.42(16), N(1)-Pd(1)-C(20) = 88.74(9), N(2)-Pd(2)-C(40) = 90.19(9), Pd(1)-Pd(2)-O(1) = 82.09(5), Pd(1)-Pd(2)-O(4) = 80.88(5), C(33)-C(34)-C(35) = 119.0(2), C(13)-C(14)-C(15) = 118.8(2).

This complex crystallised in the $P2_1/c$ space group ($Z = 4$), with several DMSO molecules in the unit cell. By contrast with [Pd(OAc)(C[^]N)] · CH₃CN, *N*-coordination to Pd^{II} exhibits a pseudo-*syn* relationship and the two quinolinylligands π - π stack intramolecularly, causing both palladacyclic moieties to form twisted boat conformations. The Pd(1)-Pd(2) bond distance is 2.9539(3) Å, and is shorter than that found in [Pd(OAc)(C[^]N)].CH₃CN dimer complex.

A similar series of reactions was repeated by using an impure batch of Pd(OAc)₂ (*ca.* 81% Pd₃(OAc)₅NO₂). Cyclopalladation of papaverine **87** using impure Pd(OAc)₂ in presence of dry CH₃CN and under a N₂ atmosphere gave an interesting result. The ¹H NMR spectrum of this material revealed the presence of a mixture of products.

Although the starting material was fully consumed, the reaction solution was filtered while hot to remove metallic palladium formed during the reaction and was left for precipitation. No precipitate was obtained from CH₃CN solution. The reaction was then repeated in the presence of air giving a similar product. A comparison of the ¹H NMR spectrum for the different products obtained under the various reaction conditions is given in Figure 13.

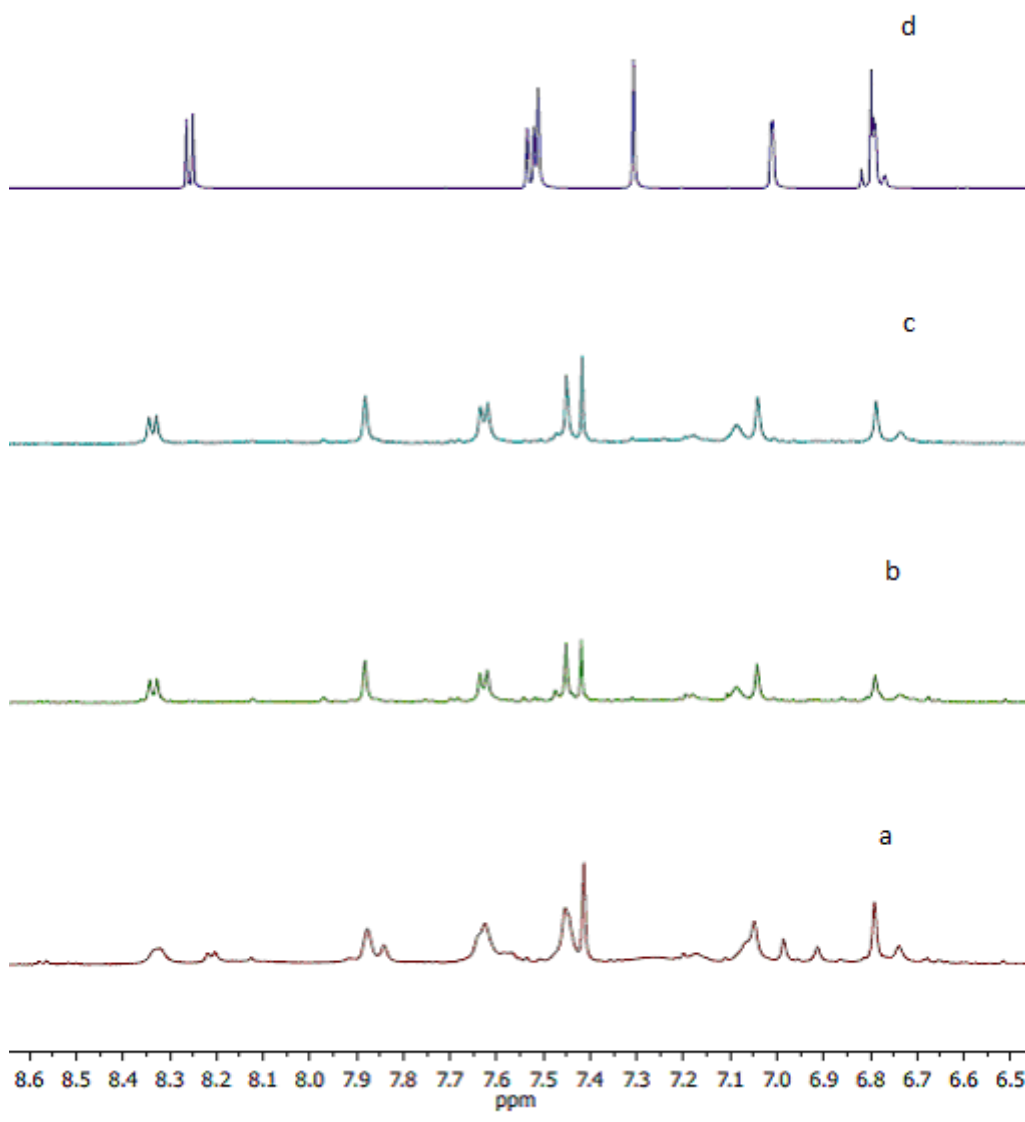
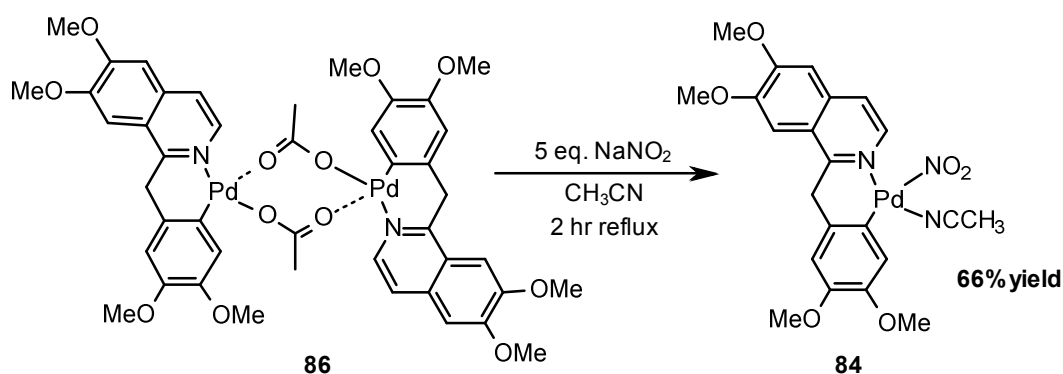


Figure 13: ¹H NMR spectra (400 MHz, in DMSO-*d*₆). **A:** Reaction of papaverine with impure Pd(OAc)₂ (red) **B:** Reaction of papaverine with pure Pd(OAc)₂ (green). **C:** Crystals of Pd-dimer (blue). **D:** papaverine 83 (note: the signal at δ 6.8 integrates for 2H, thus 7H in total in the aromatic region) (purple).

Spectrum A corresponds to the product obtained by reacting impure batch of Pd(OAc)₂ with papaverine. It shows the presence of two products. ¹H NMR spectroscopy was used to check the ratio of OAc:NO₂ containing-products, which was found to be 1:0.6 and whilst this does not match the OAc:NO₂ ratio in the impure Pd(OAc)₂ batch, it can be accounted for by the low overall yield (27%) (which is consistent with considerable Pd^{II} degradation and Pd⁰ black formation).

To account for the other major component in spectrum A (Figure 16) an authentic sample of **84** needed to be prepared. Reaction of **86**·CH₃CN with NaNO₂ (10 eq.) gave **84** in 66% yield (exact composition [Pd(NO₂)(C[^]N)CH₃CN]1.5H₂O, which compares well to the reported composition of [Pd(NO₂)(C[^]N)CH₃CN]3H₂O (Scheme 6).



Scheme 6: Synthesis of an authentic sample of [Pd(NO₂)(C[^]N)CH₃CN]·1.5H₂O, (84**).**

The comparison of the ¹H NMR spectra for the complex **88** (reported and synthesized) is given in Table 2^a. The ¹H NMR spectroscopic data confirmed the formation of NO₂-palladated papaverine.

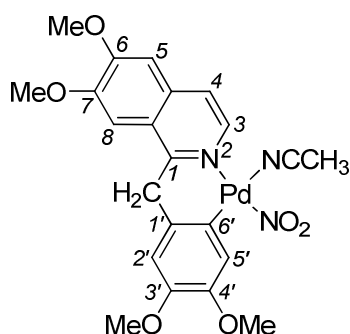


Table 2: The comparison of ^1H NMR spectrum of **88 (reported²⁵⁸ and synthesized).**

^1H signal	$[\text{Pd}(\text{NO}_2)(\text{C}^{\wedge}\text{N})\text{CH}_3\text{CN}] \cdot 3\text{H}_2\text{O}^b$ complex 88 (reported)	$[\text{Pd}(\text{NO}_2)(\text{C}^{\wedge}\text{N})\text{CH}_3\text{CN}] \cdot 1.5\text{H}_2\text{O}^c$ complex 88 (synthesized)
H-3	8.26 (d, $J = 6.3$)	8.23 (br s)
H-4	7.62 (d, $J = 6.3$)	7.58 (br s)
H-5,8	7.47 (s)	7.44 (s)
	7.88 (s)	7.85 (s)
H-5',6'	7.04 (s)	6.98 (s)
	6.96 (s)	6.91 (s)
CH₂	4.79 (s)	4.74 (br s)
OCH₃	4.11 (s)	4.07 (s)
	3.99 (s)	3.95 (s)
	3.70 (s)	3.65 (s)
	3.66 (s)	3.61 (s)

^a Reported atom-numbering was used.

^b Reported data for the palladium-nitrito adduct (in DMSO- d_6 , 400 MHz).²⁵⁸

^c in DMSO- d_6 at 400 MHz, 300 K.

A comparison of the ^1H NMR spectrum of $[\text{Pd}(\text{NO}_2)(\text{C}^{\wedge}\text{N})\text{CH}_3\text{CN}]1.5\text{H}_2\text{O}$ (in DMSO- d_6) **D** is done with the two products obtained in spectrum **A** and is found to resemble with one of the component in the reaction of **83** with impure $\text{Pd}(\text{OAc})_2$ (orange circles) (Figure 14). Thus, using impure $\text{Pd}(\text{OAc})_2$ both CH_3CN adducts of **84** and **86** are observed under the reaction conditions.

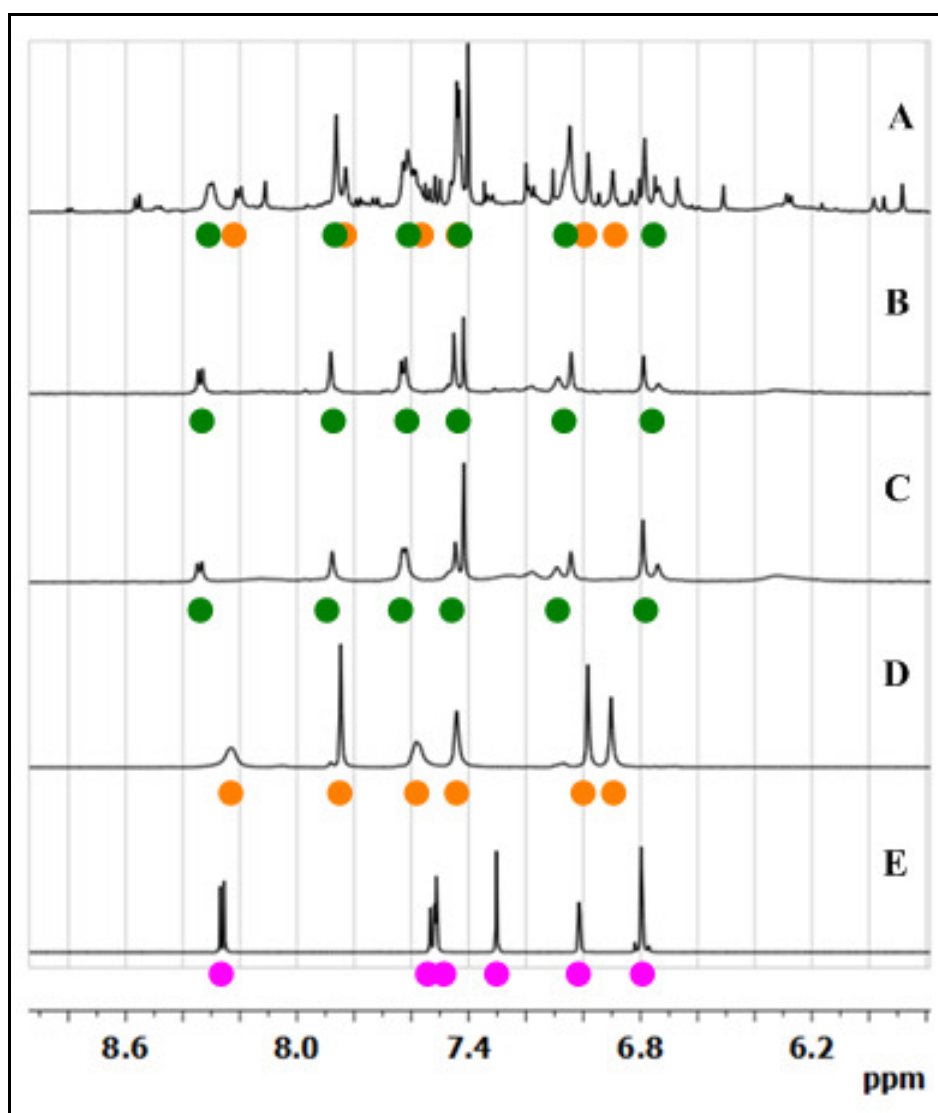


Figure 14: ^1H NMR spectra (400 MHz, in $\text{DMSO-}d_6$). A: Reaction of papaverine with impure $\text{Pd}(\text{OAc})_2$ B: Reaction of papaverine with pure $\text{Pd}(\text{OAc})_2$. C: Crystals of Pd-dimer **86**. D: Reaction of Pd-dimer with NaNO_2 . E: papaverine **83** (note: the signal at $\delta 6.8$ integrates for 2H, thus 7H in total in the aromatic region) (purple).

In an attempt to synthesize $[\text{Pd}(\text{NO}_2)(\text{C}^{\wedge}\text{N})\text{CH}_3\text{CN}]\cdot 1.5\text{H}_2\text{O}$ complex we come across an interesting result which is the formation of an unexpected $[\text{Pd}(\text{N-Hpap})_2(\text{NO}_2)_2]$, **88** complex formed during a reaction of complex **86**, with the NaNO_2 in refluxing CH_3CN (a single crystal was picked from the bulk material), giving the structure shown in Figure 15.

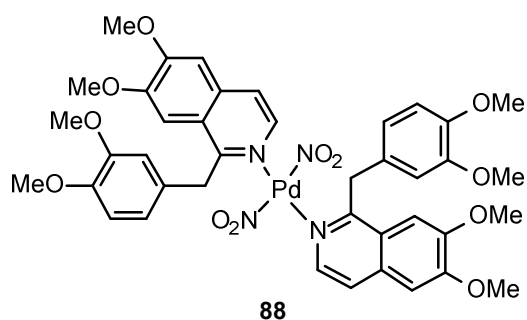


Figure 15: The structure of unexpected Pd-dinitro complex $[\text{Pd}(\text{N-Hpap})_2(\text{NO}_2)_2]$, **88.**

The X-ray crystal structure of the complex **88** is given in Figure 16.

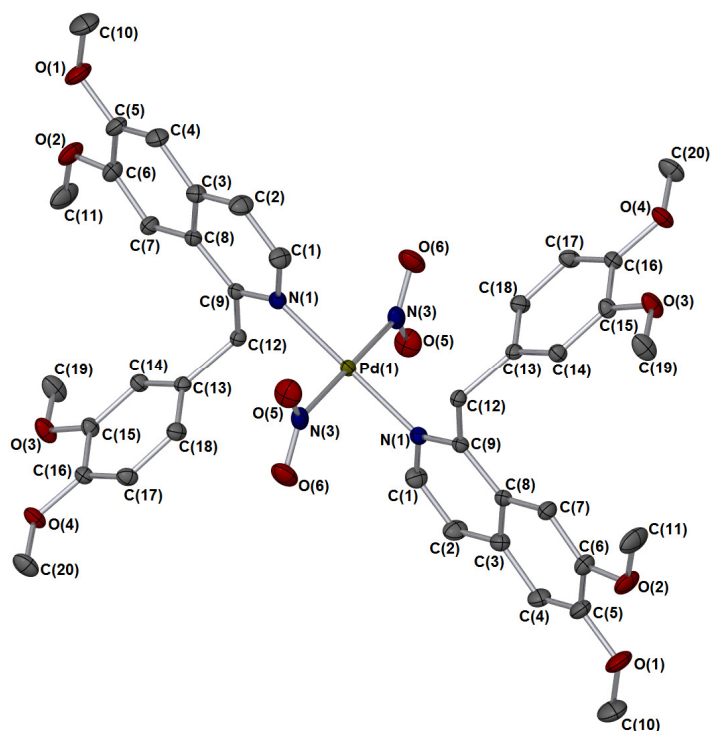
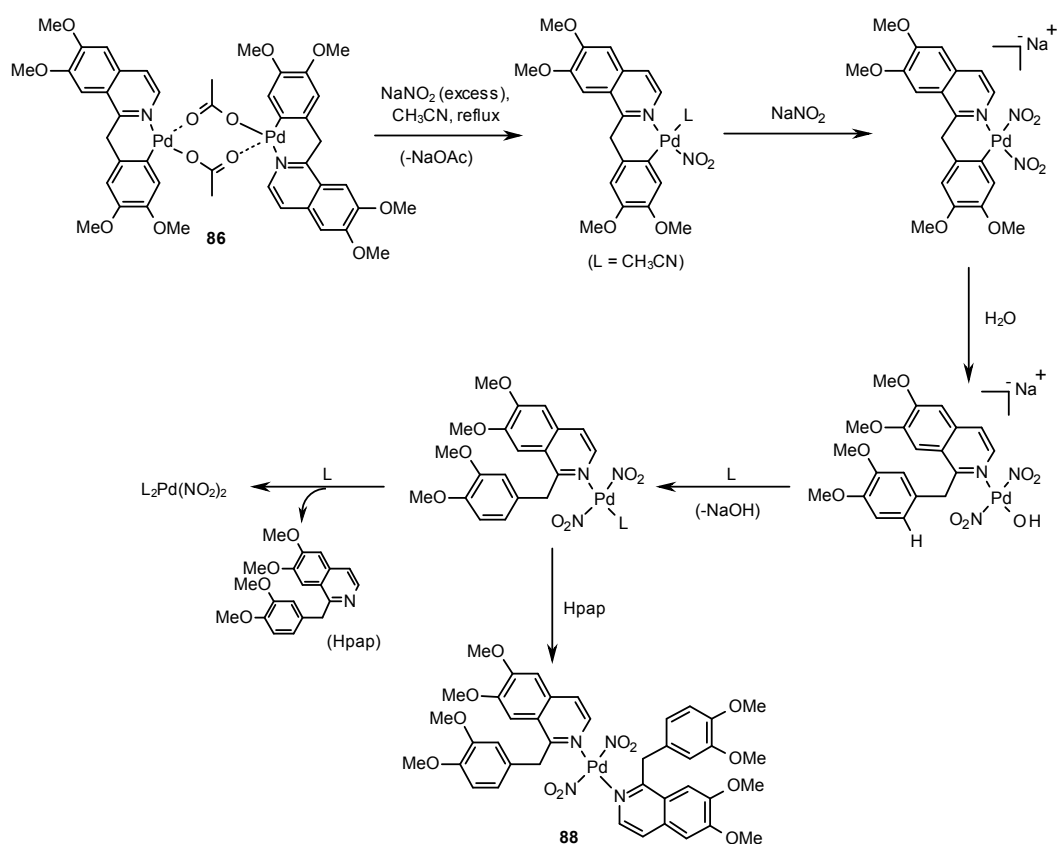


Figure 16: X-ray structure of unexpected $[\text{Pd}(\text{N-Hpap})_2(\text{NO}_2)_2]$ complex, **88**

Solvent and hydrogen atoms are removed for clarity. Thermal ellipsoids shown at 50%. Bond lengths (\AA): Pd(1)-N(1) = 2.0408(14), Pd(1)-N(3¹) = 2.0359(15), N(1)-Pd(1) = 2.0407(14), N(3)-Pd(1) = 2.0359(14), N(3)-O(5) = 1.220(2), N(3)-O(6) = 1.238(2), C(9)-N(1) = 1.340(2), C(1)-N(1) = 1.366(2), Bond Angles ($^\circ$): N(1)-Pd(1)-N(3) = 90.97(6), O(5)-N(3)-O(6) = 121.74(16), N(3)-Pd(1)-N(3¹) = 180.000(2), N(1)-Pd(1)-N(1¹) = 180.000(1), N(3)-Pd(1)-N(1) = 90.97(6), C(1)-N(1)-Pd(1) = 113.76(11), C(9)-N(1)-Pd(1) = 125.08(11).

The formation of $\text{Pd}(\text{N-Hpap})_2(\text{NO}_2)_2$ **88** from complex **86** requires some explanation. We did speculate that **86** may not have formed fully, leaving $\text{Pd}(\text{N-Hpap})_2(\text{OAc})_2$ as an initially formed complex prior to palladacycle formation. However, we have so far been unable to independently prepare $\text{Pd}(\text{N-Hpap})_2(\text{OAc})_2$ (an obvious precursor to $\text{Pd}(\text{N-Hpap})_2(\text{NO}_2)_2$ by reaction of Hpap with $\text{Pd}(\text{OAc})_2$). On this basis a tentative mechanism which may explain the formation of $\text{Pd}(\text{N-Hpap})_2(\text{NO}_2)_2$ is given in the Scheme 7. Further studies are needed to be done to independently prepare this complex, allowing its full characterisation to be accomplished and chemical reactivity to be assessed.



Scheme 7: Proposed mechanism explaining the formation of $\text{Pd}(\text{N-Hpap})_2(\text{NO}_2)_2$, **88.**

Reaction of papaverine with pure $\text{Pd}(\text{OAc})_2$ (>99%) gave a product similar to that of the crystals of Pd-dimer (Figure 17). This material is either a mixture of isomeric dinuclear compounds in $\text{DMSO-}d_6$ solution, or mononuclear and dinuclear compounds. In order to further confirm this the Pd-dimer crystals obtained were dissolved in

pyridine-*d*₅ giving a single mononuclear complex [Pd(OAc)(C[^]N)pyr-*d*₅]¹, (**85**·pyr-*d*₅) as shown by the ¹H NMR spectrum (Figure 17).

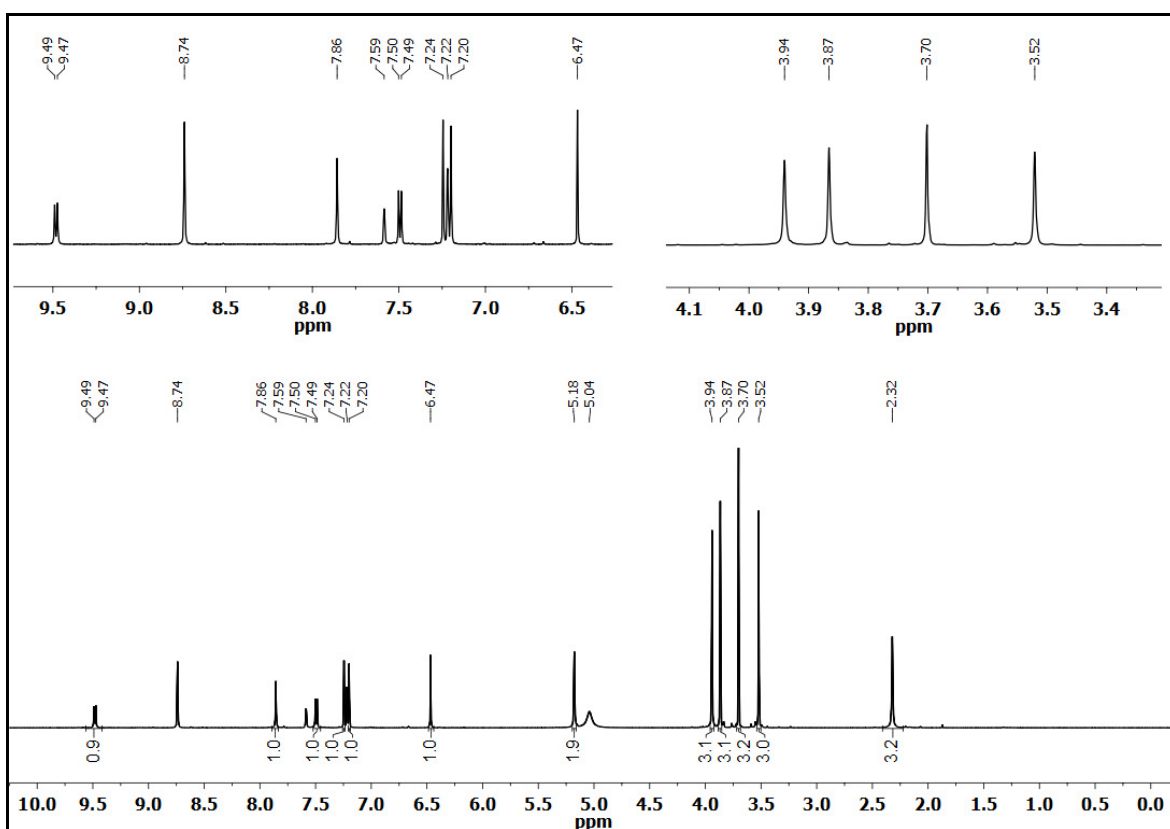
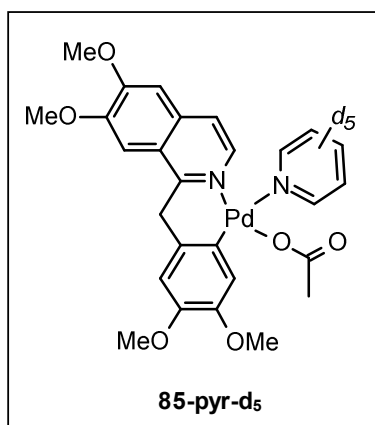
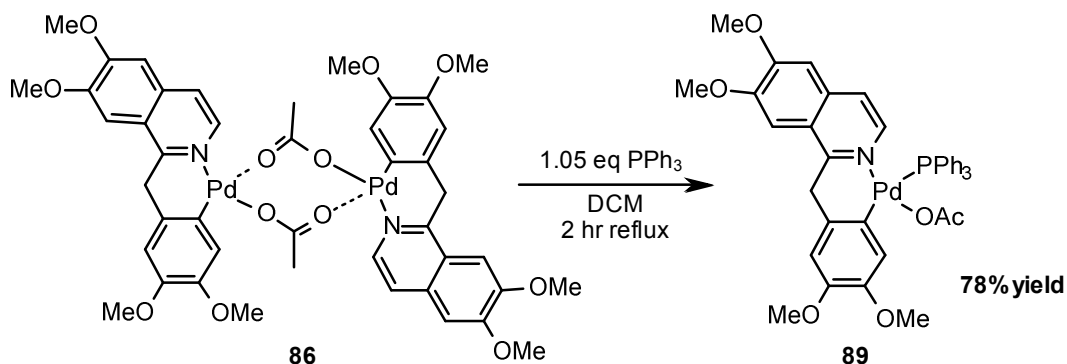


Figure 17: ¹H NMR spectra of complex **85** in pyridine-*d*₅ (400 MHz).

In order to further confirm the presence of a mononuclear compound, a stable phosphine adduct of papaverine Pd-dimer **86** was obtained by reacting Pd-dimer crystals with with PPh₃ (1:1, Pd^{II}:PPh₃) in DCM affording mononuclear complex [Pd(OAc)(C[^]N)PPh₃] **89** in 78% yield. The reaction takes 2 h. The reaction mixture was concentrated to one fifth of its initial volume. Slow addition of diethyl ether completed the crystallization of the

¹ Experiment performed by Prof. I. J. S. Fairlamb.

complex, which was filtered off, washed with ether and air-dried (Scheme 8).



Scheme 8: Synthesis of [Pd(OAc)(C^N)PPh₃].

¹H NMR spectroscopy showed the expected four singlet proton resonances for the methoxy groups at δ 4.09, 3.97, 3.69 and 2.91; proton resonances for papaverine and phenyl moieties, two pseudo-diastereotopic palladacyclic methylene protons (*ca.* δ 4.89), and methyl singlet resonance for the acetoxy group (δ 1.21). We manage to obtain the crystals for the [Pd(OAc)(C^N)PPh₃] product **89**, which were analysed by XRD studies. An X-ray structure of a single crystal is given in Figure 18.

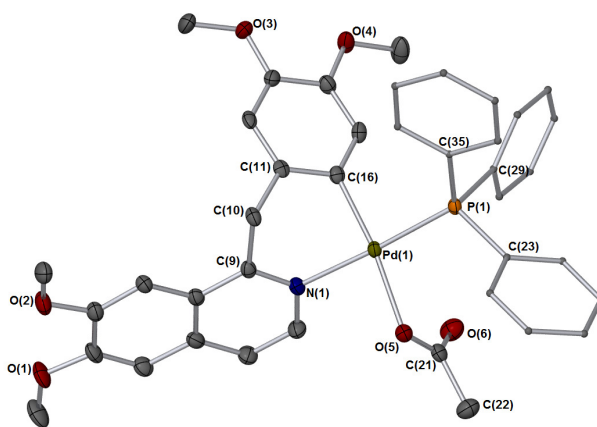


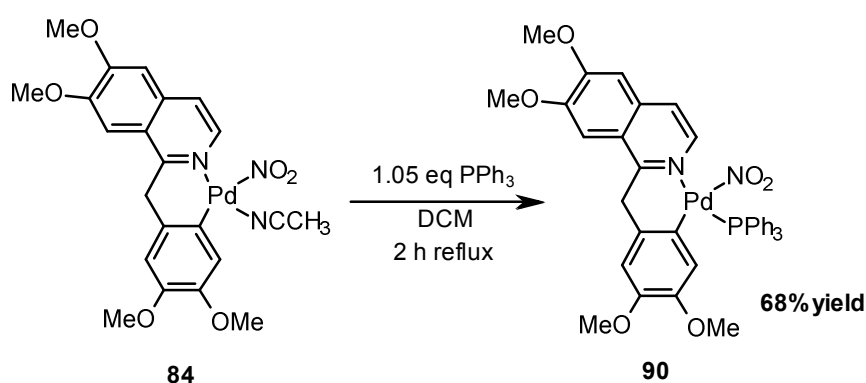
Figure 18: X-ray structure of [Pd(OAc)(C^N)PPh₃], **89.**

Solvent and hydrogen atoms are removed for clarity. Thermal ellipsoids shown at 50%. Bond lengths (\AA): Pd(1)-P(1) = 2.2434(7), Pd(1)-C(16) = 1.990(3), N(1)-Pd(1) = 2.091(2), O(5)-Pd(1) = 2.111(2), N(1)-C(9) = 1.328(4), P(1)-C(35) = 1.822(3), P(1)-C(29) = 1.818(3), P(1)-C(23) = 1.821(3), O(5)-C(21) = 1.261(4), O(6)-C(21) = 1.242(4), C(21)-C(22) = 1.515(4), Bond Angles ($^\circ$): N(1)-Pd(1)-C(16) = 85.43(10), C(16)-P(1)-Pd(1) = 118.48(9), C(29)-P(1)-Pd(1) = 113.98(10), C(23)-P(1)-Pd(1) = 112.29(2), C(35)-P(1)-C(29) = 104.27(13), C(29)-P(1)-C(23) = 103.92(13).

The XRD data showed that the PPh₃ complex crystallised in the monoclinic *C2/c* space group. The palladacycle once again sits in a boat conformation. The N(1)-Pd(1) bond distance (2.091(2) Å) is longer than the equivalent N-Pd bond found in Pd-dimer **86** (2.033(2) Å). The dihedral angle for C(9)-N(1)-Pd(1)-P(1) showed *synperiplanar* conformation (-3.9 °) whereas P(1)-Pd(1)-O(5)-(C21) exhibited *synclinal* and O(5)-Pd(1)-N(1)-C(9) exhibited *anticlinal* conformation with torsion angle of -76.98(19) ° and 124.6(2) ° respectively.

Hence by using pure Pd(OAc)₂, **86** is the only product (as a mixture isomeric, mononuclear or dinuclear compounds, verified by the independent synthesis of **89**). It can therefore be concluded that nitrite impurities explain the formation of nitrite adducts from Pd(OAc)₂ and papaverine **83** (in the presence or absence of air).

Repeated attempts to crystallize the [Pd(NO₂)(C[^]N)CH₃CN].1.5H₂O complex from both CH₃CN and DMSO failed. We were keen to crystallize the complex to further confirm the formation of pap-NO₂ complex, **84**. Whilst this was not possible for either **84**·CH₃CN or **84**·DMSO, it was possible to prepare the PPh₃ adduct by the reaction of **84**·CH₃CN with PPh₃ (in a 1:1 ratio) in CH₂Cl₂ at reflux for 2 h (Scheme 21). The product was characterized by NMR spectroscopy, mass spectrometry and elemental analysis, and found to be [Pd(NO₂)(C[^]N)PPh₃] **90** (Scheme 9).



Scheme 9: Synthesis of [Pd(NO₂)(C[^]N)PPh₃] complex (90).

It was possible to crystallize complex 90 from DCM. The light yellowish crystals obtained were analysed by XRD. The XRD analysis showed an interesting structure where the NO₂ was coordinated to palladium as expected but as a mixture of ‘Pd-η¹-

NO_2 ' (**90a**) and 'Pd- η^1 -ONO' (**90b**) isomers (Figure 19).

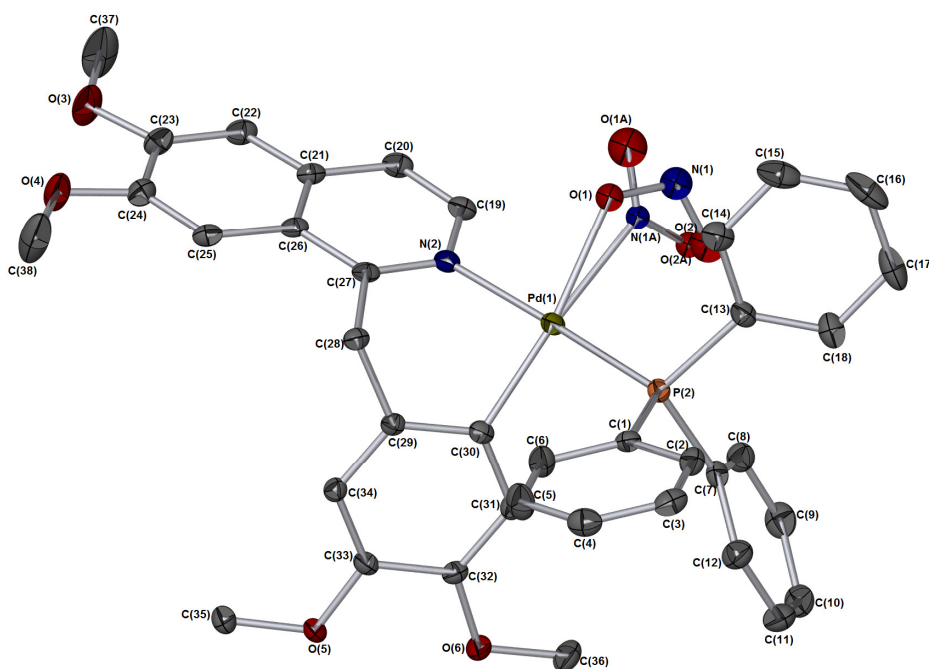


Figure 19: X-ray diffraction analysis of complex. Ground state structure (150 K) showing a mixture of 'Pd- η^1 -NO₂' (90a**) and 'Pd- η^1 -ONO' (**90b**).**

Solvent and hydrogen atoms are removed for clarity. Thermal ellipsoids shown at 50%. Bond lengths (Å): Pd(1)-P(2) = 2.2661(5), Pd(1)-C(30) = 2.004(2), N(2)-Pd(1) = 2.1149(17), O(1)-Pd(1) = 2.144(2), Pd(1)-N(1A) = 2.185(7), N(1A)-O(1A) = 1.104(10), O(1)-N(1) = 1.258(4), O(2)-N(1) = 1.225(4), P(2)-C(1) = 1.826(2), P(2)-C(7) = 1.823(2), P(2)-C(13) = 1.825(2), Bond Angles (°): C(30)-Pd(1)-N(2) = 85.39(7), C(30)-Pd(1)-P(2) = 93.46(6), C(30)-Pd(1)-N(1A) = 159.78(19), C(30)-Pd(1)-O(1) = 170.00(8), N(2)-Pd(1)-P(2) = 174.29(5), N(2)-Pd(1)-N(1A) = 90.07(18), O(1)-Pd(1)-N(1A) = 21.59(17), O(1)-N(1)-O(2) = 117.6(3), O(1A)-N(1A)-O(2A) = 124.3(9).

There were two binding modes for the nitro/nitrito ligand. The ratio of nitrito (bound by one oxygen, N1, O1, O2 with Pd cis to O2) and nitro (N-bound, N1a O1a O1b) refined to 74:26. The nitro/nitrito atoms were modelled isotropically and the N-O distance for the nitro were restrained to be equal. Similar nitrito complexes of Ni^{II} have been previously reported²⁵⁹ and are found to be effectively in use in data storage devices. These nitrito complexes of Ni^{II} exhibit linkage isomerisation (by photoexcitation). Coppens has pioneered this area and has determined the structures of a number of metastable linkage isomers including metal nitrosyl,²⁶⁰ metal nitrite²⁶¹ and metal sulphur dioxide complexes.²⁶² Hence, a detailed study of these complexes was investigated and

some more comprehensive photocrystallographic experiments were conducted using synchrotron radiation.

5.5 Photocrystallographic study of [Pd(NO₂)(C[^]N)PPh₃] complex; (Crystallographic experiments conducted by Bath investigators)

Photocrystallography is a rapidly growing technique that allows the full three-dimensional structures of short-lived and metastable photoactivated species to be determined using X-ray diffraction method. By using this technique we can not only determine the structure of a transient species but can also follow a dynamic process within a crystal. The XRD analysis for [Pd(NO₂)(C[^]N)PPh₃] complex (**90**) showed an interesting result where NO₂ was coordinated to palladium as expected but as a mixture of ‘Pd-η¹-NO₂’ (**90a**) and ‘Pd-η¹-ONO’ (**90b**) isomers. The group of Prof. Paul Raithby (University of Bath) has been working on similar kind of complexes and so a collaboration was initiated. A series of experiments were carried out to study the linkage isomerisation behaviour for the complex, [Pd(NO₂)(C[^]N)PPh₃], including the ratio for the two isomers under both photochemical and thermal conditions.

5.5.1 XRD studies

5.5.2 Instrumentation

X-ray diffraction studies on complex **90** were conducted on beamline I19 at the Diamond Light Source, Rutherford Appleton Laboratory, UK and on Station 11.3.1 of the Advanced Light Source, Lawrence Berkeley National Laboratory, California, USA. Single crystal data collections at Diamond were carried out on a Rigaku Saturn CCD diffractometer equipped with an Oxford Cryosystems Cobra cryostream, while at the ALS data were collected using a Bruker APEXII CCD diffractometer equipped with a Oxford Cryosystems Cryostream Plus.

5.5.3 Photocrystallographic Experiment

An X-ray data set was collected in the absence of light at 150 K and the structure was solved and refined. The complex **90** crystallizes in the monoclinic space group $P2_1/c$ and exists as a *ca.* 3:1 mixture of ‘Pd-η¹-NO₂’ (**90a**) and ‘Pd-η¹-ONO’ (**90b**) linkage isomers (Table 6) at this temperature. The crystal was then irradiated at 150 K using a specifically designed LED ring,²⁶³ which supports six 400 nm LEDs in a circle, 1 cm from the crystal to ensure uniform irradiation. After 1 h the crystal structure was

redetermined and it was found that the photoactivated nitrito complex ‘Pd- η^1 -ONO’ (**90b**) is fully formed (100% conversion). Further irradiation (1.5 h) caused no appreciable change, confirming the 100% nitrito form to be a photostationary state. Notably, this isomer is retained at 150 K in the dark (over 1 h), showing that the system is metastable under these conditions. The Pd- η^1 -ONO’ (**90b**) isomeric structure remains in the same space group $P2_1/c$, with little change in the packing arrangement and only a $\Delta V = 0.14\%$ increase in the unit cell volume observed, in comparison to the initially determined mixed-isomer structure. Variable temperature parametric studies (VT) determined that the metastable state exists on warming to 180 K, however further heating to 200 K causes the system to revert back to its mixed-isomer structure initially observed at 150 K.

Table 6: Crystallographically determined percentage ratios of 90a and 90b in a single crystal as a function of exposure to 400 nm radiation and variable temperature. ^a GS = ground state. ^b Photostationary state. ^c System is metastable at 150 K (8b). ^dVT = variable temperature.

Experiment	Irridation time / h	Temp / K	Conversion %	
			90a	90b
GS ^a	0	150	23	77
UV	1	150	0	100
UV	1.5	150	0	100
1 h Dark	1.5	150	0	100
VT ^d	1.5	160	0	100
VT ^d	1.5	180	0	100
VT ^d	1.5	200	23	77

5.5.4 Thermal Crystallographic Experiment

Recent studies for another mixed nitro:nitrito Ni^{II} complex have shown that conversion between isomers can also be controlled thermally.²⁶⁴ As such, in separate experiments on Station 11.3.1 at the Advanced Light Source, Berkeley, California, USA, a single crystal of **90** was slow-cooled *in-situ* and a series of identical datasets collected at regular intervals to monitor any changes in nitro:nitrito occupation. Conversion to the nitro isomer, **90a**, was found to increase, from 77% at ambient temperature to a

maximum 86% on slow-cooling to 150 K (Table 3).

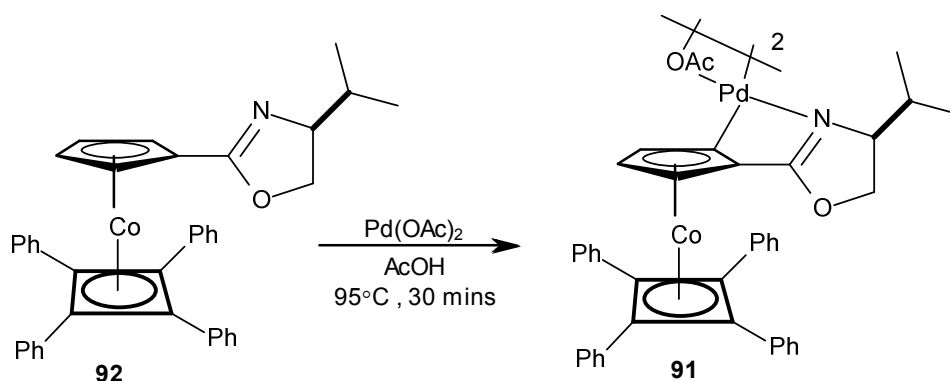
Table 3: Crystallographically determined percentage of 90b in a single crystal as a function of temperature.

Temp / K	Conversion / %
298	76
250	78
200	84
150	86

The increase in **90a** on slowly decreasing the temperature indicates that the major component is the more thermodynamically stable isomer at lower temperatures, which correlates with results obtained for the Ni^{II} system. The matching 77% conversion between the room temperature structure and the initial structure determined in the photocrystallographic experiments indicate that flash-cooling of the crystal appears to thermally trap the system in its ambient state.

5.6 Further studies with pure and impure Pd(OAc)₂

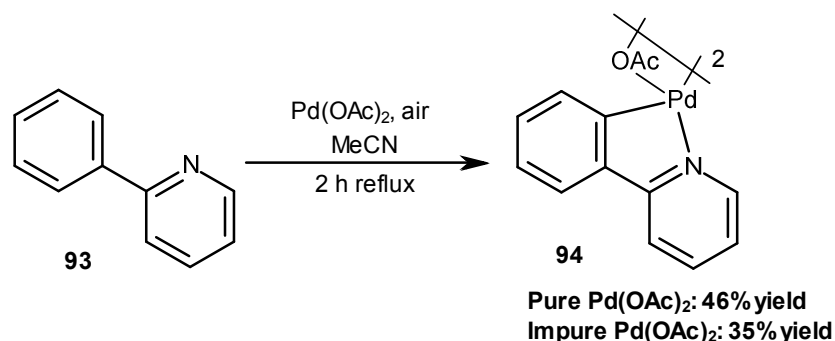
In order to further confirm that there was no oxidation of CH₃CN observed during the cyclopalladation reaction and it was the nitrite impurity in the Pd(OAc)₂ catalyst, which was the cause of the nitrito-derived palladated products. Further experiments were conducted. Dr. C. J. Richards and co-workers in 2007 reported the synthesis of series of COP catalysts, di- μ -acetatobis[(η^5 -(S)-(pR)-2-(2'-(4'-methyleneethyl)oxazolanyl)cyclopentadienyl, 1-C, 3'-N)(η^4 -tetraphenylcyclobutadiene)cobalt]dipalladium ([COP-OAc]₂) **91** was synthesized by reacting (η^5 -(S)-2-(4-methyleneethyl)oxazolanyl-cyclopentadienyl)-(η^4 -tetraphenylcyclobutadiene)cobalt **92** with Pd(OAc)₂ in glacial acetic acid (Scheme 10). The red solution was then heated to 95 °C for 0.5 h giving an orangish precipitate. The solution was cooled to room temperature, filtered, washed with glacial acetic acid and dried under vacuum to afford **91** as a mustard-coloured solid.



Scheme 10: Synthesis of [(COP-OAc)₂] catalyst, **91**.

The same chemistry was repeated and the synthesis of [(COP-OAc)₂] **91** was carried out using both pure and impure batch of Pd(OAc)₂. In both cases a pure product was obtained as confirmed by ¹H NMR spectroscopic analysis and there was no formation of Pd(II) nitrito adduct was observed in either case.²⁶⁵

The same cyclopalladation chemistry was repeated using 2-phenylpyridine **93** (Scheme 11). 2-Phenyl pyridine was treated with both a pure and impure batch of Pd(OAc)₂. In the first reaction a mixture of 2-phenyl pyridine (1 mmol) and ultra-pure Pd(OAc)₂ (1 mmol) in acetonitrile was heated at reflux for 3.5 hr with stirring. The solution was filtered whilst hot and left in fridge for crystallization. After 1 week a yellowish precipitate started appearing in the flask, which was then filtered, washed with hexane and dried. The product was obtained with a yield of 46%. The product was run for its mass spectrometry (LIFDI) and was found to have a peak at 637.9620 which corresponds to [Pd₂(C₂₆H₂₂N₂O₄)] showing the formation of a cyclopalladated product and there is no nitrito adduct for Pd^{II} was observed.



Scheme 11: Cyclopalladation of 2-phenylpyridine, (**93**).

Similarly, in the second reaction 2-phenylpyridine was treated with impure Pd(OAc)₂.

The reaction was carried out under similar conditions. Yellowish precipitates started appearing after a week, which were then filtered, washed with hexane and dried to give the product with a yield of 35%. The LIFDI mass spectrum for the product gave the peak at 637.9683 corresponding to formation of cyclopalladated product $[\text{Pd}_2(\text{C}_{26}\text{H}_{22}\text{N}_2\text{O}_4)]$. The ^1H NMR confirmed the presence of a mixture of product as expected for the impure $\text{Pd}(\text{OAc})_2$.

The yellowish product obtained was soluble in most of the organic solvents (e.g. DCM, chloroform, benzene, ethyl acetate) and hence attempts were done to crystallize the cyclopalladated product formed. Light yellowish crystals started appearing in a DCM solution of product. The crystals were submitted for their XRD studies and were found to have the following structure (Figure 20).

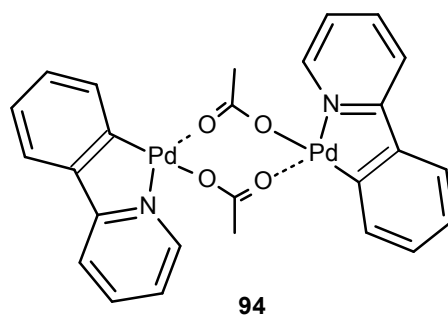


Figure 20: The structure of cyclopalladated 2-phenylpyridine, 94.

The X-ray crystal structure of the complex **94** is given in Figure 21.

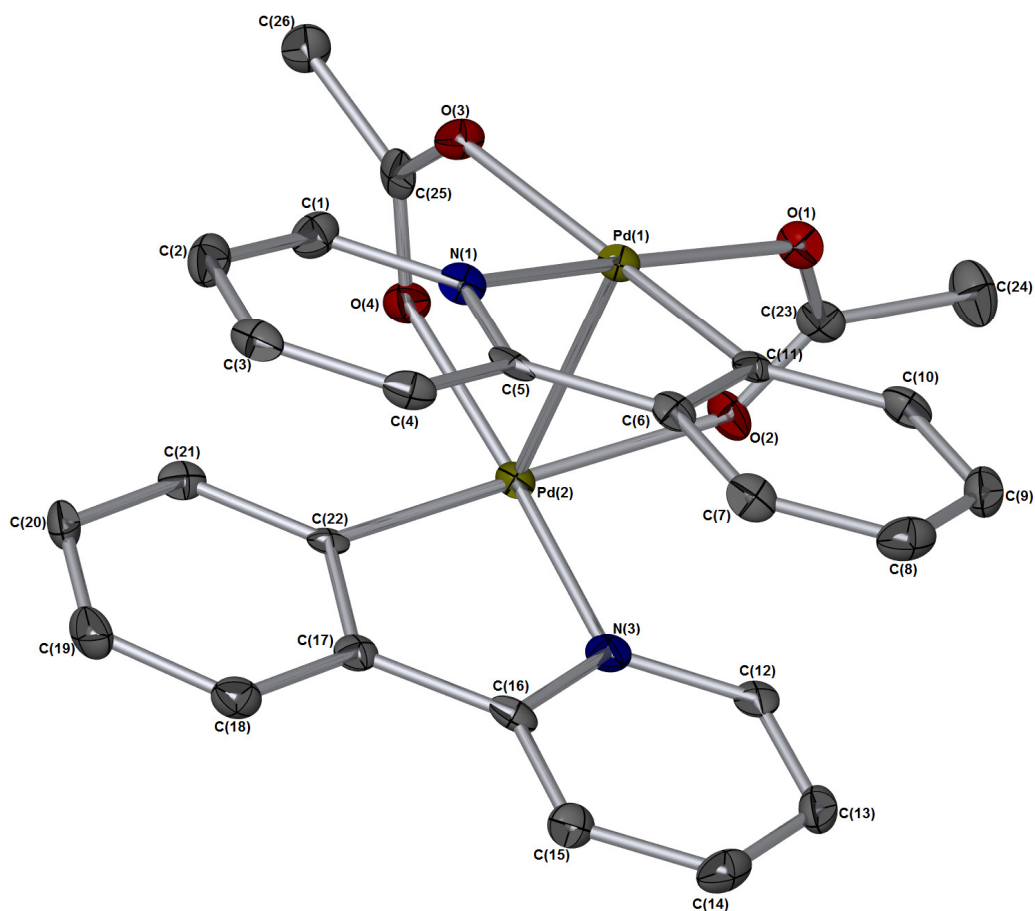


Figure 21: X-ray crystal structure of complex 94.

Solvent and hydrogen atoms are removed for clarity. Thermal ellipsoids shown at 50%. Bond lengths (Å): Pd(1)-Pd(2) = 2.8693(5), Pd(1)-N(1) = 2.014(3), Pd(2)-N(3) = 2.012(3), Pd(1)-C(11) = 1.962(4), Pd(2)-C(22) = 1.967(4), Pd(1)-O(1) = 2.057(3), Pd(1)-O(3) = 2.157(3), Pd(2)-O(2) = 2.149(3), Pd(2)-O(4) = 2.056(3), C(23)-O(1) = 1.272(5), C(23)-O(2) = 1.249(5), C(25)-O(3) = 1.265(5), C(25)-O(4) = 1.255(5), Bond Angles (°) O(1)-Pd(1)-O(3) = 93.80(11), O(3)-C(25)-O(4) = 126.0(4), O(2)-Pd(2)-O(4) = 98.37(11), N(3)-Pd(2)-C(22) = 81.84(5), N(1)-Pd(1)-C(11) = 81.49(15), O(3)-Pd(1)-Pd(2) = 73.81(8), Pd(1)-Pd(2)-O(2) = 82.06(8), N(1)-Pd(1)-O(1) = 172.51(13), N(1)-Pd(1)-O(3) = 93.03(12), N(3)-Pd(2)-O(2) = 94.84(13), N(3)-Pd(2)-O(4) = 175.34(12).

The complex crystallizes in the monoclinic space group $P2_1/c$. The Pd(1)-Pd(2) bond distance (2.8693(5) Å) is shorter than that of Pd-dimer **86** (3.0258(4) Å). The bond distances for Pd(1)-N(1) (2.014(3) Å) and Pd(2)-N(3) (2.012(3) Å) in complex **94** are similar to that of Pd(1)-N(1) (2.033(2) Å) and Pd(1)-N(2) (2.032(2) Å) in complex **86**.

5.7 Experimental

5.7.1 General Information

^1H -NMR spectra were obtained in the solvent indicated using a JEOL EXC400 or JEOL ECS400 spectrometer (400MHz for ^1H , 100 MHz for ^{13}C and 162 MHz for ^{31}P). Chemical shifts were referenced to the residual undeuterated solvent of the deuterated solvent used (CHCl_3 $\delta_{\text{H}} = 7.26$ and $\delta_{\text{C}} = 77.16$ (CDCl_3), CDHCl_2 $\delta_{\text{H}} = 5.31$ and $\delta_{\text{C}} = 54.0$ (CD_2Cl_2), $(\text{CHD}_2)\text{SO}(\text{CD}_3)$ $\delta_{\text{H}} = 2.50$ and $\delta_{\text{C}} = 39.52$ $\{\text{SO}(\text{CD}_3)_2\}$, ^1H and ^{13}C , respectively).. NMR spectra were processed using MestrNova software. All ^{13}C NMR spectra were obtained with ^1H decoupling. ^{31}P NMR were externally referenced to H_3PO_4 , and obtained with ^1H decoupling. For ^{13}C NMR spectra the coupling constants are quoted to ± 1 Hz. For the ^1H NMR spectra the resolution varies from ± 0.15 to ± 0.5 Hz; the coupling constants have been quoted to ± 0.5 Hz in all cases for consistency.

Melting points were recorded using a Stuart digital SMP3 machine. IR spectroscopy was undertaken using a Jasco/MIRacle FT/IR-4100typeA spectrometer with an ATR attachment on solid and liquid compounds; solution and KBr IR spectra were obtained on a Nicolet Avatar 370 FT-IR spectrometer. The relative intensities of the peaks are denoted by (s) = strong, (m) = medium and (w) = weak, whilst (br) is used to describe broad peaks. MS spectra were measured using a Bruker Daltronics micrOTOF MS, Agilent series 1200LC with electrospray ionisation (ESI and APCI) or on a Thermo LCQ using electrospray ionisation, with < 5 ppm error recorded for all HRMS samples. LIFDI mass spectrometry was carried out using a Waters GCT Premier MS Agilent 7890A GC (usually for analysis of organometallic compounds when ESI or APCI are not satisfactory ionisation methods). Mass spectral data is quoted as the m/z ratio along with the relative peak height in brackets (base peak = 100). Elemental analysis was carried out on an Exeter Analytical CE-440 Elemental Analyser. UV-visible spectra were recorded using a JASCO V-560 instrument with quartz cells (1 cm path length). Spectra were processed in SigmaPlot version 10.0 (2006 Systat Software, Inc.).

Dry and degassed acetonitrile and dichloromethane were obtained from a Pure Solv MD-7 solvent purification system. 'Dry' dimethyl sulfoxide was obtained from Acros (99.7+% extra dry over molecular sieves). Acetonitrile used some reactions (indicated below in individual reactions) was dried and purified by triply distilling over anhydrous AlCl_3 , then Li_2CO_3 and finally CaH_2 , according to a procedure reported by Walter and

Ramaley (*method A*).²⁶⁶ Nitrogen gas was oxygen-free and dried immediately prior to use by passage through a column containing sodium hydroxide pellets and silica. Commercial chemicals were purchased from Sigma-Aldrich or Alfa Aesar.

All air sensitive procedures were carried out using Schlenk techniques (high vacuum, liquid nitrogen trap on a standard in-house built dual line). Where necessary a glove (dry) box was used (<0.5 ppm O₂). Room temperature upper and lower limits are stated as 13-25 °C, but typically 21 °C was recorded. Commercial chemicals were purchased from Sigma-Aldrich and Alfa Aesar and used directly unless otherwise stated in the text. Brine refers to a saturated aqueous solution of NaCl.

Pd(II) dimer complex (86): Reactions of Hpap (83) with Pd(OAc)₂ (>99%)

a) In air using reagent grade CH₃CN

A mixture of Pd(OAc)₂ (224 mg, 1 mmol) and Hpap (339 mg, 1 mmol) in acetonitrile (30 mL) was refluxed for 3.5 h (under air atmosphere) with stirring. The resultant dark coloured solution was filtered whilst hot to remove metallic palladium formed during the reaction. The filtrate was then kept in the fridge which led to yellow crystals being formed. After 14 days, the yellow semi-crystalline material was filtered, washed with hexane and dried *in vacuo* to give **86** (0.415 g, 82%).

b) In air using triply-distilled CH₃CN

Procedure identical to as given above. After 14 days, the yellow semi-crystalline material was filtered, washed with hexane and dried *in vacuo* to give **86** (0.225 g, 44%).

c) Under N₂ atmosphere using triply-distilled CH₃CN

Procedure identical to as given above, with the exception that the reaction was conducted under N₂ (Schlenk techniques). After 14 days, the yellow semi-crystalline material was filtered, washed with hexane and dried *in vacuo* to give **86** (0.339 g, 67%).

¹H NMR (400 MHz, **pyr-*d*₅**) δ 9.48 (d, *J* = 6.5 Hz, 1H), 7.86 (s, 1H), 7.49 (d, *J* = 6.5 Hz, 1H), 7.24 (s, 1H), 7.20 (s, 1H), 6.47 (s, 1H), 5.18 (s, 2H), 3.94 (s, 3H), 3.87 (s, 3H), 3.70 (s, 3H), 3.52 (s, 3H) and 2.32 (s, 3H) (**note:** after 24 h in solution this complex does degrade to give other uncharacterised species); Mp 225-226 (decomp.)°C; LIFDI MS *m/z* 503 ([M]⁺), 337 (100); HR-MS *m/z* 503.0524 ([M]⁺) (calc. for Pd(C₂₂H₂₃NO₆

503.0560) {**note:** a complex mixture of ions were observed at m/z 1002-1014 (dimer), but an accurate mass could not be determined}; IR (KBr) ν cm^{-1} 2938, 2835, 1618, 1575, 1511, 1484, 1465, 1423, 1274, 1254, 1239, 1207, 1159, 1043, 1027, 987, 857, 824, 781, 681; Elemental Analysis, Calcd. for $\text{C}_{48}\text{H}_{58}\text{N}_2\text{O}_{14}\text{Pd}_2\text{S}_2$ (**6**·2DMSO) (found) %: C 49.53 (48.98), H 5.02 (4.82), N 2.41 (2.37) (**note:** elemental analysis on crystalline material derived from DMSO).

Reactions of Hpap (83) with impure $\text{Pd}(\text{OAc})_2$ {mixture of $\text{Pd}_3(\text{OAc})_6$ and $\text{Pd}_3(\text{OAc})_5\text{NO}_2$ }

a) In air using triply-distilled CH_3CN

Procedure (and scale) identical to that used for $\text{Pd}(\text{OAc})_2$. The reaction in this case was done with impure $\text{Pd}_3(\text{OAc})_6$ {*ca.* 81% $\text{Pd}_3(\text{OAc})_5\text{NO}_2$ }. After 14 days, the yellow semi-crystalline material was filtered, washed with hexane and dried *in vacuo* to give a mixture of compounds (0.137 g, *ca.* 27%); The ^1H NMR spectrum of this material was quite complicated (mixture of products), MS analysis reveals only the presence of a $[\text{Pd}(\text{C}^{\wedge}\text{N})(\text{OAc})]$ adduct – LIFDI MS m/z 503.06 ($[\text{M}]^+$); Elemental analysis of this material, Found: C, 48.73; H, 4.45; N, 4.20 (high nitrogen content).

b) Under N_2 atmosphere using triply-distilled CH_3CN

Procedure (and scale) identical to that used for $\text{Pd}(\text{OAc})_2$. The reaction in this case was done with impure $\text{Pd}_3(\text{OAc})_6$ {*ca.* 81% $\text{Pd}_3(\text{OAc})_5\text{NO}_2$ }. After 14 days, the yellow semi-crystalline material was filtered, washed with hexane and dried *in vacuo* to give a mixture of compounds (0.175 g, *ca.* 35 %); The ^1H NMR spectrum of this material was quite complicated (mixture of products), MS analysis reveals only the presence of a $[\text{Pd}(\text{pap})(\text{OAc})]$ adduct – LIFDI MS m/z 503.01 ($[\text{M}]^+$), 339.12 (100); Elemental analysis of this material, Found: C, 47.9; H, 4.64; N, 8.62 (high nitrogen content).

Complex 89, $[\text{Pd}(\text{OAc})(\text{C}^{\wedge}\text{N})\text{PPh}_3]$

Palladium complex **6** (150 mg, 0.15 mmol) was dissolved in dichloromethane (15 mL) containing triphenylphosphine (39.1 mg, 0.15 mmol, 1 eq. per Pd) was added. The solution was refluxed at 40 °C for 2 h, and then concentrated *in vacuo* to one fifth of its initial volume. Slow addition of diethyl ether led to precipitation of the complex, which was filtered off, washed with diethyl ether and air-dried to afford a pale yellow solid

(0.089 g, 78%). Mp 135-137 (decomp.); ^1H NMR (400 MHz, CD_2Cl_2) δ 8.53 (d, $J = 6.3$ Hz, 1H), 7.55-7.66 (br m, 7H), 7.41-7.45 (br m, 3H), 7.34-7.39 (br m, 7H), 7.03 (s, 1H), 6.81 (s, 1H), 6.04 (d, $J = 4.5$ Hz, 1H), 4.96 (br d, *ca.* 12 Hz, 1H), 4.82 (br d, *ca.* 12 Hz, 1H), 4.09 (s, 3H), 3.97 (s, 3H), 3.69 (s, 3H), 2.91 (s, 3H), 1.21 (s, 3H); ^{13}C NMR (101 MHz, CD_2Cl_2) δ 177.3 (4°), 158.3 (4°), 154.8 (4°), 151.5 (4°), 146.3 (4°, d, $J = 2.5$ Hz), 146.1 (4°), 142.8 (CH), 135.5 (CH, d, $J = 11.5$ Hz), 134.5 (4°), 131.5 (4°, d, $J = 48$ Hz), 131.1 (4°), 130.9 (CH, d, $J = 1.5$ Hz), 128.8 (CH, d, $J = 10.5$ Hz), 122.9 (4°, d, $J = 2.5$ Hz), 119.9 (CH, d, $J = 11$ Hz), 119.2 (CH), 112.8 (CH), 105.9 (CH), 104.6 (CH), 56.7 (CH₃), 56.6 (CH₃, 2C), 55.1 (CH₃), 45.1 (CH₂), 24.1 (CH₃); ^{31}P NMR (162 MHz, CD_2Cl_2) δ 34.6 (s, 1P); IR (KBr) ν cm^{-1} 2935, 2834, 1619, 1575, 1510, 1483, 1464, 1422, 1337, 1312, 1274, 1238, 1207, 1160, 1096, 1042, 987; LIFDI MS m/z 765 [M]⁺, 503 (100), HR-MS m/z 765.1260 ([$\text{M}+\text{H}$]⁺) (calc. for $\text{C}_{40}\text{H}_{38}\text{NO}_6\text{PdP}$ 766.1312).

Complex 84, authentic sample of $[\text{Pd}(\text{NO}_2)(\text{C}^{\wedge}\text{N})\text{CH}_3\text{CN}]\cdot 1.5\text{H}_2\text{O}$

To a stirred solution of NaNO_2 (73.8 mg, 1.07 mmol, 5 eq.) in CH_3CN (10 mL) was added semi-crystalline $\mathbf{6}\cdot\text{CH}_3\text{CN}$ (0.112 g, 0.107 mmol, 0.5 eq.). The mixture was refluxed for 2 h (temperature *ca.* 90 °C, solution turned from yellow to green), and then filtered through dried Celite® whilst hot to remove any insoluble material (trace palladium black and insoluble $\text{NaNO}_2/\text{NaOAc}$). The title complex precipitated out of solution overnight (left open to air), which was filtered and washed with diethyl ether and then dried *in vacuo* affording a pale yellow solid (78.0 mg, 69%). Mp 204-206 (dec.); ^1H NMR (400 MHz, $\text{DMSO}-d_6$) δ 8.23 (br s, 1H, H-3), 7.85 (s, 1H, H-8), 7.58 (br s, 1H, H-4), 7.44 (s, 1H, H-5), 6.98 (s, 1H, H-5'), 6.91 (s, 1H, H-6'), 4.74 (br s, 2H, CH₂), 4.07 (s, 3H, OCH₃), 3.95 (s, 3H, OCH₃), 3.65 (s, 3H, OCH₃), 3.61 (s, 3H, OCH₃), 2.07 (s, 2H, liberated CH_3CN); ^{13}C NMR (101 MHz, $\text{DMSO}-d_6$, note: weak spectrum – an improved spectrum was recorded in CD_2Cl_2 , see below) δ 158.7, 154.1, 150.9, 146.0, 144.9, 141.4, 133.3, 122.0, 118.1, 111.9, 105.8, 104.9, 56.4, 56.1, 56.0, 55.6, 48.6, 30.7, 1.2 (liberated CH_3CN); ^{13}C NMR (101 MHz, CD_2Cl_2) δ 159.0, 155.5, 152.1, 147.4, 146.3, 142.2, 134.6, 128.4, 123.2, 119.8, 117.2, 111.9, 105.8, 104.6, 56.9, 56.8, 56.7, 55.7, 44.3; IR (KBr) ν cm^{-1} 2970, 2839, 2283, 1619, 1564, 1512, 1484, 1462, 1451, 1424, 1378, 1336, 1273, 1237, 1207, 1160, 1043, 988; LIFDI MS m/z 490.05 [$\text{M}-\text{CH}_3\text{CN}$]⁺, 339.15 (100); Elemental Analysis, Calcd. for $\text{Pd}(\text{C}_{22}\text{H}_{26}\text{N}_3\text{O}_{7.5})$ (found) %: C 47.28 (47.42), H 4.69 (4.35), N 7.52 (7.86) (**note:** the complex is mononuclear and

assigned as $[\text{Pd}(\text{NO}_2)(\text{C}^{\wedge}\text{N})\text{CH}_3\text{CN}] \cdot 1.5\text{H}_2\text{O}$.

Complex 90, $[\text{Pd}(\text{NO}_2)(\text{C}^{\wedge}\text{N})\text{PPh}_3]$

Complex $[\text{Pd}(\text{NO}_2)(\text{C}^{\wedge}\text{N})\text{CH}_3\text{CN}] \cdot 1.5\text{H}_2\text{O}$ (0.035 g, 0.063 mmol) was dissolved in CH_2Cl_2 (10 mL). PPh_3 (16.4 mg, 0.063 mmol, 1 eq.) was then added. The solution was refluxed (40 °C) for 2 h, and then concentrated *in vacuo* to one fifth of its initial volume. Addition of diethyl ether (5 mL) led to product precipitation, which was filtered, washed with diethyl ether (2 x 5 mL) and air-dried (32.3 mg, 68%). Mp 185-187 (decomp.); ^1H NMR (400 MHz, CD_2Cl_2) δ 8.24 (br d, J ca. 5 Hz, 1H), 7.63-7.56 (m, 7H), 7.50-7.45 (m, 3H), 7.41-7.34 (m, 7H), 7.09 (s, 1H), 6.77 (s, 1H), 6.01 (d, J = 4.7 Hz, 1H), 5.01 (d, J = 14.1 Hz, 1H), 4.84 (d, J = 14.1 Hz, 1H), 4.10 (s, 3H), 3.98 (s, 3H), 3.68 (s, 3H), 2.98 (s, 3H); ^{13}C NMR (101 MHz, CD_2Cl_2) δ 158.6 (4°), 155.1 (4°), 151.8 (4°), 146.54 (4°), 146.46 (4° d, J = 4.0 Hz), 141.9 (CH), 137.0 (4°), 135.2 (CH, d, J = 11.5 Hz), 134.7 (4°), 131.3 (CH, d, J = ca. 3 Hz), 131.0 (4° d, J = ca. 45 Hz), 130.8 (4°), 129.0 (CH, d, J = 10.5 Hz), 123.2 (4° d, J = 3.5 Hz), 120.5 (CH, d, J = 12 Hz), 119.3 (CH, d, J = 2.5 Hz), 112.5 (CH), 106.0 (CH), 104.7 (CH), 56.73 (CH_3), 56.7 (2C, CH_3), 55.3 (CH_3), 45.1 (CH_2) {confirmed by DEPT135 experiment}; ^{31}P NMR (162 MHz, CD_2Cl_2) δ (ppm): 32.7 (s, 1P); LIFDI MS m/z 706.22 $[\text{C}_{38}\text{H}_{35}\text{NO}_4\text{PPd}]^+$ (base peak); Elemental Analysis, Calcd. For $\text{C}_{38}\text{H}_{35}\text{N}_2\text{O}_6\text{PdP} \cdot 1.25\text{CH}_2\text{Cl}_2$ (found) %: C 54.86 (54.37), H 4.40 (4.46), N 3.26 (3.35) (**note**: dichloromethane adduct).

Synthesis of COP-catalyst, 91

A flame-dried, single-necked, 250-mL round-bottomed flask was fitted with a stirring bar and an argon-inlet. The flask was evacuated, refilled with argon and then, while temporarily removing the argon inlet, charged with $(\eta^5\text{-}(\text{S})\text{-}2\text{-}(4\text{-methylethyl)oxazolinylcyclopentadienyl})\text{-}(\eta^4\text{-tetraphenylcyclobutadiene})\text{cobalt}$ (0.08 g, 0.135 mmol) and 0.8 mL of glacial acetic acid. Palladium(II) acetate (0.03 g, 0.135 mmol) was then added and the red solution was heated at 95°C. After some time orange precipitate started forming. After 30 mins the solution was cooled to room temperature and filtered to provide an orange solid. Which was then washed with 0.4 mL glacial acetic acid and dried under vacuum to gave the mustrad coloured solid. ^1H NMR (400 MHz, CD_2Cl_2) δ 7.42-7.44 (m, 8H), 7.19-7.29 (m, 14H), 5.13-5.14 (m, 1H), 5.05 (m, 1H), 4.78 (q, J = 2.5 Hz, 1H), 4.70 (q, J = 2.5 Hz, 1H), 3.61 (d, J = 9.5 Hz, 1H), 3.46 (t,

$J = 8.0$ Hz, 1H), 3.37-3.41 (m, 1H), 1.26 (s, 4H), 0.94 (d, $J = 6.6$ Hz, 3H), 0.74 (d, $J = 6.5$ Hz, 3H).²⁶⁷

NMR data(using impure Pd(OAc)₂): The ¹H NMR spectrum was quite complicated (mixture of products).

Cyclopalladation of 2-phenylpyridine, 94

a) Using pure Pd(OAc)₂ (>99%)

A mixture of Pd(OAc)₂ (224 mg, 1 mmol) and 2-phenylpyridine (155 mg, 1 mmol) in acetonitrile (30 ml) was refluxed for 3.5 h with stirring and the resulted dark coloured solution was filtered while hot to remove metallic palladium formed during the reaction. The filtrate was then kept in fridge for precipitation. After a week, yellow precipitate formed. The yellow solid product was filtered, washed with hexane and dried (0.148 g, 46.4%). ¹H NMR (400 MHz, CD₂Cl₂) δ 8.09 (d, $J = 3.5$ Hz, 1H), 7.33-7.36 (m, 1H), 7.23-7.25 (m, 1H), 7.08-7.16 (m, 3H), 6.84-6.88 (m, 2H), 6.69-6.81 (m, 1H), 6.71-6.75 (td, $J = 7.8, 1.6$ Hz, 1H), 6.62 (ddd, $J = 8.5, 4.3, 2.0$ Hz, 1H), 6.44 (d, $J = 8.1$ Hz, 1H), 6.29 (dd, $J = 8, 1.5$ Hz, 1H), 6.20-6.24 (m, 2H), 5.81 (ddd, $J = 7.2, 6, 1.2$ Hz, 1H), 1.65 (s, 3H), 1.42 (s, 3H); HRMS (LIFDI) $[M]^+$ m/z 637.9620 (Calcd. for [Pd₂(C₂₆H₂₂N₂O₄)] 637.9649); Anal. Calcd for [Pd₂(C₂₆H₂₂N₂O₄):C, 48.84; H,3.46; N,4.38. Found: C, 53.67; H, 3.82; N, 4.97.

b) Using impure Pd(OAc)₂ {mixture of Pd₃(OAc)₆ and Pd₃(OAc)₅NO₂}

A mixture of Pd(OAc)₂ (224 mg, 1 mmol) and 2-phenylpyridine (155 mg, 1 mmol) in acetonitrile (30 ml) was refluxed for 3.5 h with stirring and the resulted dark coloured solution was filtered while hot to remove metallic palladium formed during the reaction. The filtrate was then kept in fridge for precipitation. After 2 to 3 weeks, a yellow precipitate formed. The yellow solid product was filtered, washed with hexane and dried (0.113 g, 35.4%). HRMS (LIFDI) $[M]^+$ m/z 637.9683 (Calcd. for [Pd₂(C₂₆H₂₂N₂O₄)] 637.9649); Anal. Calcd for [Pd₂(C₂₆H₂₂N₂O₄):C, 48.84; H,3.46; N,4.38. Found: C, 50.28; H, 3.67; N, 6.30.

5.7.2 X-ray crystallography

5.7.2.1 X-Ray Diffraction Data for compound 90

The programs CrystalClear and APEXII were used for collecting frames, indexing reflections and determination of lattice parameters at Diamond and the ALS respectively, and the program SADABS was used for absorption correction at the ALS while CrystalClear was used to apply absorption corrections for the Diamond synchrotron data. The structures were solved by direct methods using SHELXS-86²⁶⁸ and refined by full-matrix least-squares on F^2 using SHELXL-97.²⁶⁹ In all the structures the ordered non-hydrogen atoms were refined with anisotropic displacement parameters, while disordered atoms were refined with occupancies summed to unity. Hydrogen atoms were placed in idealised positions and allowed to ride on the relevant carbon atoms. Refinements continued until convergence was reached.

Table 4: Details of the photoexcitation experiments with compound 90.

Compound reference	90_GS150K	90_UV150K	90_VT200K
Formula	C ₃₉ H ₃₇ Cl ₂ N ₂ O ₆ PPd	C ₃₉ H ₃₇ Cl ₂ N ₂ O ₆ PPd	C ₃₉ H ₃₇ Cl ₂ N ₂ O ₆ PPd
Formula weight	837.98	837.98	837.98
Cryst syst	Monoclinic	Monoclinic	Monoclinic
a(Å)	10.7223(5)	10.7119(4)	10.7245(5)
b(Å)	21.7779(13)	21.7420(12)	21.8948(15)
c(Å)	16.3387(7)	16.4105(6)	16.3488(8)
A(°)	90.00	90.00	90.00
B(°)	105.321(4)	105.404(4)	105.251(5)
Γ(°)	90.00	90.00	90.00
V (Å ³)	3679.6(3)	3684.7(3)	3703.7(4)
Temp (K)	150(2)	150(2)	190(2)
Space group	<i>P2(1)/c</i>	<i>P2(1)/c</i>	<i>P2(1)/c</i>
No. of formula units per unit cell, <i>Z</i>	4	4	4
Absorption coefficient, μ/mm ⁻¹	0.743	0.742	0.738
No. of reflections measured	41375	40979	41224
No. of independent reflections	11231	11231	11279
<i>R</i> _{int}	0.0398	0.0380	0.0526
Final <i>R</i> _I values (<i>I</i> > 2σ(<i>I</i>))	0.0340	0.0328	0.0417
Final <i>wR</i> (<i>F</i> ²) values (<i>I</i> > 2σ(<i>I</i>))	0.0789	0.0771	0.1001
Final <i>R</i> _I values (all data)	0.0429	0.0407	0.0546
Final <i>wR</i> (<i>F</i> ²) values (all data)	0.0836	0.0814	0.1092
Goodness of fit on <i>F</i> ²	1.044	1.046	0.949

Table 5: Details of the slow cool experiments with compound 90.

Compound reference	298K	250K	200K	150K
Formula	C ₃₉ H ₃₇ Cl ₂ N ₂ O ₆ PPd	C ₃₉ H ₃₇ Cl ₂ N ₂ O ₆ P Pd	C ₃₉ H ₃₇ Cl ₂ N ₂ O ₆ P Pd	C ₃₉ H ₃₇ Cl ₂ N ₂ O ₆ PPd
Formula weight	837.98	837.98	837.98	837.98
Cryst syst	Monoclinic	Monoclinic	Monoclinic	Monoclinic
a(Å)	10.786(8)	10.7248(5)	10.7075(7)	10.6878(7)
b(Å)	22.362(17)	22.0346(11)	21.8698(14)	21.7334(14)
c(Å)	16.405(12)	16.3099(8)	16.3273(10)	16.3349(10)
A(°)	90.00	90.00	90.00	90.00
B(°)	104.945(9)	105.1660(10)	105.3090(10)	105.4190(10)
Γ(°)	90.00	90.00	90.00	90.00
V (Å³)	3823(5)	3720.1(3)	3687.7(4)	3657.7(4)
Temp (K)	298(2)	250(2)	200(2)	150(2)
Space group	<i>P2(1)/c</i>	<i>P2(1)/c</i>	<i>P2(1)/c</i>	<i>P2(1)/c</i>
No. of formula units per unit cell, <i>Z</i>	4	4	4	4
Absorption coefficient, μ/mm^{-1}	0.715	0.735	0.741	0.747
No. of reflections measured	38082	39374	38982	39140
No. of independent reflections	11705	11236	11142	11046
<i>R</i>_{int}	0.0518	0.0560	0.0576	0.0793
Final <i>R</i>_I values (<i>I</i> > 2σ(<i>I</i>))	0.0465	0.0454	0.0455	0.0472
Final <i>wR</i>(<i>F</i>²) values (<i>I</i> > 2σ(<i>I</i>))	0.1399	0.1312	0.1341	0.1207
Final <i>R</i>_I values (all data)	0.0618	0.0606	0.0572	0.0563
Final <i>wR</i>(<i>F</i>²) values (all data)	0.1521	0.1408	0.1422	0.1262
Goodness of fit on <i>F</i>²	1.004	0.988	1.006	1.071

5.7.2.2 Crystallographic data for compounds analysed and solved in York

Diffraction data for complex **86**.(CH₃CN) and **87**.(DMSO) are given in Table 6 whereas for [Pd(OAc)(C[^]N)PPh₃] complex **89** and the unexpected [Pd(*N*-Hpap)₂(NO₂)₂] complex **88** are given in Table 7. The diffraction data for [Pd(NO₂)(C[^]N)PPh₃] complex **90** and cyclopalladated 2-phenylpyridine **94** is given in Table 8. The data was collected at 110 K on a Bruker Smart Apex diffractometer with Mo-K_α radiation ($\lambda = 0.71073 \text{ \AA}$) using a SMART CCD camera. Diffractometer control, data collection and initial unit cell determination was performed using “SMART”.¹ Frame integration and unit-cell refinement was carried out with “SAINT+”.¹ Absorption corrections were applied by SADABS.¹ Structures were solved by “direct methods” using SHELXS-97 (Sheldrick, 1997)¹ and refined by full-matrix least squares using SHELXL-97 (Sheldrick, 1997).¹

Table 6: Single crystal X-Ray details for complex (86-CH₃CN) and (87-DMSO).

Compound reference	ijfl1020m (86.CH₃CN)	ijssf1109 (87.DMSO)
Formula	C ₄₄ H ₄₆ N ₂ O ₁₂ Pd ₂ ·3(C ₂ H ₃ N)	C ₄₄ H ₄₂ N ₂ O ₁₄ Pd ₂ ·2(C ₂ H ₆ OS)
Formula weight	1130.79	1191.85
temp (K)	110(2)	110.0
Cryst syst	Triclinic	Monoclinic
Space group	P-1	P2 ₁ /c
a(Å)	11.1250(17)	13.3081(5)
b(Å)	15.392(2)	26.2365(10)
c(Å)	15.758(2)	14.0067(6)
α(°)	74.695(3)	90.00
β(°)	77.903(3)	99.483(4)
γ(°)	70.463(3)	90.00
V (Å³)	2430.9(6)	4823.7(3)
Z	2	4
D_{calcd.} (Mg M⁻³)	1.545	1.641
F(000)	1156	2432
M(mm⁻¹)	0.808	0.906
Crystal size (mm³)	0.22 × 0.19 × 0.09	0.165 × 0.132 × 0.032
θ range for data	1.75 to 28.31	6.08 to 61.24
Collection (°)	-14 ≤ h ≤ 14,	-18 ≤ h ≤ 18,
Index ranges	-20 ≤ k ≤ 20,	-37 ≤ k ≤ 37,
	-20 ≤ l ≤ 21	-20 ≤ l ≤ 19
No. of rflns collected	24776	20629
Refinement method	Full-matrix least-squares on F ²	Full-matrix least-squares on F ²
GOOF on F²	1.045	0.884
R1, wR2(I > 2σ(I))	R1 = 0.0387, wR2 = 0.0932	R1 = 0.0381, wR2 = 0.0708
R1, wR2(all data)	R1 = 0.0507, wR2 = 0.0993	R1 = 0.0644, wR2 = 0.0755

Table 7: Single crystal X-Ray details for complex [Pd(OAc)(C[^]N)PPh₃] (89) and [Pd(*N*-Hpap)₂(NO₂)₂] (88).

Compound reference	ijf1042 (89)	ijsf1110 (88)
Formula	C ₄₀ H ₃₈ NO ₆ PPd·CH ₂ Cl ₂	C ₃₈ H ₄₂ N ₆ O ₁₂ Pd·2(C ₂ H ₃ N)
Formula weight	851.01	959.28
temp (K)	110.15	109.9
Cryst syst	Monoclinic	Triclinic
Space group	C2/c	P-1
a(Å)	47.4181(14)	8.4350(6)
b(Å)	11.0136(3)	10.2678(5)
c(Å)	17.7382(6)	13.5105(7)
α(°)	90.00	77.953(4)
β(°)	107.608	76.502(5)
γ(°)	90.00	72.666(5)
V(Å ³)	8829.7(5)	1073.86(11)
Z	8	1
D _{calcd.} (Mg M ⁻³)	1.280	1.483
F(000)	3488	496
M(mm ⁻¹)	0.619	0.503
Crystal size (mm ³)	0.336 × 0.2842 × 0.2773	0.1827 × 0.1176 × 0.042
θ range for data	5.84 to 50.22	6.28 to 64.16
Collection (°) Index ranges	-56 ≤ h ≤ 56, -13 ≤ k ≤ 13, -21 ≤ l ≤ 21	-12 ≤ h ≤ 12, -15 ≤ k ≤ 15, -20 ≤ l ≤ 20
No. of rflns collected	42881	16535
Refinement method	Full-matrix least-squares on F ²	Full-matrix least-squares on F ²
GOOF on F ²	1.095	1.060
R1, wR2(I>2σ(I))	R1= 0.0373, wR2= 0.1018	R1= 0.0345, wR2= 0.0839
R1, wR2(all data)	R1= 0.0407, wR2= 0.1038	R1= 0.0377, wR2= 0.0861

Table 8: Single crystal X-Ray details for complex 90 and 94.

Compound reference	ijf1039 (90)	ijf1021 (94)
Formula	C ₃₉ H ₃₇ Cl ₂ N ₂ O ₆ PPd	C ₂₆ H ₂₂ N ₂ O ₄ Pd ₂
Formula weight	837.98	639.26
temp (K)	110.0	110.0
Cryst syst	monoclinic	monoclinic
Space group	P2 ₁ /c	P2 ₁ /c
a(Å)	10.66940(17)	9.8702(3)
b(Å)	21.6101(3)	13.0105(5)
c(Å)	16.3379(3)	17.5786(6)
α(°)	90.00	90.00
β(°)	105.5155(17)	94.524(3)
γ(°)	90.00	90.00
V (Å³)	3629.69(10)	2250.35(13)
Z	4	4
D_{calcd.} (Mg M⁻³)	1.533	1.887
F(000)	1712	1264
M(mm⁻¹)	0.753	1.636
Crystal size (mm³)	0.2413 × 0.1145 × 0.114	0.1414 × 0.0734 × 0.0509
θ range for data	6.22 to 54.96	2.9041 to 49.9998
Collection (°)	-13 ≤ h ≤ 13,	-11 ≤ h ≤ 11,
Index ranges	-28 ≤ k ≤ 15, -21 ≤ l ≤ 21	-15 ≤ k ≤ 15, -20 ≤ l ≤ 20
No. of rflns collected	15420	22605
Refinement method	Full-matrix least-squares on F ²	Full-matrix least-squares on F ²
GOOF on F²	1.059	1.101
R1, wR2(I>2σ(I))	R ₁ = 0.0315, wR ₂ = 0.0725	R ₁ = 0.0357, wR ₂ = 0.0575
R1, wR2(all data)	R ₁ = 0.0378, wR ₂ = 0.0769	R ₁ = 0.0466, wR ₂ = 0.0606

Chapter 6: Conclusions

The principal aim of this project was to synthesise novel bidentate alkene phosphine ligands and phosphine sulfide ligands, based on a ferrocenyl-chalcone ligand framework, which would allow their metal coordination study and use in homogenous catalysis. Previously, considerable work has been done individually on alkene and phosphine ligands; very little is known about ligands involving both alkene and phosphine moiety within the same ligand, especially in coordination chemistry studies.

The project detailed in this thesis involved the synthesis of bidentate phosphino-alkene and phosphine sulfide ligand with a chalcone backbone, which contains one enone moiety (unlike dba which is a 1,4-dien-3-one). The synthesis of β -biaryl acryl ferrocene is relatively straight-forward and was accomplished by a Claisen-Schmidt condensation reaction. The target ligands, ferrochalcone **32** and thio-ferrochalcone **33**, were synthesised from acetyl ferrocene **35** and 2-(diphenylphosphino)benzaldehyde **39** or 2-(diphenylthiophosphino)-benzaldehyde **40** in good yield. The thio-variant of the Lei ligand (**17**) has been reported previously. The structure of both **32** and thio-Lei ligand **46** was confirmed by XRD studies.

Following the successful synthesis of these novel ligands, in the next step the metal coordination studies of these ligands were conducted using transition metals such as Pt, Pd, Rh, Cu and Au. A comparison of the metal complexes of the chalcone ferrocene ligand **32** with metal complexes of Lei ligand **17** was also performed. The plan was to use these ligands for catalysis so a detailed study of the metal coordination behaviour of these ligands was deemed necessary. We were encouraged by discussions with Prof. Aiwen Lei (when he visited York in 2009), who was keen to see further coordination studies on his and related ligands pursued.

The Pd^{II} complex for the ferrochalcone ligand **32** was first synthesised. The NMR spectroscopic analysis confirmed that only the phosphine moiety was interacting with the metal and that there was no Pd^{II}-alkene interaction. The product crashes out of solution instantaneously; solubility was a continuing problem for this complex, and is best explained by extensive polymerisation.

Pt^{II} and Pt⁰ complexes were synthesised for both ferrochalcone **32** and Lei ligand **17**. For the Pt^{II} complexes the NMR spectroscopic analysis showed that the phosphorus was interacting with Pt^{II}, but as with Pd^{II} there was no evidence of a Pt^{II}-alkene interaction. However, the XRD analysis showed that the Pt^{II} complexes acted as a bidentate ligand binding through both alkene and phosphine moieties. It appears in both Pd^{II} and Pt^{II} complexes, that the M^{II}Cl₂(P)₂ complexes are kinetically preferred, whereas the M^{II}Cl₂(P, η^2 -alkene) are thermodynamically more stable. Similarly, Pt⁰ metal complexes were obtained for both the chalcone ferrocene ligand **32** and Lei ligand **17**. Reaction of Pt⁰(dba)₂ with ferrochalcone **32** in benzene gave a novel Pt⁰ species, namely Pt⁰(P, η^2 -alkene)₂. The crystallisation of the solid material in benzene gave light red crystals. The XRD studies showed that each of the two molecules of the ligand were both P and π -alkene bound to Pt⁰. Interestingly, the metal coordination by the two P atoms and two π -alkenic bonds is intermediate between square-planar and tetrahedral. The Pt⁰ metal complex for the Lei ligand **17** was obtained by reaction with Pt⁰(PPh₃)₂(η^2 -C₂H₄), which gave a product, Pt⁰(P, η^2 -alkene)₂, confirmed by NMR spectroscopic and mass spectrometric analysis and XRD studies. The crystal structure exhibited a geometry which is intermediate between square-planar and tetrahedral.

Coordination studies with rhodium were also conducted. Most of the rhodium complexes (all Rh^I) were found to be air-sensitive, and reactions needed to be conducted in the glove box. The Rh^I complex for the ferrochalcone ligand **32** was obtained by a reaction of the ligand with [Rh(cod)Cl]₂ in THF in a ligand to metal ratio of 2:1. The complex was analysed by NMR spectroscopy. The ³¹P NMR spectrum exhibited two sets of signals which were found as a doublet of doublets. The coupling constant values showed that the Rh^I was bonded to two different phosphorus atoms giving rise to an AB system. Other phosphorous species (downfield) were also observed by ³¹P NMR spectroscopy. An X-ray structure determination revealed [Rh₂(ferrochalcone ligand)₂] **57b**, where the Rh^I was bonded to two bridging ligands. The ligand spans two Rh^I centres by P, alkene-coordination to one Rh and then carbonyl *O*-coordination to the other Rh^I atom. The X-ray structure shows that ferrochalcone **32** acts as a tridentate ligand. The Rh^I complex exhibits a distorted square-planar geometry. A comparative study was conducted using Lei ligand **17**. Interestingly, the Rh^I complex is stable in air and the reaction was conducted outside the glove box (in the absence of light). The successful synthesis of the Rh^I complex of **17** was confirmed by NMR and IR

spectroscopic, and mass spectrometric studies. The singlet peak at δ -13.0 (^{31}P NMR) in the ligand had shifted to give a pair of doublet of doublets, akin to the Rh^{I} complex of ferrochalcone **32**. Interestingly, other phosphorus species were minimal for ligand **17**. The yellow product obtained was crystallised from dichloromethane giving fine yellow needles. The Rh^{I} metal was found to be coordinated to two ligands of **17**. The metal was found to be coordinated by two P atoms and two alkenic bonds.

Copper was shown to show interesting coordination behaviour toward the thiophosphine ligands. Cu^{I} complexes for ferrochalcone **32** were formed by reacting the ligand with $[\text{Cu}(\text{MeCN})_4]\text{PF}_6$ and $[\text{CuCl}]$. The structure of the complex was analysed by NMR and mass spectrometric techniques. Similarly, the Cu^{I} complex for thioferrochalcone **33** was obtained by similar reactions. Comparison of the NMR spectra for the free ligand with the complexed ligand revealed the clean formation of a Cu^{I} complex in both cases. The structure of the Cu^{I} complex was analysed by X-ray diffraction studies and found to have a trigonal-planar geometry. The ligand **33** acted as a bidentate ligand, binding through both the sulphur and the alkene moiety. The same reaction was repeated for the Lei ligand **17**, allowing a comparative study of their metal coordination behaviour. Reaction of the Lei ligand **17** with $[\text{Cu}(\text{MeCN})_4]\text{PF}_6$ in a ligand to metal ratio of 2:1, gave a cationic $[\text{Cu}^{\text{I}}(\text{P})_2\text{CH}_3\text{CN}]\text{PF}_6$ complex. Whereas, reaction of CuCl with **17** in a metal/ligand ratio of 1:1 gave a neutral $\text{Cu}^{\text{I}}(\text{P},\eta^2\text{-alkene})\text{Cl}$ complex. The formation of Cu^{I} complexes was confirmed by NMR and IR spectroscopic and mass spectrometric analysis.

The Au^{I} complexes containing the alkene-phosphine ligands were synthesised and characterised. Ferrochalcone gold(I) chloride complex **70** was synthesised. The X-ray structure of a single crystal shows that the ferrochalcone **32** acts as a monodentate ligand binding through the phosphorus moiety only and there is no evidence for a Au^{II} -alkene interaction. The complex showed a linear geometry. The same reaction was repeated for the Lei ligand **17**. The LIFDI mass spectrum for complex **71** showed a peak at m/z 624.05 corresponding to $[\text{Au}(\text{C}_{27}\text{H}_{21}\text{PO})\text{Cl}]^+$. The crystals were analysed by XRD analysis. Surprisingly a [2+2] cycloaddition product was also found to have formed. A 70:30 ratio of the dimer:monomer, respectively, was determined. A Au^{I} complex containing monodba-thiophos was also synthesised from the same metal precursor. It is worthy of note that the [2+2] cycloaddition reaction occurred on the most hindered

alkene. The presence of a mixture of compounds in the crystal suggested that a photochemical [$\pi 2s + \pi 2s$] reaction was occurring in the solid-state.

One of the aims of this project was to design and synthesise a new ligand and to use it in catalysis. The reactivity of Au^I complexes of these ligands were evaluated as catalysts for the cycloisomerisation of 4-phenyl-1-hexen-5-yne, and some interesting results obtained.

Cyclic voltammetric studies on both ferrochalcone **32** and ferrochalcone Au^I complex **70** were conducted. The cyclic voltammogram displayed a quasi-reversible ferrocene-based oxidation, between 0.30 - 0.40 V (*i.e.* harder to oxidise than ferrocene itself). There was also an irreversible vinyl-ketone based-reduction (chemical). However, the Au^I complex **70** exhibited a reversible cycle at $E_{1/2} = 0.32$ V, corresponding to the redox process of the ferrocenyl unit and an anodic peak (E_{pa}) value of -1.12 V.

An important part of this project, although providing a completely different direction, was to investigate the purity of palladium(II) acetate, Pd(OAc)₂, and its employment in stoichiometric cyclopalladation reactions. It goes back to the work reported by Nonoyama on the cyclopalladation of papaverine using Pd(OAc)₂ where they observed a nitro-palladated product on reacting papaverine with Pd(OAc)₂ in the presence of acetonitrile and air. The cyclopalladation reactions were conducted under various conditions. In this project none of the nitro-palladated product was obtained using ultra pure Pd(OAc)₂. Instead, a novel palladium-dimer **86**, with bridging acetate ligands, was obtained from CH₃CN. When crystallised from DMSO, a Pd^{II}-dimer with an oxidised methylene was obtained (**87**). A novel Pd^{II}-nitrito complex **90** was also observed exhibiting linkage isomerisation (by photoexcitation).

Overall, this project has led to the successful synthesis of a new class of phosphino-alkene ligands and their phosphine sulfide variants. Extensive coordination studies show that the ligands act as hemilabile bidentate ligands. The Au^I complexes have been successfully used in catalysis. A number of findings require further research, especially Pd, Pt and Rh mediated reactions. What is clear is that the chalcone phosphine ligands exhibit a range of coordination modes to transition metal centres, which could be exploited in various catalytic processes (*e.g.* cross-coupling, hydroformylation, 1,4-conjugate addition reactions *etc.*).

References for Chapter 1

- ¹ Helldorfer, M.; Backhaus, J.; Alt, H. G. *Inorg. Chim. Acta* **2003**, *351*, 34.
- ² Fischer, C.; Defieber, C.; Carreira, E. M.; Suzuki, T. *J. Am. Chem. Soc.* **2004**, *126*, 1628.
- ³ Glorius, F. *Angew. Chem. Int. Ed.* **2004**, *43*, 3364.
- ⁴ Shul'pin, G. B. *J. Mol. Catal. A.* **2002**, *189*, 3911.
- ⁵ (a) Wender, P. M.; *Chem. Rev.* **1996**, *96*, 1. (b) Trost, B. M.; *Science.* **1991**, *254*, 1471.
- ⁶ Pearson, R. G. *J. Am. Chem. Soc.* **1963**, *85*, 3533.
- ⁷ Heck, R. F.; Nolley, J. P. *J. Am. Chem. Soc.* **1968**, *90*, 5518.
- ⁸ Negishi, E. I.; Baba, S. *J. Chem. Soc. Chem. Commun.* **1976**, 596.
- ⁹ Milstein, D.; Stille, J. *J. Am. Chem. Soc.* **1978**, *1000*, 3636.
- ¹⁰ Miyaura, N.; Suzuki, A. *Chem. Rev.* **1995**, *95*, 2457.
- ¹¹ Sonagashira, K.; Tohda, Y.; Hagihara, N. *Tetrahedron Lett.* **1975**, 4467.
- ¹² Keiji, M. *Nippon Kagakkai Koen Yokoshu* **1999**, *76*, 960
- ¹³ For a comprehensive review of NHCs: Kantchev, E. A. B.; O'Brien, C. J.; Organ, M. G. *Angew. Chem. Int. Ed.* **2007**, *46*, 2768.
- ¹⁴ Hermes, A-R.; Girolami, G. S. *Inorg. Chem.* **1988**, *27*, 10.

-
- ¹⁵ Pignolet, L. H. *Homogenous catalysis with Metal Phosphine Complexes*; Plenum: New York, **1983**.
- ¹⁶ a) Hofmann, A. W. *Ann. Chem. Pharm.* **1857**, *104*, 1. b) Malerbi, B. W. *Platinum Metal Rev.* **1965**, *9*, 47.
- ¹⁷ Tolman, C. A.; Seidel, W. C.; Gosser, L. W. *J. Am. Chem. Soc.* **1996**, *118*, 53.
- ¹⁸ a) Lever, A. B. P. *Inorg. Chem.* **1990**, *29*, 1271. (b) Perrin, L.; Clot, E.; Eisenstein, O.; Loch, J.; Crabtree, R. H. *Inorg. Chem.* **2001**, *40*, 5806.
- ¹⁹ Tolman, C. A. *Chem. Rev.* **1997**, *77*, 313.
- ²⁰ Astruc, D. *Organometallic Chemistry and Catalysis*, Springer, **2007**, 608.
- ²¹ Schlummer, B.; Scholz, U. *Adv. Synth. Catal.* **2004**, *346*, 1599.
- ²² Barder, T. E.; Walker, S. D.; Martinelli, J. R.; Buchwald, S. L. *J. Am. Chem. Soc.* **2005**, *127*, 4685.
- ²³ Hamze, A.; Provot, O.; Alami, M.; Brion, J. D. *J. Organomet. Chem.* **2008**, *693*, 2789.
- ²⁴ Kranenburg, M.; van der Burgt, Y. E. M.; Kamer, P. C. J.; van Leeuwen, P. W. N. M. *Organometallics* **1995**, *14*, 3081.
- ²⁵ Rovis, T.; Johnson, J. B. *Angew. Chem. Int. Ed.* **2008**, *47*, 840.
- ²⁶ Fairlamb, I. J. S.; Kapdi, A. R.; Lee, A. F. *Org. Lett.* **2004**, *6*, 4435.
- ²⁷ Fairlamb, I. J. S. *Org. Biomol. Chem.* **2008**, *6*, 3645.

-
- 28 Kurosawa, H.; Kajimaru, H.; Ogoshi, S.; Yoneda, H.; Ikeda, I. *J. Am. Chem. Soc.* **1971**, *93*, 3350.
- 29 Zenkina, O. V.; Karton, A.; Shimon, L. J. W.; Martin, J. M. L.; van der Boom, M. *E. Chem. Eur. J.* **2009**, *15*, 10025.
- 30 Tromp, D. S.; Tooke, D. M.; Spek, A. L.; Deelman, B.-J.; Elsevier, C. J. *Organometallics* **2005**, *24*, 6411.
- 31 Johnson, J. B.; Rovis, T. *Angew. Chem., Int. Ed.* **2008**, *47*, 840.
- 32 Firmansjah, L.; Fu, G. *J. Am. Chem. Soc.* **2007**, *129*, 11340.
- 33 Zeise, W. C. *Mag. Pharm.* **1830**, *35*, 105.
- 34 For general introductions and leading references, see:(a) Hartley, F. R. *Chem. Rev.* **1969**, *69*, 799. (b) Tshipis, C. A. *Coord. Chem. Rev.* **1991**, *08*, 63. (c) Crabtree, R. H. *The Organometallic Chemistry of the Transition Metals*, Wiley, New York, **2003**.
- 35 Hunt, L. B. *Platinum Metals Rev.* **1984**, *28*, 76.
- 36 a) Wunderlich, J. A.; Mellor, D. P.; *Acta Crystallogr.* **1954**, *7*, 130. (b) Wunderlich, J. A.; Mellor, D. P.; *Acta Crystallogr.* **1955**, *8*, 57.
- 37 a) Dewar, M. J. S. *Bull. Soc. Chim. Fr.* **1951**, *18*, 79. (b) Chatt, J.; Duncanson, L. *A. J. Chem. Soc.* **1953**, 2929.
- 38 Ozawa, F.; Ito, T.; Nakamura, Y.; Tamamoto, A. *J. Organomet. Chem.* **1979**, *168*, 375.
- 39 Nakamoto, K. *Infrared and Raman Spectra of Inorganic and Coordination*

Compounds, Part B: Applications in Coordination, Organometallic, and Bioinorganic Chemistry; Wiley-Blackwell: Chichester, **2009**.

- 40 Jeffrey, J. C.; Rauchfuss, T. B. *Inorg. Chem.* **1979**, *18*, 2658.
- 41 Slone, C. S.; Weinberger, D. A.; Mirkin, C. A. *Inorg. Chem.* **1999**, *48*, 233.
- 42 Bennett, M. A.; Kouwenhoven, H. W.; Lewis, J.; Nyholm, R. S. *J. Chem. Soc.* **1964**, 4570.
- 43 a) Maire, P.; Deblon, S.; Breher, F.; Geier, J.; Bohler, C.; Ruegger, H.; Schonberg, H.; Grutzmacher, H. *Chem. Eur. J.* **2004**, *10*, 4198. b) Fischbach, U.; Ruegger, H.; Grutzmacher, H. *Eur. J. Inorg. Chem.* **2007**, 2654.
- 44 Defieber, C.; Ariger, M. A.; Moriel, P.; Carreira, E. M. *Angew. Chem. Int. Ed.* **2007**, *46*, 3139.
- 45 Tokunaga, N.; Otomaru, Y.; Okamoto, K.; Ueyama, K.; Shintani, R.; Hayashi, T. *J. Am. Chem. Soc.* **2004**, *126*, 13584.
- 46 Kasak, P.; Arion, V. B.; Widhalm, M. *Tetrahedron:Asymmetry* **2006**, *17*, 3084.
- 47 Lewis, J. C.; Berman, A. M.; Bergman, R. G.; Ellman, J. A. *J. Am. Chem. Soc.* **2008**, *130*, 2493.
- 48 Luo, X.; Zhang, H.; Duan, H.; Liu, Q.; Zhu, L.; Zhang, T.; Lei, A. *Org. Lett.* **2007**, *6*, 4571.
- 49 Williams, D. B. G.; Shaw, M. L. *Tetrahedron* **2007**, *63*, 1624.
- 50 a) Luo, X.; Zhang, H.; Duan, H.; Liu, Q.; Zhang, T.; Lei, A. *Org. Lett.* **2007**, *9*, 4571.
b) Zhang, H.; Luo, X.; Wongkhan, K.; Duan, H.; Li, Q.; Zhu, L.; Wang, J.;

-
- Batsanov, A. S.; Howard, J. A. K.; Marder, T. B.; Lei, A. *Chem. Eur. J.* **2009**, *15*, 3823.
- ⁵¹ Cao, Z.; Liu, Z.; Liu, Y.; Du, H. *J. Org. Chem.* **2011**, *76*, 6401.
- ⁵² Du, H.; Cao, Z.; Liu, Z.; Feng, X.; Zhuang, M. *Org. Lett.* **2011**, *13*, 2164.
- ⁵³ Shintani, R.; Duan, W-L.; Okamoto, K.; Hayashi, T. *Tetrahedron: Asymmetry* **2005**, *16*, 3400.
- ⁵⁴ a) Hashmi, A. S. K. *Angew. Chem. Int. Ed.* **2005**, *44*, 6990. b) Zhang, L. *et al. Adv. Synth. Catal.* **2006**, *348*, 2271.
- ⁵⁵ a) Bruneau, C. *Angew. Chem. Int. Ed.* **2005**, *44*, 2328. b) Gorin, D. J.; Toste, F. D. *Nature* **2007**, *446*, 395.
- ⁵⁶ a) Li, Z.; Brouwer, C.; He, C. *Chem. Rev.* 2008, *108*, 3239. b) Hashmi, A. S. K.; Hutchings, G. *J. Angew. Chem. Int. Ed.* **2006**, *45*, 7896.
- ⁵⁷ Yamamoto, Y.; Nishina, N. *Synlett.* **2007**, *11*, 1767.
- ⁵⁸ Shibata, T.; Ueno, Y.; Kanda, K. *Synlett.* **2006**, 411.
- ⁵⁹ Echavarren, A. M.; Wang, Y.; Alvarado, C. R. S. *J. Am. Chem. Soc.* **2011**, *133*, 11952.
- ⁶⁰ a) Alexakis, A.; Albrow, V.; Biswas, K.; d'Augustin, M.; Prieto, O.; Woodward, S. *Chem. Commun.* **2005**, 2843-2845. b) Alexakis, A.; Benhaim, C. *Eur. J. Org. Chem.* **2002**, 3221.
- ⁶¹ Zhu, L.; Li, G.; Luo, L.; Guo, P.; Lan, J.; You, J. *J. Org. Chem.* **2009**, *74*, 2200.

-
- ⁶² Noh, D.; Chea, H.; Ju, J.; Yun, J. *Angew. Chem., Int. Ed.* **2009**, *48*, 6062.
- ⁶³ a) Burke, A. J.; Carreiro, E. d. P.; Chercheja, S.; Moura, N. M. M.; Ramalho, J. P. P.; Rodrigues, A. I.; dos Santos, C. I. M. *J. Organomet. Chem.* **2007**, *692*, 4863. b) Eggers, F.; Luning, U. *Eur. J. Org. Chem.* **2009**, 2328.
- ⁶⁴ De Ornellas, S.; Storr, T. E.; Williams, T. J.; Baumann, C. G.; Fairlamb, I. J. S. *Curr. Org. Synth.* **2011**, *8*, 79.
- ⁶⁵ Kaddouri, H.; Vicente, V.; Ouali, A.; Ouazzani, F.; Taillefer, M. *Angew. Chem., Int. Ed.* **2009**, *48*, 333.
- ⁶⁶ Drinkel, E.; Briceño, A.; Dorta, R.; Dorta, R. *Organometallics* **2010**, *29*, 2503.
- ⁶⁷ Fairlamb, I. J. S.; Jarvis, A. G.; Whitwood, A. C. *Dalton Trans.* **2011**, *40*, 3695.
- ⁶⁸ Ferrer, C.; Benet-Buchholz, J.; Riera, A.; Verdaguer, X. *Chem. Eur. J.* **2010**, *16*, 8340.
- ⁶⁹ Hayashi, T.; Togni, A. *Ferrocenes, Homogenous Catalysis, Organic Synthesis and Materials Science*, ed. VCH, Weinheim, Germany, **1995**.
- ⁷⁰ Halterman, R. L.; Togni, A. *Metallocenes*, ed. VCH, Weinheim, Germany, **1998**.
- ⁷¹ Long, N. J. *Metallocenes, An introduction to Sandwich Complexes*, Blackwell Science, Oxford, UK, **1998**.
- ⁷² Pauson, P. L. *Organomet. Chem.* **2001**, *3*, 637.
- ⁷³ Dombrowski, K. E.; Baldwin, W.; Sheats, J. E. *J. Organomet. Chem.* **1986**, *302*, 281.

-
- ⁷⁴ Connelly, N. G.; Geiger, W. E. *Chemical Redox Agents for Organometallic Chemistry*. *Chemical Reviews*. **1996**, *96*, 877.
- ⁷⁵ Hembre, R. T.; McQueen, J. S. *Angew. Chem., Int. Ed.* **1997**, *109*, 79.
- ⁷⁶ Dyson, P. J.; Sava, G. *Dalton Trans.* **2006**, 1929.
- ⁷⁷ Huxham, L. A.; Cheu, E. L. S.; Patrick, B. O. *Inorg. Chim. Acta.* **2003**, *352*, 238.
- ⁷⁸ Prokop, A.; Jesse, P.; Kater, L.; Hunlod, A.; Kater, B. *J. Cancer. Res. Clin. Oncol.* **2011**, *137*, 639.
- ⁷⁹ Meunier, P.; Ouattara, I.; Gautheron, B.; Tirouflet, J.; Camboli, D.; Besancon, J. *Eur. J. Med. Chem.* **1991**, *26*, 351.
- ⁸⁰ Top, S.; Tang, J.; Vessieres, A.; Carrez, D.; Provot, C.; Jaouen, G. *Chem. Commun.* **1996**, 955.
- ⁸¹ Dori, Z.; Gershon, D.; Scharf, Y. Demande FR, 2, 598, 616 (Cl. A61K31/12), 20 Nov. **1987**, US Appl. 862, 804, 13 May **1986**, p. 13.
- ⁸² Koepf-Maier, P.; Koepf, H. Neuse EW. *Angew. Chem., Int. Ed.* **1984**, *23*, 456.
- ⁸³ Koepf-Maier, P.; Koepf, H. *Drugs Future* **1986**, *11*, 297.
- ⁸⁴ Biot, C.; Francois, N.; Maciejewski, L.; Brocard, J.; Poulain, D. *Med. Chem. Lett.* **2000**, *10*, 839.
- ⁸⁵ Itoh, T.; Shirakami, S.; Ishida, N.; Yamashita, Y.; Yoshida, T.; Kim, H-S.; Wataya, Y. *Bioorg. Med. Chem. Lett.* **2000**, *10*, 839.

-
- 86 Baldoli, C.; Maiorana, S.; Licandro, E.; Zinzalla, G.; Perdicchia, D. *Org. Lett.* **2002**, *4*, 4341.
- 87 Haque, M. E.; Hossen, M. F.; Pervin, M. M.; Hassan, P.; Khalekuzzaman, M. *J. App. Sci.* **2006**, *6*, 988.
- 88 Hayashi, T in *Ferrocenes. Homogenous Catalysis, Organic Synthesis, Materials Science* (Eds.: Togni, A.; Hayashi, T), VCH, Weinheim. **1995**, 105.
- 89 Kagan, H. B.; Riant, O. *Adv. Asymmetric. Synth.* **1997**, *2*, 189.
- 90 Richards, C. F.; Lock, A. J. *Tetrahedron: Asymmetry* **1998**, *9*, 2377.
- 91 Togni, A in *Metalloenes* (Eds.: Togni, A.; Halterman, R, L) Wiley, New York. **1998**, 685.
- 92 Santelli, M.; Laurenti, D. *Org. Prep. Proced. Int.* **1999**, *31*, 245.
- 93 Dai, L. X.; Tu, T.; Deng, W. P.; Hou, X. L. *Acc. Chem. Res.* **2003**, *36*, 659.
- 94 Fache, F.; Schulz, E.; Tommasino, M. L.; Lemaire, M. *Chem. Rev.* **2000**, *100*, 2159.
- 95 McManus, H. A.; Guiry, P. *J. Chem. Rev.* **2004**, *104*, 4151.
- 96 Breuer, M.; Ditrach, K.; Habicher, T.; Kebeler, M.; Zelinski, T. *Angew. Chem.* **2004**, *43*, 788.
- 97 Hansen, K. B.; Rosner, T.; Kubryk, M.; Domer, P. G. *Org. Lett.* **2005**, *7*, 4935.
- 98 Lu, S. M.; Han, X. W.; Zhou, Y. G. *Adv. Synth. Catal.* **2004**, *346*, 909.

-
- ⁹⁹ Dyson, P.; Hartinger, C. G. *J. Chem. Soc. Rev.* **2009**, 38, 391.
- ¹⁰⁰ Metzler-Nolte, N.; Salmain, T. In *Ferrocenes Ligand, Materials and Biomolecules*; Ed.; Wiley: West Sussex. **2008**, 499.
- ¹⁰¹ Wu, X.; Wilairat, P.; Go, M. L. *Bioorg. Med. Chem. Lett.* **2002**, 12, 2299.
- ¹⁰² Zhao, B.; Lu, W. Q.; Wu, Y. *J. Mater. Chem.* **2000**, 10, 1513.
- ¹⁰³ Belavaux-Nicot, B.; Fery-Forgues, S. *Eur. J. Inorg. Chem.* **1999**, 1821.
- ¹⁰⁴ McMurry, J. *Organic Chemistry*, 6th Ed. Thomson-Brooks/cole, NY, **2007**.
- ¹⁰⁵ Fairlamb, I. J. S.; Moulton, B. E.; Sawle, P.; Green, C. J.; Motterlini, R. *Chem. Res. Toxicol.* **2008**, 21, 1484.
- ¹⁰⁶ a) Sun, M.; Shi, Q.; Huang, G.; Liang, Y.; Ma, Y. *Synthesis* **2005**, 15, 2482. b) Zhou, W. J.; Ji, S. J.; Shen, Z. L. *J. Organomet. Chem.* **2006**, 691, 1356.
- ¹⁰⁷ Wu, X.; Tiekink, E. R. T.; Kostetski, I.; Go, M. L. *Eur. J. Pharm. Sci.* **2006**, 27, 175.
- ¹⁰⁸ Wolfe, H.; Kopacka, H.; Ongania, K-H.; Bildstein, B. *J. Org. Chem.* **2006**, 691, 1197.
- ¹⁰⁹ Miyaura, N.; Buchwald, S. L. *Cross coupling reactions. Springer.* **2002**, 248.
- ¹¹⁰ Zhang, H.; Luo, X.; Zhu, L.; Marder, T. B.; Lei, A. *Chem. Eur. J.* **2009**, 0, 0.

References for Chapter 2

- 111 Mitoraj, M. P.; Michalak, A. *Inorg. Chem.* **2010**, *49*, 578.
- 112 a) Maire, P.; Deblon, S.; Breher, F.; Geier, J.; Bohler, C.; Ruegger, H.; Schonberg, H.; Grutzmacher, H. *Chem. Eur. J.* **2004**, *10*, 4198. b) Mariz, R.; Briceno, A.; Dorta, R.; Dorta, R. *Organometallics* **2008**, *27*, 6605. c) Stepnicka, P.; Lamac, M.; Cisarova, I. *J. Organometallic. Chem.* **2008**, *693*, 446. d) Shintani, R.; Duan, W.-L.; Okamoto, K.; Hayashi, T. *Tetrahedron Asymmetry* **2005**, *16*, 3400. e) Hennessy, E. J.; Buchwald, S. L. *Org. Lett.* **2002**, *4*, 269.
- 113 a) Fairlamb, I. J. S.; Kapdi, A. R.; Lee, A. F.; McGlacken, G. P.; Weissburger, F.; de Vries, A. H. M.; Schmieder-van de Vondervoort, L. *Chem. Eur. J.* **2006**, *12*, 8750. b) Fairlamb, I. J. S.; Kapdi, A. R.; Lee, A. F. *Org. Lett.* **2004**, *6*, 4435.
- 114 Luo, X.; Zhang, H.; Duan, H.; Liu, Q.; Zhu, L.; Lei, A. *Org. Lett.* **2007**, *9*, 4571.
- 115 Kudar, V.; Zsoldos-Mady, V.; Simon, K.; Csampai, A.; Sohar, A. *J. Organometallic. Chem.* **2005**, *690*, 4018.
- 116 a) Lopez, E. A. V.; Klimova, T.; Klimova, E. I.; Toledano, A.; Garcia, M. M. *Synthesis*. **2004**, *15*, 2471. b) Nagy, A. G.; Marton, J.; Sohar, P. *Acta. Chim. Hung.* **1991**, *128*, 961.
- 117 Kudar, V.; Zsoldos-Mady, V.; Simon, K.; Csampai, A.; Sohar, P. *Organometallic. Chem.* **2005**, *690*, 4018.
- 118 a) Tolman, C. A. *J. Am. Chem. Soc.* **1970**, *92*, 2656. b) Tolman, C. A. *J. Am. Chem. Soc.* **1970**, *92*, 2953.
- 119 Bandgar, B. P.; Patil, S. A.; Gacche, R. N.; Korbadi, B. L.; Kinkar, S. N.; Jalde, S. S. *Bioorg. Chem. Lett.* **2010**, *20*, 730.
- 120 McMurry, M. *Organic Chemistry. 6th ed, Thomson-Brooks/Cole, NY, 2007.*

-
- 121 a) Tarraga, A.; Molina, P.; Lopez, J. L. *Tetrahedron Lett.* **2000**, *41*, 2479. b) Tarraga, A.; Molina, P.; Curiel, D.; Lopez, J. L.; Velasco, M. D. *Tetrahedron.* **1999**, *55*, 14701.
- 122 a) Tanaka, K.; Tada, F. *Chem. Rev.* **2000**, *100*, 1025. b) Rothenberg, G.; Downie, A. P.; Raston, C. L.; Scott, J. L. *J. Am. Chem. Soc.* **2001**, *123*, 8701. c) Liu, W.; Xu, Q.; Chen, B.; Liang, Y.; Ma, Y.; Liu, W. *J. Organometallic Chem.* **2001**, *782*, 637. d) Liu, W.; Xu, Q.; Chen, B.; Ma, Y. *Synth. Commun.* **2002**, *32*, 171.
- 123 Ji, S. J.; Shen, Z. L.; Wang, S. Y. *Chin. Chem. Lett.* **2003**, *14*, 663.
- 124 Villemin, D.; Martin, B.; Puciova, M.; Toma, S. J. *Organometallic Chem.* **1994**, *27*, 484.
- 125 <http://chemistry.uah.edu/faculty/vogler/LectureNotes332/CH332Chapter18.pdf>
- 126 Song, Q-B.; Lin, R-X.; Yang, Z-P.; Qi, C-Z. *Molecules.* **2005**, *10*, 634.
- 127 Fang, J.; Jin, Z.; Li, Z.; Liu, W. *J. Organometal. Chem.* **2003**, *674*, 1. and references therein.
- 128 <http://www.as.utexas.edu/astronomy/education/spring07/scalo/secure/LoudonCh4 Alkenes.pdf>
- 129 <http://www.chem.mun.ca/homes/fmkhome/Schlenks.htm>
- 130 Wade, L. G. *J. Chem. Educ.* **1978**, *55*, 208.
- 131 Luo, X.; Zhang, H.; Duan, H.; Liu, Q.; Zhu, L.; Zhang, T.; Lei, A. *Org. Lett.* **2007**, *6*, 4571.
- 132 "SHELXS-97" - program for structure solution. Sheldrick, G. M. *University of Göttingen, Göttingen, Germany, 1997.*

-
- 133 "SHELXL-97" - program for the Refinement of Crystal Structures. Sheldrick, G. M. *University of Göttingen, Göttingen, Germany, 1997.*
- 134 "SHELXS-97" - program for structure solution. Sheldrick, G. M. *University of Göttingen, Göttingen, Germany, 1997.*
- 135 "SHELXL-97" - program for the Refinement of Crystal Structures. Sheldrick, G. M. *University of Göttingen, Göttingen, Germany, 1997.*

References for Chapter 3

- 136 Bennett, M. A.; Knorr, W. R.; Nyholm, R. S. *Inorg. Chem.* **1968**, *7*, 552.
- 137 a) Platinum Metal Rev., **2005**, *49*, 77. b) Cao, Z.; Liu, Z.; Du, H. *J. Org. Chem.* **2011**, *76*, 6401. c) Bruyere, D.; Monteiro, N.; Bouyssi, D.; Balme, G. *Organometallic* **2003**, *22*, 466. d) Dias, H. V. R.; Lu, H-L.; Kim, H-J.; Polach, S. A.; Goh, T. K. H. H.; Browning, R. G.; Lovely, C. J. *Organometallics* **2002**, *21*, 1466. e) Perez, P. J.; Brookhart, M.; Templeton, J. L. *Organometallics*, **1993**, *12*, 261. f) Lang, F.; Chen, G.; Li, L.; Xing, J.; Han, F.; Liao, J. *Chem. Eur. J.* **2011**, *17*, 5242. g) Nishimura, T.; Kawamoto, T.; Nagaosa, M.; Kumamoto, H.; Hayashi, T. *Angew. Chem. Int. Ed.* **2010**, *49*, 1638.
- 138 Luo, X.; Zhang, H.; Duan, H.; Liu, Q.; Zhu, L.; Lei, A. *Org. Lett.* **2007**, *9*, 4571.
- 139 a) Slone, C. S.; Weinburger, D. A.; Mirkin, C. A. *Prog. Inorg. Chem.* **1999**, *48*, 233. b) Braunstein, P.; Naud, F. *Angew. Chem., Int. Ed.* **2001**, *40*, 680.
- 140 Rovis, T.; Johnson, J. B. *Angew. Chem. Int. Ed.* **2008**, *47*, 840.
- 141 a) Cotton, F. A.; Wilkinson, G. *Advanced Inorganic Chemistry: A Comprehensive Text*, 2nd Ed.; Interscience: New York, 1966. b) Five-coordinate compounds have been observed for alkene complexes with N,N-donor ligands: Albano, V. G.; Natile, G.; Panunzi, A. *Coord. Chem. Rev.* **1994**, *133*, 67.
- 142 Gray, G. M.; George, J. M.; Jan, M. *Inorganica Chimica Acta* **2001**, *314*, 133.
- 143 Jarvis, A. G. Phd Thesis University of York **2011**.
- 144 Pongracz, P.; Petocz, G.; Shaw, M.; Williams, D. B. G.; Kollar, L. *J. Org. Chem.* **2010**, *29*, 2503.
- 145 Al-Najjar, I. M. *Inorg. Chim. Acta* **1987**, *128*, 93.

<http://www.as.utexas.edu/astronomy/education/spring07/scalo/secure/LoudonCh4Alkenes.pdf>

- 147 Metallinos, C.; Zaifman, J.; Belle, L. V.; Dodge, L.; Pilkington, M. *Organometallic* **2009**, *28*, 4534.
- 150 Head, R. A. *Inorg. Synth.* **1990**, *28*, 132.
- 151 Tromp, D. S.; Duin, M. A.; Elsevier, C. J. *Inorg. Chim. Acta* **2002**, *327*, 90.
- 152 March, F. C.; Mason, R.; Scollary, G. R. *Aust. J. Chem.* **1977**, *30*, 2407.
- 153 a) Shintani, R.; Narui, R.; Hayashi, S.; Hayashi, T. *Chem. Comm.* **2011**, *47*, 6123. b) Gladiali, S.; Grepioni, F.; Medici, S.; Zucca, A.; Kollar, L. *Eur. J. Inorg. Chem.* **2003**, 556.
- 154 a) Faraone, F.; Arena, C. G.; Rcondo, E. *J. Organomet. Chem.* **1991**, *419*, 399. b) Colquhoun, I. J.; McFarlane, W. *J. Magnetic Resonance* **1982**, *46*, 525. c) Gambaro, J. J.; Hohman, W. H.; Meck, D. W. *Inorg. Chem.* **1989**, *28*, 4154. d) Pandey, K. K.; Nehete, D. T.; Sharma, R. B. *Polyhedron* **1990**, *9*, 2013.
- 155 a) Steel, P. J. *Coord. Chem. Rev.* **1990**, *106*, 227. b) Panthi, B.; Gipson, S. L.; Franken, A. *Acta. Cryst.* **2008**, *E64*, m1330.
- 156 Benech, J-M.; Piguet, C.; Bernardinelli, G.; Hopfgartner, G. *J. Chem. Soc. Dalton Trans.* **2001**, 684.
- 157 Pearson, R. G. *J. Am. Chem. Soc.* **1963**, *85*, 3533.
- 158 "SHELXS-97" - program for structure solution. Sheldrick, G. M. *University of Göttingen, Göttingen, Germany*, **1997**.
- 159 "SHELXL-97" - program for the Refinement of Crystal Structures. Sheldrick, G. M. *University of Göttingen, Göttingen, Germany*, **1997**.

-
- 160 Dolomanov, O.V.; Bourhis, L. J.; Gildea, R. J.; Howard, J. A. K.; Puschmann, H.
OLEX2: a complete structure solution, refinement and analysis program. *J. Appl.
Cryst.* **2009**, *42*, 339, using "SHELXS-97" - program for structure solution.
Sheldrick, G. M. University of Göttingen, Göttingen, Germany, 1997.
- 161 "SHELXL-97" - program for the Refinement of Crystal Structures. Sheldrick, G. M. University
of Göttingen, Göttingen, Germany, 1997.
- 162 "smtbx-flip" plug-in module to "Olex2" crystallography software, *J. Appl. Cryst.* **2009**, *42*, 339.

References for Chapter 4

- 163 a) Lightman, A. *Chemical & Engineering news. American Chemical Society* **2003**, *81*, 150. b) Al'brekht, V. G.; Zhurnal, G. *Izvestiya Vysshikh Uchebnukh Zavedenii* **2001**, *6*, 33.
- 164 a) Niinistoe, L. *Kemia* **2002**, *29*, 15. b) Elisabeth, L. *Praxis der Naturwissenschaften Chemie in der Schule* **2007**, *56*, 31.
- 165 Casini, A.; Hartinger, C.; Gabbiani, C.; Mini, E.; Dyson, P. J.; Keppler, B. K.; Messori, L. *J. Inorg. Biochem.* **2008**, *102*, 564.
- 166 Messori, L.; Marcon, G. In *Metal ions and their complexes in medication*; Sigel, A., Ed.; CRC Press: 2004, 280.
- 167 Food Standards Agency's web site. Current EU approved additives and their E Numbers.
<http://www.food.gov.uk/safereating/chemsafe/additivesbranch/enumberlist>
(accessed on July 1st, 2009)
- 168 a) Nolan, S. P. *Nature*. **2007**, *445*, 496. b) Hashmi, A. S.K. *Chem. Rev.* **2007**, *107*, 3180. c) Furstner, A. *Chem. Soc. Rev.* **2009**, *38*, 3208.
- 169 a) Skouta, R.; Li, C.J. *Tetrahedron*. **2008**, *64*, 4917. b) Gorin, D. J.; Toste, F. D. *Nature* **2007**, *446*, 395. c) Hashmi, A.S. K.; Hutchings, G, J. *Angew. Chem., Int. Ed.* **2006**, *45*, 7896. d) Hashmi, A. S. K.; Salathe, R.; Frost, T. M. *Appl. Catal. A.* **2005**, *291*, 238.
- 170 Pradal, A.; Toullec, P, Y.; Michelet, V. *Synthesis* **2011**, *10*, 1501.
- 171 Bone, W. A.; Wheeler, R. V. *Philos. Trans. R. Soc. London, Ser. A* **1906**, *206*, 1-67.
- 172 a) Gorin, D. J.; Toste, F. D. *Nature* **2007**, *446*, 395. b) Hutchings, G. J. *Catal. Today*. **2007**, *122*, 196. c) Hashmi, A. S. K.; Hutchings, G. J. *Angew. Chem., Int.*

-
- Ed. **2006**, 45, 7898. d) Hashmi, A. S. K. *Angew. Chem., Int. Ed.* **2005**, 44, 6990.
e) Dyker, G. *Angew. Chem., Int. Ed.* **2000**, 39, 4237.
- 173 a) Furstner, A.; Davies, P. W. *Angew. Chem., Int. Ed.* **2007**, 46, 3410. b) Gorin, D. J.; Sherry, B. D. Toste, F. D. *Chem. Rev.* **2008**, 108, 3351.
- 174 a) Haug, T. T.; Harschneck, T.; Duschek, A.; Binder, J. T.; Kirsch, S. F. J. *Organomet. Chem.* **2009**, 694, 510. b) Blanc, A.; Alix, A.; Weibel, J.-M.; Pale, P. *Eur. J. Org. Chem.* **2010**, 1644.
- 175 a) Sanz, S.; Jones, L. A.; Mohr, F.; Laguna, M. *Organometallics* **2007**, 26, 952.
- 176 Nieto-Oberhuber, C.; Perez-Galam, P.; Herrero-Gomez, E.; Lauterbach, T.; Rodriguez, C.; Lopez, S.; Echavarren, A. M. *J. Am. Chem. Soc.* **2008**, 130, 269.
- 177 a) Marion, N.; Gealageas, R.; Nolan, S. P. *Org. Lett.* **2007**, 9, 2653. b) Witham, C. A.; Mauleon, P.; Shapiro, N. D.; Sherry, B. D.; Toste, F. D. *J. Am. Chem. Soc.* **2007**, 129, 5838.
- 178 Diez-Gonzalez, S.; Nolan, S. P. *Acc. Chem. Res.* 2008, 41, 349.
- 179 Guan, B. T.; Xing, D.; Cai, G. X.; Yu, N.; Fang, Z.; Shi, Z. J. *J. Am. Chem. Soc.* **2005**, 127, 18004.
- 180 Hashmi, A. S. K.; Schafer, S.; Wolfle, M.; Gil, C. D.; Fischer, P.; Gimeno, M. *C. Angew. Chem. Int. Ed.* **2007**, 46, 6184.
- 181 Li, X. Q.; Li, C.; Song, F. B. *J. Chem. Res.* **2007**, 722.
- 182 Brouwer, C.; He, C. *Angew. Chem. Int. Ed.* **2006**, 45, 1744.
- 183 a) Zhang, L. M.; Sun, J. W.; Kozmin, S. A. *Adv. Synth. Catal.* **2006**, 348, 2271.
b) Bruneau, C. *Angew. Chem., Int. Ed.* **2005**, 44, 2328.
- 184 a) Haruta, M.; Kobayashi, T.; Sano, H.; Yamada, N. *Chem. Lett.* **1987**, 405. b) Haruta, M.; Yamada, N.; Kobayashi, T.; Iijima, S.; *J. Catal.* **1989**, 115, 301. c) Guzman, J.; Gates, B. C. *J. Am. Chem. Soc.* **2004**, 126, 2672. d)

-
- Luengnaruemitchai, A.; Thoa, D. T. K.; Osuwan, S. *Int.J. Hydrogen. Energy.* **2005**, *30*, 981.
- 185 Hua, J.; Zheng, Q.; Zheng, Y.; Wei, K.; Lin, X. *Catal. Lett.* **2005**, *102*, 99.
- 186 Corma, A.; Abad, A.; Garcia, H. *Angew. Chem. Int. Ed.* **2005**, *44*, 4066.
- 187 a) Carrettin, s.; Guzman, J.; Corma, A. *Angew. Chem. Int. ed.* **2005**, *44*, 2242. b) Hashmi, A. S. K.; Schwarz, L.; Choi, J.-H, Frost, T. M. *Angew. Chem. Int. Ed.* **2000**, *39*, 2285.
- 188 Toste, F. D. *Gold catalysis for organic synthesis*. Thematic series in the Open access *Beilstein Journal of Organic Chemistry*.
- 189 a) Gorin, D. J.; Toste, F. D. *Nature* **2007**, *446*, 395. b) Chianese, A. R.; Lee, S. J.; Gagne', M. R. *Angew. Chem., Int. Ed.* **2007**, *46*, 4042. c) Ma, S.; Yu, S.; Gu, Z. *Angew. Chem., Int. Ed.* **2006**, *45*, 200. d) Bruneau, C. *Angew. Chem., Int. Ed.* **2005**, *44*, 2328.
- 190 a) Li, Z.; Brouwer, C.; He, C. *Chem. Rev.* **2008**, *108*, 3239. b) Jimenez-Nuñez, E.; Echavarren, A. M. *Chem. Rev.* **2008**, *108*, 3326. c) Bongers, N.; Krause, N. *Angew.Chem., Int. Ed.* **2008**, *47*, 2178. d) Furstner, A.; Davies, P. W. *Angew. Chem., Int.Ed.* **2007**, *46*, 3410. e) Zhang, L.; Sun, J.; Kozmin, S. A. *Adv. Synth. Catal.* **2006**, *348*, 2271. f) Hashmi, A. S. K.; Hutchings, G. J. *Angew. Chem., Int. Ed.* **2006**, *45*, 7896.
- 191 a) Hashmi, A. S. K.; Salathe, R.; Frey, W. *Chem. Eur. J.* **2006**, *12*, 6991. b) Harkat, H.; Dembele, A. Y.; Weibel, J.-M.; Blanc, A.; Pale, P. *Tetrahedron.* **2009**, *65*, 1871.
- 192 Hashmi, A. S. K. *Angew. Chem., Int. Ed.* **2008**, *47*, 6754.
- 193 Lee, Y. T.; Kang, Y. K.; Chung, Y. K. *J. Org. Chem.* **2009**, *74*, 7922.
- 194 a) Lloyd-Jones, G. C. *Org. Biomol. Chem.* **2003**, *1*, 215. b) Echavarren, A. M.; Nevado, C. *Chem. Soc. Rev.* **2004**, *33*, 431. c) Diver, S. T.; Giessert, A. *J. Chem. Rev.* **2004**, *104*, 1317.

-
- 195 Park, Y.; Kim, S. Y.; Park, J. H.; Cho, J.; Kang, Y. K.; Chung, Y. K. *Chem. Comm.* **2011**, *47*, 5190.
- 196 a) Soriano, E.; Macro-Contelles, J. *Acc. Chem. Res.* **2009**, *42*, 1026. b) Hashmi, A. S. K.; Rudolph, M. *Chem. Soc. Rev.* **2008**, *37*, 1766. c) Lee, Y. T.; Kang, Y. K.; Chung, Y. K. *J. Org. Chem.* **2009**, *74*, 7922.
- 197 a) Trost, B. M.; Toste, F. D. *J. Am. Chem. Soc.* **2000**, *122*, 714. b) Trost, B. M.; Toste, F. D. *J. Am. Chem. Soc.* **2004**, *126*, 15592.
- 198 Trost, B. M.; Lautens, M.; Hung, M. H. *J. Am. Chem. Soc.* **1984**, *106*, 7641.
- 199 a) Trost, B. M.; Chand, V. K. *Synthesis* **1993**, 824. b) Chatani, N.; Morimoto, T.; Muto, T.; Murai, S. *Organometallics* **2001**, *20*, 3704.
- 200 Shibtata, T.; Kobayashi, Y.; Maekawa, S.; Toshida, N.; Takagi, K. *Tetrahedron* **2005**, *61*, 9018.
- 201 a) Grigg, R.; Stevenson, P.; Worakun, T. *Tetrahedron* **1988**, *44*, 4967. b) Cao, P.; Wang, B.; Zhang, X. *J. Am. Chem. Soc.* **2000**, *122*, 6490.
- 202 Fehr, C.; Farris, I.; Sommer, H. *Org. Lett.* **2006**, *8*, 1839.
- 203 Michelet, V.; Toullec, P. Y.; Genet, J. P. *Angew. Chem. Int. Ed.* **2008**, *47*, 4268.
- 204 Marion, N.; De-Fremont, P.; Lemiere, G.; Stevens, E. D.; Nolan, S. P. *Chem. Commun.* **2006**, 2048.
- 205 Luzung, M. R.; Markham, J. P.; Toste, F. D. *J. Am. Chem. Soc.* **2004**, *126*, 10858.
- 206 Axen, U.; Lincoln, F. H.; Thompson, J. L. *J. Chem. Soc. D. Chem. Commun.* **1969**, 303.
- 207 Furstner, A.; Hannen, P. *Chem. Eur. J.* **2006**, *12*, 3006.

-
- 208 Staben, S. T.; Kennedy-Smith, J. J.; Huang, D.; Corkey, B. K.; Toste, F. D.
Angew. Chem. Int. Ed. **2006**, *45*, 5991.
- 209 Ishiuchi, K.; Kubota, T.; Morita, H.; Kobayashi, J. *Tetrahedron Lett.* **2006**, *47*,
3287.
- 210 Marion, N.; Fremont, P.-D.; Lemiere, G.; Stevens, E. D.; Fensterbank, L.; Nolan,
S. P. *Chem. Commun.* **2006**, 2048
- 211 Montaudou, G.; Caccamese, S. *J. Org. Chem.* **1973**, *38*, 710.
- 212 Karpuk, E.; Schollmeyer, D.; Meier, H. *Eur. J. Org. Chem.* **2007**, 1983.
- 213 Garvis, A. J. PhD Thesis. University of York 2011.
- 214 Schmidt, G. M. J. *Pure Appl. Chem.*, **1971**, *27*, 647.
- 215 Alcock, N. W.; de Meester, P.; Kemp, T. J. *J. Chem. Soc., Perkin Trans. II* **1979**,
921.
- 216 <http://www.as.utexas.edu/astronomy/education/spring07/scalo/secure/LoudonCh4Alkenes.pdf>
- 217 Luzung, M. R.; Markham, J. P.; Toste, F. D. *J. Am. Chem. Soc.* **2004**, *126*,
10858.
- 218 a) Cunningham, A. J.; Underwood, A. L. *Cyclic voltammetry of the pyridine
nucleotides and a series of nicotinamide model compounds. Biochem.* **1967**, *6*,
266. b) Ti-Tien, H. *Cyclic voltammetry of bilayer lipid membranes. J. Phys.
Chem.* **1984**, *88*, 3172.
- 219 Ito, N.; Saji, T.; Aoyagui, S. *J. Organomet. Chem.* **1983**, *247*, 301.
- 220 a) Sharp, M.; Petersson, M.; Edstrom, K. *J. Electroanal. Chem.* **1980**, *109*, 271.
b) Montenegro, M. I.; Pletcher, D. *J. Electroanal. Chem.* **1986**, *200*, 371.
- 221 <http://www.chem.mun.ca/homes/fmkhome/Schlenks.htm>

-
- 222 Faggiani, R.; Howard-Lock, H. E.; Lock, C. J. L.; Turner, M. A. *Can. J. Chem.* **1987**, *65*, 1568.
- 223 Schwier, T.; Rubin, M.; Gevorgyan, V. *Org. Lett.* **2004**, *6*, 1999.
- 224 Luzung, M. R.; Markham, J. P.; Toste, F. D. *J. Am. Chem. Soc.* **2004**, *126*, 10858.
- 225 "SMART" - control software Bruker SMART Apex X-ray Diffractometer. v5.625, Bruker-AXS GMBH, Karlsruhe, Germany.
- 226 "SAINT+" - integration software for Bruker SMART detectors. v6.45, Bruker-AXS GMBH, Karlsruhe, Germany.
- 227 "SADABS" - program for absorption correction. v2.10. Sheldrick, G. M. Bruker AXS Inc., Madison, Wisconsin, USA, 2007.
- 228 "SHELXS-97" - program for structure solution. Sheldrick, G. M. University of Göttingen, Göttingen, Germany, 1997.
- 229 "SHELXL-97" - program for the Refinement of Crystal Structures. Sheldrick, G. M. University of Göttingen, Göttingen, Germany, 1997.
- 230 CrysAlisPro, Oxford Diffraction Ltd. Version 1.171.34.40.
- 231 Empirical absorption correction using spherical harmonics, implemented in SCALE3 ABSPACK scaling algorithm within CrysAlisPro software, Oxford Diffraction Ltd. Version 1.171.34.40.
- 232 Dolomanov, O.V.; Bourhis, L. J.; Gildea, R. J.; Howard, J. A. K.; Puschmann, H. OLEX2: a complete structure solution, refinement and analysis program. *J. Appl. Cryst.* **2009**, *42*, 339, using "SHELXS-97" - program for structure solution. Sheldrick, G. M. University of Göttingen, Göttingen, Germany, 1997.

References for Chapter 5

- 233 <http://en.wikipedia.org/wiki/Palladium>
- 234 Palladium. International Platinum Group Metals Association.
<http://www.ipa-news.com/pgm/index.htm>.
- 235 a) Stille, J. K. *Angew. Chem.* **1986**, *98*, 504. b) Heck, R. F. *Comprehensive Organic Synthesis*. Pergamon. Oxford. **1991**, *4*, 833. c) Miyaura, N.; Suzuki, A. *Chem. Rev.* **1995**, *95*, 2457. d) Luh, T. Y.; Leung, M. K.; Wong, K. T. *Chem. Rev.* **2000**, *100*, 3187. e) Hiyama, T. J. *Organomet. Chem.* **2002**, *653*, 58. f) Negishi, E. -i.; Hu, Q.; Wang, G. *Aldrichimica. Acta.* **2005**, *38*, 71. g) Trost, B. M.; Crawley, M. L. *Chem. Rev.* **2003**, *103*, 2921. h) Surry, D. S.; Buchwald, S. L. *Angew. Chem.* **2008**, *120*, 6438. i) Hartwig, J. F. *Nature.* **2008**, *455*, 314. j) Denmark, S. E.; Regens, C. S. *Acc. Chem. Res.* **2008**, *41*, 1486.
- 236 Chen, X.; Engle, K. M.; Yu, J-Q. *Angew. Chem. Int. Ed.* **2009**, *48*, 5094.
- 237 Cope, A. C.; Siekman, R. W. *J. Am. Chem. Soc.* **1965**, *87*, 3272.
- 238 Cope, A. C.; Friedrich, E. C. *J. Am. Chem. Soc.* **1968**, *90*, 909.
- 239 Iyer, S.; Ramesh, C. *Tetrahedron Lett.* **2000**, *41*, 8981.
- 240 Weissmann, H.; Milstein, D. *Chem. Commun.* **1999**, 1901.
- 241 Nonoyama, M. *Synth. React. Inorg. Met.-Org. Chem.* **1999**, *29*, 119.
- 242 Nonoyama, M.; Nakajima, K. *Polyhedron.* **1999**, *18*, 533.
- 243 Stephenson, T. A.; Morehouse, S. M.; Powell, A. R. *J. Chem. Soc.* **1965**, 667.
- 244 Cheng, C. D.; Gonela, R. K.; Gu, Q.; Haynie, D. T. *Nano Lett.* **2005**, *5*, 175.
- 245 a) Skapski, A. C.; Smart, M. L. *J. Chem. Soc.* **1970**, 658. b) Cotton, F. A.; Han, S. *Rev. Chim. Miner.* **1985**, *22*, 277.

-
- 246 a) Romm, I. P.; Buslaeva, T. M.; Lyalina, N. N.; Simitsyn, N. M. *Koord. Khim.* **1992**, *18*, 165. b) Stoyanov, E. S. *J. Struct. Chem.* **2000**, *41*, 440.
- 247 Marson, A.; VanOort, A. B.; Mul, W. P. *Eur. J. Inorg. Chem.* **2002**, 3028.
- 248 Zhang, R.; Ma, C.; Yin, H. *Huaxue Shiji.* **1994**, *16*, 383.
- 249 M. Walter, and L. Ramaley. *Anal. Chem.* **1973**, *45*, 165.
- 250 Bakhmutov, V. I.; Berry, J. F.; Cotton, F. A.; Murillo, C. A. *Dalton Trans.* **2005**, 1989.
- 251 The fully balanced equation is: $3\text{Pd}^0 + 6\text{HNO}_3 + 6\text{HOAc} \rightarrow \text{Pd}_3(\text{OAc})_6 + 6\text{NO}_2 + 6\text{H}_2\text{O}$.
- 252 $\text{Pd}_3(\text{OAc})_5\text{NO}_2$ can only be isolated by manual picking of the crystals from $\text{Pd}_3(\text{OAc})_6$
- 253 In the original paper (ref. 14a), crystalline material precipitated within a day.
- 254 Walter, M.; Ramaley, L. *Analytical Chemistry* **1973**, *45*, 165.
- 255 Kukushkin, Yu. N.; Vyazmenskii, Yu. E.; Zorina, L. I. *Neorg. Khim.* **1968**, *13*, 1595.
- 256 Kukushkin, Yu. N. *Coord. Chem. Rev.* **1995**, *139*, 375.
- 257 Santoro, A.; Wegrzyn, M.; Whitwood, A. C.; Bruce, D. W. *J. Am. Chem. Soc.* **2010**, *132*, 10689.
- 258 M. Nonoyama, *Synth. React. Inorg. Met.-Org. Chem.*, 1999, **29**, 119.
- 259 Warren, M. R.; Brayshaw, S. K.; George, M. W.; Warren, J. E.; Teat, S. J. *Angew. Chem. Int. Ed.* **2009**, *48*, 5711.

-
- 260 a) Pressprich, M. R.; White, M. A.; Coppens, P. *J. Am. Chem. Soc.* **1994**, *116*, 5233. b) Fomitechev, D. V.; Coppens, P. *Inorg. Chem.* **1996**, *35*, 7021.
- 261 a) Kubota, M.; Ohba, S. *Acta Crystallogr. Sect. B.* **1992**, *48*, 627. b) Kovalevsky, A. Yu.; Bagley, K. A.; Coppens, P. *Chem. Eur. J.* **2005**, *11*, 7254.
- 262 Kovalevsky, A. Yu.; Coppens, P. *J. Am. Chem. Soc.* **2002**, *124*, 9241.
- 263 S. K. Brayshaw, J. W. Knight, P. R. Raithby, T. L. Savarese, S. Schiffers, S. J. Teat, J. E. Warren, and M. R. Warren, *J. App. Cryst.*, 2010, **43**, 337.
- 264 L. E. Hatcher, M. R. Warren, D. R. Allan, S. K. Brayshaw, A. L. Johnson, S. Fuertes, S. Schiffers, A. J. Stevenson, S. J. Teat, C. H. Woodall, and P. R. Raithby, *Angew. Chem. Int. Ed.*, 2011, **50**, 8371.
- 265 Anderson, C. E.; Kirsch, S. F.; Overman, L. E.; Richards, C. J.; Watson, M. P. *Organic syntheses* **2007**, *84*, 148.
- 266 M. Walter, and L. Ramaley, *Anal. Chem.*, 1973, **45**, 165.
- 267 Anderson, C. E.; Kirsch, S. F.; Overman, L. E.; Richards, C. J.; Watson, M. P. *Organic syntheses* **2007**, *84*, 148.
- 268 G. M. Sheldrick, *Acta Crystallogr., Sect. A*, 1990, **46**, 467.
- 269 G. M. Sheldrick, *Acta Crystallogr., Sect. A*, 2008, **64**, 112.